Use of flexible and ductile roof diaphragms in the seismic design of single-storey steel buildings

By

Kishor Mohan Shrestha ©

McGill

Department of Civil Engineering and Applied Mechanics

McGill University, Montréal, Canada

August 2011

A thesis submitted to the Faculty of Graduate and Postdoctoral Studies
in partial fulfillment of the requirements for the degree of
Doctor of Philosophy
in
Civil Engineering

Abstract

This thesis documents an investigation of the use of the roof diaphragm flexibility in the seismic design and analysis procedure of single-storey steel buildings designed otherwise in accordance with the provisions of the 2010 NBCC and the 2009 CSA S16. The design approach considers the members of the vertical bracing system as the ductile fuse elements in the seismic force resisting system (SFRS), whereas the diaphragm remains elastic. An alternative design approach was also examined in which the steel deck roof diaphragm acts as a ductile fuse element in the SFRS; at present this procedure is not permitted by the NBCC or CSA S16.

The investigation was reliant on a complementary three phase test program in which nineteen large-scale (7.31 m x 21.02 m) roof diaphragm specimens were dynamically excited with a sequence of increasing amplitude loading protocols: low amplitude vibration to measure the dynamic properties of the specimens, variable amplitude excitation up to yielding to evaluate the change in dynamic properties and extreme earthquake excitation to examine the change from elastic to inelastic response. The specimens were assembled of components commonly found in the roofs of single-storey steel buildings. The first part of the study comprised the development of a deep horizontal plane truss numerical model using the OpenSees software platform to reproduce the dynamic characteristics as well as the elastic and inelastic response of the nineteen test specimens. Diagonal truss elements composed of the Pinching4 material model were used to represent the measured strength and stiffness degradation as well as the pinched hysteretic response of the diaphragm, while placing an emphasis on the shear representation of the models. The predicted fundamental period of vibration, the elastic response and the inelastic hysteretic response were compared with the test results and the models were calibrated accordingly. In all cases except for weld and button punched deck diaphragm specimens, it was essential to reduce by 30%, on average, the shear stiffness G' of test specimens, as obtained from the Steel Deck Institute (SDI), in order to match the predicted and measured deformations and natural period of vibration. Pinching behaviour along with degradation of shear stiffness and strength under cyclic loading in the inelastic range could be closely reproduced.

In the second part of the study, the detailed design and non-linear time history dynamic analyses of representative medium size (30 m × 60 m × 7 m) and large size (30 m × 60 m × 7 m) single-

storey steel buildings were carried out. The intent was to evaluate the overall behaviour of four structural systems whose design was tailored to either rely on the flexibility of the diaphragm or to allow the roof decking / connections to deform inelastically. Different design cases were considered; such as with and without period limitation in design as well as with reduced SDI diaphragm shear stiffness. The designed buildings were modelled elastically in SAP 2000 to verify the initial assumption of fundamental period of vibration and allowable drift limit. OpenSees building models were developed by integrating a non-linear brace model with the non-linear diaphragm model. Dynamic analyses were performed on the designed buildings using the corresponding OpenSees building model and responses were evaluated under a suite of design level earthquake signals. The study illustrated that the analytically predicted fundamental period of vibration which includes the influence of the roof deck diaphragm could be used in the design of such single-storey steel buildings. This finding leads to the recommendation to revise the expression given in 2010 NBCC for the fundamental period of vibration as well as for the period limitation. Further, compared to the different structural systems, the buildings designed with EBF structural system were found most promising in terms of the relative capacity force on the steel deck diaphragm and the building response. The study also found that the diaphragms in the EBF and CBF structural systems could be designed for the force corresponding to the seismic base shear with $R_d R_o = 2$, if it controls the design. Moreover, significant shear strength degradation and concentration of inelastic demand were observed in the diaphragm at the edge of the buildings when the steel decks were parallel to the loading direction and the diaphragm was designed as a ductile fuse element. This illustrates that the value of 2.0 that was assumed for the seismic force reduction parameter R_d may not be appropriate in the design of such buildings. Similar strength degradation and concentration of inelastic demand in the diaphragm were observed in the buildings with a Type CC structural system, which shows that the diaphragm may need to be designed corresponding to the elastic seismic force.

Résumé

La présente thèse porte sur une recherche sur l'utilisation de la flexibilité du diaphragme de toit dans la conception et l'analyse parasismiques des bâtiments d'un seul étage en acier conçus selon les dispositions parasismiques des normes de construction CNBC 2010 et CSA S16-09. L'approche de conception consiste à considérer les diagonales de contreventement faisant partie du système de résistance aux forces sismiques (SRFS) comme les éléments ductiles, alors que le comportement du diaphragme de toit demeure dans le domaine élastique. Une approche différente a aussi été examinée selon laquelle le diaphragme de toit en acier agit comme un élément ductile dans le SFRS, approche qui n'est pas autorisée dans les codes CNBC et CSA S16 présentement en vigueur.

L'étude est tributaire d'un programme d'essais complémentaires en trois phases durant lequel dix-neuf spécimens de diaphragme de toit à grande échelle (7.31m x 21.02m) ont été soumis à des essais dynamiques selon un protocole de chargement à amplitude variable: vibrations à faible amplitude permettant de mesurer les propriétés dynamiques des spécimens, amplitude d'excitation variable jusqu'à la plastification permettant d'évaluer le changement des propriétés dynamiques et chargement sismique extrême permettant d'examiner le changement de comportement de l'état élastique à l'état inélastique. Les spécimens étaient constitués de composantes couramment utilisées dans les toitures des bâtiments en acier d'un seul étage. La première partie de l'étude a porté sur l'élaboration avec le logiciel OpenSees d'un modèle numérique de diaphragme de toit composé d'un système de treillis afin de reproduire les caractéristiques dynamiques de même que les comportements élastique et inélastique des dix neuf spécimens. Pour les éléments de treillis des modèles, on a utilisé le matériau "Pinching4" permettant de reproduire la dégradation en résistance et en rigidité qui a été observée de même que le pincement du comportement hystérétique des diaphragmes, le tout en mettant l'emphase sur le comportement à l'effort tranchant des modèles.

Les prédictions de la période fondamentale de vibration, du comportement élastique et de la réponse sous sollicitation inélastique cyclique ont été comparées aux résultats des essais au laboratoire, et les modèles ont été ajustés en conséquence. Dans tous les cas sauf ceux dans lequel ou les feuilles de tablier étaient fixées avec des soudures et sertissages, on a dû réduire de

30% la rigidité en cisaillement G' du spécimen du test obtenue par la méthode SDI (Steel Deck Institute) afin d'obtenir une corrélation entre les déformations et les périodes fondamentales de vibration prédites et mesurées. Le pincement (pinching), de même que la dégradation de la rigidité et de la résistance en cisaillement sous chargement cyclique dans le domaine inélastique ont pu être reproduits de près.

Dans le seconde partie du programme d'essais, la conception de différents bâtiments à un étage de taille moyenne (30m x 60m x 7m) et de taille grande (40m x 90m x 8m), ainsi que l'analyse non-linéaire de ceux-ci, a été complétée. L'objectif était d'évaluer le comportement global de quatre systèmes structuraux dont la conception avait été adaptée pour prendre en compte la flexibilité du diaphragme de toit ou permettre les déformations inélastiques des connecteurs du tablier métallique. Différents cas de conception ont été considérés, incluant ceux où on a considéré ou ignoré dans la conception la limite imposée sur la période de vibration et la réduction de la rigidité en cisaillement du diaphragme obtenue de la méthode SDI. Les bâtiments ainsi conçus ont été modélisés dans le domaine élastique avec le logiciel SAP2000, afin de vérifier les hypothèses initiales quant à la période fondamentale de vibration et la conformité des structures quant aux limites de déformations. Des modèles des bâtiments ont été développés avec le logiciel OpenSees, en intégrant un modèle non linéaire des diagonales et le modèle non linéaire du diaphragme. Des analyses dynamiques des bâtiments ainsi conçus ont été réalisées avec le logiciel OpenSees et leur comportement a été évalué sous un ensemble de mouvements de sol sismique d'amplitude correspondant au niveau sismique de conception. L'étude à démontré que la période qui inclus l'influence du diaphragme peut être utilisée dans la conception d'un bâtiment à un étage en acier avec ce type de construction. Cette découverte mène à la recommandation de réviser l'expression du CNBC 2010 pour la période fondamentale du bâtiment ainsi que la limite empirique sur celle-ci. Les bâtiments construits avec un système de contreventements de type excentrique sont les plus prometteurs au niveau de la capacité relative du diaphragme en acier et la comportement du bâtiment. L'étude a aussi démontré que les diaphragmes qui sont unis avec un système de contreventements concentriques ou excentriques peuvent êtres conçus pour la force qui correspond au cisaillement calculé avec $R_d R_o$ = 2, si celui-ci contrôle la conception du diaphragme. Il faut aussi noter qu'une dégradation significative de la capacité en cisaillement et une concentration de la demande élastique à été observée aux côtés des bâtiments quand la tôle est installée parallèle à la direction de la charge et

quand le diaphragme est conçu comme l'élément sacrifiant. Ceci illustre le fait que la valeur de 2.0 assumé pour la ductilité du système (R_d) n'est pas nécessairement appropriée pour la conception de ce genre de bâtiments. Cette même concentration de la demande aux côtes et dégradation du système a aussi été observée dans les bâtiments conçus avec un système latéral de type 'construction conventionnelle' ce qui veut dire que le diaphragme devrait sans doute être construit pour la force sismique élastique.

Preface

This thesis is submitted to the McGill University, for the degree of Doctor of Philosophy. The work described in this thesis was carried out by the candidate during the years 2007 to 2011 in the Department of Civil Engineering at the McGill University under the supervision of Professor Colin A. Rogers and Professor Robert Tremblay.

In accordance with the by-laws of the McGill University governing the requirements for the degree of Doctor of Philosophy, the candidate submits that the work presented in this thesis is original unless otherwise referenced within the text. In particular the numerical non-linear modeling of steel roof diaphragms using the OpenSees platform along with the proposed values of Pinching4 material parameters and the seismic evaluation of single storey steel buildings with non-linear flexible diaphragms exhibiting pinched hysteretic response and strength degradation are claimed as original. A total of 7 supporting journal and conference papers have been published, submitted or accepted for publication based on the related work presented in this thesis.

Journal Papers:

Massarelli, R., Franquet, J., Shrestha, K., Tremblay, R., and Rogers, C. A. (2011), "Dynamic Seismic Response of Large Scale Steel Deck Diaphragms", J. Constr. Steel Research (Submitted)

Shrestha, K., Rogers, C.A., Tremblay, R., (2011), "Numerical modelling and calibration of steel roof deck diaphragms under dynamic loading", J. Constr. Steel Research (In preparation)

Conference Papers:

Franquet, J., Massarelli, R., Shrestha, K., Tremblay, R., Rogers, C.A. (2010), "Dynamic tests of 0.76 & 0.91 mm steel deck diaphragms for single-storey buildings", 9th US National & 10th Canadian Conference on Earthquake Engineering, Toronto, Canada, Paper No. 1008.

Massarelli, R., Franquet, J., Shrestha, K., Tremblay, R., Rogers, C.A. (2011), "Dynamic tests of 0.76 to 1.21 mm steel deck diaphragms for single-storey buildings", 6th International Conference on Thin-Walled Structures, Timisoara, Romania. (Paper accepted)

Proulx, J., Boulanger, B., Bakhti, F., Shrestha, K., Tremblay, R., Rogers, C.A., Lamarche, C.-P., Paultre, P. (2012), "Field measurements and numerical predictions of the dynamic properties of a low-rise steel building with a flexible steel roof deck diaphragm", STESSA 2012 – 7th International Conference on the Behaviour of Steel Structures in Seismic Areas, Santiago, Chile. (Paper submitted)

Shrestha, K., Franquet, J., Rogers, C.A., Tremblay, R. (2009), "OpenSees modeling of the inelastic seismic response of steel roof deck diaphragms", STESSA 2009 – 6th International Conference on the Behaviour of Steel Structures in Seismic Areas, Philadelphia, USA, 775-780.

Tremblay, R., Rogers, C.A., Lamarche, C.-P., Nedisan, J., Franquet, J., Massarelli, R. and Shrestha, K (2008b), " Dynamic seismic testing of large size steel deck diaphragm for low-rise building applications" 14th World Conference on Earthquake Engineering, October 12-17, 2008, Beijing, China.

Kishor M. Shrestha

Acknowledgements

I would like to thank all the individuals who in one way or another contributed their valuable support throughout this study.

First and foremost, I would like to express my sincerest gratitude to my supervisors Professor Colin A. Rogers and Professor Robert Tremblay who guided me on this long journey from beginning to end, and provided continuous support and encouragement. Your diligence and patience has made this an invaluable learning experience. Thank you very much!

Thank you to the whole diaphragm team: John Franquet, Robert Massarelli and Camelia Nedisan, for carrying out the three phases of dynamic tests on the steel roof diaphragms. It was wonderful to work with you all and to be involved in the testing program. Thank you to David Ek, Derek Kozak and William Franquet, as well as the technical staff of the Structures Laboratory of École Polytechnique for your support in successfully completing the tests. Also, a special thanks to Dr. Ali Roufegarinejad, Prof. Kenneth Elwood and Prof. Perry Adebar of the University of British Columbia for their helpful comments and suggestions.

Additionally, it was an honour for me to be recognized by McGill University by being awarded the prestigious Tomlinson Fellowship for my research. I would also like to acknowledge the financial support provided by the Natural Sciences and Engineering Research Council of Canada, the Steel Structures Education Foundation, the Canadian Sheet Steel Building Institute and the member companies of the Vancouver Steel Deck Diaphragm Committee (listed on the following pages), as well as the following companies: Hilti Corporation, Canam Group Inc., Sofab Structural Steel Inc. and Lainco Inc..

Finally, I would like to thank my parents, my wife Rupa and children Rukesh and Kriti, as well as all my siblings, relatives and friends for their belief, passion and constant encouragement. I would never have accomplished what I have without you, so thank you, again and again.

Vancouver Diaphragm Committee

Structural Engineering Companies

Bianco Lam Consultants, Bogdonov Pao Associates Ltd., Bush Bohlman, CA Boom, CWMM, Glotman Simpson Consulting Engineers, John Bryson & Partners, Krahn Engineering , Lang Structural Engineering Inc., Mainland Engineering, Omicron Consulting Group, Phoenix Structural Designs Ltd., PJB Engineering Ltd., Pomeroy Engineering, RDJ Structural, Read Jones Christoffersen Ltd., Reliable Equipment Rentals, Siefken Engineering Ltd., Tabet Engineering Ltd., Thomas Leung Structural Engineering Inc., Weiler Smith Bowers Consulting Structural Engineers

Decking Installers

Continental Steel Ltd., Contura Building Corp., Dominion Construction Company Inc., ICC Integrated Cons Concepts Ltd., Opus Building Canada Inc., Overon Designs, Porte Realty Ltd., Prism Construction Ltd., Rite-Way Metals Ltd., Rockwell Pacific, Sun Life Financial (Real Estate Investment Division), Teck Construction LLP, The Beedie Group ,Ventana Construction Corporation, Wales McLelland Construction Co. (1988) Ltd.

Architectural Design

D Forcier Designs, Sanford Designs Ltd.

Table of Content

List of Figures

List of Tables

Chapter 1 - Introduction

1.1 Introduction

Single-storey steel buildings comprise a significant portion of the building stock in North America. These types of steel framed buildings have been widely used for industrial, commercial, educational as well as for recreational purpose. They typically include a cold-formed steel roof deck diaphragm which transfers the lateral forces due to wind or strong ground motion to the vertical bracing bents through the collector elements (Figure 1.1, a). The satisfactory performance of these buildings under any extreme earthquakes is of prime importance to protect the safety of the occupants and to avoid potential collapse. As such, the 2010 National Building Code of Canada (NBCC) (NRCC 2010) requires the use of capacity design principles for the seismic design of buildings, which direct designers to determine the size of the elements of the seismic force resisting system (SFRS) and to detail them to dissipate seismic energy through cyclic inelastic response. Current seismic design principles, such as those found in the 2010 NBCC and the Canadian Standards Association (CSA) S16 Design of Steel Structures Standard (CSA, 2009) require that inelastic demand be limited to the vertical bracing bents of the building, while the roof diaphragm and the other remaining elements in the SFRS are designed to carry loads corresponding to the probable capacity of the bracing bents (Figure 1.1, b). These design requirements have forced engineers to choose thicker deck panels and more closely spaced fastener patterns for the roof diaphragm compared with past practice, causing the structural system of a building to become more costly. Furthermore, in larger buildings the use of a roof deck diaphragm may not be possible due to capacity based forces that exceed the shear resistance of the deck / connection configurations commonly available in North America. An increase in cost is more pronounced when one has to design this type of building with tension/compression braces (Tremblay and Rogers 2005, Rogers and Tremblay 2010). The braces, which are selected based on their compression resistance, inherently possess significant reserve strength in tension; the surrounding elements, including the roof diaphragm, must be designed accounting for the large force in the braces as defined by the probable tension yield capacity $A_gR_yF_y$, where A_g is the member cross-sectional area and R_yF_y is the expected yield stress. An alternative design approach, which at present is not permitted by the NBCC or CSA

S16, could be to consider the steel deck roof diaphragm to act as the ductile fuse element in the SFRS instead of the braces (Figure 1.1, c). This could reduce the structural cost significantly as the shear resistance of the diaphragm can be more easily matched to the seismic design force, thus minimizing the overstrength of the fuse element in the SFRS. Given that the roof accounts for a large percentage of the steel contained in the building compared with just a few bracing bents the overall cost of the structure will typically be less if an inelastic roof diaphragm design approach is implemented. The inelastic behaviour of the steel deck roof diaphragm and the possibility of using it as a fuse element are presented in this thesis.
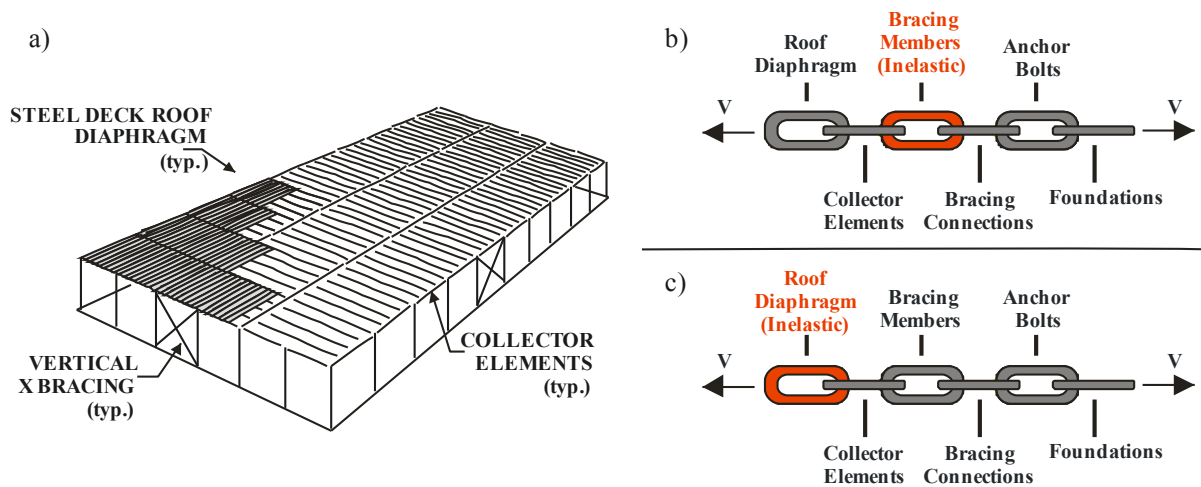
Figure 1.1– a) Typical single-storey steel building structure; b) Weak brace design; and c) Weak diaphragm design

Further, the seismic base shear largely depends on the fundamental period of vibration of the structure, which is used to obtain the design spectral acceleration $S(T_a)$ (Figure 1.2). The period of vibration, T_a, calculated using the NBCC recommended expressions is solely a function of the type of SFRS and the height of the building, regardless of the impact of the diaphragm flexibility. For a building with a braced steel frame, the period is given by the empirical equation $T_a = 0.025h_n$, where h_n is the total building height. The NBCC also allows for the use of a period that is estimated from dynamic analysis; however, this value should not be greater than $0.05h_n$. Past studies have shown that the in-plane flexibility of the roof diaphragm can affect the dynamic response of low-rise buildings (Naman and Goodno 1986, Tremblay and Stiemer 1996, Medhekar 1997, Tremblay et al. 2003, 2004, Rogers et al. 2004). It has been demonstrated

through analytical means that the period of a single-storey steel building with a flexible roof diaphragm may be longer than that which is based on the stiffness of the vertical SFRS (Tremblay and Stiemer 1996, Medhekar 1997, Tremblay et al. 2008a). Significant savings in the cost of the lateral load resisting system could be achieved if this longer period of vibration were exploited in the design of single-storey steel buildings, mainly because of the lower seismic load that would result (Tremblay et al. 2002, Tremblay and Rogers 2005, Rogers and Tremblay 2010). On the other hand, ambient vibration studies of these buildings have shown that the fundamental period of vibration may not be as long as that obtained from analytical predications (Medhekar 1997, Paultre et al. 2004, Tremblay et al. 2008a, Lamarche et al. 2009). However, the level of excitation during ambient vibration tests is low and, consequently, forces and deformations on structures are equally small. Most likely, these forces may not be large enough, compared to seismic induced forces, to overcome the connection rotational capacities of the structure arising from built in friction and restraint (Tremblay et al. 2008a). The recent dynamic testing of roof deck diaphragms showed clear evidence of an increase in the fundamental period with an increase in amplitude of loading (Tremblay et al. 2008b, 2011; Massarelli et al. 2011). Hence, period estimates based solely on ambient vibration measurements are likely to be shorter than the building period that will exist during high seismic force excitation. The behaviour and dynamic inelastic response of single-storey buildings having flexible roof diaphragms are presented in this thesis as well as a study covering the upper limit of the fundamental period of vibration set by the 2010 NBCC.
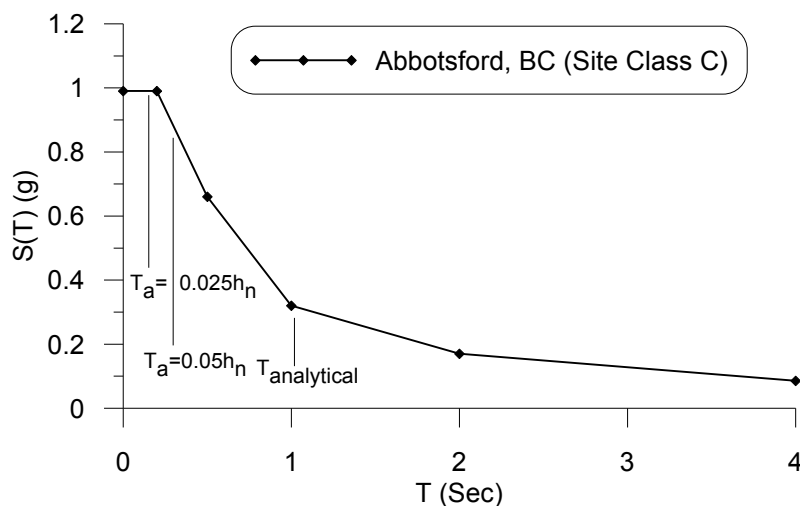
Figure 1.2 – Uniform hazard spectrum

1.2 Objectives

The general objective of the study is to enhance knowledge on the behaviour of single-storey steel buildings with flexible roof diaphragms and to understand the influence of the roof diaphragm on the seismic design and analysis procedure in accordance with the provisions of the NBCC (2010) and CSA S16 (2009), and thus to provide guidance for making recommendations on:

a) the use of an analytically computed fundamental period of vibration of single-storey steel buildings with flexible steel roof deck diaphragms,

b) the design of single-storey steel buildings using the steel deck roof diaphragm as a ductile fuse element, and

c) further experimental and analytical research.

To give the guidance for making the above recommendations, this research study has the following specific objectives:

a) to develop a non-linear inelastic numerical model of steel deck roof diaphragms,

b) to compare and calibrate this model with data obtained from the dynamic and reversed cyclic testing of representative roof deck diaphragms,

c) to incorporate this diaphragm model in a dynamic model of representative single-storey braced frame buildings, and

d) to use the building model to study and develop an improved understanding of the seismic dynamic behaviour and inelastic response of single-storey concentrically braced frame and eccentrically braced framed buildings.

1.3 Scope and limitations

The work includes:

a) a review of the literature on the analysis, design and behaviour of single-storey steel buildings along with their steel roof deck diaphragms,

4

b) a description of the large-scale dynamic diaphragm tests carried out by Franquet (2010) and Massarelli (2011) as a related component of the research project and the analysis of the resulting test data,

c) the development of a non-linear inelastic numerical model of the roof diaphragm test specimens using the Open System for Earthquake Engineering Simulation (OpenSees) platform (McKenna, F. 1997, Mazzoni et al. 2009) and its calibration based on the test data,

d) the calculation of the shear stiffness of the dynamic roof diaphragm test specimens using the model and the test data,

e) the design and analysis of representative concentrically braced frame (CBF) single-storey steel buildings and a study on the influence of diaphragm flexibility and period limitation on such buildings,

f) the design and analysis of representative eccentrically braced frame (EBF) single-storey steel buildings and a study on the influence of diaphragm flexibility and period limitation on such buildings,

g) the design and analysis of braced frames of the conventional construction (CC) category for single-storey steel buildings and a study on the influence of diaphragm flexibility and period limitation on such buildings,

h) the design and analysis of CBF buildings using the steel deck roof diaphragm as the inelastic fuse element in the SFRS and a study on the behaviour of such buildings under design level earthquake ground motions, and

i) the development of numerical building models in the OpenSees platform to evaluate and understand the behaviour of the designed buildings, i.e. items e, f, g and h.

The analytical study is limited to medium sized (30m × 60m × 7m) and large sized (40m × 90m × 8m) rectangular single-storey steel buildings located in Montreal, Quebec and Abbotsford near Vancouver, British Columbia that are located on the reference soil condition Class C. The vertical lateral resisting systems of the building structures to be analysed are of the moderately ductile class of CBF, and the ductile class of EBF. Tension compression CBFs are used for the CC type seismic force resisting system. Openings in the steel roof deck diaphragm are not considered in the analyses. Stiffness contribution from the non-structural components of the roof diaphragms and vertical wall claddings are also not considered in the study.

1.4 Outline of thesis

The thesis consists of five chapters. An overview of the research work is given in Chapter 1 along with a literature review, which covers the following topics:

a) 2010 NBCC seismic design guidelines,

b) seismic design of steel structures according to CSA S16,

c) diaphragm design guidelines,

d) analytical and experimental studies of low rise buildings and

e) experimental investigation of steel roof deck diaphragms.

Chapter 2 describes the development of a numerical model for the roof diaphragm test specimens using the OpenSees software platform and calibration of the model based on the data obtained from dynamic testing of diaphragms. It also includes an evaluation of the numerical models using other existing diaphragm test data.

Chapter 3 is devoted to the design of single-storey steel buildings with CBF, EBF and CC type seismic force resisting systems. Design of representative buildings, where the diaphragm is used as the inelastic weak element in the SFRS, is also presented in this chapter. In addition, a comparison of the design approaches used for these categories of buildings is also presented.

The behaviour of the buildings that are designed in Chapter 3 is presented in Chapter 4. It includes the development of the non-linear building models and dynamic analysis of the single-storey buildings under design level ground motions. Modeling and design recommendations are also presented in this chapter. A summary and conclusion of the thesis along with recommendation for further experimental and analytical research work is presented in Chapter 5.

1.5 Literature review
1.5.1 NBCC 2010 Seismic design guidelines
1.5.1.1 General overview

In Canada the design of the SFRS of a single-storey steel building includes the determination of the seismic base shear as per the 2010 NBCC, the analysis and design of the vertical lateral

resisting system along with collector elements as per CSA S16 (2009) and the design of the steel roof diaphragm. To determine the seismic forces required to be resisted by the SFRS the 2010 NBCC presents two methods; a) equivalent static force procedure (ESFP) and b) dynamic analysis procedure. The NBCC also requires that the building has a clearly defined SFRS to resist 100% of the seismic forces and related effects.

1.5.1.2 Equivalent static force procedure

The 2010 NBCC permits the use of an equivalent static load procedure to determine the design seismic base shear for regular structures, or for irregular structures which satisfy certain stringent conditions. Designers generally follow this procedure when dynamic analysis is not mandatory because of the building's simplicity. Single-storey steel buildings usually satisfy the stringent conditions and are typically designed using the procedure in which the design base shear is calculated using the following formula:

$$V = \frac{S(T_a)M_v\,I_E W}{R_d R_o} \leq \frac{\frac{2}{3}\,S(0.2)I_E W}{R_d R_o} \geq \frac{S(2.0)M_v\,I_E\,W}{R_d R_o} \qquad 1.1$$

where T_a is the fundamental period of vibration of the structure, M_v is the base shear adjustment factor for higher mode effects, I_E is the importance factor, W is the seismic weight of the structure, $S(T_a)$ is the spectral acceleration response at the fundamental period of the structure and R_d and R_o are the ductility related and over strength related force modification factors, respectively. The 2010 NBCC provides spectral acceleration S(T) values with 2% probability of being exceeded in 50 years for very dense soil or soft rock (reference soil condition, class C). An acceleration based site coefficient (F_a) and velocity based site coefficient (F_v) are given in the code to determine the spectral acceleration for the actual site conditions. The method also provides upper and lower limits on the base shear calculation as presented in Equation 1.1. The upper limit is applicable only for SFRSs having $R_d \geq 1.5$. In Equation 1.1, the fundamental period T_a is determined by either using formulae given by the NBCC or by performing a dynamic analysis of the structure. For the brace framed buildings being considered in this study, the period is a function of the building height, h_n, and is given as:

$$T_a = 0.025h_n \qquad\qquad 1.2$$

A longer period of vibration estimated by the use of dynamic analysis is allowed to be used in the design force calculation; however, this should not be greater than two times the period given by Equation 1.2 for this type of building. Limits are defined for the maximum drift as well, which depend on the importance of the structure; in the case of normal buildings an inelastic drift limit of 0.025 times the inter-storey height is applicable.

The other requirement defined in the NBCC is the consideration of accidental torsion. Dynamic analysis is mandatory if the building is sensitive to torsion. The accidental torsion must also be accounted for in regular buildings, which are not sensitive to torsion, by taking into account a 10% eccentricity of the plan dimension perpendicular to the direction of seismic loading. A detailed explanation for the seismic design provisions can be found in the publications by Mitchell et al. (2003), Humar et al. (2003), Humar and Mahgoub (2003) and Heidebrecht (2003).

1.5.1.3 NBCC 2010 diaphragm design provisions

In Clause 4.1.8.15.1 of the 2010 NBCC it is stated that diaphragms and their connections shall be designed so as not to yield. The load path that transfers inertia forces to the collector elements and then to the vertical bracing system must be clearly defined, and hence the design should account for the shape of the diaphragm and its openings. The 2010 NBCC further specifies that the diaphragms should be designed for the governing load case as defined below:

a) The design force for the diaphragms should be determined taking into account the probable capacity of the SFRS. In addition, forces must be applied to the diaphragm to account for the transfer of loads between lateral load carrying elements of the SFRS. The discontinuities and change in stiffness presented in these elements should also be considered.

b) The minimum design force for the diaphragms at any level is determined by dividing the design base shear by the number of storeys.

According to NBCC Clause 4.1.8.15.7, the forces determined based on a) above need not exceed the forces determined with $R_dR_o = 1.0$ unless otherwise permitted by the applicable reference

design standard and, in this case the NBCC allows these forces to be limited to those corresponding to $R_dR_o = 1.3$. As described in Section 1.5.2, it is permitted to use this lower limit in CSA S16 for all steel SFRSs. In addition, when the diaphragms are designed and detailed according to applicable reference design standards to exhibit ductile behaviour, Clause 4.1.8.15.2 of the 2010 NBCC allows the use of seismic design forces corresponding to the base shear calculated using $R_dR_o = 2.0$. As also described in Section 1.5.2, this additional reduction currently is only permitted for diaphragms of SFRSs of the conventional construction (Type CC) category that meet the ductility detailing requirements prescribed in Clause 27.11 of CSA S16.

1.5.2 Design of steel structures CSA S16

The Canadian Standards Association CSA S16 Standard (2009) is the governing document for the design of hot-rolled steel structures in Canada. For the seismic design of steel structures it follows capacity design principles which are documented in Clause 27. The seismic force reduction factors for various design systems, R_d and R_o, are presented in this Clause and are consistent with the NBCC provisions. This Clause also contains the design and detailing requirements such that the structure will perform at a level consistent with the R_d and R_o selected for the calculation of seismic loads.

The standard states that the diaphragms and the collector elements should be capable of transferring the loads developed at each floor to the vertical seismic resisting system. It provides an upper limit for the design force on diaphragms and other elements of the SFRS corresponding to the base shear calculated using $R_dR_o = 1.3$, as permitted in the 2010 NBCC. However, as per Clause 27.11 of CSA S16, it is also permitted that the diaphragms of conventional construction (Type CC) category buildings be designed for seismic forces corresponding to $R_dR_o = 1.5 \times 1.3 = 1.95$, provided that the diaphragm and its connections exhibit a ductile mode of failure. In the Commentary to CSA S16 (CISC, 2010), it is mentioned that recent tests have shown that diaphragms made of thin steel deck sheets (0.76 and 0.91 mm thick) with power-actuated frame fasteners and screwed side-laps can accommodate some inelastic deformations under cyclic loading, whereas other diaphragm designs such as those constructed with welded frame connections and button punched side-laps have not shown adequate ductile behaviour.

1.5.3   Diaphragm design guidelines

1.5.3.1 General

Cold-formed steel deck panels are used primarily to carry the roof or floor gravity loads. The steel deck is usually considered as a continuous beam member spanning between the joists and designed for bending, web crippling and deflection using CSA S136 (2007).

These panels when integrally connected to the underlying framework and to one another also act as a diaphragm (Luttrell, 1981, 2004). Steel roof deck diaphragms are capable of transferring the lateral loads induced by seismic or wind loads to the vertical bracing system. The diaphragm design methods commonly available are: a) Steel Deck Institute (SDI) method (Luttrell, 2004), b) Tri Services method (1973, 1982) and c) Stressed skin method (Davies and Bryan, 1982). Among these methods, the SDI method and the Tri Services method are more common in North America. A continued review and comparison of these design methods is presented in a Sheet Steel Fact published by the Canadian Sheet Steel Building Institute (CSSBI) (2007).

1.5.3.2 Steel Deck Institute (SDI) Design Method

The Steel Deck Institute (SDI) design method (Luttrell, 1981, 2004) is based on numerous tests and analyses of steel deck diaphragms carried out at the University of West Virginia since 1965. The design recommendations are compiled in the SDI manual, and are applicable to steel decks of thickness 0.36 mm to 1.63 mm and depths ranging from 14.3 mm to 76.2 mm, which cover the steel deck profiles commonly found in North America. The design method assumes the diaphragm to act as a simply supported deep beam spanning horizontally between the vertical bracing elements of the building; equations are provided to determine the in-plane shear strength and shear stiffness. The shear strength and shear stiffness depend heavily on the strength and flexibility of the connections. The shear strength and shear stiffness values for various types of side-lap connections and frame fasteners are given in the SDI manual (Luttrell, 2004). Information on the inelastic cyclic response and the ultimate capacity of various types of side-lap connections and frame fasteners can also be found in the work of Rogers and Tremblay (2000, 2003a, 2003b).

The SDI method provides three basic equations to determine the nominal shear strength of diaphragms, among which the lowest governs the strength. These equations represent the following failure mechanisms:

a) Shear strength of connections
b) Localised panel buckling at corner connections
c) Overall shear buckling of the diaphragm

Strength calculations also account for the combined action of shear forces acting along both orthogonal directions for the corner fasteners. This method also provides an expression for the determination of the in-plane shear stiffness (G') of the steel roof deck diaphragm (Equation 1.3). The method accounts for the influence of shear deformation and warping of the steel deck as well as connection flexibility on the diaphragm shear stiffness.

$$G' = \frac{Et}{2(1 + \mu)\left(\frac{s}{d}\right) + \rho D_N + C} \qquad 1.3$$

Where,

$E =$ Young's Modulus of elasticity

$t =$ Thickness of steel deck

$\mu =$ Poisson's ratio

$d =$ Panel corrugation pitch

$s =$ Flute length developed per panel pitch d

$\rho =$ Parameter to account for the number of spans within the deck sheet length

$D_N =$ Warping coefficient

$C =$ Slip coefficient

1.5.3.3 Tri Services Design Method

The Tri Service (1973) method was originally developed for the design of buildings for the U.S. Army, Navy and Air Force. The Canadian Sheet Steel Building Institute guideline (2006) includes both the SDI method (Luttrell, 1981, 2004) and the Tri Services method for the design of steel deck diaphragms in Canada. Each method is based on the assumption that the diaphragm acts as a deep horizontal beam; the determination of shear strength and stiffness is independent of the orientation of the steel deck panels. The Tri Services method is more empirical in nature compared with the SDI method and applicable only to diaphragms with arc-spot welded frame fasteners and button punch or seam weld side-lap connections.

The Tri Services method accounts for the theoretical flat plate shear deformation, the number of spans for a single deck and sheet distortion as well as fastener deformation for the determination of diaphragm flexibility. For the determination of shear strength, this method accounts for the elastic shear buckling resistance and the connection failure of diaphragms. It is noted that more recent guidelines for the seismic design of buildings for the U.S. Army, Navy and Air Force (e.g., USACE, 1998) now recommend the use of the SDI method for the design of steel roof deck diaphragms.

1.5.3.4 Stressed skin method

The stressed skin design method was developed by Davies and Bryan (1982) and documented in their book called "Manual of Stress Skin Diaphragm Design". This is the European recommendation for the design of steel deck diaphragms, which can also be considered applicable for use in North America. In this method the shear strength is determined based on the least of the following resistances: seam failure, sheet or shear connector failure, overall shear buckling failure, sheet or purlin fastener failure, and compression failure in the edge member. Determination of the diaphragm flexibility includes the effects of: the sheet profile distortion, axial strain in the edge member as well as shear strain and fastener stiffness. This method is very comprehensive in nature and accounts for the orientation of deck sheets with respect to the direction of loading. Further detail about the method can be found in a paper by Davies (2006).

1.5.4 Analytical and experimental study of low rise buildings

1.5.4.1 Naman and Goodno (1986)

Naman and Goodno (1996) performed a detailed seismic evaluation of a two storey steel office building located in Atlanta, Georgia which was designed for gravity and wind loads only. The dynamic properties of the building were estimated using a three dimensional computer model. Particular attention was made to observe the effects of diaphragm flexibility and accidental torsion on the response of the building. The roof diaphragm thickness was varied in the two models to study the effects of diaphragm flexibility. The effective thickness of the diaphragm was used in the first model, which was determined by dividing the diaphragm shear stiffness with the shear modulus of steel. In the second model, actual steel thickness was used to study the influence of diaphragm flexibility on the dynamic response of the building. It was observed that using the effective roof thickness in the first model resulted in a flexible modal distortion in contrast to the rigid diaphragm behaviour of the second model.

1.5.4.2 Tremblay and Stiemer (1996)

Tremblay and Stiemer (1996) examined the non-linear response of 36 uniform rectangular single-storey steel buildings having flexible steel roof diaphragms located in various cities across Canada. The computer program DRAIN-2DX (Allahabadi and Powell, 1988) was used to model the dynamic properties of the structures. The structures studied were found to respond mainly in their first mode (in-plane deformation of diaphragm) which implies that the fundamental period of vibration is a representative seismic design parameter for uniform rectangular single-storey steel buildings with a flexible roof diaphragm. In addition, due to the flexibility of the roof diaphragms, fundamental periods estimated from the analysis were found to be significantly longer than the values given by the 1990 NBCC (NRCC, 1990). The ratio between the computed period and the design period was found to be in the range of 1.35 to 6.52 for the buildings studied. When compared to the building model with a rigid diaphragm, the periods were observed approximately 1.5 times longer in the shorter direction (loads parallel to long direction) and in the range of 2 to 3 times longer in the other direction. Further, dynamically induced deformations of the roof exceeded the static values by a factor equal to 2.3 and the in-plane shear

force profile along the diaphragm span was found to exceed the values predicted by the straight line variation assumed in static analysis. The study also examined an approach, generally used in design, for predicting the inelastic drift by multiplying the total elastic drift by the seismic force modification factor R and proposed to amplify only the inelastic action that will take place in the vertical bracing bents.

1.5.4.3 Medhekar (1997) and Medhekar and Kennedy (1999)

Medhekar (1997) and Medhekar and Kennedy (1999) evaluated the seismic performance of uniform rectangular single-storey steel buildings having flexible roof diaphragms and concentrically braced frames (CBFs). Five seismic zones in Western Canada were considered for the study. The buildings were designed in accordance with the 1995 NBCC (NRCC, 1995) and CSA S16.1 94 (CSA, 94). The analytical study found that the fundamental period of the low-rise buildings predicted analytically was significantly longer than the period estimates from the NBCC. Further, it was found that the existing code did not ensure that yielding would be restricted to the vertical bracing elements. In moderate to high seismic zones yielding was also found in the roof diaphragms. Dynamic amplification of diaphragm in-plane deformations and shear force demand was also observed in the analyses. An expression was proposed for the distribution of the shear forces along the diaphragm span. Ambient vibration tests on a single-storey steel building were also carried out. The mode shapes from the tests provided evidence that the roof diaphragm behaved in a flexible manner. In addition, the study also examined two approaches for predicting the inelastic drift of buildings which were; 1) by multiplying the total elastic drift with the seismic force modification factor R and 2) an approach proposed by Tremblay and Stiemer (1996). A reasonable estimate of the inelastic drift was found with both of the approaches.

Moreover, analytical expressions to calculate the fundamental frequency of a rectangular diaphragm (Equation 1.5) and fundamental period of rectangular single-storey steel buildings (Equation 1.10) were also developed. In these expression K_d is diaphragm stiffness, ω_1 is the fundamental frequency of diaphragm, M_d is the mass of roof diaphragm, EI is the flexural stiffness of perimeter beams, $\overline{m}$ ($= M_d/L$) is the mass per unit length of the diaphragm, L is the

span of diaphragm, GA_s is the shear rigidity of perimeter beams, ω is the fundamental frequency of the building, K_f is lateral stiffness of the end wall (braced frame and cladding wall), M_f is the mass of the end walls, M is sum of M_f and M_d, and K_iL is the lateral stiffness of the interior walls.

$$K_d = \omega_1^2 M_d \qquad\qquad 1.4$$

$$\omega_1^2 = \frac{EI}{m} \frac{(\pi/L)^4}{1 + (EI/GA_s)(\pi/L)^2} \qquad\qquad 1.5$$

$$\alpha\lambda^2 + \beta\lambda + \gamma = 0 \qquad\qquad 1.6$$

Where $\lambda = \omega^2$ and the constants α, β and γ are

$$\alpha = M_f M_d \qquad\qquad 1.7$$

$$\beta = -(MK_d + M_d K_f + M_f K_i L) \qquad\qquad 1.8$$

$$\gamma = K_f K_d + K_i L(K_f + K_d) \qquad\qquad 1.9$$

The fundamental period of the building is:

$$T = 2\pi/\omega \qquad\qquad 1.10$$

When the mass and stiffness of the end walls and the lateral stiffness of the interior partition walls are small and can be neglected, the formula for the fundamental period can be simplified as (Tremblay et al. 2000):

$$T = 2\pi \sqrt{\frac{(K_B + K_D)}{K_B K_D} \frac{W}{g}} \qquad\qquad 1.11$$

In this Equation, K_D is the equivalent stiffness of the diaphragm (Equation 1.12), including in-plane flexural and shear deformations;

$$K_D = \frac{\pi^2}{\dfrac{L^3}{\pi^2 EI} + \dfrac{L}{G'b}} \qquad\qquad 1.12$$

The other parameters: K_B is the lateral stiffness of the vertical bracing system, g is the acceleration due to gravity, W is the total seismic weight, L and b are respectively the diaphragm span and depth, EI is the flexural stiffness of the diaphragm, and G' is the diaphragm shear stiffness. In this thesis, this simplified expression (Equation 1.11) is referred to as the Medhekar equation for the period.

1.5.4.4 Tremblay, Berair and Filiatrault (2000)

Tremblay et al. (2000) investigated the behaviour of low-rise steel buildings with flexible diaphragms by conducting shake table tests on a 1: 7.5 reduced scale building model. The tests validated the simplified analytical expression adapted from Medhekar to estimate the fundamental period of single-storey buildings. The tests also confirmed the dynamic amplification of drift compared with the static values as found in the analytical study by Tremblay and Stiemer (1996). Dynamic amplification of the shear forces in the diaphragm was also confirmed by the tests. The SDI method was found not applicable to the roof diaphragm assembly that was used in the study. It was noted that the measured shear stiffness of the roof diaphragm was considerably different than the SDI theoretical value. Furthermore, significant strain rate effects on the yield resistance of the bracing members were observed in the test. This effect would result in an increase in shear force on the roof diaphragm during strong ground shaking. The first mode damping ratio of the model was found to vary between 3.1% and 4.3%.

1.5.4.5 Tremblay and Rogers (2005)

Tremblay and Rogers (2005) investigated the impact of capacity design provisions and period limitations on the seismic design of low-rise steel buildings by examining several design strategies. The design strategies included: design without a capacity based approach, capacity design with ductile vertical bracing and capacity design considering the roof diaphragm as the ductile element in the SFRS. The effect of relaxing the period limitation as specified in the 2005 NBCC (NRCC, 2005) and the capacity forces on the roof diaphragm were also studied. Significant negative impacts on the cost of these buildings were observed with the use of the

capacity design approach, particularly when tension-compression bracing was used. The buildings designed without period limitation had a notably longer period of vibration than the code limitation; furthermore, the design of these buildings was not governed by the drift limitations due to the lower seismic design force associated with the longer period. Non-linear dynamic analysis for a typical single-storey steel building located in Vancouver was also performed using a numerical model wherein the diaphragm was modelled as a deep horizontal plane truss (Martin, 2002) using the Ruaumoko computer program (Carr, 2001). The resulting buildings obtained from the various design approaches were used to perform the non-linear analysis. A 1994 Northridge earthquake record scaled to match the design response spectrum for Vancouver was used to examine the response of the building. Recommendation was made for doing additional studies in this area to make final design recommendations.

1.5.4.6 Agüero et al. (2006)

Agüero et al. (2006) developed a concentrically braced frame model in the OpenSees software platform to simulate the hysteretic response of steel bracing members. Rectangular and square steel HSS bracing members were considered for the study. Non-linear beam-column elements with a fibre representation and with Giuffré-Menegotto-Pinto constitutive model (Steel02) were used for the bracing members. The initial out-of-plane imperfection at mid-length of the braces was considered in the analysis. Rotational zero length spring elements were also included in the model to account for the end restraint conditions induced by the gusset plates. Model predictions were compared with past individual and full-scale test results. The forced based elements model and displacement based elements models were also compared. The forced based formulation provided higher accuracy in comparison to the displacement based formulation. The influence of modeling parameters including number of integration points along the element length, number of elements along the brace length and number of fibres to define a cross section were also investigated in the study. The study found that sufficient accuracy could be obtained if 8 elements per brace length were used in the model together with 16 fibres for cross-section discretization. Jin J. and El-Tawil S. (2003) and Uriz P. (2005) also studied the behaviour of

concentric braced frame and proposed numerical models to predict inelastic response of the braced frame.

1.5.4.7 Tremblay et al. (2008a)

Tremblay et al. (2008a) carried out ambient vibration tests of a single-storey steel building located in Magog, Quebec to estimate the fundamental period of vibration in the two principal directions of the building. Analysis of the test data allowed for the calculation of periods of 0.39 seconds and 0.3 seconds and first model damping values of 3.4% and 2.5% in the two principal directions, respectively. A 3D elastic model in SAP (CSI, 2000) was then created in order to reproduce the field measurements. The SDI method (Luttrell, 2004) was used to determine the shear stiffness of the roof diaphragm which was modeled using shell elements. Initially, a general model was formulated using assumptions generally accepted by practicing engineers; i.e., all the frame members were assumed to be pin connected at their ends. The fundamental period of vibration using this formulation was found to be approximately three times longer (1.11 seconds, 1.00 seconds) than the field measurements. It was believed, however, that the reason for measuring the shorter periods in the tests was because of the excitation level of ambient vibration, which was not large enough to overcome the inherent friction present in the steel deck diaphragm connections and other connections in the structure. Hence, it was further believed that the apparent lateral stiffness of the building, measured by means of ambient vibration tests, would not exist in the event of anticipated design level earthquakes. Changes were made in the numerical model to simulate the field conditions gradually; by fixing all the members at their ends, by restraining side-lap and deck to frame connections of the roof diaphragm and by restraining end overlaps of the diaphragm to prevent warping of the steel deck. A better match of the period (0.34 seconds, 0.23 seconds) was found when all the assumed field conditions were considered in the numerical model.

1.5.4.8 Lamarche et al. (2004, 2009)

Work carried out by Lamarche et al. (2004, 2009) included ambient vibration tests on 22 buildings in Eastern and Western Canada. The building structures comprised steel roof deck diaphragms and vertical bracing systems, and varied in size, roof mass and location of vertical steel braces. The measured periods of the structures did not correlate well with the periods computed from the formula given in the 2010 NBCC (Eq. 1.2). The periods were found more closely correlated to the parameters D_{neff}, which is the maximum distance between vertical brace lines, and to the height of structure h_n. From the study, a simple expression accounting for these two parameters was formulated to calculate the fundamental period of vibration of single-storey steel buildings under low level of vibration.

1.5.4.9 Koboevic et al. (2011)

Koboevic et al. (2011) studied the seismic response of three and eight storey eccentrically braced frame (EBF) structures designed for western and eastern North American locations by carrying out dynamic non-linear time history analyses using three computer programs including the OpenSees software platform. The inelastic behaviour of the EBF link element was predicted using the Giuffré-Menegotto-Pinto (Steel02) hysteretic material. The parameters for the Steel02 material were determined from calibration with past test results of EBF specimens. Rotational zero length spring elements were also included at the brace ends to account for the end restraint conditions induced by the gusset plates. Realistic responses of the frame members, other than the link element, were also obtained by modeling them with eight non-linear beam-column elements together with 16 fibres for cross-section discretization. The study found a strong correlation between the plastic link rotations and the inter-storey drifts. The study also confirmed that the flexural yielding of outer beams is acceptable for EBFs with short and intermediate links under certain circumstances.

1.5.5 Dynamic tests of large scale diaphragms – Phase I, II and III

A three phase dynamic test program of large-scale steel deck diaphragms was conducted at Ecole Polytechnique, Montreal to examine their dynamic behaviour under higher level vibrations than those that would occur during ambient conditions. The main objectives of the experimental study were; firstly, determination of diaphragm stiffness under various dynamic loadings, consequently period of vibration of the diaphragms, and secondly, study of the ductile behaviour of diaphragms to estimate the ductility related seismic force reduction factors. The Phase I test program was completed in 2007 and Phase II and III were completed in 2009. The findings of the research works are presented in papers by Tremblay et al. (2008b), Shrestha (2009) and Franquet et al. (2010). More detailed information on the experimental works and results can be found in the recent Master's dissertations of Franquet (2010) and Massarelli (2010). Since these experimental works are one of the major parts of the study documented herein, they are presented in Chapter 2 separately. An experimental research study on the in-plane shear response of roof diaphragms under the monotonic and reversed cyclic loading was also carried out at the University of British Columbia by the Earthquake Engineering Research Facility (EERF) in 2008. Details of the test program can be found in the report by EERF (2008).

1.5.6 Past experimental investigation of steel roof diaphragms
1.5.6.1 Essa et al (2001)

Essa et al. (2001) investigated the inelastic behaviour of steel roof diaphragms by conducting monotonic and reversed cyclic loading tests on 18 6.1 m x 3.66 m cantilever diaphragm specimens. Steel deck of nominal depth 38 mm and thickness of 0.76 mm or 0.91 mm was used in a 36/4 pattern with 305 mm side-lap spacing. Nine combinations of deck-to-frame and deck-to-deck fasteners were tested in order to investigate the inelastic energy dissipation capacity. The experimental study found that; inelastic behaviour and ductility of the roof deck was dependent on the type of connection, strength degradation was observed and diaphragms with screw side lap and nail frame fasteners exhibited ductile behaviour. The strength degradation occurred due to the failures of side-lap and deck-to-frame connections. The failure of side-lap connections were characterized mainly by total separation of component sheets in button punched side-laps

and screws pulling out in the screwed side-laps. And, the failure of frame fasteners were characterized mainly by; tearing and separation of deck panels from the whole perimeter of weldment in welded fasteners and bearing failure of the deck panel against nails or screws. The degradation was significantly higher in the diaphragms with welded deck-to-frame fasteners. In order to maintain the shear strength of a diaphragm at greater than 80% of its ultimate capacity, the study recommended limiting the plastic shear deformation (γ_p) to 0.01 radian for the diaphragms with nail deck to frame fasteners and screw side-lap fasteners. The plastic shear deformation γ_p was defined as shown in Figure 1.3.
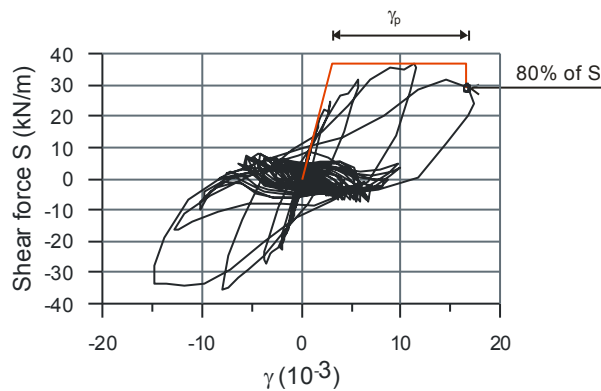
Figure 1.3 Typical measured hysteretic shear response of diaphragm and definition of γ_p

1.5.6.2 Martin (2002)

Martin (2002) studied the inelastic response of steel roof deck diaphragms under simulated seismic loadings. Non-linear time history dynamic analyses were carried out to determine the seismic demand on three different buildings located in Victoria, British Colombia, and Quebec City, Quebec. Based on the analyses, loading protocols were developed to simulate the expected inelastic behaviour of the roof diaphragms. Inelastic tests, subjected to the simulated seismic loading protocol, were performed on 19 diaphragm test specimens using a similar test setup to Essa et al. (2001). A numerical model was also developed to predict the seismic response of single-storey steel buildings using the RUAUMOKO (Carr 2004) computer program (Martin, 2002; Rogers et al., 2004). The roof diaphragm was modeled as a deep horizontal plane truss. A Stewart hysteretic model (Stewart, 1987) was selected for the diagonal truss members to reproduce the cyclic inelastic response measured for the screwed-nailed diaphragm system. It

was noted that the diaphragm could perform in the inelastic deformation range; the inelastic demand, however, may concentrate at the edge of a roof diaphragm leading to undesirable failure. The software and the hysteretic model, however, did not allow for simulation of the shear strength degradation which was observed in the testing of diaphragm specimens. Martin found that the inelastic behaviour was dependent on the type of connections, and that the screw and nail connection configuration provided satisfactory ductile performance. The study recommended using R_d of 2.0 and R_o of 1.67 for nail screw diaphragms when assumed to act as the fuse element in the SFRS.

1.5.6.3 Yang (2003)

Twelve steel roof diaphragm specimens were tested using a similar test setup to Essa et al. (2001) to examine their inelastic behaviour and the influence of non-structural components and end overlaps. A significant increase in strength and stiffness of the diaphragm was observed when the non-structural components were added to a bare steel roof diaphragm in the test. Further, the use of shorter deck length along with the longitudinal overlap between panels significantly decreases the stiffness of the diaphragm compared to the diaphragm without the longitudinal overlap. Non linear dynamic analyses of single-storey steel buildings was also carried out; it was found that the nail and screw connected diaphragms could be used as an energy dissipating element. The study also recommended using R_d of 2.0 and R_o of 1.67 for nail screw diaphragms when assumed to act as the fuse element in the SFRS. The torsional effect was found to be lower when the flexibility of the diaphragm was considered in the building analysis. Further, the study also found the importance of including the shear and bending flexibility of the diaphragm in the analysis to calculate storey drifts and inelastic demand on the vertical bracing because the inelastic demand on the vertical braces was found to be higher when a flexible diaphragm was considered for design.

1.5.6.4 Avci et al. (2004)

Avci et al. (2004) conducted five full-scale cantilever static tests on diaphragm specimens having aluminum panels to evaluate their strength and stiffness. The side laps and the deck to frame connections were made using screws. The SDI method was used to determine the shear strength and stiffness, which were then compared with the measured values from the test specimens. The material properties as well as connection properties of aluminum panels were used in the SDI strength and stiffness calculations. The study found a good match between the test values of diaphragm strength and the strength calculated using the SDI method. A modification factor K = 2/3 was proposed for the SDI stiffness to match with the experimental diaphragm stiffness.

1.5.6.5 Mastrogiuseppe (2006) and Mastrogiuseppe et al. (2008)

The effect of non-structural components on the shear stiffness of steel roof diaphragms was also investigated experimentally by Mastrogiuseppe, (Mastrogiuseppe, 2006, Mastrogiuseppe *et al.*, 2008). The effects of non-structural components were found mainly dependent on the steel deck thickness as well as the connection pattern. Higher effects were found in the thinner deck diaphragms having fewer connections. However, a complementary study involving the linear elastic analysis of buildings found that the effects of these non-structural components are not significant enough to change the fundamental period of vibration of the structure (Mastrogiuseppe et al. 2008). Large-scale diaphragm tests (Franquet, 2010) recently demonstrated that the stiffening effects of the non-structural components may not exist in the case of loading that brings the diaphragm to the factored shear resistance level and into the inelastic range of behaviour.

1.5.6.6 Engleder and Gould (2010)

Engleder and Gould carried out static and dynamic testing on cantilever steel roof deck diaphragm specimens to examine their seismic performance at Hilti headquarters in Schaan. The diaphragm specimens consisted of 0.76mm, 0.91mm and 1.21mm thick steel deck placed over a

9.14m by 7.32 m test frame. The fastener patterns were also varied from test to test. The mechanical fasteners (screws and nails) were used for side laps and deck to frame connections. A reversed cyclic loading protocol developed by Tremblay et al. (2004) was used to push the diaphragm specimens into the inelastic range. The tests found that the response from the simulated seismic loading tracked the static reference curve well. The static tests as well as dynamic tests on the diaphragm specimens of different thickness and fastener patterns confirmed the ductile behaviour of such constructions. Diaphragm ductility was provided by the sheet bearing failure and tilting of the screws at side-laps as well as sheet slotting failure at the deck to frame connections. For the specimens with thicker (1.21 mm) steel, the powder-actuated deck-to-frame fasteners at the end lap connection lost anchorage capacity and could be manually removed after the test.

1.5.7 Literature review - Conclusion

Tremblay and Rogers (2005) investigated the impact of capacity design provisions and period limitations on the seismic design of low-rise steel buildings by examining several design strategies. The study observed significant negative impacts on the cost of these buildings with the use of the current capacity design approach. Among the various design strategies studied, weak-diaphragm design without period limitation, i.e., capacity design considering the roof diaphragm as the ductile element in the SFRS and without limiting the period of vibration, gave the most economical design. The study recommended however not to use the full period relaxations or weak-diaphragm design until adequate information is available. This clearly reveals the need of further study on the use of flexibility and ductility in the design of low rise buildings.

Inelastic cyclic loading tests on cantilever diaphragm specimens (Essa et al. 2003; Tremblay et al 2004; Engleder and Gould 2010) and the recent dynamic tests on simply supported large-scale diaphragm assemblies (Tremblay et al. 2008b, 2011; Massarelli et al. 2011) showed that metal roof deck diaphragms may exhibit inelastic deformation capacity. To use the ductility of the diaphragm in design, one would have to establish the ductility related seismic force modification factor R_d by evaluating the performance of buildings through non-linear dynamic analysis. This

requires an accurate non-linear model capable of predicting the complex inelastic behaviour of the diaphragm. Limited study has been previously attempted on the development of a non-linear steel roof diaphragm model. Martin (2002), Tremblay and Rogers (2005) and Tremblay et al. (2008b) developed a non-linear steel roof diaphragm model to study its elastic and inelastic response in the Ruaumoko software (Carr 2004). A Stewart (Stewart 1987) hysteretic element with stiffness degradation and pinching characteristics was used in the model to mimic the shear response of the deck. These initial models were, however, not capable of simulating the strength degradation that was observed during testing. It is believed that pinching characteristic, stiffness degradation as well as strength degradation can significantly influence the distribution and amplitude of inelastic demand in a large roof diaphragms and it is therefore necessary to develop a non-linear model that includes these characteristics to accurately predict the inelastic response and collapse behaviour of these building structures.

The 2010 NBCC does not explicitly allow for yielding of the diaphragms or their connections. However, it relies on a certain level of yielding when the diaphragm is designed and detailed according to the applicable reference design standards to exhibit ductile behaviour. In that case, the diaphragm design can be done with reduced seismic design loads corresponding to the base shear calculated using $R_dR_o = 2.0$. This relaxation is recognized in CSA S16-09 as this design strategy is permitted for Type CC SFRSs that are designed with $R_dR_o = 1.95$. These diaphragms are then expected to experience inelastic response under strong ground motion. The seismic performance of structures so-designed has not been examined in past studies and there is a need to validate this design approach as it is currently allowed in codes. In particular, capacity design principles need not be applied for Type CC SFRSs, which means that the inelastic demand can develop in the diaphragm, the vertical bracing or both, depending on the relative strength and inelastic response of these elements. Further, the failure modes of this type of structure under large earthquake ground motions are still not well understood. The seismic response of a Type CC structure designed according to current codes is therefore examined later in this thesis.

The design approach for Type CC structures is rather simple as capacity design rules need not apply. However, this may lead to ineffective design solutions as would be the case if yielding concentrates in the vertical bracing: the ductility detailing provided for the roof diaphragm, as required by CSA S16, will be not be mobilized and would be useless. A more rational design

method where capacity design principles are enforced to ensure that the diaphragm forms the energy dissipative element and the vertical bracing elements are sized to remain essentially elastic may represent a more effective solution, as was pointed out by Rogers and Tremblay (2005). The performance of this design approach with intended inelastic diaphragm response is also examined in this thesis with proper consideration of diaphragm inelastic response in the model. For these two first cases, the vertical bracing consists of concentrically braced frames (CBFs).

As a basis of comparison, the response of ductile steel SFRSs designed in accordance with the seismic provisions specified in CSA S16-09 standard are also studied. Two systems will be examined: Type MD (moderately ductile) steel concentrically braced steel frames (CBFs) designed with $R_dR_o = 3.9$ and Type D (ductile) steel eccentrically braced frames (EBFs) designed with $R_dR_o = 6.0$. As described earlier, these structures are designed so that yielding develops in the framing members and the diaphragm responds elastically. However, the design procedure was slightly modified compared to current code requirements: an upper limit corresponding to $R_dR_o = 2.0$ was used for the design of the diaphragms, i.e., a lower limit compared to the upper limit corresponding to $R_dR_o = 1.3$ that is currently specified in CSA S16-09. This modification would be applicable to diaphragms detailed to exhibit ductility, so as to comply with NBCC requirements. This is to achieve uniformity in design forces for ductile diaphragms when used in Type D, MD (or LD) systems when compared with Type CC SFRSs. Examination of the performance of these buildings will permit to determine whether this is an acceptable approach for future code editions.

Study on the response of buildings that are designed with and without the use of period relaxation is also lacking. The influence of the design period is therefore also examined in this thesis for the building cases studied. Also, the stiffness of the diaphragm could have significant influence on the ductility demand of the SFRS and thus on the non linear behaviour of the buildings, which will be incorporated in the study.

Non-linear models of CBFs have been proposed by Jin and El-Tawil (2003) and Uriz (2005). Further, non-linear models have been recently developed in the OpenSees platform to accurately reproduce the inelastic response of bracing members of CBFs (Agüero et al., 2006) and link

beams of EBFs (Koboevic et al., 2011). A non-linear roof diaphragm model could also be developed in the OpenSees platform which then could be integrated with these numerical brace models to study the overall inelastic behaviour of such single-storey steel buildings.

Chapter 2 - Numerical modeling of roof diaphragm test specimens

2.1 General

One of the primary objectives of this study was to develop a numerical model of a steel roof deck diaphragm; to calibrate it with test data, and then to integrate the numerical diaphragm model with a building model for a single-storey building. This numerical model would then be used to evaluate the inelastic behaviour of representative buildings when subjected to design level ground motions. This chapter describes the numerical modeling phase of this research in which a diaphragm model, that reproduces the degradation of shear stiffness and strength under cyclic loading in the inelastic range, was developed and validated against the Phase I through III dynamic diaphragm test (Franquet 2010, and Massarelli 2010) results. Evaluation of the model is discussed by comparing the numerical predictions of stiffness, period of vibration, displacement time history response, hysteretic response, deformation profile and shear force distribution along the length of diaphragm to the test results. Values of the parameters required for the material model are proposed for different diaphragm designs. The accuracy of this model is then validated by means of a blind comparison with the results obtained from reversed cyclic uniform shear tests performed on small-scale cantilever diaphragm specimens by Essa et al. (2001, 2003) and Martin (2002).

2.2 Large-scale roof diaphragm test

Nineteen large-scale roof diaphragm specimens were tested in a three phase program using a rectangular (7.31 m x 21.02 m) test frame on which steel deck was laid (Figure 2.1). The diaphragm test specimens were assembled of components commonly found in the roofs of single-storey steel buildings. They comprised of the typical North American 38 mm deep x 914 mm wide x 0.76 mm, 0.91 mm or 1.21 mm thick deck panels (F_y = 230 MPa, F_u =310 MPa) connected using standard fastener patterns (Table 2.1). The P-3615 Canam deck panels were used for the diaphragms with weld and button punch connections whereas P-3606 Canam deck

panels were used for the diaphragm specimens with nail or weld frame fasteners and screw side lap fasteners. Note, that these two profiles are consistent with other deck manufacturers such as

a)
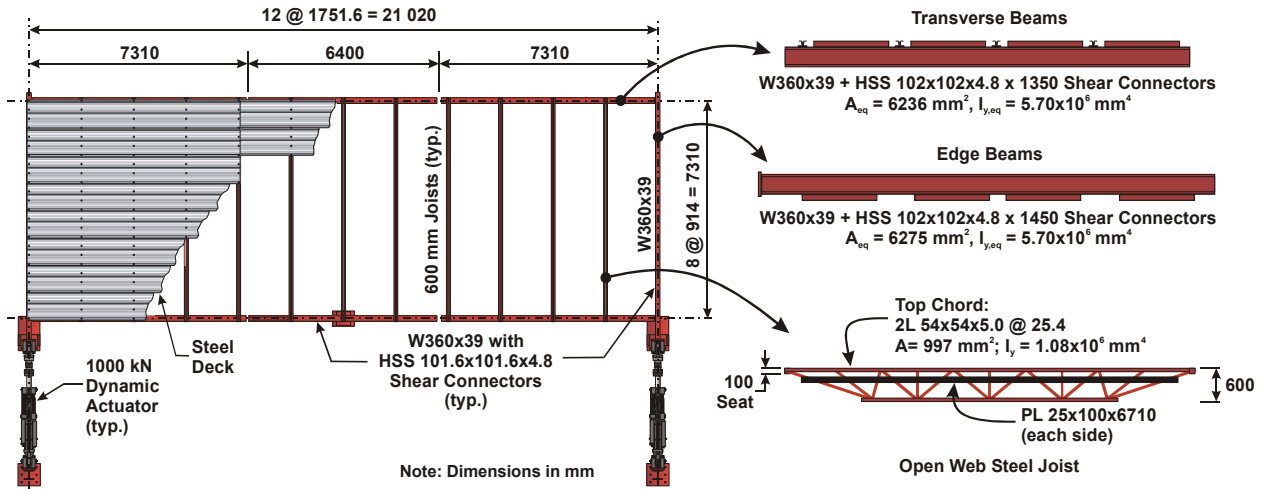
b)

Figure 2.1 – Test setup (Layout I): a) Plan view and detail of the perimeter beams and steel joists; b) Photos during assembly and after installation of the deck, instrumentation and additional steel bars.

Table 2.1 – Test matrix and SDI strength and stiffness prediction

Phase / Layout	Test. Spec. No.	Sheet t (mm)	Frame fasteners	Fastener pattern	End overlap	Sidelap Fastener	Sidelap spacing (mm)	SDI Prediction G' (kN/mm)	Sn (kN/m)	Inelastic Loading Signals Signal	Freq (Hz)
I/I	1	0.76	Nails	36/4	36/4	Screws	152	4.2	13	0.80SS2	4
	1R	0.76	Nails	36/4	36/4	Screws	153	4.2	13	0.80SS2	4
	2	0.76	Nails	36/4	no overlap	Screws	154	4.2	13	0.80SS2	4
II/I	3	0.76	Nails	36/4	36/7	Screws	152	16.8	23.5	20SS3	N/A
	3R	0.76	Nails	36/7	36/7	Screws	152	17.0	24.4	20SS3	N/A
	4	0.76	Nails	36/7	36/7	Screws	152	17.0	24.4	0.80SS2	4
	4R	0.76	Nails	36/9	36/9	Screws	152	17.4	29.2	0.80SS2	5
	5	0.76	Nails	36/9	36/9	Screws	152	17.4	29.2	0.80SS2	5
	5R	0.76	Nails	36/9	36/9	Screws	102	18.3	35.3	0.92SS2	5
	6	0.76	Nails	36/11	36/11	Screws	152	17.6	31.8	0.92SS2	5
	6R	0.76	Nails	36/11	36/11	Screws	102	18.5	38.6	0.92SS2	5
	7	0.91	Nails	36/7	36/7	Screws	152	21.8	29.2	0.80SS2	5
	7R	0.91	Nails	36/9	36/9	Screws	152	22.4	34.9	0.80SS2	5
	8	0.91	Nails	36/9	36/9	Screws	152	22.4	34.9	0.80SS2	5
	8R	0.91	Nails	36/9	36/9	Screws	102	23.9	42.2	0.80SS2	5
	9	0.91	Nails	36/11	36/11	Screws	152	22.8	38.0	0.80SS2	5
	9R	0.91	Nails	36/11	36/11	Screws	102	24.1	46.1	0.80SS2	5
	10	0.76	16 mm welds	36/4	36/4	B-P	305	3.6	8.5	0.80SS2	4
	10R	1.76	Nails	36/4	36/4	Screws	305	4.2	14.1	0.80SS2	4
III/I	11*	0.76	16 mm welds	36/4	36/4	B-P	305	16.3	24.5	0.80SS2	5
	12	1.21	Nails	36/7	36/7	Screws	152	31.1	38.6	0.92SS2	5
	12R	1.21	Nails	36/7	36/7	Screws	152	31.1	38.6	0.92SS2	5
	13	1.21	19 mm welds	36/7	36/7	Screws	152	31.3	44.7	0.92SS2	5
	13R	1.21	Nails	36/7	36/7	Screws	152	31.1	38.6	0.92SS2	5.25
	14	1.21	Nails	36/9	36/9	Screws	102	34.8	55.7	0.92SS2	5.25
III/II	15	0.76	16 mm welds	36/4	36/4	B-P	305	3.6	8.1	0.80SS2	4
	15R	0.76	Nails	36/4	36/4	Screws	305	4.3	12.6	0.80SS2	5
	16	0.76	Nails	36/7	36/7	Screws	152	17.1	23.6	0.80SS2	4
	16R	0.76	Nails	36/9	36/9	Screws	152	17.5	28.2	0.80SS2	5
	17	0.91	Nails	36/7	36/7	Screws	152	21.9	28.2	0.80SS2	5
	17R	0.91	Nails	36/9	36/9	Screws	152	22.5	33.7	0.80SS2	5
	18**	0.91	Nails	36/7	36/7	Screws	Tailored	23.6	34.8	0.92SS2	5
	18R	0.91	Nails	36/7	36/7	Screws	102	23.6	34.8	0.92SS2	5
	19	1.21	19 mm welds	36/7	36/7	Screws	152	31.1	43.1	0.92SS2	5
	19R	1.21	Nails	36/7	36/7	Screws	152	30.9	37.3	0.92SS2	5

R-Repaired, * Retrofitted with screw side lap and nail frame fasteners, ** Designed as per demand

VicWest, Agway Metals, Ideal Roofing, and Westform Metals. The deck panels were connected to the top chord of steel joists and to the HSS shear connectors using Hilti X-EDNK22 powder driven fasteners and to the top flanges of beams using Hilti X-EDN19 fasteners; arc-spot welds were also used for some test specimens. Hilti S-MD 12-14x1 self drilling screws with 102 mm and 152 mm spacing or button punches with 305mm spacing were used for side-lap connections. Two identical high performance 1000 kN actuators acting in phase were used to apply the dynamic excitation. Inertia forces were induced along the span of the diaphragm due to the mass of the steel deck-frame assembly, steel bars on the top of the diaphragm and steel plates welded to the web members of the steel joists. Two panel orientations were used to examine the influence of having the side-laps perpendicular or parallel to the direction of seismic loading. In one of the tests (Specimen 18), the connection pattern was tailored to follow the expected shear demand under the loading.

The tests were performed at various amplitudes of loading: low amplitude vibration to measure the dynamic properties of the specimens, variable amplitude excitation up to yielding to evaluate the change in dynamic properties, and extreme earthquake excitation (signal SS1, SS2 and SS3) to examine the change from elastic to inelastic response (Table 2.1). The SS1 signal was an acceleration record from the 1989 Loma Prieta earthquake (Stanford Univ. 360°) having a time scale factor of 1/3 with a peak value of 0.29 g and duration of 10 seconds. The SS2 signal was a sinusoidal harmonic signal with a peak displacement of 30 mm and total duration of 10 s (Figure 2.6). The frequency and the amplitude of the loading signal SS2 were varied in the final non-linear tests to push the diaphragms into the inelastic range (Table 2.1). The SS3 signal was an acceleration record from the Northridge Earthquake (Big Tujunga, 352°) having a time scale factor of 1/2.5 with a peak value of 0.245 g and a duration of 12 seconds. The earthquake signals were mainly used for elastic tests except for specimen 3 and specimen 3R in which the amplified (20 times) SS3 signal was used to push the diaphragm into the inelastic range. Additional information on the test program can be found in the two companion papers (Tremblay et al., 2011; Massarelli et al., 2011). A detailed description of this dynamic diaphragm test program is presented in the work of Franquet (2010) and Massarelli (2010).

2.3 Cantilever cyclic quasi-static shear tests

Essa et al. (2001, 2003) and Martin (2002) tested a series of full-scale cantilever steel roof diaphragm specimens (3.658 m by 6.096 m) under monotonic and reversed cyclic loading signals to investigate their ductile behaviour (Figure 2.2). It was concluded that the diaphragms with screwed side-laps and either nailed or welded-with-washer frame fasteners showed ductile performance over other connection patterns. In all the tests carried out by Essa et al. alternate flutes of deck sheets were connected to the underlying frame (36/4 pattern). The test setup used by Martin (2002) was similar to that used by Essa et al. (2001). Diaphragm tests 28 and 31 comprised of nail frame fasteners and screw side-lap connectors with 0.76 mm thick roof deck panels. A short duration displacement based loading protocol, which was devised from the non-linear analyses of representative buildings, was used for both tests. Test 35 was also constructed with nail frame fasteners and screw side-lap connections except that 0.91 mm thick deck panels were used and the long duration loading protocol was applied for testing. Test 36 had weld frame-to-deck and button punch side-lap connections with 0.76 mm deck sheets; it was subjected to the short duration loading protocol. Note; both the short and long duration protocols were not symmetric (Martin, 2002).The Steel Deck Institute (SDI) method (1987) was used to determine the shear strength and stiffness of the diaphragm assemblies. The comparison of measured stiffness and strength of diaphragm specimens to the SDI prediction is discussed in Section 2.4.4.
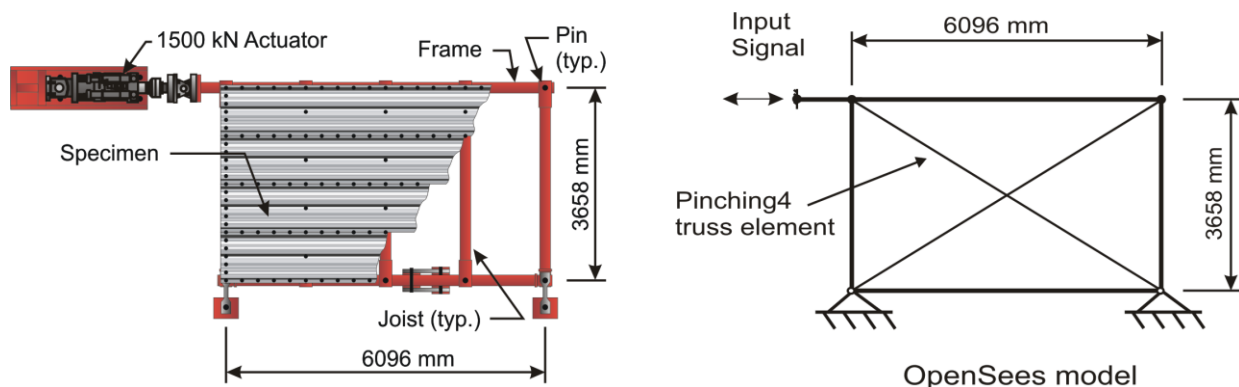
Figure 2.2 – Cantilever test setup (Essa et al., 2001) and OpenSees model

2.4 Numerical Simulation

2.4.1. Development and calibration of the numerical models

A deep horizontal plane truss model representing half of the specimen length was developed using the OpenSees software platform (McKenna 1997, Mazzoni et al. 2009) to predict the elastic and inelastic dynamic responses of the steel deck diaphragm test specimens (Figure 2.3a). The model is similar to that used by Tremblay and Rogers (2005) and, more recently, by Tremblay et al. (2008b) in studies of inelastic diaphragm response. In this previous work, the Ruaumoko software (Carr 2004) was used and a Stewart (1987) hysteretic element with stiffness degradation and pinching characteristics was selected for the diagonal roof truss members to mimic the shear response of the deck. These initial models were, however, not capable of simulating the strength degradation that was observed during testing. In the study described herein the Pinching4 hysteretic uniaxial material model originally developed by Lowes et al. (2004) and available in OpenSees was selected for the diagonal truss elements (Figure 2.3b). It represents a 'pinched' load-deformation or stress strain response and exhibits stiffness as well as strength degradation under reversed cyclic loading. Calibration of the Pinching4 material model requires: 8 stress strain points to define positive and negative response envelopes, 6 parameters to define unload and reload paths, 15 parameters to define the stiffness and strength degradation, one energy dissipation parameter, and a damage type. The perimeter beams and joist top chords are modeled with elastic beam-column elements. The weak axis moment of inertia is used for the beam-column elements in the model so as to give in-plane flexibility to the diaphragm. Elastic truss elements parallel to the deck sheets are also introduced to account for the in-plane axial stiffness of the deck sheets (developed width).

The relationship between the axial stiffness of the diagonal truss element and the shear stiffness of the roof diaphragm (Figure 2.3a), shown in Equation 2.3, can be obtained with the use of Equation 2.1 and 2.2. Equation 2.1 shows relation between shear stiffness of diaphragm G' and lateral stiffness of 914 mm × 875.8 mm truss model, k_{Lat} (Figure 2.3a). Equation 2.2 shows the relationship between the lateral stiffness of truss model, k_{Lat}, and axial stiffness of the diagonal truss member, k. The relation between the ultimate strength of the diagonal truss element, σ_{Ult}, and shear strength of roof diaphragm, S_u, is shown in Equation 2.4.

$$G' = \frac{S}{\gamma} = \frac{F}{914} \times \frac{875.8}{\Delta} = \frac{k_{Lat} \times 875.8}{914} \qquad \text{2.1}$$

$$k_{Lat} = 2 \times \frac{AE}{L} \times Cos^2\theta = 2 \times k \times Cos^2\theta \qquad \text{2.2}$$

$$k = \frac{G' \times 914}{2 \times 875.8 \times Cos^2\theta} \qquad \text{2.3}$$

$$\sigma_{Ult} = \frac{P}{A} = \frac{S_U \times 914}{A \times 2Cos\theta \times 1000} \qquad \text{2.4}$$

The response obtained for each side of the specimen was assumed to be symmetric; for this reason only half of the test diaphragm was included for modeling purposes (Figure 2.3a). The inelastic shear deformations measured in tests were found higher near the support of diaphragms except for Specimen 18. Hence, this end shear response (measured over the 1752 mm joist spacing length) was used to obtain the response envelope curve. Initially, an analytical expression as shown in Figure 2.3 (c) (Medhekar 1997, Tremblay et al. 2008b) was used to estimate the shear stiffness of the diaphragm specimens to obtain the response envelope. In this expression, K_D is the equivalent stiffness of the diaphragm, including in-plane flexural and shear deformations, g is the acceleration due to gravity, L and b are respectively the diaphragm span and depth, EI is the flexural stiffness of the diaphragm, W is the total seismic weight, and G' is the diaphragm shear stiffness. The analytically computed G' was then used to calculate the area of the diagonal elements and the corresponding axial stress following the shear representation (Equation 2.3) of the truss element as shown in Figure 2.3a. The ultimate axial strength of the diagonal elements is projected from the measured shear strength per unit length (S_u) of the diaphragm (Equation 2.4). A measured typical end shear response is shown in Figure 2.4a. Figure 2.4b shows a typical axial stress vs. axial strain response obtained for a diagonal truss element projected from Figure 2.4a. The stress strain peak points of the Pinching4 material were estimated for all the tests as shown in Figure 2.4b to obtain response envelopes, which were averaged and grouped according to steel thickness of deck sheets used in the test specimens. This

34

approach was followed even though it is conservative to some extent as stated in FEMA P-440A (2009) since the average stress strain input parameters used in the model are loading history dependent.
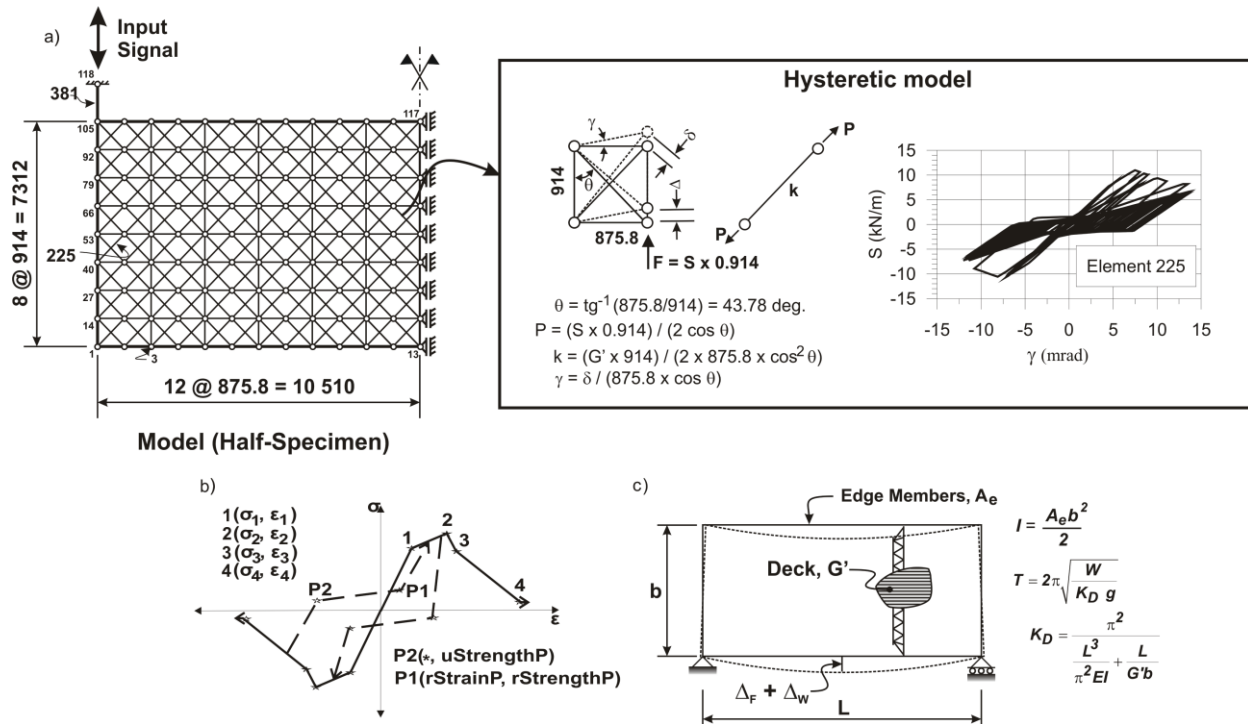
Figure 2.3 – Non-linear diaphragm truss model in OpenSees
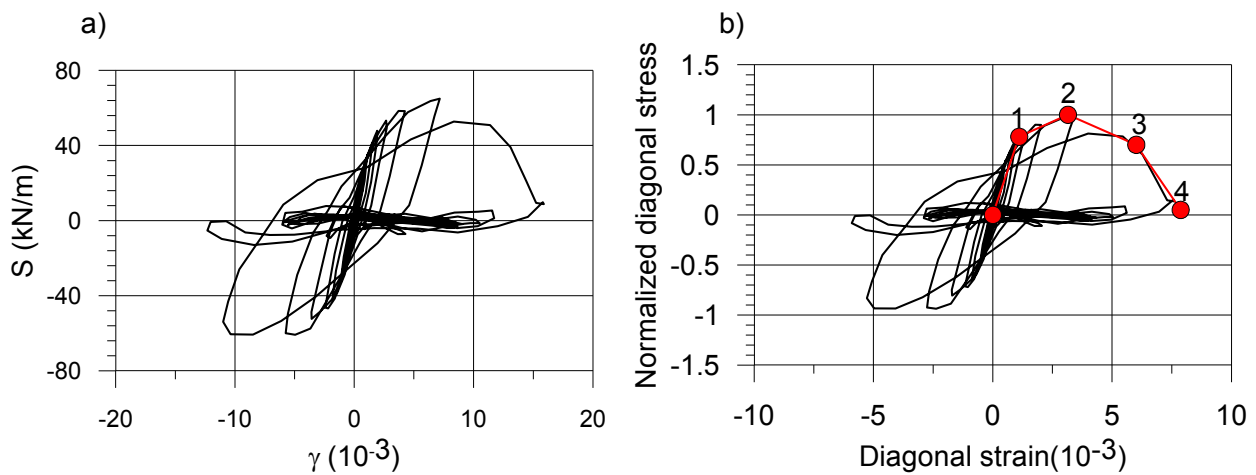
Figure 2.4 – a) Typical measured hysteretic shear response at diaphragm end; b) Typical hysteretic response of diagonal truss element and projected response envelope.

Figure 2.5 shows the normalized response envelope (positive quadrant) of diaphragm specimens in layout I (Figure 2.5a, deck panels perpendicular to loading direction) and layout II (Figure 2.5b, deck panels parallel to loading direction). The objective of this normalized response envelope is to show the relative values of four peak stress points and the actual ratios of stress-to-strain obtained at those four peak points during a diaphragm test. Average values for the different thickness of deck sheets and layout are also given in Table 2.2. The average ratios of stress to strain were then used in the numerical model to obtain the four peak strain points. The first stress point was typically found in the range of 70% to 76% of ultimate axial strength of the diagonal truss elements except for Specimen 18 (Table 2.2) for which the first stress point was found at about 95% of the ultimate axial strength. This higher value for Specimen 18 is attributed to the position of the maximum shear deformation which was not observed at the end of the diaphragm specimen. The fourth stress-strain peak point (after complete failure) was difficult to identify because the test data do not include the complete strength degradation curve in most cases. It was thus estimated using a trial and error approach during calibration of the model. In addition, the unloading and reloading pinching parameters required to define the Pinching4

a) Roof deck panel in layout I
b) Roof deck panel in layout II
*Diaphragm designed as per demand along length (Specimen 18)

×—×—× 0.76mm diaphragms
△—△—△ 0.91mm diaphragms
+—+—+ 1.21 diaphragms
☆—☆—☆ 0.91mm diaphragms*
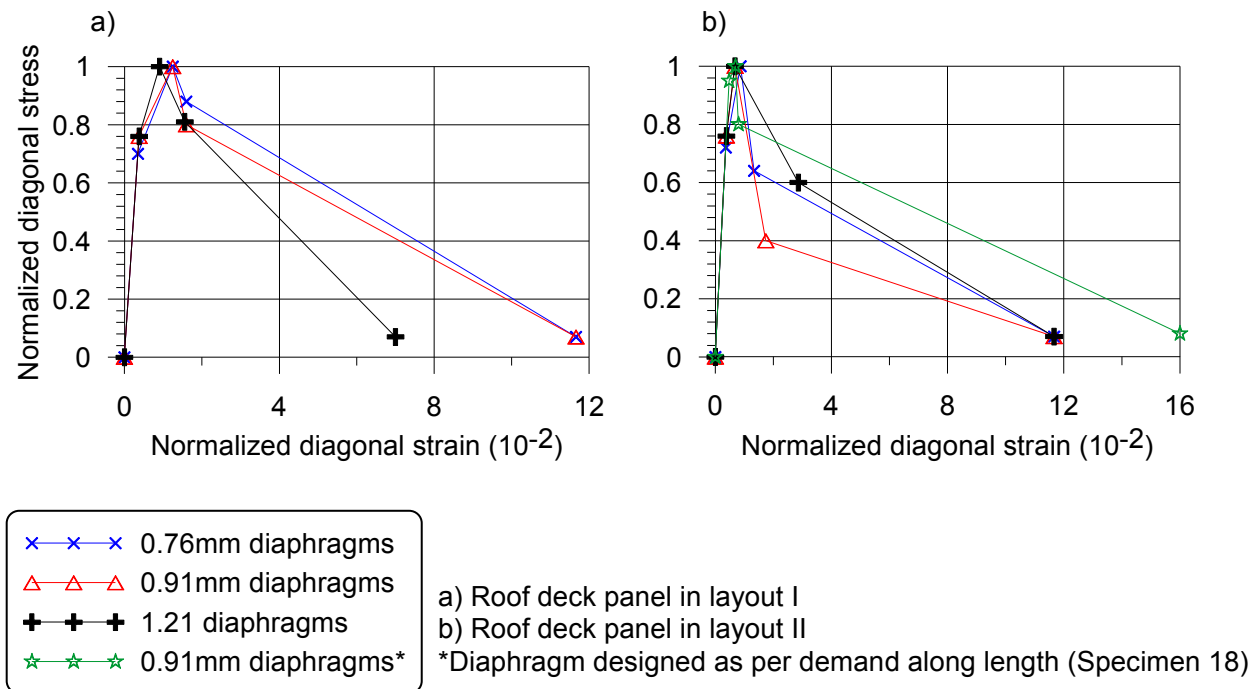
Figure 2.5 – Response envelope of diaphragms

Table 2.2 – Average stress and stress strain ratios at peak points

Layout I	Deck thickness (mm)	1		2		3		4	
		σ_1/σ_u	σ_1/ϵ_1 (kN/mm^2)	σ_2/σ_u	σ_2/ϵ_2 (kN/mm2)	σ_3/σ_u	σ_3/ϵ_3 (kN/mm2)	σ_4/σ_u	σ_4/ϵ_4 (kN/mm2)
I	0.76*	0.70	200	1.0	170	0.75	80	0.04	0.4
	0.76	0.70	200	1.0	80	0.88	55	0.07	0.6
	0.91	0.76	200	1.0	80	0.8	50	0.07	0.6
	1.21	0.76	200	1.0	110	0.81	52	0.07	1.0
II	0.76	0.72	200	1.0	115	0.64	48	0.07	0.6
	0.91	0.76	200	1.0	147	0.4	23	0.07	0.6
	1.21	0.76	200	1.0	148	0.6	21	0.07	0.6
	0.91 (Test 18)	0.95	200	1.0	145	0.8	100	0.08	0.5

*Peak points from Test 2

Table 2.3 – Pinching4 stiffness and strength degradation parameters

Layout	Deck thickness (mm)	Unloading stiffness degradation parameters gK1, gK2, gK3, gK4, gKLim	Reloading stiffness degradation parameters gD1, gD2, gD3, gD4, gDLim	Strength degradation parameters gF1, gF2, gF3, gF4, gFLim
I	0.76*	0.8 0.8 0.3 0.2 0.4	0.1 1.0 0.8 0.7 1.0	0.2 0.4 0.0 0.3 0.14
	0.76		0.2 1.0 0.4 0.7 1.0	
	0.91		0.8 1.0 0.4 0.7 1.0	0.0 0.0 0.0 0.0 0.0
	1.21		0.2 1.0 0.4 0.7 1.0	
II	0.76	0.8 0.8 0.3 0.2 0.3	0.5 1.0 0.4 0.7 1.0	0.1 0.3 0.0 0.3 0.2
	0.91		0.1 1.0 0.5 0.7 1.0	0.2 0.3 0.0 0.3 0.16
	0.91 (Test 18)		0.2 1.0 0.8 0.5 1.0	0.0 0.0 0.0 0.0 0.0
	1.21		0.8 1.0 0.5 0.7 1.0	0.1 0.3 0.0 0.3 0.1

*Parameters specifically for Test 2 using peak points from Test 2

For all tests; $rStrainP = 0.16$, $rStrengthP = 0.22$, $uStrengthP = 0.16$, $gE = 2.0$, $dmgType = energy$

element were estimated from the test data. The unloading stiffness degradation, reloading stiffness degradation and strength degradation parameters were then introduced into the model based on the match between the overall model response and the test data (Table 2.3). During calibration, it was found that the common unloading stiffness degradation parameters as given in Table 2.3 could be used for all the diaphragm specimens. However the reloading stiffness degradation parameters and strength degradation parameters are not common for the different diaphragm configurations. Rayleigh damping value of 3% was assigned in the 1st and 3rd mode of

vibration. The measured average value of damping ratio of the diaphragm test specimens was about 2.3% (Franquet, 2010 and Massarelli, 2010). Damping in the Pinching4 material model, as of energy dissipation parameter, was also existed in the numerical model. An OpenSees script written for modeling Test Specimen 6 is presented in Appendix A.

2.4.2. Evaluation of model

The elastic and inelastic response of the OpenSees truss model was evaluated with respect to the data obtained from the three diaphragm test phases (Tremblay et al., 2011; Massarelli et al., 2011). The numerical model provided a general shear force vs. deformation response that closely matched the measured response and the diaphragm shear stiffness G' values. It was found, as noted by Tremblay et al. (2008b), that the diaphragm stiffness (G') and the fundamental period of vibration (T) are needed to accurately predict the seismic demand on roof diaphragms. Diaphragm test specimen 6, composed of 0.76 mm steel deck connected with a 36/11 pattern for nail frame fasteners and screw side-lap fasteners spaced at 152 mm, is used herein to describe the matching of the numerical model with the test response. Figure 2.6 shows the measured and predicted time histories of the mid-span deflection, δ_m, and the normalized hysteretic response (end shear S_u vs. mid-span deflection δ_m) of specimen 6 under the 1.2 x SS1 (Figure 2.6a) and 0.92 x SS2 (Figure 2.6b) signals. Good agreement, both in phase and amplitude, was obtained when specifying G' = 10.7 kN/mm (SDI estimation 17.6 kN/mm) in the numerical model to match the corresponding measured period of vibration (0.155 s). Once the reduced (measured) G' was used in the model, the hysteretic response was also well predicted, including pinching and strength degradation under the stronger signal. The measured and predicted displacement profiles of Specimen 6 along the length of the diaphragm (perpendicular to loading direction) under the elastic and inelastic signals are plotted in Figure 2.7. Figures 2.7a and 2.7b show the comparison at the time when the shear force is a maximum at the support. Close matching of the displacement profile between the test data and the model is also shown for the time when there is maximum shear force at the 4th joist from the end support (Figure 2.7c).
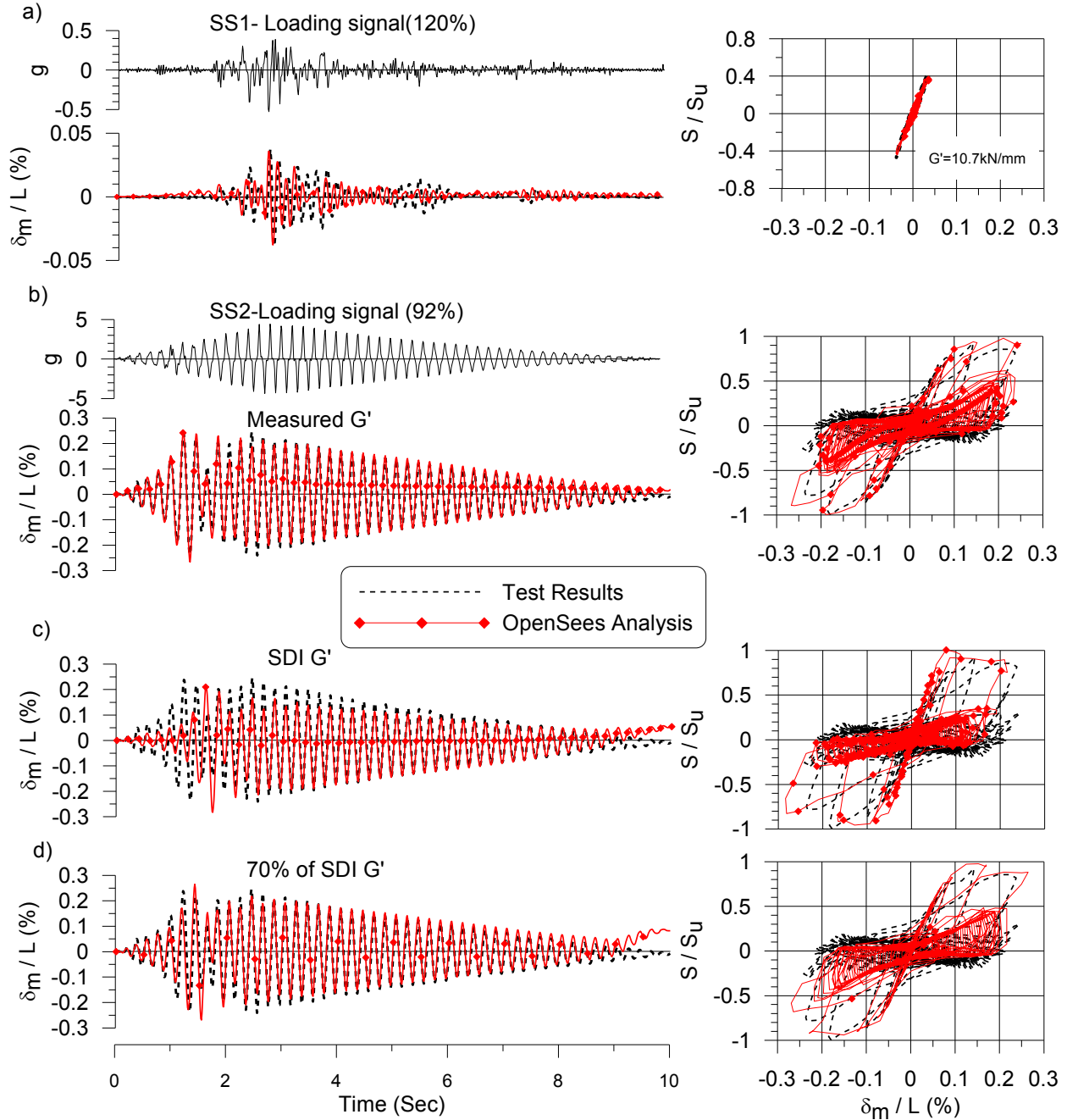
Figure 2.6 – Time history and hysteretic responses of specimen 6 under loading signal: a) l 1.2 x SS1; b) 0.92 x SS2; c) model with 100% SDI G'; d) model with 70% SDI G'

A typical steel deck sheet panel, which is the one third the length of the full diaphragm specimen, is shown in Figure 2.8a. The measured and predicted maximum shear deformation obtained for Specimen 6 under the inelastic signal 0.92 SS2 and at the panel segment 1 to 4

(Figure 2.8a) is shown in Figure 2.8b. The predicted responses matched well with the test data. Figure 2.8c shows the predicted and measured hysteretic shear response again at the position 1 to 4 under the inelastic signal. The hysteretic matching was good for segments 1 and 2 of the deck specimen. For segments 3 and 4 of the deck panel, the predicted response was mainly elastic
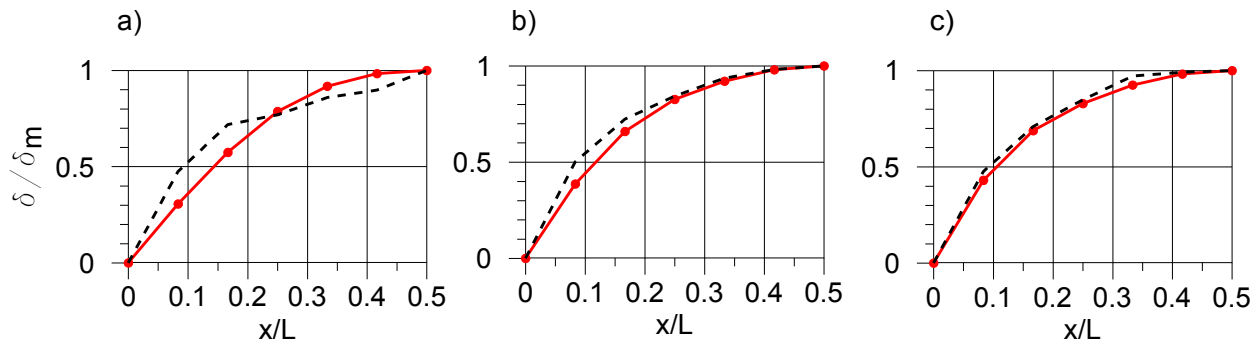
Figure 2.7 – Displacement along the length of specimen 6: a) Elastic signal 1.2 x SS1 (maximum shear at end); b) Inelastic signal 0.92 x SS2 (maximum shear at end); and c) Inelastic signal (maximum shear at 4th joist).

whereas the test still shows an inelastic response. This may have been caused by the progressive connection failure along the length of the individual panel. Since the shear force is higher at the panel end, it can be assumed that connection failure would begin at this location (segment 1). Once, the connections failed in segment 1 and then 2, the shear strength of the diaphragm at segment 3 of the panel would be reduced. Consequently, segment 3 of the panel would show inelastic response even though the shear force at that segment was about 70% of the diaphragm initial strength. Similarly, segment 4 of the panel showed inelastic response for a shear force of about 50% of the diaphragm initial strength after the failure of segments 1 to 3. This "panel effect" was not incorporated in the OpenSees model. The middle panels did not show an inelastic response because the shear force over the span of the diaphragm did not reach a level beyond that associated with elastic behaviour. Figure 2.8d shows the predicted and measured distribution of shear force along the length of the diaphragm at time t when there is maximum shear at the support. A parabolic fit for the shear force distribution as suggested by Massarelli et al. (2011) is also shown in the figure. Although the parabolic expression was developed for an elastic load it proved to be very similar for the inelastic load. Figure 2.8e shows the predicted shear force distribution and shear deformation over the depth (parallel to force) of the diaphragm
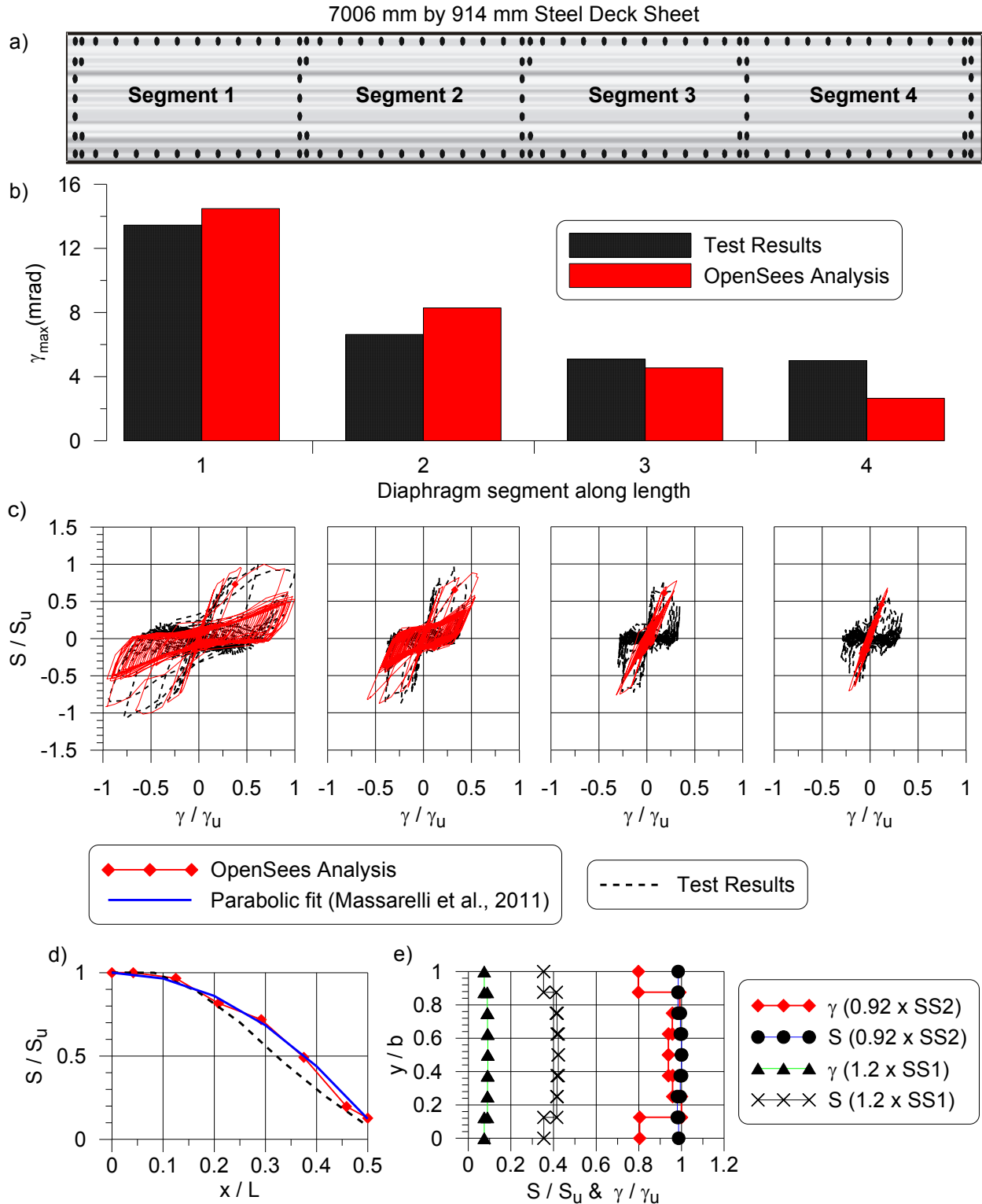
Figure 2.8 – Specimen 6: a) steel deck sheet; b) maximum shear deformation along length; c)
hysteretic response of diaphragm along length; d) shear force distribution along length; e) shear
force and deformation along depth

specimen under the elastic and inelastic loading. The model shows that there is no significant difference in the shear response over the depth. As expected, for the inelastic loading, the shear force distribution over the depth is almost constant, and for the elastic loading, the model shows that there is slightly higher shear force at the middle.

Compared with Specimen 6 and other diaphragm specimens with nail frame fasteners and screw side-lap connections, specimens 1 and 2 were constructed with frame fasteners placed at alternate flutes. Higher warping deformations of the deck ends were observed due to this less dense connection pattern. As a result, a higher variation in shear stiffness distribution was measured along the length of diaphragm specimens 1 and 2. Furthermore, the deck panel ends were not overlapped in Specimen 2, and hence the warping effect and stiffness variation were more pronounced than in Specimen 1. Good match of elastic and inelastic responses between the measured values and OpenSees prediction was found when a G' of 2.7 kN/mm (T =0.22 s) and a G' of 2.1 kN/mm (T = 0.25 s) were used in the models for Specimens 1 and 2, respectively. Four types of analysis were carried out in OpenSees for Specimen 2: Analysis 1 incorporated the response envelope and calibration parameters from Specimen 2, Analysis 2 incorporated the average parameters used for a 0.76 mm thick steel deck diaphragm (Table 2.2 and 2.3), Analysis 3 and 4 were similar to 1 and 2 respectively except the G' was varied along the length (estimated from test) from 1.0 kN/mm at the span end to 12.0 kN/mm towards the middle of the deck sheets. Figure 2.9a shows the measured and predicted time history of the mid-span deflection and the hysteretic response (S_u vs δ_m) of Specimen 2 under the 0.8 x SS2 inelastic signal. There is no significant difference between the results of Analysis 1 and Analysis 2 and hence the average Pinching4 parameters developed (Table 2.2 and 2.3) could be used in the model. Figures 2.9b and 2.9c show maximum elastic (under 1.6 × SS1) and inelastic shear deformation along the length of the diaphragm specimen (Figure 2.8a). A better match with the test data was found when G' was varied along the length (Analysis 3 and 4). Figures 2.9d and 2.9e show the displacement demand for Specimen 2 at the occurrence of maximum shear force at the end of the diaphragm under elastic and inelastic signals when a uniform G' of 2.1 kN/mm was assumed in the model (Analysis 2). The Analysis 2 procedure could be used for design purposes because only the overall response, i.e. maximum shear force and maximum displacement of the diaphragm, would likely be considered in design. Figures 2.9d and 2.9e show (test results) that
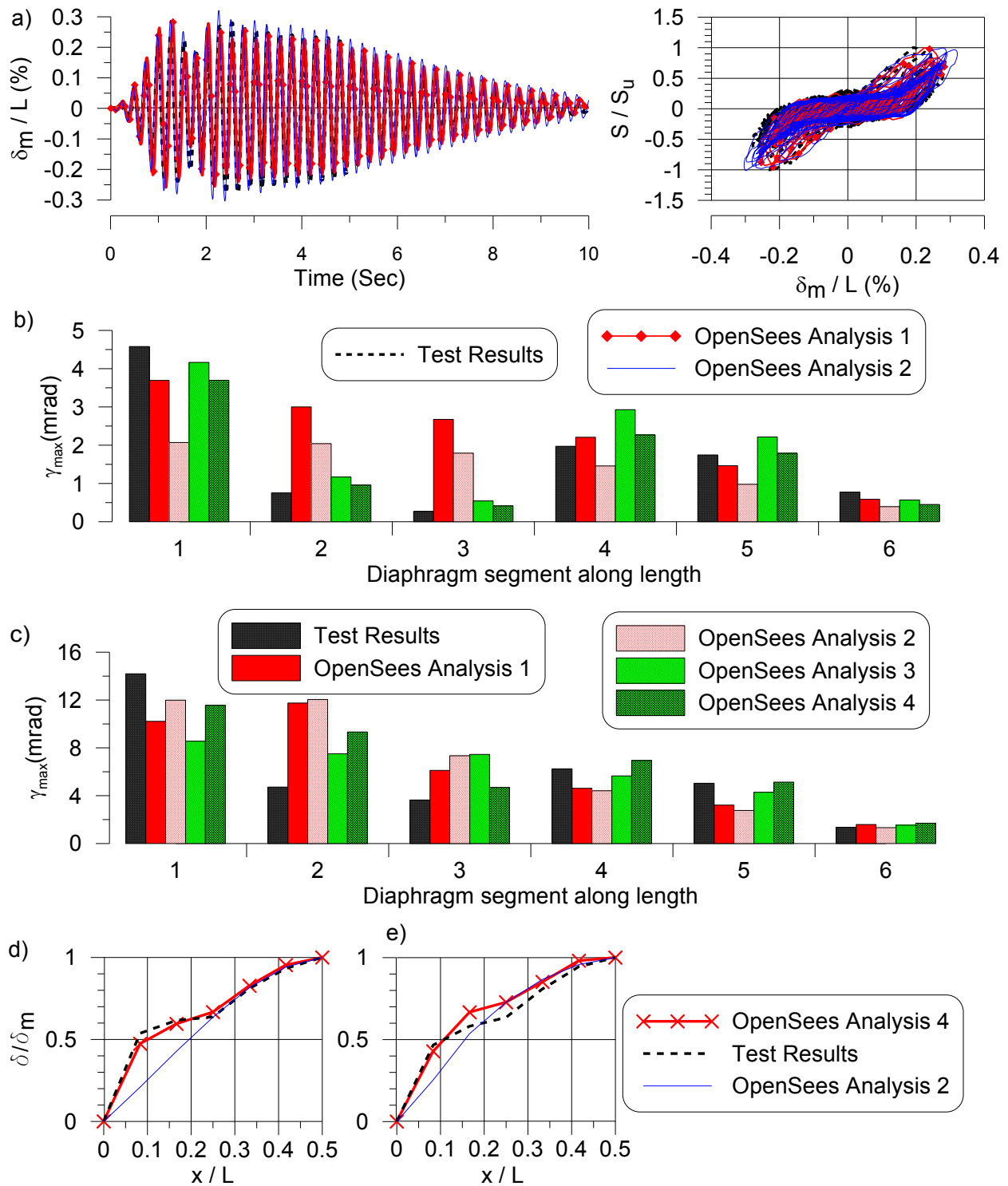
Figure 2.9 – Specimen 2: a) Inelastic time history and hysteretic response; b) to c) elastic, inelastic maximum shear deformation along length of diaphragm; d) to e) elastic, inelastic deformation profile along length of diaphragm.

43
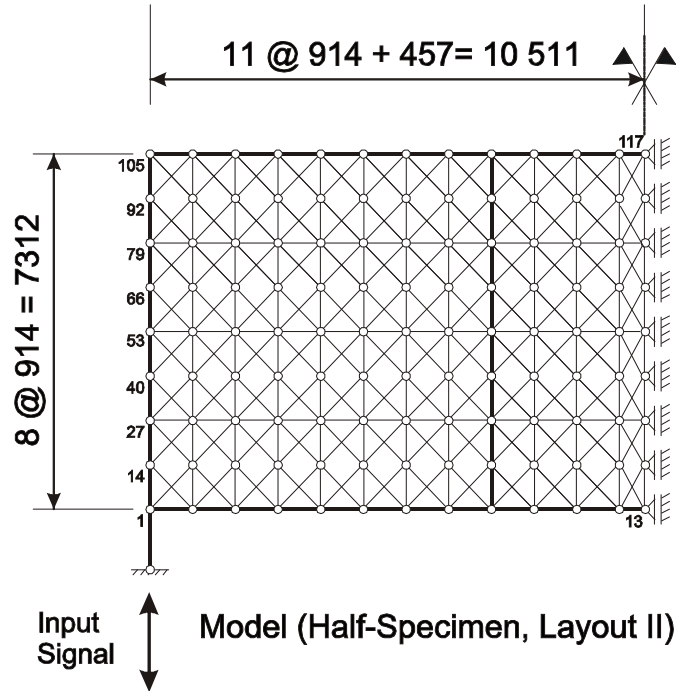
Figure 2.10 – Non-linear diaphragm truss model in OpenSees (Layout II)

the stiffness is significantly lower at the end of the test specimen due to warping. To incorporate this in the model the G' was varied along the length in OpenSees Analysis 4. Using a model (Analysis 4) that contained a variation of stiffness allowed for the displacement pattern along the length to better match with the test data under both the elastic and inelastic signals (Figures 2.9d and 2.9e). The change in shear stiffness along the length of the test diaphragms having all flutes connected was significantly less; as such the variation in shear stiffness was found to not significantly affect the displacement pattern. For such diaphragms (e.g. Specimen 6), the assumption of uniform shear stiffness along the length of the model was adequate to match the observed displacement demand.

Close matching of displacement profile and hysteretic response between the test data and model was also found for the thicker deck diaphragms and for the weld and button-punched diaphragms (Layout I and II) when the G' values corresponding to their measured period of vibration were used in each respective model (Table 2.4). Test results and numerical prediction from the OpenSees truss models for the elastic and inelastic response of all the new diaphragms specimens that were tested in the Phase I to Phase III large scale diaphragm test program are presented in Appendix B.
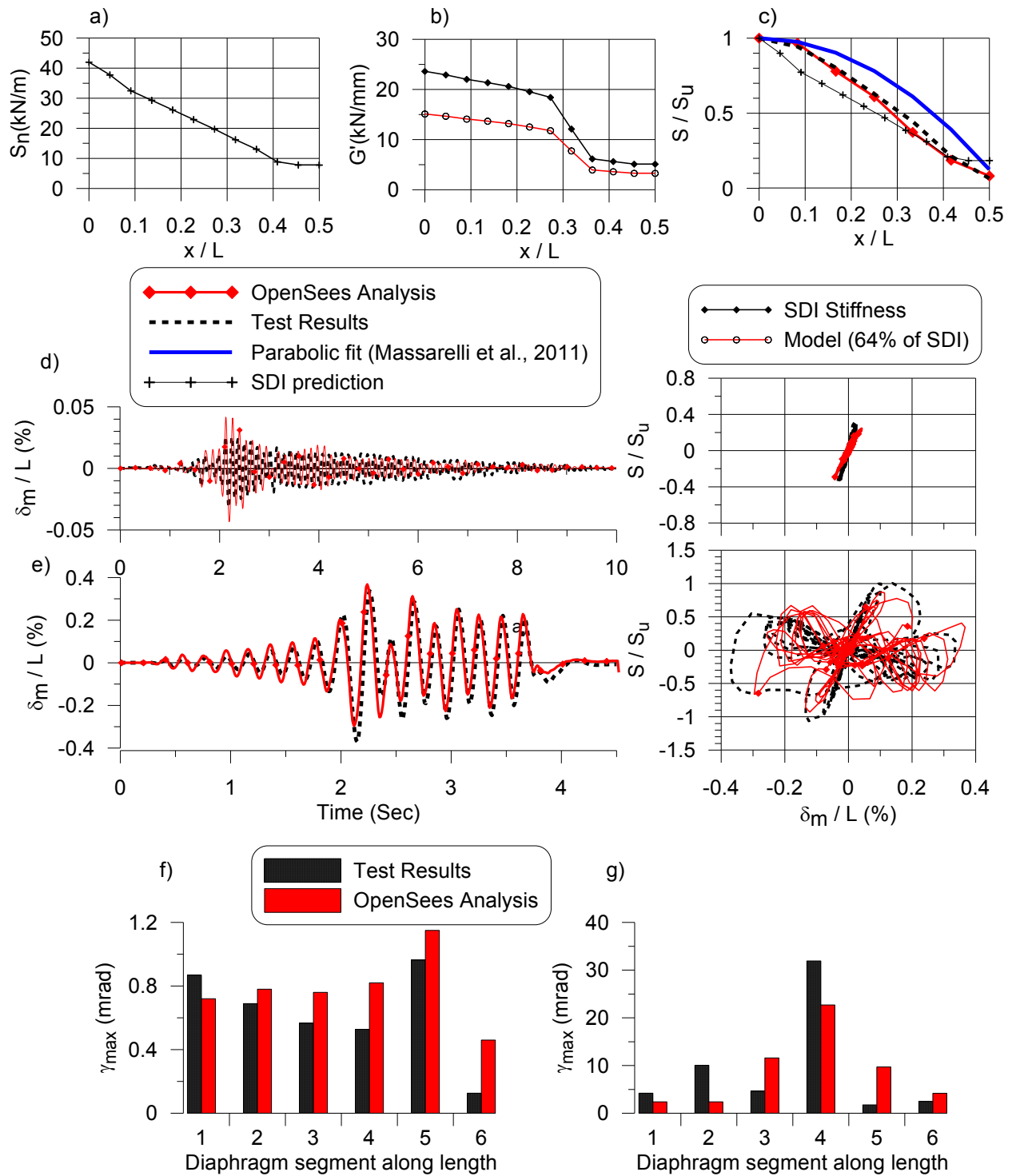
Figure 2.11 – Specimen 18: a) SDI strength profile; b) stiffness profile; c) shear force distribution along length of diaphragm; d) to e) elastic, inelastic time history and hysteretic response; f) to g) elastic, inelastic maximum shear deformation.

45

Adjustment to the model was made for Layout II specimens to account for the change in direction of the steel decks and joists as well as for the addition of two interior beams (Figure 2.10). Figure 2.11 shows the shear strength (Figure 2.11a) and shear stiffness (Figure 2.11b) along the length of Specimen 18, whose connection pattern was tailored to follow the expected shear demand under loading. The measured strength (S_u) of the diaphragm at the support was found to be close to the SDI prediction (S_n) and hence the predicted strength along the length was used in the model. A good match in response was found under the elastic ($1.0 \times SS1$) and inelastic ($0.92 \times SS2$) loading signals only when 64% of the SDI predicted stiffness along the length was used in the model; this corresponds to a measured period of vibration of 0.13 Sec (Figures 2.11d and 2.11e). This result is further indication that the SDI method overestimates the shear stiffness for diaphragms under dynamic loading conditions. Figure 2.11c shows the measured and predicted shear force distribution at the occurrence of maximum shear force at the end along the length of the diaphragm under the inelastic signal. The normalized SDI prediction and parabolic fit suggested by Massarelli et al. (2011) is also plotted in Figure 2.11c. The measured and predicted maximum shear deformations along the length of the diaphragm under the elastic and inelastic signals are shown in Figures 2.11f and 2.11g. The diaphragm segments 1 to 6 represent half of a test specimen in size. The maximum elastic and inelastic shear deformation were observed towards the middle of the diaphragm in the test which was well captured by the model.

2.4.3. Modeling of cantilever diaphragm test specimens

The OpenSees truss model was also evaluated by modeling the cantilever diaphragm specimens that were tested by Essa et al. (2001) and by Martin (2002) to verify the values of the material model parameters. Note that the aspect ratios of the cantilever diaphragm test specimens were not similar to that of the three phase diaphragm test specimens (3:5 vs. 1:3). The numerical model (Figure 2.2) was developed using a similar concept to that applied for the dynamic diaphragm truss model (Figure 2.3a). Elastic truss elements were used for the beam members. Measured stiffness and strength was used in the model. Figure 2.12a shows the hysteretic response of test 7, 0.76 mm deck with screw side-lap and nail deck-to-framed connections (Essa

46

et al., 2001), under the reversed cyclic loading signal. The response obtained by the OpenSees model provided a good fit with the test data. The response shown in Figure 2.12a was obtained by using the normalized response envelope (Figure 2.5a) and pinching parameters (Table 2.2 and 2.3) that were incorporated in the original numerical truss model for the 0.76 mm dynamic diaphragm specimens.
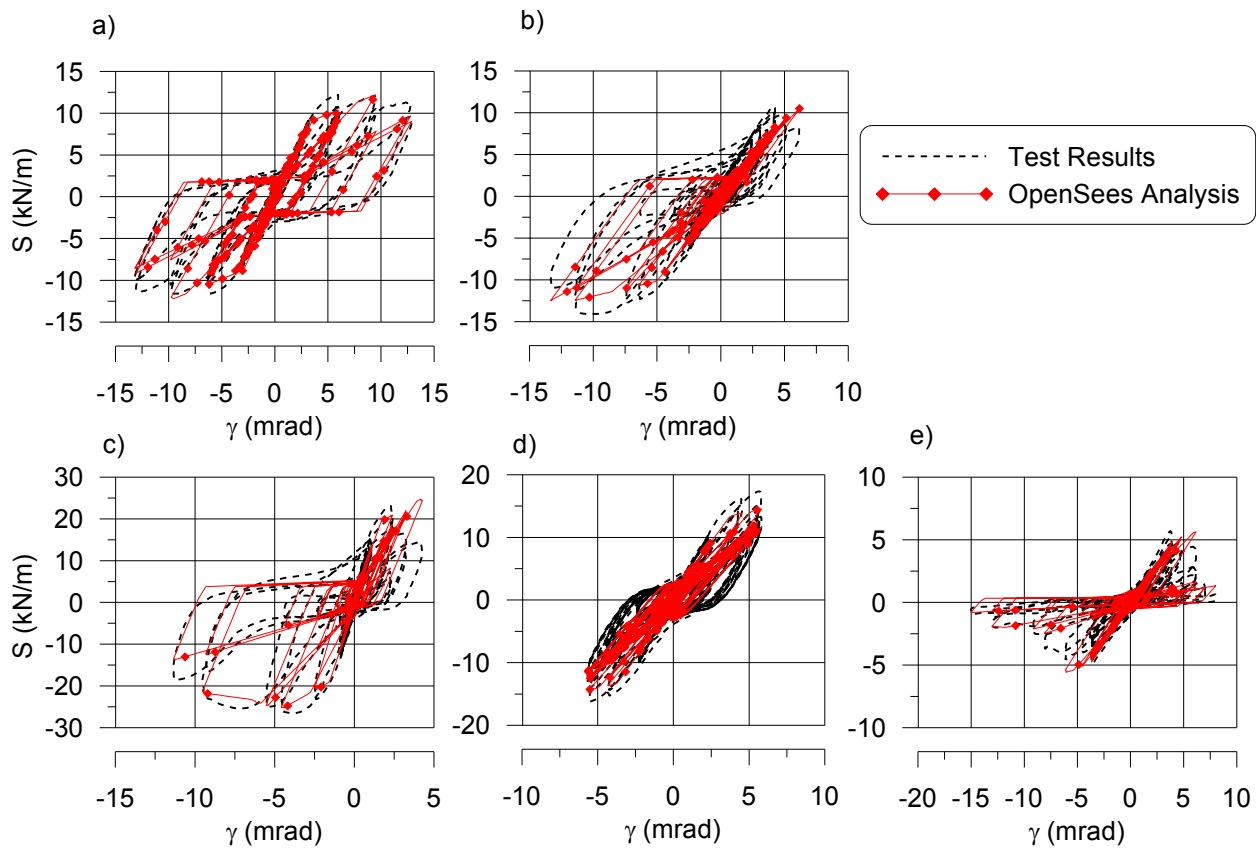
Figure 2.12 – Hysteretic responses of diaphragm test specimens; a) test number 7 (Essa et al. 2001), b) to e) test number 28, 31, 35 and 36 (Martin, 2002)

Figures 2.12b to 2.12e show the response of diaphragm tests 28, 31, 35 and 36, respectively (Martin, 2002). Good match between the test data and numerical model was found in all cases except for test 35 when the corresponding normalized response envelope and pinching4 parameters used in the truss model along with the measured strength and stiffness was used in the model. For test 35 (0.91mm deck sheets), the good match was found only after allowing for a greater decrease in stiffness degradation of Pinching4 elements in the numerical model. This

could be possibly due to the higher stiffness degradation in each subsequent cycle in the thicker deck panel diaphragms under the dynamic loading conditions.

2.4.4. Analysis and discussion

The measured fundamental period of vibration and the shear stiffness (G') of diaphragm test specimens estimated by the SDI (Luttrell, 2004) method, numerical model and the Medhekar analytical expression (Medhekar 1997, Tremblay et al. 2008b) are presented in Table 2.4. The shear stiffness values of the diaphragm test specimens estimated by the numerical model were based on the matching of the measured response and the fundamental period. The stiffness predicted by the numerical model was almost equal to that obtained by the use of the Medhekar analytical expression. The average numerical model / analytical expression stiffness ratios ranged from 0.98 to 1.03. It should be noted that the Medhekar analytical expression was validated by the shake table testing by Tremblay and Bérair (1999) and Tremblay et al. (2000). In both of the methods, the measured fundamental period of vibration of each diaphragm specimen under the largest elastic seismic signal (SS1 or SS3) or the largest white noise signal (whichever gave the maximum fundamental period) was the basis for computing its stiffness. Even though the numerical model and the analytical expression showed almost equal stiffness for all the diaphragm specimens, these values were found to be lower than the stiffness estimated using the SDI method except for the weld and button punch diaphragm specimens. The average ratios between the stiffness obtained by the numerical model and the SDI method were 0.58, 0.68 and 0.73 for the 0.76 mm, 0.91 mm and 1.21 mm deck sheet diaphragm specimens (overall average 0.67), respectively. For weld and button punched diaphragm specimens having 0.76 mm deck panels, the measured stiffness was close to the predicted SDI stiffness.

Essa et al. (2001) compared the measured stiffness of their test diaphragms with the SDI method and found an average ratio of 0.81 under monotonic loading and 0.76 under reversed cyclic loading signals. The measured stiffness under monotonic load was the tangent at the level of 40% of ultimate strength (S_u) of diaphragms. Under the cyclic loadings, the positive portion of the 7th cycle was used to measure the stiffness of the diaphragms. For weld and button punched diaphragms, the average ratio was 0.77 under both monotonic and cyclic loading. Furthermore,

Table 2.4 – Shear stiffness (G') of test specimens

Test No.	Measured time period	Shear Stiffness G' (kN/mm)			Ratio between (Model and Medhekar)	Ratio between (Model and SDI)
		SDI	OpenSees Model	Medhekar Eq.		
0.76 mm thick steel diaphragms						
1	0.220	4.2	2.7	2.7	1.00	0.64
2	0.250	4.2	2.1	2.1	1.00	0.50
3	0.183	16.8	7.5	7.2	1.04	0.45
4	0.180	17.0	7.7	7.5	1.03	0.45
5	0.160	17.4	10	9.7	1.04	0.57
6	0.155	17.6	10.7	10.4	1.03	0.61
11	0.147	16.3	10.9	11.6	0.94	0.67
16	0.134	17.1	12.1	12.8	0.95	0.71
				Mean	**1.01**	**0.58**
				C.o.V.	**0.03**	**0.16**
0.91 mm thick steel diaphragms						
7	0.133	21.8	15.3	14.8	1.03	0.70
8	0.135	22.4	14.8	14.3	1.03	0.66
9	0.134	22.8	15.0	14.6	1.03	0.66
17	0.129	21.9	14.5	14.1	1.03	0.66
18	0.130	23.6†	13.2††	13.9	0.95	0.56
				Mean	**1.03**	**0.65**
				C.o.V.	**0.00**	**0.032**
1.21 mm thick steel diaphragms						
12	0.115	31.1	21.8	21.5	1.02	0.70
13	0.107	31.3	25.6	25.6	1.00	0.82
14	0.111	34.8	23.8	23.4	1.02	0.68
19	0.116	31.3	19.0	18.7	1.02	0.61
				Mean	**1.01**	**0.73**
				C.o.V.	**0.01**	**0.12**
0.76 Weld and button punch diaphragms						
10	0.256	3.6	3.6	3.6	1.00	1.00
15	0.247	3.5	3.3	3.5	0.96	0.94
				Mean	**0.98**	**0.97**
				C.o.V.	**0.03**	**0.04**

†G' at the diaphragm end,

†† Assuming uniform G' in model

Martin (2002) reported that the measured diaphragm shear stiffness is significantly lower than the SDI prediction. The average ratio was 0.7 and 0.88 for diaphragms with 305 mm and 152 mm spacing connection patterns, respectively. The slight differences in the average ratios compared to those obtained by Martin (2002) and Essa et al. (2001) could be due to the loading condition of the diaphragm specimens. Nonetheless, these studies showed that the measured shear stiffness could be considerably lower than the SDI prediction when a diaphragm is subjected to dynamic large amplitude loading. The average ratio of measured shear strength to the SDI prediction was about 1.1 and 0.85 in the tests carried out by Martin (2002) and Essa et al. (2001) respectively.

A design engineer requires the shear stiffness of the diaphragm to calculate the maximum roof deflection (NRCC 2010). The shear stiffness of the diaphragm will also be required when numerical modelling is carried out in the design process. Diaphragm stiffness can affect the overall building period of vibration, which in turn affects the lateral load used for seismic design. Figure 2.6 shows the measured and predicted (original truss model) response of Specimen 6 under the inelastic signal; predicted responses were also shown using the measured stiffness (61% of SDI stiffness), SDI stiffness, and 70% of SDI stiffness (close to overall average) in Figures 2.6b, 2.6c and 2.6d, respectively. From the analysis, it was found that the use of 70% of SDI stiffness in the model provides for an adequate match with the displacement time history and the normalized force vs. displacement hysteretic test data. The model gave a fundamental period of 0.125 s with 100% of SDI stiffness and 0.146 s with 70% SDI compared to the measured period of 0.155 s (Table 2.4).

2.5 Selection of mesh size for building application

In the modeling of the cantilever diaphragm specimens (Figure 2.2), mesh size equal to the size of specimen was used mainly because of two considerations; the shear force is equal throughout the specimen and the specimen size is small. However, for the modeling of the large scale diaphragm specimens (Figure 2.3a) of the dynamic tests (Tremblay et al., 2011; Massarelli et al., 2011), a smaller mesh size of 875.8mm by 914mm was used in the numerical model considering both shear force and shear strain could vary over the span and depth of the specimen. In medium
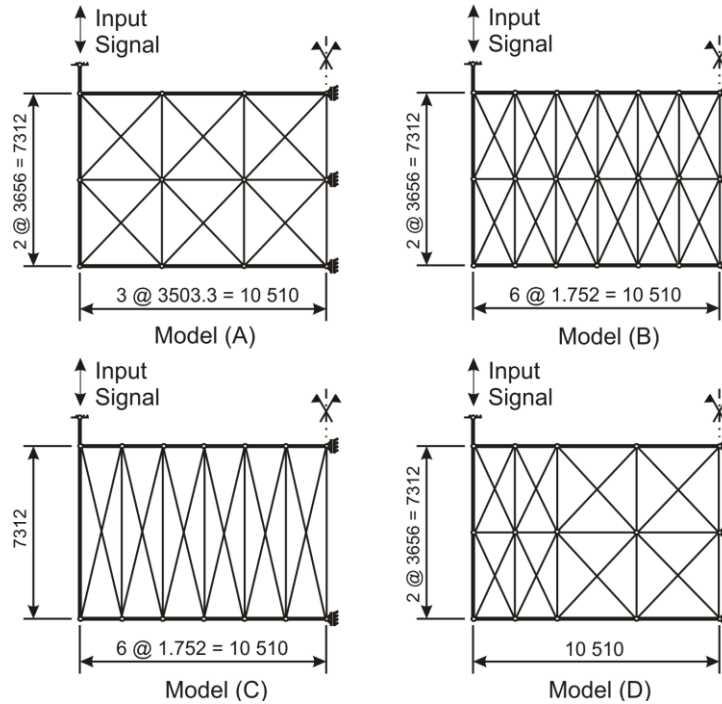
Figure 2.13 – OpenSees models with large mesh size for the dynamic diaphragm test specimens (dimensions in mm)

to large sized single-storey steel buildings, using the smaller mesh size in a model as used for the diaphragm specimens of the dynamic test can take longer time and more effort to analyze. As the numerical response of the test specimen showed that the shear response does not change significantly over the depth of the specimens (Figure 2.8e), the diaphragm can also be modelled using a strip mesh size. To study the influence of mesh size on the inelastic response, truss models with a larger mesh size were developed for the diaphragm specimens of dynamic tests in OpenSees and their responses were compared with the original OpenSees truss model (Figure 2.3a). Figure 2.13 shows the four OpenSees models (Model A to D) of the Phase I to III large-scale dynamic diaphragm tests. The response envelope and the parameters of the Pinching4 non-linear material model were kept identical to the original OpenSees truss model. All the models, including the original truss model, have identical measured shear stiffness and strength. The total mass was distributed uniformly along the direction of excitation as a lumped mass over the nodes. Layout I diaphragm Specimen 6 was selected for the comparison.
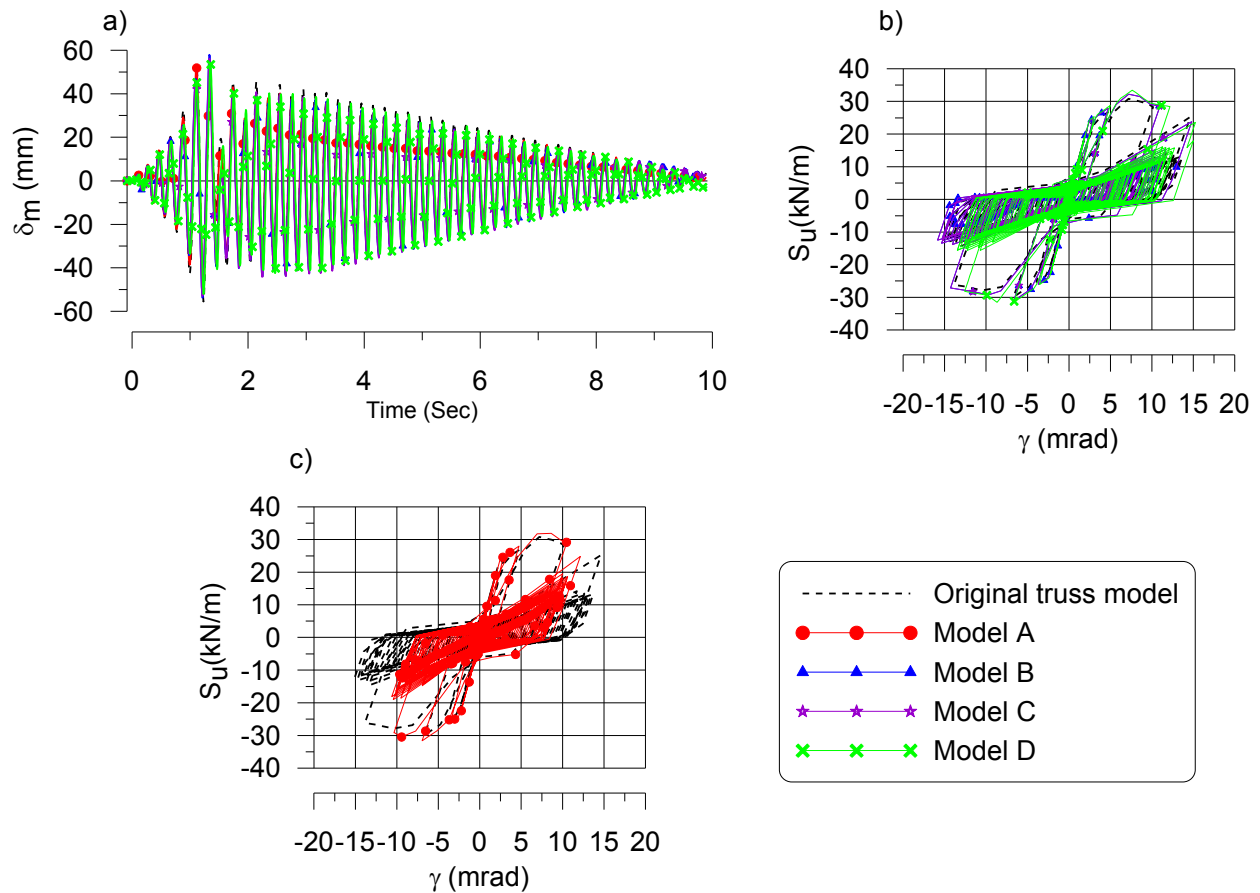
Figure 2.14 – Response with large mesh in OpenSees model ; a) Inelastic displacement time history at mid span; b) and c) inelastic shear response near the end of diaphragm

Figure 2.14a shows a comparison of the mid-span displacement time history of Specimen 6 obtained from all the models including the original truss model. Figure 2.14b shows comparison of the end shear response (S_u Vs γ) of Specimen 6 obtained from Model B to D and from the original truss model. Model A provided a good match in terms of the overall mid-span displacement time history with the results obtained from the original truss model (Figure 2.14a). The local inelastic demand, however, was lower than that obtained from the original fine mesh truss model (Figure 2.14c). To capture a similar response to the original truss model it was necessary to change the mesh size to 1.752 m by 3.656 m in Model B and 1.752 m by 7.312 m in Model C. Note that 1.752 m is the joist spacing for the layout I diaphragm specimens. Model B and C provided almost identical results as shown in Figures 2.14a and 2.14b. Model C is better than Model B in terms of time of computation with the same level of accuracy and hence can be
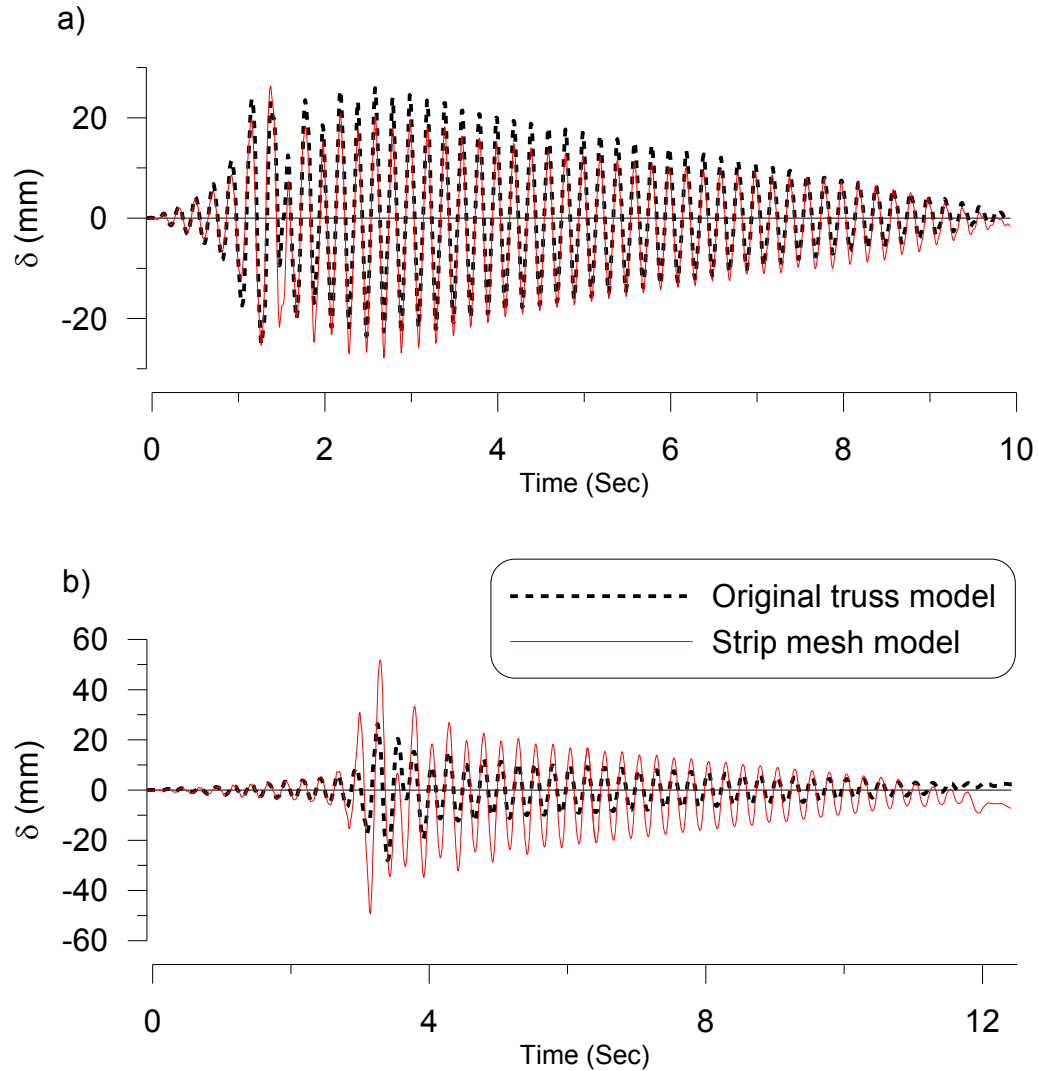
Figure 2.15 – Local inelastic displacement time history; a) Specimen 6 (Layout I), at 1.75m from diaphragm end,   b) Specimen 16 (Layout II), at 1.828m from diaphragm end

recommended for the building application where the deck sheets are perpendicular (Layout I) to the loading. Changing the mesh size from smaller at end to larger towards the middle (Model D) could be an option for modelling large buildings but will be inappropriate for the diaphragms with tailored connection patterns as the shear strength and shear stiffness will change in such diaphragms.

The strip mesh model (Model C) may not be suitable for Layout II diaphragms where the deck sheets are parallel to the loading direction as shown in Figure 2.15. Figure 2.15a shows the displacement time history of Specimen 6 (Layout I) at the 1.75m distance from the end of

diaphragm under the inelastic loading signal (0.92SS2). The fine mesh original truss model and the strip model (Model C) provided similar displacement time history response (Figure 2.15a). A similar strip model (1.828 m × 7.312 m) was developed for Layout II diaphragm Specimen 16. Figure 2.15b shows the displacement time history of Specimen 16 (Layout II) at the distance of 1.828m from the end of diaphragm under the inelastic loading signal (0.80SS2). The strip model for layout II diaphragm (Specimen 6) provided significantly higher inelastic displacement demand compared to the results obtained by the fine mesh original truss model for Layout II. The difference in displacement inelastic demand between the strip model and the original truss model for Specimen 16 (Layout II) could be because of the influence of the joist members which run perpendicular to the direction of excitation.

2.6 Summary and conclusion on numerical modeling of roof diaphragms

Non-linear dynamic time-history analyses of diaphragm test specimens were performed using a truss model in the OpenSees software platform to predict the dynamic response. Diagonal truss elements with Pinching4 material models were used to represent the measured shear strength and stiffness of the diaphragm, its degradation as well as the pinched hysteretic response. Values of the Pinching4 material model were proposed after calibration of the numerical model with the recent Phase I to III dynamic diaphragm tests and validated with the results obtained from past reversed cyclic tests of cantilever diaphragm specimens. It should be noted that the average stress strain input parameters used in the numerical model are loading history dependent since these parameters are based on the envelope of the experimental data. In this aspect, the numerical model is conservative to some extent as stated in FEMA P-440A (2009).

Calibration of the numerical models revealed that in order to match the predicted response with the measured response it was essential to reduce the SDI calculated G' of test specimens in all the cases except for weld and button punch diaphragm specimens. Once a reduced G' that corresponds to the fundamental period of vibration was used in the model the elastic as well as inelastic response including the pinching and degradation could be well predicted. It was found that using 70% of the SDI stiffness provides for an adequate match with the test response for the diaphragms with nail or weld frame fasteners and screw side-lap connections. Moreover, the

change in the stiffness of the test specimens over the span length was found to have a significant effect on the displacement profile when alternate flutes were connected to the underlying frame. This was due to the high degree of warping and consequently lower stiffness at the deck panel ends under high level excitation. The change in stiffness over the span length was found necessary to incorporate in the model to match with the measured displacement profile. In contrast, when all the deck flutes were connected to the underlying frame warping was reduced; the change in stiffness was minimal and thus did not affect the displacement profile significantly. Use of an uniform shear stiffness, corresponding to the measured period, in all truss elements of the numerical model allowed for an adequate match of the displacement profile in this case. Further, use of uniform shear stiffness over the span length in the model was found competent to predict the overall diaphragm response of alternate or all flute connected diaphragms, i.e. shear force at the end and displacement at the middle. In addition, whether alternate flutes or all the flutes are connected to the underlying frame, the uniform stiffness could be used in the model for design purposes because only the overall response, i.e. maximum shear force and maximum displacement of the diaphragm, would likely be considered.

The possible use of the strip mesh size for diaphragm modeling for building application was also studied. The use of the strip mesh size in the models was found applicable for modeling Layout I roof diaphragms where deck sheets were perpendicular to the loading directions. Strip model "Model C" was found most appropriate for building application for Layout I diaphragms. Whereas, the strip models were not found appropriate to model Layout II diaphragms to predict the inelastic response of the diaphragms.

Chapter 3 –Design of single-storey steel buildings

3.1 General overview

In the seismic design of a single-storey steel building, vertical bracing is typically provided to resist the design lateral forces. The current model building code in Canada, NBCC (NRCC, 2010), lists two primary forms of lateral bracing systems: concentrically braced frame (CBF) where the braces act as fuse elements and eccentrically braced frame (EBF) where the portion of a braced beam known as the link beam acts as a fuse element. The ductility and over strength related seismic force modification factors (R_d, R_o) are given in the NBCC for the various structural systems which must be designed and detailed according to the CSA S16 Standard (CSA, 2009). The detailed design of a medium size (30m × 60m × 7m) and a large size (40m × 90m × 8m) single-storey steel building with the following four structural systems is carried out. A detailed description of the design calculations for the medium size building is presented in this chapter. A similar design procedure was followed for the large size building; for the purpose of brevity the design details are presented in Appendix D.

   A. Moderately ductile concentrically braced frame (R_d = 3.0, R_o = 1.3)
   B. Ductile diaphragm with concentrically braced frame (R_d = 2.0, R_o = 1.9)
   C. Ductile eccentrically braced frame (R_d = 4, R_o = 1.5)
   D. Conventional construction concentrically braced frame (R_d = 1.5, R_o = 1.3)

In the seismic design of a building, the lateral design load depends primarily on the period of vibration of the structure and the type of lateral structural system that is implemented. The four different structural systems (A to D) were selected for design mainly to compare their corresponding design base shear, design forces on the diaphragms and their behaviour under a design level earthquake loading. Within these structural systems, different design cases such as with and without period limitation in design as well as with SDI and reduced SDI shear stiffness of the diaphragms were considered. Structural systems A, C and D are of standard configuration as currently described in the NBCC and CSA S16. Contrary to these typical framing systems, the steel roof deck diaphragm of System B was configured to yield and dissipate energy under a

56

design level earthquake ground motion. The CBF of this building was then designed elastically since it is the diaphragm that was specified to act as the fuse element in the SFRS. The seismic force modification factors for the ductile diaphragm structure are not available from the NBCC, and as such had to be estimated; further discussion is provided in Section 3.8. The in-plane flexibility of the steel deck diaphragm and its influence on the period of vibration was considered in the design of four structural systems. Design and analysis were carried out mainly for the buildings that have roof diaphragms in Layout II scenario, in which the deck panels were parallel to the loading direction (N-S direction). From the large scale dynamic test of diaphragms (Massarelli, 2010), higher shear deformations and greater concentration of damage at the ends of diaphragms were observed in Layout II diaphragm specimens than in Layout I diaphragm specimens.

3.2 Location and geometry of buildings

These representative buildings were considered to be located in Abbotsford near Vancouver, British Columbia. Furthermore, an additional System B building (medium size), i.e. having a ductile diaphragm structural system, was considered to be located in both Abbotsford BC and
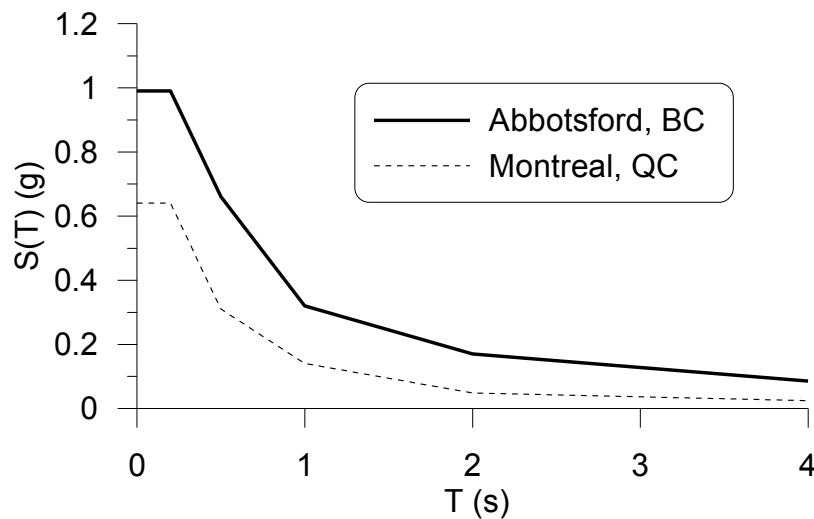
Figure 3.1 – Design NBCC(2010) uniform hazard response spectrum (UHS) for Abbotsford BC and Montreal QC
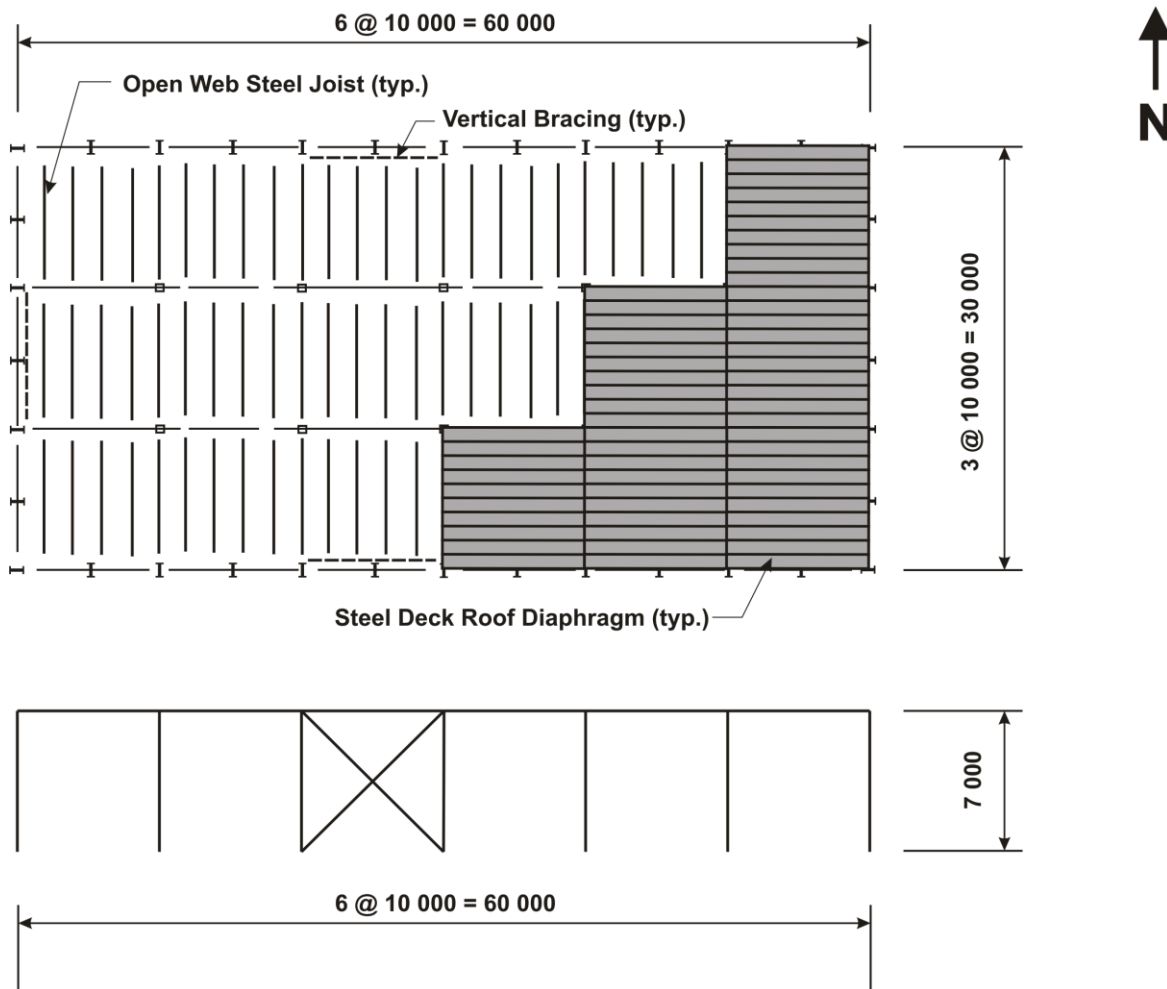
Figure 3.2 – A typical 30m×60m×7m single-storey building (Design 1) (dimensions in mm)

Montreal QC to study the influence of ground motion characteristics. Abbotsford is a western Canadian city whereas Montreal lies in the east part of Canada. However, both of the cities are considered as zones of high seismicity and heavy snowfall. A nationwide survey by Adams (1989) indicated that Vancouver and Montreal are the first and second ranked cities in terms of seismic risk. The uniform hazard spectra as given in the 2010 NBCC for both cities are shown in Figure 3.1. A site class C that represents very dense soil or soft rock was considered for the design and analysis.

The geometry of a medium size (30m×60m×7m) representative single-storey steel building with the CBF structural system is shown in Figure 3.2 and Figure 3.3. Figure 3.2 represents a Design 1 building (Layout I diaphragm) where the open web steel joists (OWSJs) are perpendicular to

the longer side of the building. The OWSJs are parallel to the longer side of the building in Design 2 (Layout II diaphragm) (Figure 3.3). The orientation of the joist members are changed to study the influence of deck orientation on the inelastic response of buildings designed with inelastic roof diaphragms. In both of the designs, the exterior and interior gravity columns are spaced 10 m apart and the open web steel joists in the roof of the building are spaced 2 m apart. Square HSS ASTM A500 Class C members were used for the interior columns and diagonal braces, whereas W-shapes G40.21 Grade 350W members were used for all other beams and columns. A 38 mm deep by 914 mm wide corrugated steel sheet deck manufactured by the Canam Group with P-3606 profile was selected for the roof diaphragm of the buildings. A bracing bent, whether a CBF or EBF, is located near the middle of each external wall. Similar layout was considered for the large sized buildings that were designed for Abbotsford, BC.
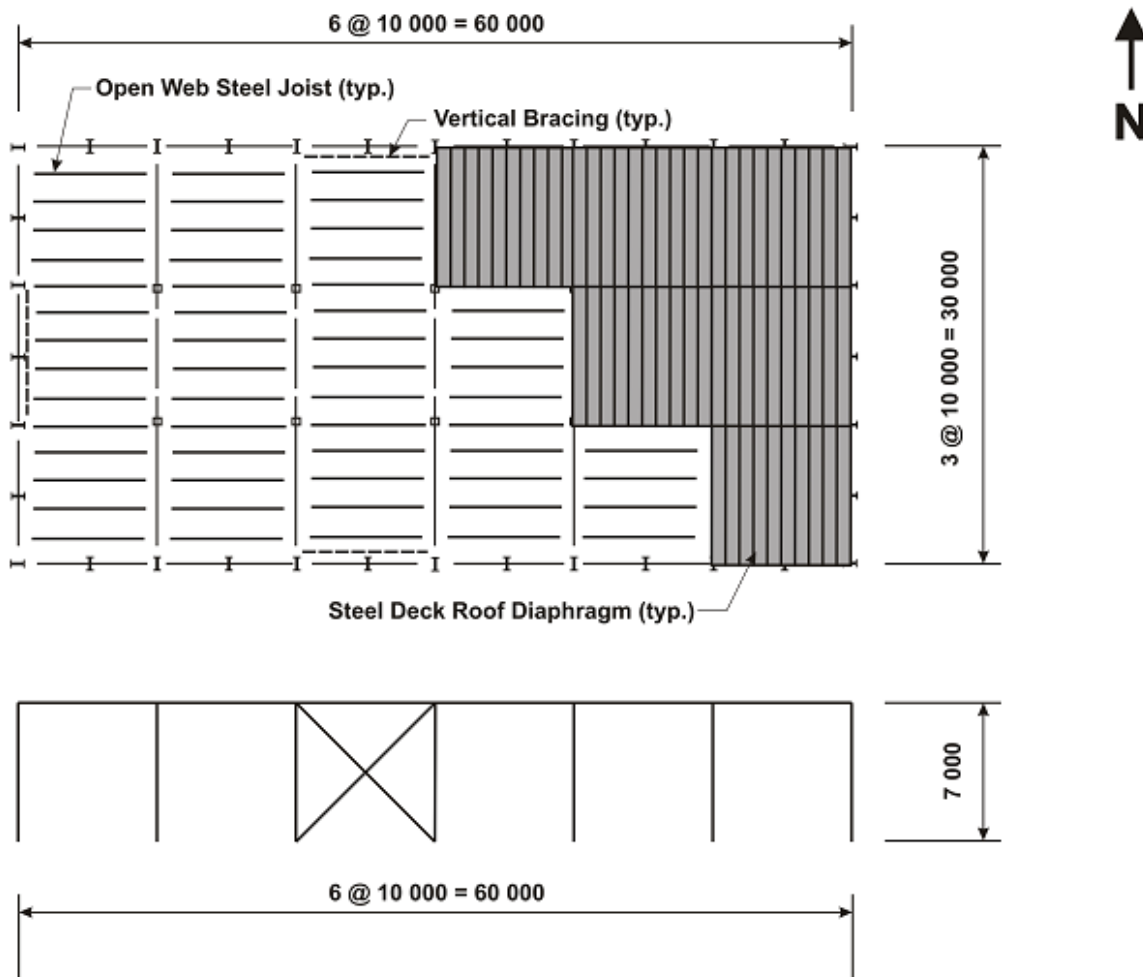
Figure 3.3 – A typical 30m×60m×7m single-storey building (Design 2) (dimensions in mm)

3.3 Design Load

The expected loads and their factored combinations were determined following Clause 4.1.3.2(2) of the 2010 NBCC. In Clause 4.1.5.5(2) of the NBCC, it is specified that only the snow load or the live load need be considered in the load combination for exterior areas (inaccessible to pedestrians). Since the snow load was relatively high for both Abbotsford and Montreal compared to the 1.0 kPa live load for roofs not accessible to the public, only the snow load was considered in design. The seismic force resisting members, including braces, beams and column members, as well as perimeter beam members were designed for the D+E+0.25S load combination, where D, E and S are the dead load, earthquake load and snow load, respectively. Gravity load carrying members, i.e., the open web steel joists, interior columns and beams, were designed for the 1.25D + 1.5S load combination. For the design of the exterior column members, the two load combinations 1.25D + 1.5S + 0.4W (wind load) and 1.25D + 1.4W + 0.5S were considered. The seismic weight of D+0.25S was considered as defined in Clause 4.1.8.2 of the NBCC.

The roof dead load generally consists of: roof ballast, vapour retarder, HVAC units, electric and sprinkler systems, insulation systems, dead load of open web steel joists and beam members as well as the self weight of the steel deck. The estimated value of the dead load was 1.1 kPa plus the self weight of steel roof deck panels. The estimated dead load of the exterior walls was 0.35 kPa. The walls were assumed to be composed of an insulated metal cladding system having metal sheets on the interior as well as the exterior side. These values were identical to those considered by Massarelli (2010). The design snow load, wind load and seismic load are discussed in the following sections.

3.3.1 Snow load

The 2010 NBCC provides a basic equation to determine snow loads:

$$S = I_s[S_s(C_b C_w C_s C_a) + S_r] \tag{3.1}$$

Where,

S =   Specified snow load (kPa)

S_s, S_r =   1-in-50 year ground snow load and associated rain load, (kPa)

C_b =   Basic roof snow load factor

I_s =   Importance factor for snow load, 1.0

C_w =   Wind exposure factor, 1.0

C_s =   Roof slope factor, 1.0

C_a =   Roof shape factor, 1.0

Snow accumulation due to the HVAC units was also considered, as given in the 2005 NBCC Commentary G-11, and assumed uniformly distributed over the entire roof area since the exact position of the units was not specified. This increased the snow load by about 7%. The values of the snow load parameters I_s, C_w, C_s and C_a were considered 1.0. The values of other snow load parameters S_s, S_r, C_b and S for the building considered are given in Table 3.1. The total snow loads, S_{total} , which includes the snow accumulation load due to the HVAC units are also provided.

Table 3.1 – Snow load and parameters

Snow load and parameters	Location	
	Abbottsford	**Montreal**
S_s (kPa)	2.0	2.6
S_r (kPa)	0.3	0.4
C_b	0.8	0.8
S (kPa)	1.9	2.48
S_{total} (kPa)	2.03	2.58

3.3.2 Wind load

Wind loading was considered in the design of the exterior columns based on Cl. 4.1.7 of the 2010 NBCC (Equation 3.2). The wind was assumed to act independently in the N-S and E-W directions (Figure 3.2 and Figure 3.3). The reference velocity pressure *q* for the 50 years return period was 0.44 kPa for Abbottsford, BC and 0.42 kPa for Montreal. The exposure factor C_e was

taken as $(h/10)^{0.2}$ where h is the height of the buildings. The calculated specified external pressure in the high pressure zone, considering critical wind direction which is parallel to the east-west direction, is given in Table 3.2. The corner columns were designed for biaxial moments considering these wind pressures. Other external columns were designed conservatively by taking into account the high pressure zone wind pressure. Since the buildings were located in high seismic zones, the lateral force due to wind load on the lateral resisting members, including steel roof diaphragms, was significantly lower than the lateral force due to earthquake. The lateral deflection of the buildings due to wind load was lower than the allowable drift h/200 for industrial buildings.

$$p = I_w q C_e C_g C_p \qquad (3.2)$$

Where,

$p =$ Specified external pressure acting normal to the surface (kPa)

$I_w =$ Importance factor for wind, 1.0

$q =$ Reference velocity pressure

$C_e =$ Exposure factor

$C_g =$ Gust effect factor

$C_p =$ External pressure coefficient

Table 3.2 – Specified external pressure (kPa) in the high pressure zone

Abbottsford, BC		Montreal	
E-W	N-S	E-W	N-S
0.47	- 0.37	0.45	-0.35

3.3.3 Seismic load

The seismic load on a building depends on several factors including the type of seismic force resisting system and the fundamental period of the structure. An overview of the seismic force

calculations is provided in Section 1.5.1.2. The design base shear was determined using the equivalent static load procedure (NBCC, 2010) (Equation 1.1). Equation 1.2 provides the fundamental period (T_a) of 0.175 s for the medium size building (7 m height); therefore, 0.35 s is the limiting period of vibration as per the 2010 NBCC for the four medium sized buildings considered (Structural system A through D). The accidental torsion effects were considered to calculate the lateral brace forces (and to calculate shear force on the diaphragm) by using a 10% eccentricity in the plan dimension perpendicular to the direction of seismic loading. All the buildings were designed for normal importance ($I_E = 1$) and assumed to be built over very dense soil or soft rock (reference soil condition class C); hence, the acceleration based site coefficient (F_a) and velocity based site coefficient (F_v) were 1.0. Similarly, the base shear adjustment factor, M_v, for higher mode effect was set to 1.0 for all the buildings. The seismic mass consisted of the dead load plus 25% of the snow load including the accumulation effects. The top half of the perimeter walls was considered to contribute to the seismic weight in the roof.

CSA S16 (2009) requires that the P-Δ effects along with a horizontal notional load be considered to determine the design member forces induced by seismic loads. The horizontal notional load was taken as 0.5% of the total gravity load on the building. The effects of lateral forces including the notional load should be multiplied by a factor U_2, as given by Equation 3.3, to account for the P-Δ effects. However, as written in the NBCC Commentary (2005), Cl. 4.1.8.3 (8), the U_2 factor can be taken as 1.0 if the value provided by Eq. 3.3 is less than 1.1. The value of the U_2 factor was less than 1.1 for the four buildings, and hence 1.0 was taken for design.

$$U_2 = 1 + \frac{\sum C_f R_d \Delta_f}{\sum V_f h} \tag{3.3}$$

Where,

$U_2 =$ Amplification factor to account for second-order effects

$C_f =$ Total gravity load carried by columns

$R_d =$ Ductility-related force modification factor

Δ_f = First-order displacement of the structure due to factored loads

V_f = Factored shear force on the structure

h = Height of the structure

3.4 Design of Gravity resisting members

As mentioned in Section 3.3, the gravity load carrying members including the open web steel joists, interior columns and beams were designed for the 1.25D + 1.5S load combination. Two load combinations, 1.25D + 1.5S + 0.4W (wind load) and 1.25D + 1.4W + 0.5S were considered for the design of the exterior column members. The open web steel joists (OWSJs) consisted of double angle section top chord which was designed and selected from the Canam joist catalogue (Canam Group Inc., 2008a). The depths of the OWSJs for Abbotsford and Montreal were 650 mm and 700 mm, respectively, which provided for the most economical design. The interior beams were cantilevered to a 20% length of span over the supporting columns to form a Gerber system so as to reduce the span moment. Link (suspended) beams were designed to span the remaining distance. The external column members were assumed to be braced laterally in their weak axis at the mid height by a girt system attached to the columns.

Table 3.3 – Design Summary of Gravity members

Members	Location	
	Abbotsford (BC)	**Montreal (QC)**
Joist top chord section (in.)	1 ¾ × 1 ¾ × 5/32	1 ¾ × 1 ¾ × 5/32
Interior columns	HSS 178 × 178 × 6.4	HSS 178 × 178 × 8.0
Exterior columns	W200 × 31	W200 × 36
Corner columns	W200 × 31	W360 × 39
Gerber cantilever beams	W530 × 85	W530 × 85
Gerber link beams	W460 × 60	W460 × 60

A summary of the shape and size of the gravity resisting members (excluding perimeter beam members) of the medium size building is presented in Table 3.3. The gravity design loads were higher for buildings located in Montreal than those in Abbotsford due to the larger snow load. However, the design gravity loads for each location were nearly equal in all the structural

systems, and hence, the design sections of gravity members remained unchanged. Regarding the design of the perimeter beams, in addition to the gravity load, an axial compressive force should also be accounted for. The axial compressive force on the beams was the greater of two actions: the force due to the flexural response of the diaphragm, or if the load was from the other direction, the force due to the transfer of shear force from the diaphragm to the bracing bents. The design of the perimeter beam members were also checked such that the compressive resistance of the top flange of the beam section was greater than the total compressive force on it; the total force being compressive due to flexural response of the diaphragm under earthquake load and the compressive force due to strong axis bending under gravity load. However, this check was not a standard practice. It was done with the assumption that the bottom flange of the beam was not laterally braced and hence, as a result of the lateral torsional buckling of the member, it would not be able to carry the compression force due to the flexural response of the diaphragm. The top flanges of the perimeter beams, that were perpendicular to the OWSJs, were assumed to be laterally braced by the OWSJs. For the perimeter beam members that were parallel to the OWSJs, it was considered that the steel deck would provide continuous lateral bracing at their top flange.

3.5 Design of Steel deck roof diaphragms

The 38 mm deep by 914 mm wide P-3606 corrugated steel deck profile manufactured by the Canam Group was selected for the buildings. The panels are cold rolled from ASTM A 653M SS Grade 230 steel having a minimum yield strength, ultimate tensile strength and modulus of elasticity of F_y = 230 MPa, F_u = 310 MPa and E = 203,000 MPa, respectively. The diaphragm action was obtained by fastening Hilti X-EDNK19 and X-EDNK22 powder-actuated pins to the underlying frame and using #12 self-tapping screws to connect the panels to each other. The two different frame fastening powder actuated pins were selected to satisfy installation requirements for the different thickness of frame members.

The SDI methodology (Luttrell, 2004), as discussed in the Section 1.5.3.2, was used for the design of the roof diaphragm. The factored shear strength of the diaphragm was calculated by multiplying the SDI nominal shear resistance S_n with a resistance factor ϕ = 0.6 as specified in

CSA S136 (2007) for mechanical fasteners. The deck sheets were assumed to be of 10 m total length spanning over open web steel joists spaced at 2.0 m o/c. The design force on the diaphragm depends upon the type of structural system used in design (A through D) and hence is discussed separately in the design section of the each structural system. The steel deck were also checked for the gravity load (1.25D+1.5S) using Canam steel deck catalogue (Canam Group Inc., 2008b)

3.6 SAP 2000 building model

The designed buildings were modeled in SAP 2000 (CSI, 2010) to verify the initial assumption of fundamental period of vibration and to ensure compliance with the 2010 NBCC inelastic drift limit of $0.025h_s$ for normal buildings under seismic load, where h_s is the storey height of a building. Figure 3.4 shows a CBF building model in SAP 2000; a similar model for the EBF buildings was also developed. Frame elements were used to model all the longitudinal members. Pinned connections were used between all the members except for the Gerber cantilevered beams which were continuous up to the link beams. Also, the pin connections were used at the base of the external and the internal column members. However fixed connections were used for the bases of column members of the braced frames assuming stiff foundations at those places.

Shell elements (2 m × 2 m) with the thickness of the steel deck panel were used to represent the diaphragm where mass and stiffness modifiers were applied to account for the roof mass and diaphragm shear stiffness. The mass modifier was calculated using Equation 3.4. The shear stiffness modifier as given in Equation 3.5 was also needed as the shear stiffness of a corrugated deck sheet will be less than that of a flat plate of the same thickness. An axial stiffness modifier was also used in the both direction of the deck sheet. The axial stiffness modifier in the longitudinal direction of deck sheet was equal to the ratio of actual cross sectional area of corrugated deck sheet and the cross sectional area considering it as a flat plate. Negligible axial stiffness was provided in the perpendicular direction of deck length as the deck was considered to be very flexible in that direction. The OWSJs were modeled by specifying only the top chord (double angle section); this approach was taken because it was assumed that only the top chord would participate in the flexural as well as axial response of an OWSJ when subjected to
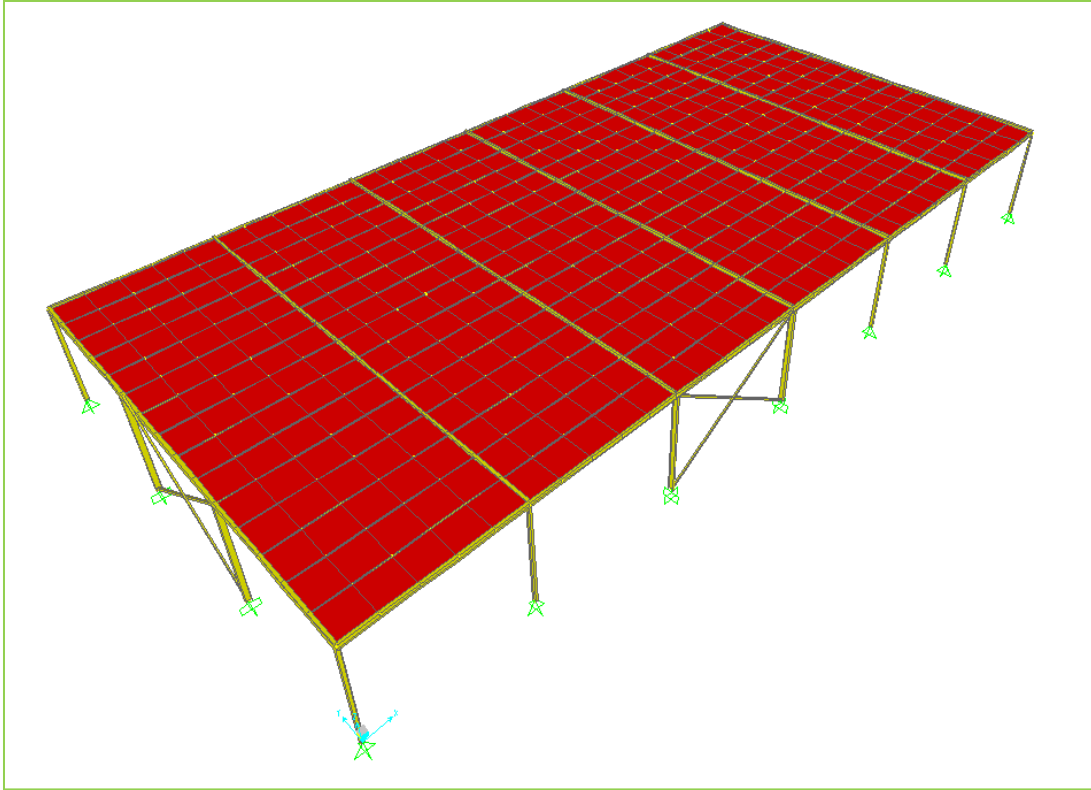
Figure 3.4 – CBF Building model in SAP 2000

$$\text{Mass modifier} = \frac{w_f}{\gamma t} \tag{3.4}$$

Where,

$w_f =$ Factored seismic weight per unit area on the roof (1.0D+0.25S)

$\gamma =$ Weight per unit volume of cold-formed steel

$t =$ Thickness of steel deck

$$\text{Shear stiffness modifier} = \frac{G'}{G/t} \tag{3.5}$$

$G' =$ Diaphragm shear stiffness

$G =$ Shear modulus of cold-formed steel

$t =$ Thickness of steel deck

horizontal loading in two different principal directions. The seismic weight of the perimeter wall was assigned as lumped mass to the nodes of the perimeter beams.

3.7 Design of type MD concentric braced framed buildings (System A)

The moderately ductile (MD) concentrically braced frame buildings (R_d = 3.0, R_o = 1.3) were designed to dissipate energy mainly by inelastic elongation and buckling of the vertical brace members. All other structural members in the SFRS including the roof diaphragm were designed considering the probable yield tensile resistance and the probable compression resistance as well as the post buckling compression capacity of the bracing members. This system is examined only for the Abbotsford site. For the design of roof diaphragms, a modified approach was used, i.e., the capacity design forces were limited to those corresponding to R_dR_o =2 instead of R_dR_o of 1.3 as currently specified in CSA S16. This design assumption may result in the diaphragm entering into the inelastic range of behaviour. Design forces in the other structural members were determined following the seismic capacity procedure required by the 2010 NBCC. As part of this research the performance of the so-designed structure was examined to determine whether the modified design method is acceptable (see Section 4.4.1). Various bracing configurations are permitted under the type MD concentrically braced frame category (structural system A) in the 2010 NBCC. Among them, the popular X configuration tension / compression bracing was chosen for design and analysis. To analyze the effects of diaphragm flexibility and period limitation on design and on the dynamic response, three design cases were selected for the medium sized buildings as shown in Table 3.4. However, for the large sized buildings, only two design cases were selected. The detailed design of the large sized buildings is presented in Appendix D (Table D2 to D4).

The design case AVM0 is representative of current design practice and is as per the 2010 NBCC. For that case, the diaphragm shear stiffness was set equal to that obtained from the SDI method. For the AVM1 and AVM2 designs, 70% of the SDI shear stiffness was retained for design, which was close to the average shear stiffness found in the Phase I, II and III diaphragm tests (Franquet, 2010 and Massarelli, 2010), as discussed in Sections 2.4.5 and 2.6. It is noted that label AVMx denotes: A for structural system, V for Vancouver (Abbotsford is close to

Vancouver city), M for medium size building and x for the design case (0, 1 or 2). In design cases AVM0 and AVM1, the limitation provided by the 2010 NBCC on the fundamental period of vibration of such buildings was applied. Hence the period was limited to $T_a = 0.35$ s. In the design case AVM2, the period was not constrained by the 2010 NBCC limit. For the design of AVM2, an iterative "design and analysis" process was carried out until both the design and the analysis (SAP 2000 model) provided the same fundamental period of vibration. In other words, the design period was determined from the numerical model (SAP 2000) following the iteration of "design and analysis". The initial trial fundamental period was set equal to $T_a = 0.35$ s.

Table 3.4 – Design matrix of CBF buildings (System A) (Abbotsford, BC)

Building size	30m×60m×7m			40m×90m×8m	
Diaphragm shear stiffness	SDI G'	70% of SDI G'		SDI G'	70% of SDI G'
Time period limitation	$T_a = 0.35$ s	$T_a = 0.35$ s	NL	$T_a = 0.4$ s	NL
Design Case	AVM0	AVM1	AVM2	AVL0	AVL2

3.7.1 Design comparison and discussion

As discussed in Section 3.3.3, the values of the higher mode factor (M_v), the acceleration based site coefficient (F_a) and the velocity based site coefficient (F_v) were set equal to 1.0. Hence, the design spectral value $S(T_a)$ and the 5% damped spectral response acceleration values $S_a(T_a)$ were equal. As given in Equation 1.1, the upper limit on the seismic design base shear corresponding to 2/3 of S(0.2) was considered in design. For Abbotsford, BC, 2/3 $S_a(0.2) = 0.66$ which, coincidentally, is equal to the value of $S_a(0.5)$.

Table 3.5 shows the dynamic characteristics and design parameters for the AVM0 AVM1, and AVM2 buildings in the N-S direction. Period limitation was used for the AVM0 and AVM1 buildings, and the upper limit of design base shear from Equation 1.1 controlled the base shear force. The use of 70% SDI stiffness in the AVM1 building resulted in a slightly longer period in comparison to the AVM0 building for which G' was not reduced. Similarly, the actual period is slightly longer in the AVM2 building compared to the actual period of the AVM1 building for which the period was limited to $T_a = 0.35$ s. Since the actual periods were used as design periods in the AVM2 building, there existed the potential for some decrease in the design spectral value

and base shear force; however, as the design period was not considerably longer than 0.5 s, the base shear was not significantly lower than the upper limit of the base shear. Because of this, the use of an unlimited period in design has no significant effects on member design forces. This was not a case in the design of a large building (Appendix D, Table D3). Fundamental periods in the E-W directions are also given in Table 3.5 for completeness. Because of the shorter diaphragm span, the difference between the actual periods and NBCC limit are smaller. The periods computed with rigid diaphragm assumptions are also given in the Table 3.5. These periods are close to the code upper limit, which is in consistent with rigid diaphragm assumption behind NBCC period values. Because of the longer span, diaphragm effects are more significant along the N-S direction.

Design details of AVM0, AVM1 and AVM2 are given in Table 3.6. Since the bracing system was tension/compression CBF, the design lateral forces were equally shared between the compression and tension diagonal members. The diagonal members were designed for the compression force as the tensile strength of the member would be much higher than its compressive strength. The design force in the brace members was only slightly lower in the

Table 3.5 – Seismic properties of CBF buildings (System A) (Abbotsford, BC)

Details	Design case		
	AVM0	AVM1	AVM2
Actual fundamental period with diaphragm flexibility and design period (shown in bracket)			
N-S Direction (s)	0.49 (0.35)	0.52 (0.35)	0.54 (0.54)
E-W Direction (s)	0.41 (0.35)	0.42 (0.35)	0.43 (0.43)
Actual fundamental period with rigid diaphragm assumption			
N-S Direction (s)	0.36	0.36	0.36
E-W Direction (s)	0.36	0.36	0.36
Design spectral value S(Ta) (g)	0.825	0.825	0.640
Seismic Weight W (kN)	3347	3347	3347
Base shear V^1 (kN)	708	708	549
Upper limit on Base Shear^2 (kN)	565	565	565

[1]Corresponds to total base shear, [2]Corresponds to 2/3 S(0.2 s).

Table 3.6 – Design details of CBF buildings (System A) (Abbotsford, BC)

Details	Design case		
	AVM0	AVM1	AVM2
Vertical brace (at N-S sides)			
Factored compression force, C_f (kN)	212	212	206
Brace section (HSS)	$114 \times 114 \times 6.4$	$114 \times 114 \times 6.4$	$114 \times 114 \times 6.4$
Factored compression resistance, C_r (kN)	230	230	230
Probable tension resistance T_u (kN)	1104	1104	1104
Probable compression resistance, C_u (kN)	337	337	337
Post buckling strength, C'_u (kN)	220	220	220
Storey shear corresponding to $C_u + T_u$ (kN)	1181	1181	1181
Storey shear corresponding to $C'_u + T_u$ (kN)	1085	1085	1085
Storey shear corresponding to R_dR_o=1.3 (kN)	1274	1274	988
Storey shear corresponding to R_dR_o=2.0 (kN)	828	828	642
Column member	W310 × 39	W310 × 39	W310 × 39
Beam member	W310 × 33	W310 × 33	W310 × 28
Vertical brace (at E-W sides)			
Factored compression force, C_f (kN)	212	212	206
Brace section	$114 \times 114 \times 6.4$	$114 \times 114 \times 6.4$	$114 \times 114 \times 6.4$
Factored compressive resistance, C_r (kN)	230	230	230
Probable tension resistance, T_u (kN)	1104	1104	1104
Probable compression resistance, C_u (kN)	337	337	337
Post buckling strength, C'_u (kN)	220	220	220
Storey shear corresponding to $C_u + T_u$ (kN)	1181	1181	1181
Storey shear corresponding to $C'_u + T_u$ (kN)	1085	1085	1085
Storey shear corresponding to R_dR_o=1.3 (kN)	1274	1274	1139
Storey shear corresponding to R_dR_o=2.0 (kN)	828	828	740
Column member	W310 × 39	W310 × 39	W310 × 39
Beam member	W410 × 60	W410 × 60	W410 × 54
Perimeter Beams			
N-S sides	W360 × 51	W360 × 51	W310 × 39
E-W sides	W360 × 51	W360 × 51	W360 × 51
Design of Diaphragm			
Shear force S_f(kN/m)	39.4	39.4	39.4
Limiting shear force S_{limit} (kN/m)	27.6	27.6	21.4
Factored shear resistance ϕS_n (kN/m)	28.4	28.4	22.2
Thickness of deck (mm)	1.21	1.21	1.21
Shear stiffness G' (kN/mm)	37.5	37.5	33.3
Frame fasteners pattern	36/7	36/7	36/7

Table 3.6 – Design details of CBF buildings (System A) (Abbotsford, BC) Cont..

Details	Design case		
	AVM0	AVM1	AVM2
Side lap spacing (mm)	100	100	150
Deflection using SAP models under seismic load at mid span (N-S)			
$\Delta R_d R_o$(mm)†	41.3	49.1	51.5
$\Delta_b R_d R_o + \Delta_d$(mm)*	26.8	29.4	29.4
Deflection using SAP models under seismic load at mid span (E-W)			
$\Delta R_d R_o$(mm)	29.2	32.0	32.0
$\Delta_b R_d R_o + \Delta_d$(mm)	25.2	26.8	26.8

* Δ_b - Elastic deformation at brace end, Δ_d - Elastic deformation of diaphragm, † Δ - Total elastic deformation at mid-span

AVM2 building because the upper limit of base shear controlled the design forces in the AVM0 and AVM1 buildings. The same brace section was selected in all three design cases due to similarity of the lateral forces. The lateral force, corresponding to the probable resistance of the brace members, in the SFRS of the AVM2 design was greater than the cut off force resulting from the base shear determined with $R_d R_o$ of 1.3 (shown in Table 3.6); hence, the cut off force was used in the design of the beam and columns of the braced frame.

The gravity load combination (1.25D+1.5S) controlled the design of the east and west side perimeter beams in the design of medium sized building. The total compression force due to earthquake load and gravity load on the top flange of the section controlled the design of the north and south side perimeter beams. This criterion controlled the design of all the perimeter beams of the large sized building. The shear force S on the diaphragms corresponding to the probable resistance of the brace members (corresponding to $C_u + T_u$) was 39.4 kN/m in all the three design cases as the same brace section was selected in each design case. The limiting shear force S_{limit} corresponding to the base shear determined with $R_d R_o$ of 2.0, which also includes the effect of accidental torsion as specified in NBCC, was smaller than the probable shear force S_f in all cases. Obviously, this value was lower than the shear determined with $R_d R_o$ of 1.3. The influence was more pronounced in the AVM2 design case as well as in the diaphragm design of the large size building (Appendix D, Table D4). The inelastic deflection at mid-span $\Delta R_d R_o$ was well below the drift limit provided by 2010 NBCC (0.025h) in all the design cases in both directions. The maximum inelastic displacement in the north to south direction at the mid-span

$\Delta R_d R_o$ was 41.3 mm in the AVM0 design case which increased to 49.1mm in AVM1 design case due to use of 70% of SDI shear stiffness for the diaphragm in the SAP model.

The maximum inelastic displacement at the mid-span of the buildings were also determined by multiplying the elastic displacement at the building edge Δ_b by $R_d R_o$ and adding to the elastic deformation of the diaphragm Δ_d. Although this method is not generally used in the practice, it was considered for study following an idea that the factor $R_d R_o$ should be applied only to the elastic displacement of the SFRS that yield under the design level earthquake loading. A similar study was done by Tremblay & Stiemer (1996) and by Medhekar and Kennedy (1999). In this structural system, the brace was expected to yield and hence the building displacement at the edge Δ_b was amplified with the factor $R_d R_o$. Values obtained with these methods are compared with the values obtained from non-linear models and discussed in Section 4.7 for all the structural systems through A to D.

3.8 Design of buildings with inelastic diaphragm (System B)

A modified 2010 National Building Code of Canada (NBCC) (NRCC, 2010) and the CSA S16 (CSA, 2009) design approach was used for the design of concentrically braced framed (CBF) single-storey steel buildings in which the diaphragms were specified as the fuse element in the SFRS. The design was carried out for two cities; Abbotsford, BC near Vancouver and Montreal, QC for the medium sized building. Where as, for the design of the large sized building, the building was assumed to be located in Abbotsford only. The X configuration tension-compression braces were selected and designed corresponding to the probable capacity of the steel roof diaphragm, and hence were intended to act as elastic elements. Tremblay and Rogers (2005) showed that a significant cost saving could be made using this design approach.

Given that a CBF building having the fuse element in the roof diaphragm is not specified as a seismic system in the NBCC or CSA S16 a trial value of the ductility related seismic force modification factor (R_d) of 2.0 was used for the design. This R_d value was recommended for diaphragms having 0.76 mm thick deck panels connected with screw side-lap and nail frame fasteners (Martin, 2002, Tremblay et al. 2004). An overstrength related force modification factor

(R_o) was evaluated using the expression $R_o = R_{size} \times R_\phi \times R_y \times R_{sh} \times R_{mech}$ (Mitchell et al., 2003). R_{size}, which is a size related overstrength factor, was selected as 1.0 because the diaphragm was designed close to the required strength by varying the spacing of its connections. A resistance factor $\phi = 0.6$ was used in design as recommended by CSA S136 (2007) and hence the factor $R_\phi = 1/\phi$ was set to 1.67. R_y corresponds to the ratio of actual strength to the minimum specified strength. From the test data of 41 screw side-laps and nail frame fasteners diaphragm tests, carried out by previous researchers (Essa 2001, Martin 2002, Yang 2003, Engleder and Gould 2010, Franquet 2010, Massarelli 2010), the weighted average ratio between the measured and the SDI prediction was obtained as 1.12. This value was set for R_y. The strain hardening related (R_{sh}) and collapse mechanism related (R_{mech}) overstrength factors were set to 1.0 because diaphragms typically do not exhibit strain hardening and redundancy. Thus the calculated R_o factor was 1.9 and the resulting R_dR_o was set to 3.8.

The seismic force on the bracing bents, perimeter beams and braced columns were calculated based on probable shear resistance of the diaphragm (R_yS_n) as shown in Figure 3.5. However, an upper limit on this capacity design force corresponding to the forces determined with $R_dR_o = 2.0$ was applied for the design of these members in consideration of their inherent ductility. This deviates from the current S16-09 provisions for ductile systems as the upper limit on capacity design forces is set to $R_dR_o = 1.3$. The value of 2.0 was selected as it approximately corresponds to the R_dR_o value of 1.95 that is assigned to Type CC (conventional construction) SFRS category. Whenever this upper limit controlled, the members also had to meet Class 2 section limits so as to delay local buckling in case the members are subjected to inelastic demand. For the design cases BVM1 and BMM1 (V = Vancouver, M = Montreal), iterations of design and analysis were carried out until both the design and analysis (SAP 2000 model) provided the same fundamental period of vibration.

Two design cases were selected for the medium and large sized buildings located in Abbotsford and Montreal as shown in Table 3.7. The shear stiffness of the diaphragm was set at 70% of the SDI value for the analysis and design of the building which was obtained from the dynamic tests of diaphragms. The building was modelled in SAP 2000 (CSI, 2010) similar to the buildings with ductile CBFs (Figure 3.4). In design cases BVM0 and BMM0, the fundamental period of vibration was limited to $T_a = 0.35$ s for design as per the 2010 NBCC. In design case BVM1 and

BMM1, the period was not limited. Detailed design calculations for the building for the design case BVM0 are presented in Appendix C. Further, for the design case BVM1, two alternatives were considered in design; in Design 1 (Figure 3.2), the open web steel joists were placed parallel to the shorter side of the building (Layout I diaphragm); in Design 2 (Figure 3.3), the joists were placed perpendicular to the shorter side of the building (Layout II diaphragm). In both designs, the joists were spaced at 2 m o/c. The dynamic tests of diaphragms specimens showed that the ductile response could be different in Layout I and Layout II orientation (Massarelli, 2010). For the BMM0 and BMM1 buildings, one of the design alternatives Design 1 was considered to study the influence of ground motion characteristics.
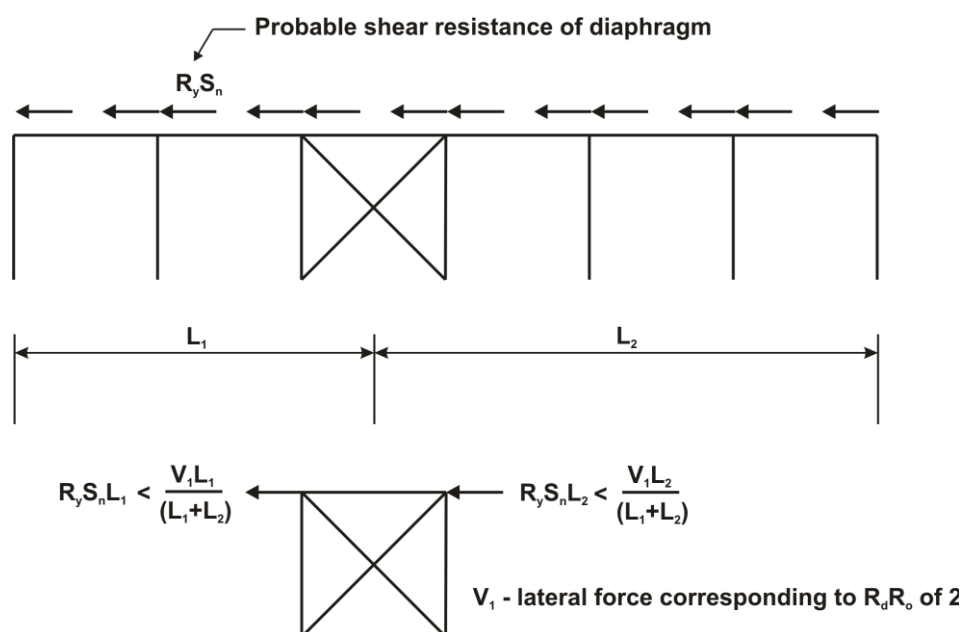
Figure 3.5 – Design lateral forces in CBF (System B)

Table 3.7 – Design matrix of buildings with inelastic diaphragm (System B)

Location	Abbotsford (BC)		Montreal (QC)		Abbotsford (BC)	
Building size	30m×60m×7m				40m×90m×8m	
Diaphragm shear stiffness	70% of SDI G'				70% of SDI G'	
Time period limitation	T_a=0.35 s	NL	T_a=0.35 s	NL	T_a=0.4 s	NL
Design Case	BVM0*	BVM1††	BMM0†	BMM1†	BVL0	BVL1

* Design 2, †† Design 1 and Design 2, † Design1

3.8.1 Design comparison and discussion

Table 3.8 shows the seismic characteristics along the shorter direction of the medium sized buildings designed for Abbotsford (BVM0 and BVM1) and Montreal (BMM0 and BMM1). The actual fundamental period of the BVM0 building and BMM0 building are 0.84 s and 0.90 s, respectively, thus significantly longer than the design period limited by 2010 NBCC ($T_a = 0.35$ s). Similar results were also found in the design of the large buildings with this structural system (Appendix D, Table D6). Diaphragms of the structural system B, particularly, are more flexible than the diaphragms of the other structural systems due to the lower design force on the diaphragm. Due to this, the discrepancy between the actual period of vibration and design period (with period limitation) is more pronounced in this system.

Table 3.8 – Seismic characteristics of buildings with ductile diaphragm (System B)

Details	Location			
	Abbotsford (BC)		Montreal (QC)	
Design Case	BVM0	BVM1	BMM0	BMM1
Actual fundamental period with diaphragm flexibility and design period (shown in bracket)				
N-S direction (s)	0.84 (0.35)	0.88 (0.88)	0.90 (0.35)	0.98 (0.98)
E-W direction (s)	0.48 (0.35)	0.52 (0.52)	0.54 (0.35)	0.58 (0.58)
Actual fundamental period with rigid diaphragm assumption				
N-S direction (s)	0.30	0.34	0.35	0.44
E-W direction (s)	0.27	0.31	0.35	0.39
Design spectral value S(Ta) (g)	0.825	0.402	0.475	0.147
Seismic Weight W (kN)	3255	3255	3505	3505
Base shear V^1 (kN)	707	344	438	135
Upper limit on Base Shear[2] (kN)	565	565	393	393

[1]Corresponds to total base shear, [2]Corresponds to 2/3 S(0.2 s).

The design of both the BVM0 and BMM0 buildings was controlled by the upper limit of the design base shear (Equation 1.1). Looking at the BVM1 and BMM1 buildings, the actual periods are only slightly longer compared to the corresponding actual periods of the BVM0 and BMM0 buildings. However, since the actual periods were used in the BVM1and BMM1 buildings as design periods, not the period corresponding to upper limit in T_a, a significant decrease in the

Table 3.9A – Design details of buildings with ductile diaphragm (System B) (Abbotsford, BC)

Details	Design case		
		BVM1	
	BVM0	**Design 1**	**Design 2**
Design of Diaphragm			
Shear force S (kN/m)	11.6	7.1	7.1
Thickness of deck (mm)	0.76	0.76	0.76
Frame fasteners patern	36/4	36/4	36/4
Side lap spacing (mm)	140	300	300
Factored shear resistance ϕS_n (kN/m)	11.6	7.3	7.3
SDI Shear stiffness G' (kN/mm)	6.5	5.9	5.9
Probable Shear Resistance $R_y S_n$ (kN/m)	21.7	13.6	13.6
Vertical brace (at N-S sides)			
Storey Shear corresponding to $R_y S_n$ (kN)	1304	820	820
Storey Shear corresponding to $R_d R_o = 2$ (kN)	806	392	392
Beam member	W310 × 39	W410 × 60	W310 × 39
Brace section (HSS)	152 × 152 × 8.0	178 × 178 × 4.8	178 × 178 × 4.8
Column member	W200 × 27	W200 × 27	W200 × 27
Vertical brace (at E-W sides)			
Storey Shear corresponding to $R_y S_n$ (kN)	652	410	410
Storey Shear corresponding to $R_d R_o = 2$ (kN)	806	631	631
Beam member	W360 × 51	W310 × 39	W360 × 45
Brace section	152 × 152 × 6.4	152 × 152 × 4.8	152 × 152 × 4.8
Column member	W200 × 27	W200 × 27	W200 × 27
Perimeter beams			
N-S sides	W310 × 39	W410 × 60	W310 × 39
E-W sides	W360 × 51	W310 × 39	W360 × 51
Deflection using SAP models under seismic load at mid span (N-S)			
$\Delta R_d R_o$(mm)†	91.6	92.0	93.8
$\Delta_d R_d R_o + \Delta_b$(mm)*	82.3	81.3	83.2
Deflection sign SAP models under seismic load at mid span (E-W)			
$\Delta R_d R_o$(mm)	50.2	51.3	55.5
$\Delta_d R_d R_o + \Delta_b$(mm)	36.2	35.9	38.7

* Δ_b - Elastic deformation at brace end, Δ_d - Elastic deformation of diaphragm, † Δ - Total elastic deformation at mid-span

design spectral values was found compared to the corresponding design base shear of the BVM0 and BMM0 buildings. The upper limit on base shear did not control for buildings BVM1 and BMM1. The change in the orientation of the deck sheets did not affect the period of the buildings and hence the design base shear was identical for the Design 1 and Design 2 BVM1 buildings. The buildings for Montreal were more flexible compared to the Abbotsford buildings due to the lower base shear which required smaller (less stiff) structural members and diaphragms.

The design details of the BVM0 and BVM1 buildings are shown in Table 3.9A. The calculated shear force on the diaphragm was 11.6 kN/m in the BVM0 building and 7.1 kN/m in the BVM1 (Design 1 and Design 2) buildings. The side-lap spacing and frame fastener patterns of the diaphragms were selected such that they provides the required shear resistance with a corresponding minimum shear stiffness to allow for a building with a longer period of vibration. The braces for all the sides of buildings were designed for the force corresponding to the probable shear resistance of the diaphragms. In most cases, the cut off force on these members corresponding to R_dR_o of 2.0 was smaller than the probable resistance of the diaphragm; as such the cut off force was used for the brace design. The perimeter beam sections are also given in Table 3.9A. The gravity load combination 1.25D+1.5S controlled the design of the perimeter beams that supported open web joist members for the buildings. Design of the large building with this structural system shows that this may not be the case for buildings having other dimensions. For the other perimeter beams where joists were not sitting directly on these members, the compressive force corresponding to the probable resistance of the diaphragms controlled their design. The inelastic mid-span deflections in the north-south and east-west directions are also presented in Table 3.9A. The inelastic deformation ΔR_dR_o for the BVM0 building at mid-span was 91.6 mm under the seismic load in the north-south direction. Use of the unlimited period in design for the BVM1 buildings did not increase the mid-span deflection considerably because the base shear was also reduced significantly due to the use of longer period in design. Also, the mid-span deflection in the Design 1 and Design 2 buildings was similar. The 2010 NBCC inelastic drift limit (0.025h) for the buildings was 175 mm.

Design details of the BMM0 and BMM1 buildings that were designed for Montreal are presented in Table 3.9B. The mid-span inelastic deflection ΔR_dR_o of the BMM0 and BMM1 buildings were smaller than the corresponding ΔR_dR_o of the BVM0 and BVM1 buildings even though the

buildings that were designed for Montreal were more flexible. This was due to the lower design spectral acceleration values for the Montreal region. The difference in design characteristics between BMM0 and BMM1 was similar to the difference between BVM0 and BVM1 as discussed above. The predicted displacements are discussed separately in Section 4.7.

Table 3.9B – Design details of buildings with ductile diaphragm (System B)
(Montreal, QC)

Details	Design case	
	BMM0	BMM1
Design of Diaphragm		
Shear force S (kN/m)	8.1	3.4
Thickness of deck (mm)	0.76	0.76
Frame fasteners patern	36/4	36/4
Side lap spacing (mm)	250	600
Factored shear resistance ϕS_n (kN/m)	8.3	4.8
SDI Shear stiffness G' (kN/mm)	6.1	5.3
Probable Shear Resistance $R_y S_n$ (kN/m)	15.6	9.0
Vertical brace (at N-S sides)		
Beam member	W 410 × 67	W410 × 67
Brace section (HSS)	152 × 152 × 4.8	127 × 127 × 4.8
Column member	W200 × 27	W200 × 27
Vertical brace (at E-W sides)		
Beam member	W310 × 28	W310 × 24
Brace section	152 × 152 × 4.8	102 × 102 × 4.8
Column member	W200 × 27	W200 × 22
Perimeter beams		
N-S sides	W410 × 67	W410 × 54
E-W sides	W310 × 28	W310 × 24
Deflection under seismic load at mid span (N-S)		
$\Delta R_d R_o$(mm)†	43.3	42.9
$\Delta_d R_d R_o + \Delta_b$(mm)*	38.3	36.8
Deflection under seismic load at mid span (E-W)		
$\Delta R_d R_o$(mm)	25.8	29.3
$\Delta_d R_d R_o + \Delta_b$(mm)	17.4	19.7

* Δ_b - Elastic deformation at brace end, Δ_d - Elastic deformation of diaphragm, † Δ - Total elastic deformation at mid-span

3.9 Design of Ductile eccentric braced framed buildings (System C)

Eccentrically braced steel frames (EBFs) ($R_d = 4$, $R_o = 1.5$) are very efficient structural systems for resisting seismic loads. They provide an excellent combination of strength, stiffness and ductility by combining the ductility characteristic of a moment frame with the stiffness characteristic of a braced frame. In this structural system the inelastic deformation is confined to a small length of the braced beam which is known as a link beam. It yields mostly in shear; however the design can be adjusted such that flexural yielding also occurs. Shorter links that yield in shear are generally preferable because of their more stable energy dissipation mechanism in comparison to the longer links that yield in flexure. The remaining elements of the seismic force resisting system including the beam sections outside the link beam and the diaphragm are designed based on the probable resistance of the link beam, and hence, are capacity protected. One issue with the EBF structures is that the yielding link element is a part of the beam; as such, the strength design and drift design of the structure are interlinked which can lead to a severely overdesigned seismic resisting system. A replaceable link element as described in Mansour et al. (2008) can be used to cancel out these coupled effects. This would not only allow for easier replacement of a damaged link following a major earthquake, but also allows the engineer to increase the size of the outer beams to resist the forces corresponding to the probable resistance of the link element. A design study of a ductile eccentrically brace framed building with a replaceable link element is presented in this section.

To ensure that the ductile capacity of the link beam has not been exceeded, the CSA S16 Standard (CSA, 2009) limits the inelastic shear link rotation γ_p to 0.08 radians for the shear critical link beam. Massarelli (2010) noted that this criterion could play an important role in the design of single storey buildings with an EBF structural system mainly because of its flexibility. The inelastic component of the total anticipated storey drift, θ_p, of the EBF for the factored seismic loading will become greater with an increase in the elastic drift demand, Δ_f, as shown in Equation 3.6. This increase in θ_p will in turn increase the inelastic shear rotation of the link beam, γ_p, as given in Equation 3.7.

$$\theta_p = \frac{3\Delta_f}{h_s} \tag{3.6}$$

θ_p =   Inelastic component of the total anticipated storey drift

Δ_f =   Elastic drift of EBF determined under factored seismic loading

h_s =   Storey height

$$\gamma_p = \frac{\theta_p L}{e} = \frac{3L\Delta_f}{eh_s} \tag{3.7}$$

γ_p =   Inelastic shear rotation of link beam relative to the outer beams, which shall not exceed the value of 0.08 radians for shear critical links (CSA, 2009)

θ_p =   As defined in Equation 3.6

L =   Bay width of EBF

e =   Length of the link beam

Two design cases were selected for the medium and large sized buildings as shown in Table 3.10. The design details of the medium sized buildings are presented in this section; for the large sized buildings, the design details are presented in Appendix D (Table D8 to D10). The shear stiffness of the diaphragm was set at 70% of the SDI value for the analysis and design of the building. The building was modelled in SAP 2000 (CSI, 2010) similar to the buildings with ductile CBFs (Figure 3.4). The fundamental period of vibration was limited to $T_a = 0.35$ s for design as per the 2010 NBCC in design case CVM0, whereas in design case CVM1, the period was not limited. For the design of these buildings, the size of the link element was initially selected to adequately resist the shear force induced by the seismic loading on it. Once the size was selected, the required length of the link was found such that only shear yielding will occur in the link. Additional requirements for the link length, as specified in CSA S16 (2009) were also considered.

Table 3.10 – Design matrix of EBF buildings (System C) (Abbotsford, BC)

Building size	30m×60m×7m		40m×90m×8m	
Diaphragm shear stiffness	70% of SDI G'		70% of SDI G'	
Time period limitation	$T_a = 0.35$ s	NL	$T_a = 0.4$ s	NL
Design Case	CVM0	CVM1	CVL0	CVL1

3.9.1 Design comparison and discussion

Table 3.11 shows the seismic characteristics along the shorter direction of the CVM0 and CVM1 buildings. The design of the CVM0 building, where a period limit was used, was controlled by the upper limit of the design base shear (Equation 1.1). The actual fundamental periods of the CVM0 and CVM1 buildings were found to be 0.64 s and 0.69 s respectively, which were significantly longer than the T_a limitation of 0.35 s. Use of unlimited fundamental period in design for the CVM1 building decreased the design base shear from 358 kN (CVM0) to 288 kN.

The length of the link beam was selected such as to satisfy the limit on inelastic shear rotation of link beam relative to the outer beams, γ_p. A link length of 660 mm was selected for the CVM0 building in both the north-south and east-west directions; this corresponds to the initial assumption of $R_d \Delta_f = 0.006 h_s$ and satisfies other shear yielding criteria as given in CSA S16. A link length of 570 mm was selected for the CVM1 building in both directions, which also corresponds to initial assumption of $R_d \Delta_f = 0.006 h_s$.

Design details of the CVM0 and CVM1 buildings are given in Table 3.12. The shear force demand on the link beam for the CVM0 design case was 165 kN, for which a W150 × 30 section

Table 3.11– Seismic properties of EBF buildings (System C) (Abbotsford, BC)

Details	Design case	
	CVM0	CVM1
Actual fundamental period with diaphragm flexibility and design period (shown in bracket)		
N-S Direction (s)	0.64 (0.35)	0.69 (0.69)
E-W Direction (s)	0.54 (0.35)	0.56 (0.56)
Actual fundamental period with rigid diaphragm assumption		
N-S Direction (s)	0.30	0.33
E-W Direction (s)	0.30	0.33
Design spectral value S(Ta) (g)	0.825	0.537
Seismic Weight W (kN)	3035	3035
Base shear V[1] (kN)	447	292
Upper limit on Base Shear[2] (kN)	358	358

[1]Corresponds to total base shear, [2]Corresponds to 2/3 S(0.2 s).

Table 3.12 – Design details of EBF buildings (System C) (Abbotsford, BC)

Details	Design case	
	CVM0	CVM1
Braced frame (at N-S sides)		
Shear force on link beam V_f (kN)	165	134
Shear resistance of link beam V'_p (kN)	196	167.3
Probable resistance of link beam $1.3R_yV'_p$ (kN)	285	242.7
Link beam	W150 × 30	W150 × 22
Length of Link Beam	660	570
Brace section (HSS)	178 × 178 × 8.0	152 × 152 × 8.0
Column member	W310 × 28	W310 × 28
Outer beam member	W310 × 33	W310 × 28
Braced frame (at E-W sides)		
Shear force on link beam V_f (kN)	165	134
Shear resistance of link beam V'_p (kN)	196	167
Probable resistance of link beam $1.3R_yV'_p$ (kN)	285	243
Link beam	W150 × 30	W150 × 22
Length of Link Beam	660	570
Brace section (HSS)	178 × 178 × 8	152 × 152 × 8.0
Column member	W310 × 28	W310 × 28
Outer beam member	W310 × 39	W310 × 28
Perimeter Beams		
N-S sides	W310 × 33	W310 × 33
E-W sides	W360 × 51	W360 × 51
Design of Diaphragm		
Shear force S (kN/m)	13.6	11.5
Limiting Shear force S_{limit} (kN/m)	26.9	17.5
Factored shear resistance ϕS_n (kN/m)	14	11.56
Thickness of deck (mm)	0.76	0.76
SDI Shear stiffness G' (kN/mm)	19.6	18.1
Frame fasteners patern	36/7	36/7
Side lap spacing (mm)	150	200
Deflection using SAP models under seismic load at mid span (N-S)		
ΔR_dR_o (mm)	72.6	80.4
$\Delta_bR_dR_o + \Delta_d$ (mm)	35.6	42.9
Deflection using SAP models under seismic load at mid span (E-W)		
ΔR_dR_o (mm)	57.0	58.8
$\Delta_bR_dR_o + \Delta_d$ (mm)	48.0	47.3

* Δ_b - Elastic deformation at brace end, Δ_d - Elastic deformation of diaphragm, † Δ - Total elastic deformation at mid-span

was selected. Using the unlimited period for design case CVM1 reduced the design shear force in the link beam to 134 kN, for which a smaller beam section W150 × 22 was selected that satisfied the inelastic rotation limit including shear yielding criteria. Similar to the other structural systems, the gravity load combination (1.25D+1.5S) controlled the design of the east and west side perimeter beams for both of the design cases. This was not the case in the design of the large size building. The total compressive force due to the earthquake load and gravity load on the top flange of the section controlled the design of the north and south side perimeter beams for both of the design cases. The inelastic deflection at mid-span $\Delta R_d R_o$ was well below the drift limit provided by 2010 NBCC in all the design cases in both directions. Further it should be noted that the limiting shear force S_{limit}, which is the force corresponding to $R_d R_o$ of 2.0, did not control the diaphragm design. The force on the diaphragm corresponding to probable resistance of link beam, S, was significantly lower than the limiting shear force S_{limit}. The probable shear resistance of the link beam was comparatively closer to the design shear force and hence the diaphragm in this system was not penalized significantly.

3.10   Design of buildings with Conventional Construction Type (System D)

Steel structures of the Conventional Construction category (Type CC structures) have limited capacity to dissipate the seismic energy input through localized yielding and friction that inherently exists in traditional design and construction practices ($R_d = 1.5$, $R_o = 1.3$). The 2010 NBCC specifies an R_d factor of 1.5 for this type of structure; therefore, their response is expected to be predominantly elastic with limited ductility demand. Cl. 27.11.1 of CSA S16 requires that diaphragms of steel framed buildings designed to resist seismic loads corresponding to R_d of 1.5 should have a ductile failure mode or the design seismic loads should be amplified by 1.5 so that the diaphragms remain mainly elastic. Inelastic cyclic loading tests on cantilever diaphragm

Table 3.13 – Design matrix of CC buildings (System D) (Abbotsford, BC)

Building size	30m×60m×7m			40m×90m×8m	
Diaphragm shear stiffness	SDI G'	70% of SDI G'		SDI G'	70% of SDI G'
Time period limitation	$T_a = 0.35$ s	$T_a = 0.35$ s	NL	$T_a = 0.4$ s	NL
Design Case	DVM0	DVM1	DVM2	DVL0	DVL2

specimens (Essa et al. 2003; Tremblay et al 2004; Engleder and Gould 2010) and dynamic tests on simply supported large-scale diaphragm assemblies (Tremblay et al. 2008b, Franquet 2010, Massarelli 2010) showed that diaphragms with screw side-lap and nail frame fasteners could exhibit inelastic deformation capacity.

Using screw side lap and nail frame fasteners connections to obtain the diaphragm action and considering its ductile behaviour, the diaphragms were designed to resist seismic loads corresponding to $R_d R_o$ of 1.95. The X configuration tension compression lateral bracing system (CBF) was chosen for design and analysis. Similar to the MD concentric brace framed building designs, three design cases were selected for the medium sized building to analyze the effects of diaphragm flexibility and period limitation on the design and on the dynamic response (Table 3.13). The design case DVM0 was the current design practice (as per the 2010 NBCC and CSA S16). The buildings were also modelled in SAP 2000 (CSI, 2010) (Figure 3.4). The fundamental period of vibration was limited to $T_a = 0.35$ s for design as per the 2010 NBCC in the design case DVM0 and DVM1, whereas in the design case DVM2 the period was not limited. For the large sized buildings, two design cases were selected. The design details of the large sized building are presented in Appendix D (Table D11 to D13).

3.10.1 Design comparison and discussion

Table 3.14 shows the seismic characteristics along the shorter direction of the DVM0, DVM1 and DVM2 buildings. Designs of the DVM0 and DVM1 buildings, where period limitation was used in the design, were controlled by the upper limit of the design base shear (Equation 1.1). The use of 70% SDI stiffness in the DVM1 building provided for a slightly longer period compared to the DVM0 building where the reduction in stiffness was not used. Similarly, the actual period was slightly longer in the DVM2 building compared to the actual period of the DVM1 building. Since the actual periods were used in the DVM2 buildings as design periods, a significant decrease in design spectral values was found. However, as the design period was not considerably longer than 0.5 s, the base shear was not appreciably less than the upper limit. In contrast, a much greater decrease in base shear was found in the design of large size building for the corresponding design case (Appendix D, Table D12).

Table 3.14 – Seismic properties of buildings with Conventional Construction (System D) (Abbotsford, BC)

Details	Design case		
	DVM0	DVM1	DVM2
Actual fundamental period and design period (shown in bracket)			
N-S Direction (s)	0.48 (0.35)	0.53 (0.35)	0.53 (0.53)
E-W Direction (s)	0.38 (0.35)	0.39 (0.35)	0.39 (0.39)
fundamental period with rigid diaphragm assumption			
N-S Direction (s)	0.30	0.30	0.30
E-W Direction (s)	0.30	0.30	0.30
Design spectral value S(Ta) (g)	0.825	0.825	0.64
Seismic Weight W (kN)	3291	3291	3291
Base shear V^1 (kN)	1392	1392	1080
Upper limit on Base Shear[2] (kN)	1114	1114	1114

[1]Corresponds to total base shear, [2]Corresponds to 2/3 S(0.2 s).

Design details of DVM0, DVM1 and DVM2 are given in Table 3.15. Although the actual fundamental period was longer to some extent in the DVM1 building than the DVM0 building, due to the use of 70% SDI shear stiffness of diaphragm, these two designs were identical as the period limit ($T_a = 0.35$ s) controlled the design in both buildings. Further, the design force on the vertical brace members and on the diaphragm were only slightly lower in the DVM2 building because the upper limit of base shear controlled the design forces in the DVM0 and DVM1 buildings. Hence, the designs in all the three case remained identical. However, this was not the case in the design of the large building with this structural system (Appendix D, Table D13). The gravity load combination (1.25D+1.5S) controlled the design of the east and west side perimeter beams for the medium sized building. The total compressive force due to earthquake load and gravity load on the top flange of the section controlled the design of the north and south side perimeter beams. This loading criterion controlled the design of all the perimeter beams in the design of large sized building. The inelastic deflection at mid-span, $\Delta R_d R_o$, was well below the drift limit provided by 2010 NBCC in all the design cases in both directions (Table 3.15). The

Table 3.15 – Design details of buildings with Conventional Construction (System D) (Abbotsford, BC)

Details	Design case		
	DVM0	DVM1	DVM2
Vertical brace (at N-S sides)			
Design force C_f (kN)	419	419	406
Brace section (HSS)	152 × 152 × 6.4	152 × 152 × 6.4	152 × 152 × 6.4
Brace resistance C_r (kN)	483	483	483
Column member	W360 × 33	W360 × 33	W360 × 33
Beam Member	W360 × 39	W360 × 39	W360 × 39
Vertical brace (at E-W sides)			
Design force C_f (kN)	419	419	406
Brace section	152 × 152 × 6.4	152 × 152 × 6.4	152 × 152 × 6.4
Brace resistance C_r (kN)	483	483	483
Column member	W360 × 33	W360 × 33	W360 × 33
Beam member	W360 × 51	W360 × 51	W360 × 51
Perimeter Beams			
N-S sides	W310 × 39	W310 × 39	W310 × 39
E-W sides	W360 × 51	W360 × 51	W360 × 51
Design of Diaphragm			
Shear force S (kN/m)	22.5	22.5	21.8
Factored shear resistance ϕS_n (kN/m)	25.0	25.0	25.0
Thickness of deck (mm)	0.91	0.91	0.91
Shear stiffness G' (kN/mm)	27.3	27.3	27.3
Frame fasteners patern	36/9	36/9	36/9
Side lap spacing (mm)	100	100	100
Deflection using SAP models under seismic load at mid span (N-S)			
$\Delta R_d R_o$ (mm)	45.6	52.2	51.5
$\Delta_d R_d R_o + \Delta_b$ (mm)	36.8	43.7	43.1
Deflection using SAP models under seismic load at mid span (E-W)			
$\Delta R_d R_o$ (mm)	27.5	28.6	28.3
$\Delta_d R_d R_o + \Delta_b$ (mm)	17.2	18.7	18.5

* Δ_b - Elastic deformation at brace end, Δ_d - Elastic deformation of diaphragm, † Δ - Total elastic deformation at mid-span

inelastic deformation $\Delta R_d R_o$ in the north to south direction was 45.6 mm in the DVM0 design case which increased to 52.2 mm in DVM1 design case.

3.11   Design comparison and conclusion

The fundamental periods of vibration in the N-S direction of the designed medium and large sized buildings, with all the structural systems and their corresponding design cases, determined using the SAP models are significantly higher than the T_a limit provided by the 2010 NBCC. The use of a rigid diaphragm assumption for the roof diaphragm in the SAP models resulted in periods of vibration close to the T_a limit. The NBCC recommended expressions for the design period are solely a function of the type of SFRS and the height of the building, regardless of the impact of the diaphragm flexibility (NRCC, 2010). The upper limit of the seismic design base shear corresponding to 2/3 S_a(0.2 s) controlled whenever the fundamental period T_a was limited to the code provision. This occurred because the design spectral acceleration value corresponding to $S(T_a)$ was greater than the value corresponding to 2/3 of S(0.2) for both the Abbotsford and Montreal regions. Also, the use of 70% SDI G' along with the $T_a = 0.35$ s period limitation did not affect the AVM1 and DVM1 designs compared to the AVM0 and DVM0 respectively where 100% SDI G' was used. Design cases corresponding to AVM1 and DVM1 were not considered for the large sized building.

Diaphragms of the structural system B, particularly, were more flexible than the diaphragms of the other structural systems. The medium and large sized buildings (BVM1 and BVL1), which contained a ductile diaphragm structural system and an unlimited design period, provided the longest fundamental period of vibration. This was mainly because the diaphragm itself acts as a fuse element in this structural system. As a result, the design seismic force on the diaphragm of this structural system was significantly lower compared to the design forces on the diaphragms of the other SFRS. Since the diaphragm was designed for this lower force, it was more flexible compared to the diaphragms of the other buildings.

Of the medium sized buildings with structural systems A and D, the use of an unlimited fundamental period in design decreased the design base shear to some extent but the decrease was not large enough to significantly change the initial designs controlled by the $T_a = 0.35$ s period limit. This was mainly because the upper limit in base shear controlled the initial designs where the period was limited to $T_a = 0.35$ s and the base shear corresponding to the actual period of structure was close to the upper limit of the base shear. The fundamental period, in general, will lengthen with an increase in the height and plan size of the buildings, whereas the upper

limit in base shear does not change with the change in the fundamental period of the structure. As a results, the design base shear for these design cases were considerably lower compared to the upper limit in the base shear in the design of large sized buildings. In a similar study by Tremblay et al. (2002) it was noted that the period computed using a numerical model was significantly longer than the period computed using the empirical formula from the NBCC. The difference between the two periods was more pronounced as the size of the building was increased.

When the period was limited to $T_a = 0.35$ s in the design of the medium sized buildings (located at Abbotsford) the design force on the diaphragm was: 27.6 kN/m for the CBF structural systems (System A), 11.6 kN/m for the ductile diaphragm structural system (System B), 13.6 kN/m for the EBF structural system (System C) and 22.5 kN/m for the CC structural system (System D). A thicker deck panel along with a more closely spaced fastener pattern was required for the diaphragm of CBF structural System A compared to all other systems due to the larger shear force. The high shear force on the diaphragm of the CBF building was attributed to the probable tension resistance of the brace member (1104 kN) which was significantly larger than the design compression force (212 kN). It is noted that the 27.6 kN/m shear force in System A was obtained even if the $R_dR_o = 2.0$ limit was applied; an even higher force equal to 39.4 kN/m would have been used if the current S16-09 requirement was applied. This difference in shear force on the diaphragm was more pronounced in the corresponding design of the large sized building (Appendix D, Table D4). In the EBF structural system however, the probable shear resistance of the link beam was comparatively closer to the design shear force and hence the diaphragm in this system was not penalized significantly. As a result, the design shear force on the diaphragm in this structural system was considerably lower compared to the design shear force on structural system A and D. For the buildings studied, the design shear force on the diaphragms with ductile diaphragm structural systems was the smallest in comparison to all other structural systems, which suggests that this design method could be an economical option in the design of the single-storey steel buildings. When the period was not limited, the difference in design shear force on the diaphragm of ductile diaphragm structural systems compared with the three other structural systems was more pronounced.

In all the design cases for buildings designed with a CBF structural system, the shear forces on the diaphragms corresponding to the probable capacity of the vertical bracing members were higher than the proposed limiting shear force based on R_dR_o of 2.0. This indicates that the response of the diaphragms in this structural system might not be fully elastic. In the design of buildings with an EBF structural system, it was found that the limit on the inelastic shear link rotation as given by the CSA S16 Standard (CSA, 2009) was more critical than the overall drift limit.

The P-Δ effects were found not to be significant in the design of the single-storey buildings for all the structural system considered. The amplification factor U_2 was less than 1.1 in all the design cases and hence the value of 1.0 was taken for it following the NBCC Commentary (2005), Cl. 4.1.8.3 (8). The inelastic deflection at mid span ΔR_dR_o was well below the drift limit $(0.025h_s)$ provided by 2010 NBCC in all the design cases in the both principle directions.

In all the medium sized building designs, the gravity load combination 1.25D+1.5S controlled the design of the perimeter beams that supported the open web joist members. However, this was not the case for the large buildings because the compressive force on beams corresponding to the shear force on the diaphragms or compressive force resulted from flexural response of the diaphragms was large enough to control their design. For the other perimeter beams where joists were not supported by these members, the total compressive force on the top flange of the section, due to the total effects of weak axis bending (earthquake load) and strong axis bending (gravity load), controlled the design (Appendix C).

Chapter 4 – Seismic behaviour of single-storey steel buildings

4.1 General

OpenSees building models were developed to perform non-linear time history dynamic analyses on the designed single-storey steel buildings, with the four structural systems and different design cases, which have been presented in Chapter 3. These models were developed to evaluate the overall behaviour of the buildings, including inelastic drift demand on the building and inelastic deformation demand on the fuse elements or/and on the diaphragm of the SFRS, under a suite of design level earthquake signals. The calibrated Pinching4 material modeling parameters obtained from the numerical modeling of the Phase I to III test specimens were used in the OpenSees building models to define the properties of the diaphragms. The calculated SDI nominal shear strength of the diaphragm (S_n) and 70% or 100% of SDI shear stiffness G', depending upon the design cases as described in Chapter 3, were used in the models. For the buildings designed with the inelastic diaphragm structural system, the non linear diaphragm model was implemented with an elastic vertical bracing system to develop the OpenSees building model. A non-linear concentric braced frame model in the OpenSees software platform, developed by Agüero et al. (2006) to simulate the hysteretic response of the vertical bracing members, was incorporated in the OpenSees models for the buildings with the CBF and CC type structural systems. For the buildings with EBF structural system, a non-linear OpenSees EBF model developed by Koboevic et al. (2011) was integrated with the non-linear OpenSees diaphragm models. Further, a study on the applicability of a strip mesh size for modeling roof diaphragms for building application is also presented in this chapter.

A series of earthquake records, and simulated ground motion signals provided by Atkinson (2009), were used in the analysis of the example buildings located in Abbotsford and Montreal. P-delta effects were included with gravity loads due to dead load plus 25% of the snow load applied to P-delta columns represented by Corotational truss elements along the diaphragm span in the model (see Figure 4.6). Rayleigh damping of 3% was specified in the first two symmetrical modes of vibration. The accidental torsion effects were not considered in the analysis. The response of the medium sized buildings designed for Abbotsford and Montreal,

using a record from the 1989 Loma Prieta earthquake and a closely matched simulated earthquake signal provided by Atkinson (2009) respectively, is presented in detail in this chapter. The response of the large sized buildings designed for Abbotsford under the design level earthquake signals is also presented.

4.2 Selection of earthquake Signals

In order to gain an understanding of the inelastic performance of the designed buildings, they were subjected to earthquake records and simulated signals that are representative of the location for which they were designed. Table 4.1 shows the historical earthquake records and simulated earthquake signals used to analyze buildings located in Abbotsford. A total of 11 earthquake signals were used to analyze the medium sized buildings. Out of these 11 earthquake signals, only 5 signals were used to analyze the large sized buildings. The historical motions were selected from the PEER ground motion data base. All the simulated ground motions were taken from the Seismic Toolbox website by G. Atkinson (2009). The selection of these ground motions, except the 1989 Loma Prieta record with next generation attenuation sequence number (NGA No.) 0805, was based on the de-aggregation of the 2% in 50 year hazard at the location, as determined from the historical seismic model. The M7.0 1989 Loma Prieta earthquake measured at the USGS (U.S. Geological Survey) Station 17 (NGA number 0805), Stanford Park Garage location (360°), which is at a epicentral distance of 50 km, was also used for the Abbotsford region, BC . Rainer et al. (1990) studied the nature and the extent of damage to buildings and lifelines due to the 1989 Loma Prieta Earthquake to predict the expected impact of similar magnitude earthquakes in the Greater Vancouver Area. They demonstrated that an earthquake with a similar frequency content and amplitude to the Loma Prieta earthquake could be expected for the Vancouver region. Since the city of Abbotsford (BC) is close to Vancouver, it was thought that this earthquake record could be used to study the response of the designed buildings. The earthquake signal was scaled with factor (SF) of 1.3 to the NBCC (2010) design uniform hazard spectrum (UHS) for Abbotsford (Site Class C) in order to match the design level ground motion for the region (Figure 4.1). The SFs applied for other earthquake signals are also show in Table 4.1. The SFs were chosen such that, at the average fundamental period of the models, the

spectral acceleration of the ground motion was approximately equal to the spectral acceleration of the UHS. The design NBCC UHS for Abbotsford and the scaled earthquake spectra of the historical earthquake records and simulated earthquake signals are shown in Figure 4.1 and in Figure 4.2 respectively. The responses of the designed buildings were evaluated by applying the design level ground motions parallel to the short direction of the buildings.

Table 4.1 – Historical earthquake records and simulated signals for Abbotsford (BC)

NGA No.	Event	M_W	Station	Dist. (km)	SF	Signal type
0805*	1989 Loma Prieta	7.0	Stanford Park Garage	50	1.3	Historical records
963*	Jan. 17, 1994 Northridge	6.7	Castaic, Old Ridge Route	21	0.6	
1005*	Jan. 17, 1994 Northridge	6.7	LA - Temple & Hope	31	1.7	
1039*	Jan. 17, 1994 Northridge	6.7	Moorpark - Fire Station	25	1.3	
1794	Oct. 16, 1999 Hector Mines	7.1	Joshua Tree	31	1.4	
15	July 21, 1952 Kern County	7.4	Taft Lincoln School	39	2.0	
10*	n/a	6.5	n/a	10	1.0	Simulated
34*	n/a	6.5	n/a	12	1.0	
13	n/a	7.5	n/a	30	1.0	
1	n/a	7.5	n/a	47	1.6	
16	n/a	7.5	n/a	65	2.0	

*Signals used for analyzing large sized buildings.
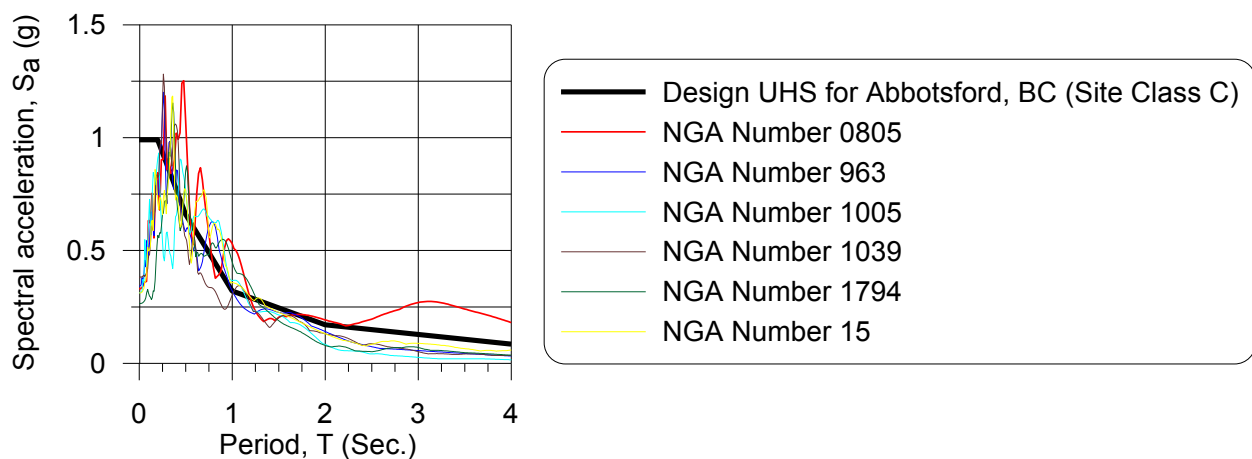
Figure 4.1 –Design NBCC(2010) UHS for Abbotsford (BC) and scaled earthquake spectra of historical records.
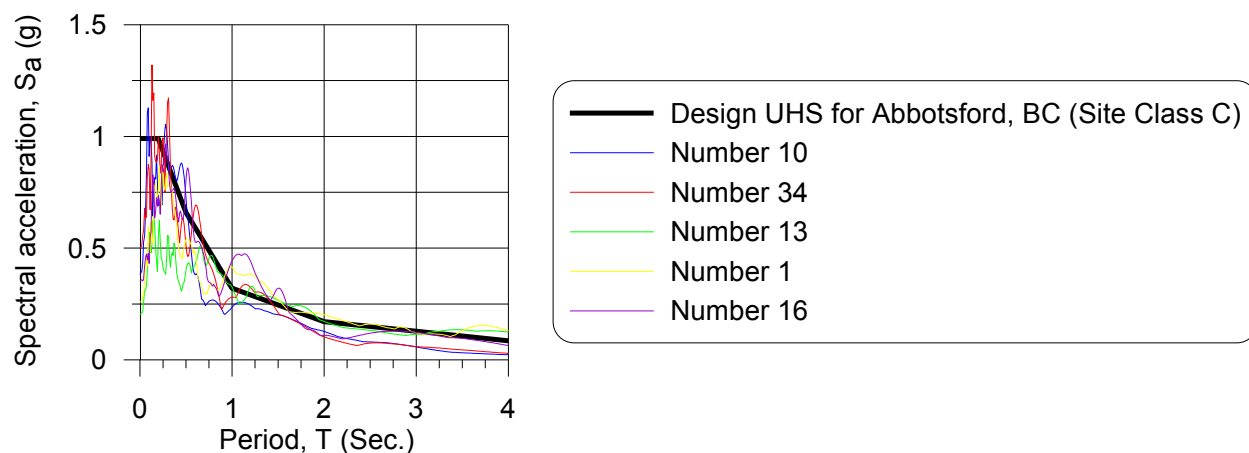
Figure 4.2 –Design NBCC(2010) UHS for Abbotsford (BC) and scaled earthquake spectra of simulated signals (5% damping).

Table 4.2 – Historical earthquake records and simulated signals for Montreal (QC)

Name/ Number	Event	Mw	Station	Dist. (kM)	SF	Signal type
CCN090	Jan. 17, 1994 Northridge	6.7	LA-Century City CC North	26	0.4	Historical records
WAI290	Jan. 17, 1994 Northridge	6.7	Huntington Beach Waikiki	57	1.3	
HNT000	Jan. 17, 1994 Northridge	6.7	Huntington Beach Lake St	76	1.6	
DEL090	Jan. 17, 1994 Northridge	6.7	Lakewood Del Amo Bvld	59	0.8	
H-E01140	Oct 15, 1979 Imperial Valley	6.5	El Centro Array #1	16	1.0	
24	n/a	7.0	n/a	70	n/a	Simulated
15	n/a	6.0	n/a	11	0.5	
1	n/a	6.0	n/a	13	0.5	
30	n/a	6.0	n/a	14	0.8	
34	n/a	6.0	n/a	17	0.8	
32	n/a	7.0	n/a	26	0.8	

In order to study the influence of ground motion characteristics, the medium sized buildings having an inelastic diaphragm as the fuse element in the SFRS were also designed for the Montreal region. Their behaviour was then evaluated by applying historical and simulated ground motions that are representative of the location (Table 4.2). The design NBCC (2010) UHS for Montreal region and the scaled earthquake spectra of the historical earthquake records and the simulated earthquake signals are shown in Figure 4.3 and in Figure 4.4, respectively. The historical ground motion set for Montreal was taken from the ensemble generated by Risk
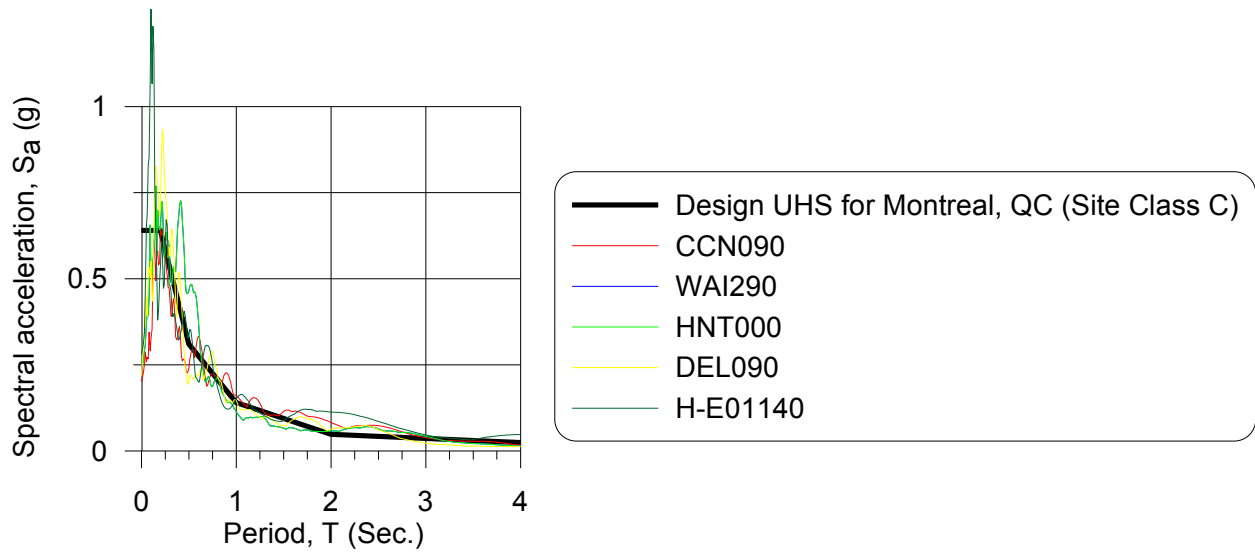
Figure 4.3 –Design NBCC(2010) UHS for Montreal (QC) and scaled earthquake spectra (Historical records).
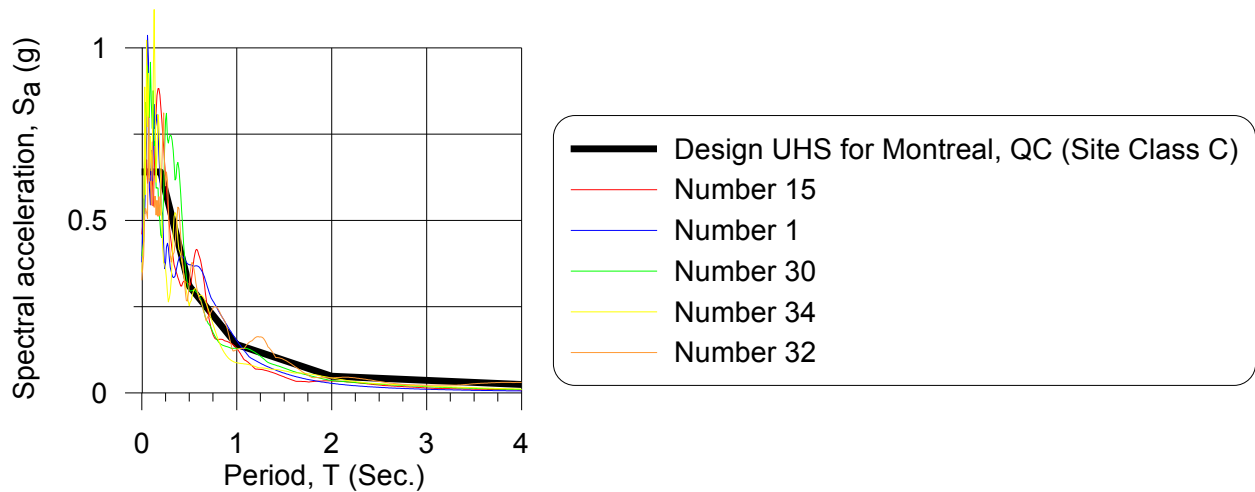
Figure 4.4 –Design NBCC(2010) UHS for Montreal (QC) and scaled earthquake spectra (Simulated signals).

Engineering, Inc. (2001) for Central Eastern US which was derived from ground motions recorded in the Western US considering the difference in crustal properties and source characteristics. The simulated ground motions were taken from the Seismic Toolbox website by G. Atkinson (2009). Again the selection of the ground motion, except for simulated signal 24, was based on the de-aggregation of the 2% in 50 year hazard at Montreal. The simulated signal 24 was characterized by a magnitude M7.0 earthquake recorded at 70 km from the epicentre and

was closely matched in the frequency domain using the SPECTRE software (Léger et al., 1993) to the Uniform Hazard Spectrum for Montreal, QC (Figure 4.5a and 4.5b).
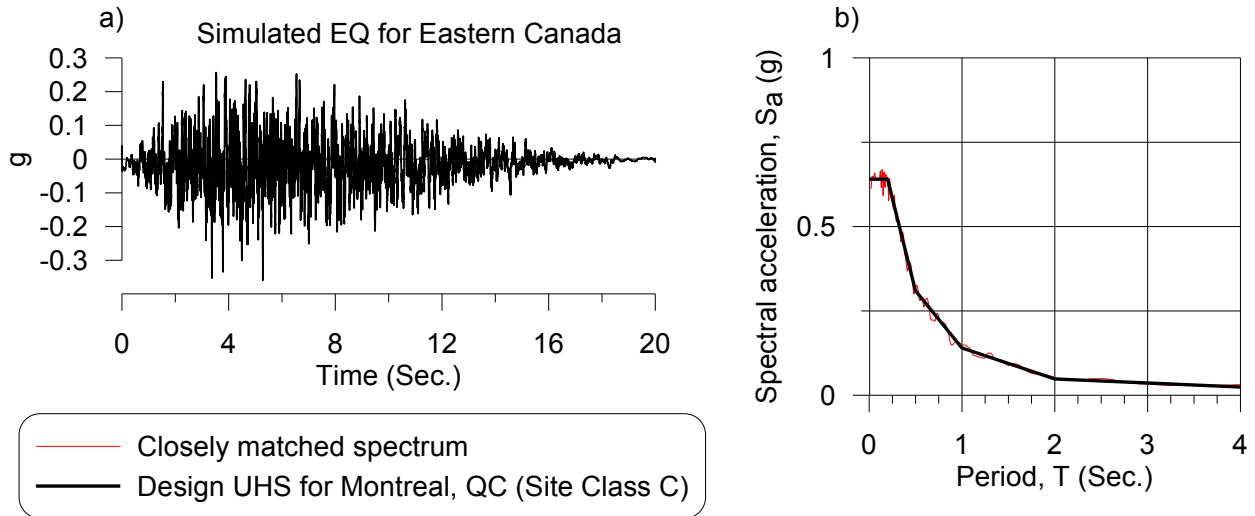
Figure 4.5 – a) Modified simulated earthquake signal, b) Design NBCC (2010) UHS for Montreal (QC) and closely matched spectrum (3% damping).

4.3 Numerical modeling of buildings designed with inelastic diaphragms (System B)

Designs of the buildings with an inelastic diaphragm as a fuse element in the SFRS are presented in Section 3.8. OpenSees models were developed for the designed buildings which were located at Abbotsford, BC, and Montreal, QC. Elastic truss elements were used to model the vertical tension/compression bracing members. The elastic bracing system was integrated with the non linear diaphragm model to develop the OpenSees building model. The Pinching4 material parameters obtained from the calibration of the numerical models of the Phase I to III diaphragm test specimens (0.76 mm thick deck) were used in the OpenSees building models. The nominal shear strength of roof diaphragm calculated using SDI method was used in the numerical model as it was comparatively closed to the probable shear strength. P-delta effects were included with gravity loads due to dead load plus 25% of the snow load applied to P-delta columns represented by Corotational truss elements.
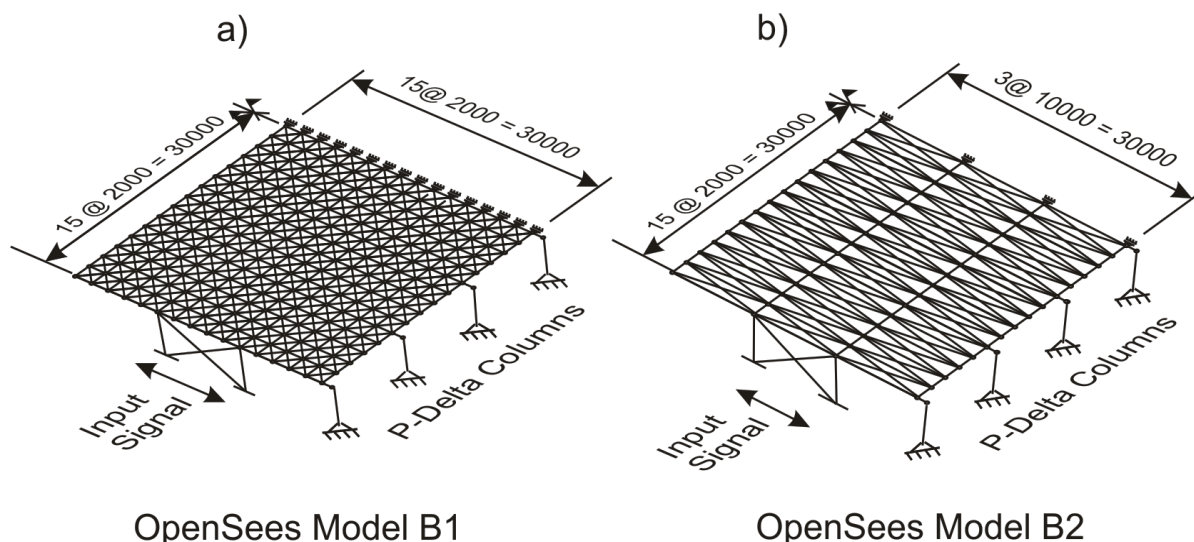
Figure 4.6 – OpenSees building models (Half of building size) with: a) 2 m by 2 m mesh size and b) 2 m by 10 m mesh size.

Table 4.3 – OpenSees models used for building designed with structural system B

Building location	Abbotsford BC					Montreal QC	
Design case	BVM0	BVM1				BMM0	BMM1
Design alternatives*	DESIGN 2	DESIGN 1		DESIGN 2		DESIGN 1	DESIGN 1
OpenSees model	B1	B1	B2	B1	B2	B1	B1

*Based on the layout type of diaphragms (Section 3.2)

Figures 4.6a and 4.6b show the 3D OpenSees models developed for the medium sized buildings with inelastic diaphragms, which due to symmetry included only half of the building. Similar to the mesh size analysis in the diaphragm test specimens modeling (Section 2.5), a 2 m by 2 m roof diaphragm mesh size and a 2 m by 10 m mesh size were used in OpenSees Model B1 and OpenSees Model B2, respectively. The types of OpenSees model used for the analysis of the medium sized buildings are given in Table 4.3. The building design case BVM1 was evaluated using both of the OpenSees models. For the other design cases (BVM0, BMM0 and BMM1), the OpenSees Model B1 was used to study the response of the buildings. The 2 m by 2 m mesh size

97

can be considered as a fine mesh size and adequate to predict the overall as well as local behaviour of the building including inelastic response of the diaphragm. In medium to large sized single-storey steel buildings, using the smaller mesh size in the model can take longer time and more effort to analyze. To address this issue, the 2 m by 10 m mesh size was selected in Model B2 to study the applicability of the strip model. Note that 10 m is the spacing of frame along the shorter direction of the building. In Table 4.3, Designs 1 and 2 for BVM1 building are identical except for the orientation of the deck panels: in Design 1, the deck panels are oriented along the E-W direction (parallel to the long walls) whereas the panels are oriented in the orthogonal direction in Design 2 (parallel to the short walls). For modeling the large sized buildings, the OpenSees Model B1 was used since the Model B2 was not able to accurately predict the inelastic response for the Design 2 buildings (see Section 4.3.1.1).

4.3.1 Results and discussion

4.3.1.1 Results of buildings designed for Abbotsford (BC)

The results obtained from the OpenSees models under the elastic signal (0.3×Loma Prieta earthquake signal) and under the design level earthquake (1.3 × Loma Prieta EQ) for the building BVM1 are first discussed as this building was evaluated using both Model B1 and B2. Further, the results based on the Loma Prieta earthquake record are presented in the beginning which will be supplemented with a comparison to the results obtained from the other earthquake records later in this chapter. The results obtained under the simulated earthquake signals are presented in Appendix E.

The OpenSees models B1 and B2 provided an identical fundamental period of vibration (0.88 s) compared to the value obtained by the SAP 2000 models for Design 1 and Design 2 of the BVM1 building. Figure 4.7 shows the predicted building responses for the Design 1 building with OpenSees Model B1 and B2. Both models provided identical results for the elastic signal as well as for the inelastic earthquake signal. Figure 4.7a shows the mid-span displacement time history (δ_m) under the elastic as well as design level earthquake signals. The mid-span displacement time history under the elastic earthquake signal obtained from SAP 2000 matches well with the results obtained from the OpenSees models (Figure 4.7a). Figure 4.7b shows the
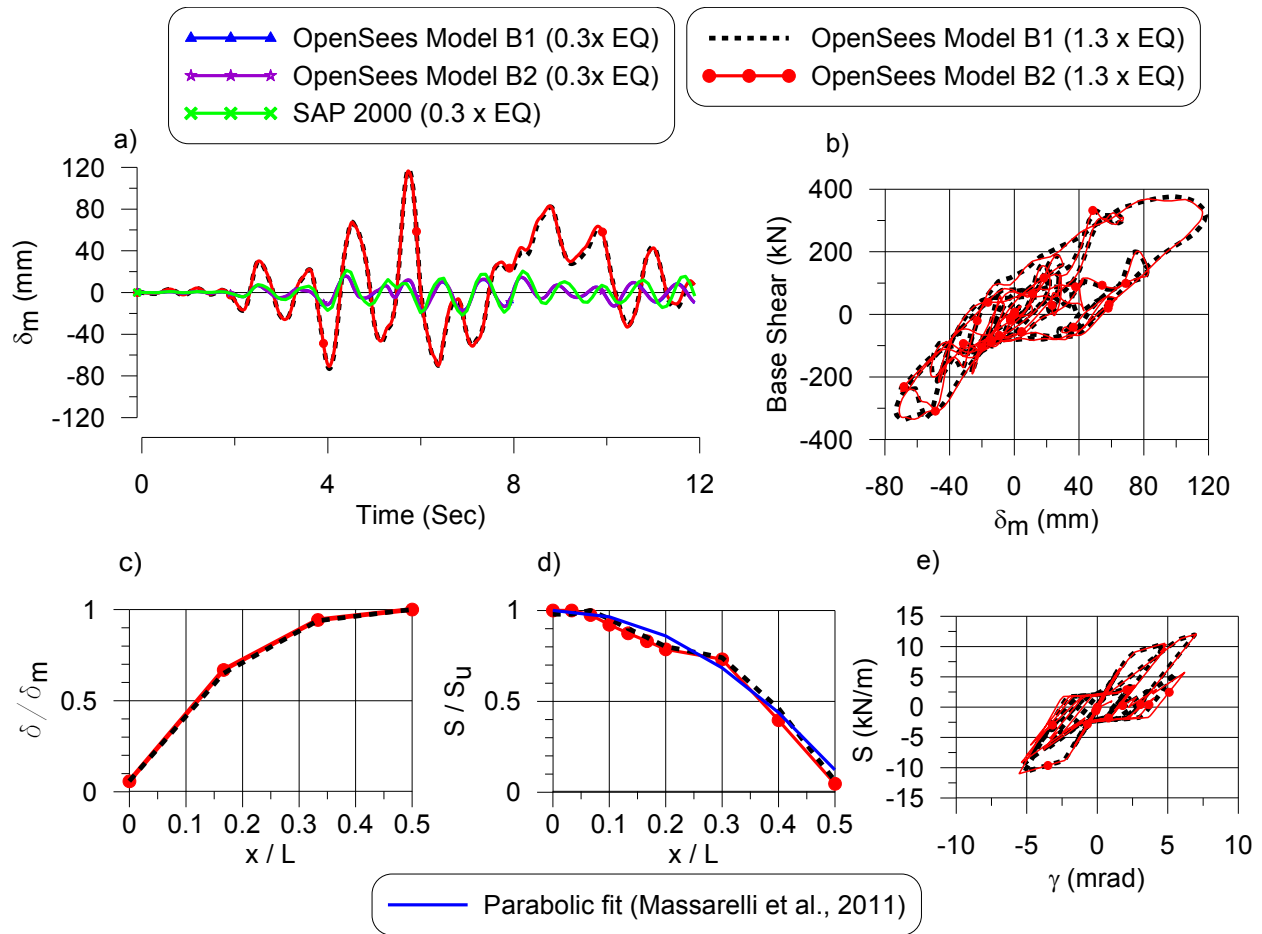
Figure 4.7 – Building response for Design 1 of BVM1 (30m×60m×7m) building under design level earthquake signal (record no. 0805): a) Displacement time history at mid-span; b) base shear vs. mid-span displacement; c) normalized maximum displacement profile along length; d) normalized shear force distribution along length; e) hysteretic response of diaphragm at the building edge.

predicted base shear (for one side of the building) vs. the mid-span displacement. Figures 4.7c and 4.7d show the normalized maximum displacement profile and the shear force distribution on the diaphragm at the occurrence of maximum shear force at the end of diaphragm along the length of building. The shear force on the diaphragm along the length of building was normalized with the maximum shear demand S_u on the diaphragm. The maximum displacement at the edge of the building was below 10% of the maximum displacement at the mid-span, which clarified that the flexibility of the diaphragm played an important role in the overall response of
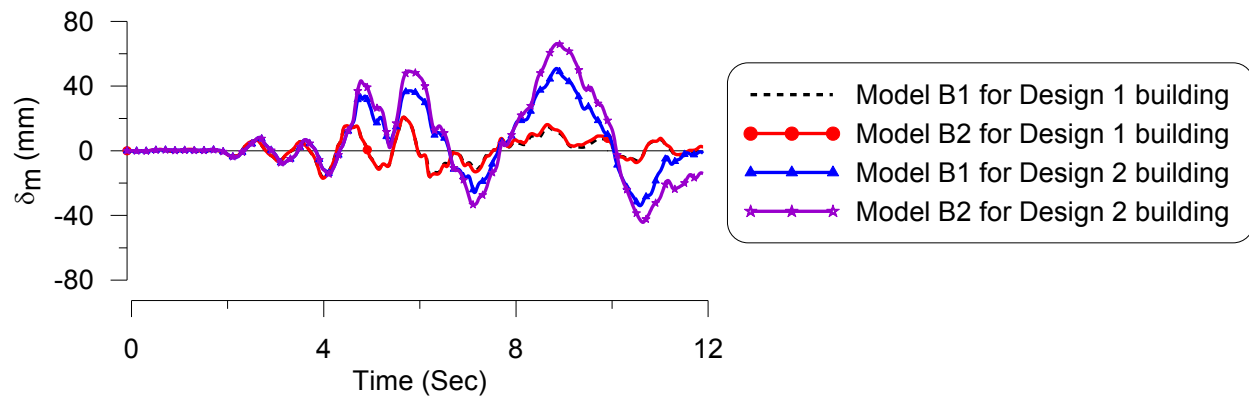
Figure 4.8 – Displacement time history for the design case BVM1 (at 2 m distance from edge) under under design level earthquake signal (record no. 0805)

the structure. The parabolic shear profile obtained from the diaphragm tests (Massarelli et al., 2011) is also shown in Figure 4.7d. The similar shear force distribution in the diaphragm tests and in the diaphragms of the designed building shows that the inelastic demand could be further spread towards the middle of the building as the length of the diaphragm increases. Inelastic shear deformation demand was observed over a distance of up to 12 m from the end of diaphragm in the analysis of the Design 1 building. Further non-linear analysis is necessary to understand the effect of the diaphragm length (building size) on the inelastic shear demand and distribution since only a single building size was considered herein for the Design 1 case (Layout I diaphragm). Figure 4.7e shows the inelastic shear hysteretic response of the diaphragm at the end of building. The identical response for the OpenSees Models B1 and B2 (Figure 4.7a to 4.7e) show the applicability of the strip model (OpenSees Model B2) for the Design 1 buildings.

Figure 4.8 shows the local displacement time history at a node, 2 m away from the building end, of the designed building BVM1 under the design level earthquake signal for the Design 1 and 2 buildings. The results as obtained using Models B1 and B2 are plotted in the figure. For the case of Design 2 buildings, the OpenSees Model B2 did not provide the same displacement time history results in comparison with the OpenSees Model B1, and hence may not be applicable for the non linear analysis of buildings when the roof deck panels are placed parallel to the direction of excitation. Similar results were obtained for the OpenSees analysis of the Layout II diaphragm

test specimens (Section 2.5). The difference in inelastic demand between Model B1 and Model B2 for the Design 2 building could be due to the influence of the joist members which run perpendicular to the direction of excitation. A higher concentration of inelastic demand was also found at the end of diaphragm in the Design 2 building than in the Design 1 building, which was as expected because a similar difference in the response of the layout I and layout II diaphragm specimens was observed in the diaphragm tests (Massarelli, 2010).
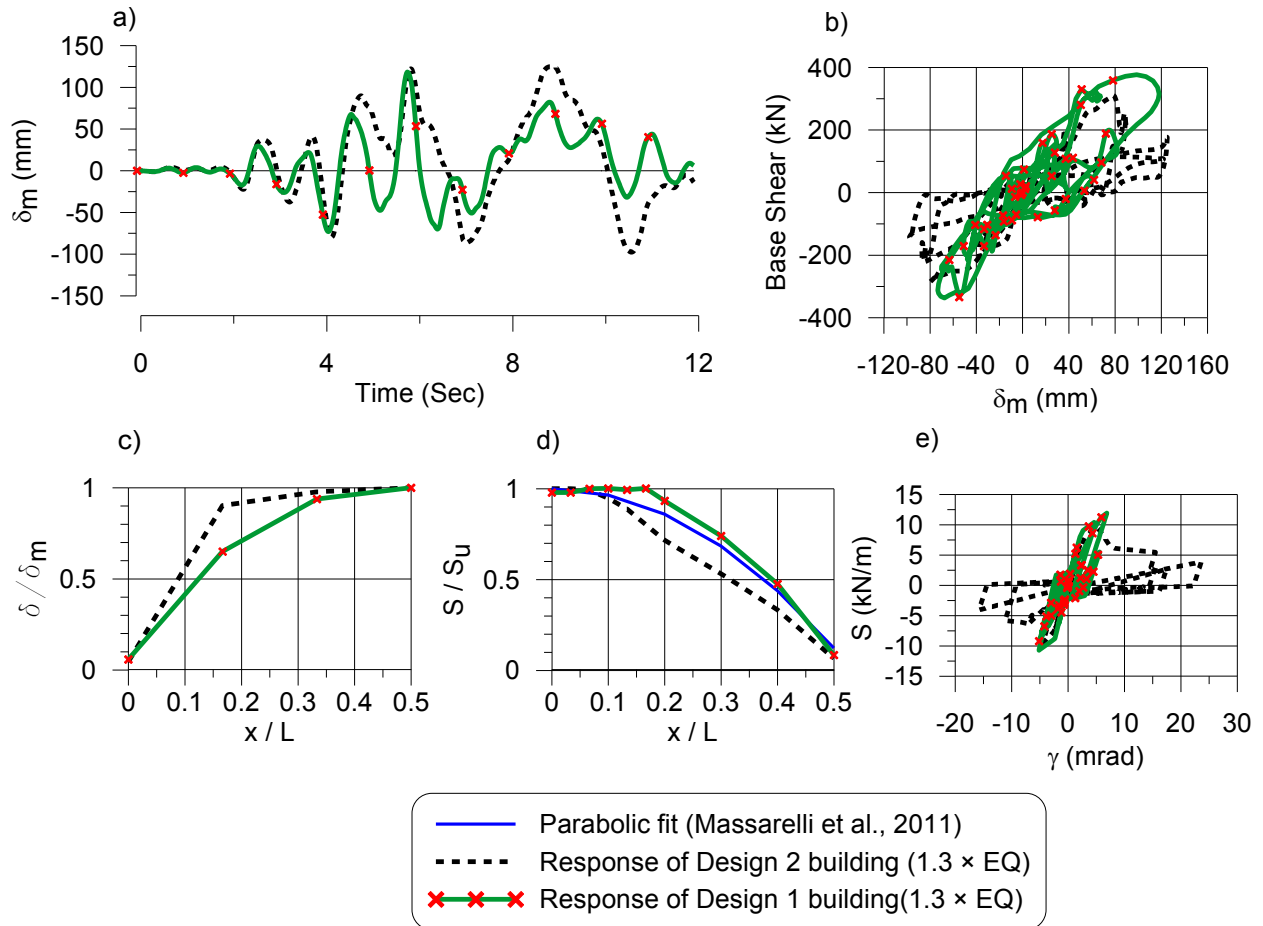
Figure 4.9 – Building response for BVM1 building (30m×60m×7m) under design level earthquake signal (record no. 0805): a) Displacement time history at mid-span; b) base shear vs. mid-span displacement; c) normalized maximum displacement profile along length; d) normalized shear force distribution along length; e) hysteretic response of diaphragm at the building edge.

Figure 4.9 shows the predicted building responses for the Design 2 BVM1 building with OpenSees Model B1 (see Table 4.3) under the design level earthquake (1.3 × Loma Prieta EQ). Response of Design 1 BVM1 building is also plotted in this figure for comparison purpose. The panel decks are parallel to the loading direction in the Design 2 BVM1 building (Layout II diaphragms). Even though the maximum deflection at the mid-span of the Design 2 BVM1 building (Figure 4.9a) was not significantly different from that of the Design 1 BVM1 building, inelastic shear deformation of the diaphragm at the building edge was significantly higher. Similar response was found under all other earthquake signals. The higher shear deformation was due to the damage concentration at the end of diaphragm in the case of the Design 2 building. Similar responses were observed in the dynamic tests of Layout II diaphragm specimens (Massarelli, 2010). The effect of damage concentration can be seen in Figure 4.9c; the maximum displacement demand at the end of the first bay from the building edge in Design 2 is about 90% of the maximum displacement at the building mid-span.

Essa et al. (2001) recommended a plastic shear deformation limit (Figure 1.3) of 0.01 radian for the diaphragms with nail deck to frame fasteners and screw side-lap fasteners in order to maintain the post-peak shear strength at greater than 80% of the ultimate capacity. In the Design 1 (BVM1) building, the maximum shear deformation demand (γ_{max}) on the diaphragm was 0.008 radian (Figure. 4.7e) under the design level earthquake, which was lower than the plastic shear deformation limit as recommended by Essa et al. The inelastic deformation demand in the range of 0.006 radian to 0.008 radian was distributed up to about 20% of the diaphragm span from the end. On the other hand, the maximum shear deformation demand in the Design 2 BVM1 building reached a value of 0.025 radians, which is significantly higher than 0.01 radian. The maximum shear deformation demand under other design level earthquake signals was also significantly higher than 0.01 radian. Such higher inelastic deformation was distributed only up to about 7% of the diaphragm span from the end, after which there was drastic decrease in the deformation demand. Figure 4.9e also clearly shows the significant strength degradation, corresponding to nearly complete failure, of the diaphragm at the building end of Design 2. The nearly complete shear failure at the diaphragm edge demonstrates that the use of $R_d = 2.0$ in the design of this type of building may not be appropriate. A lower value of R_d, probably a value of

1.5, may be used. However, a study would require for the use of appropriate R_d value in the design of the buildings with this type of structural system.
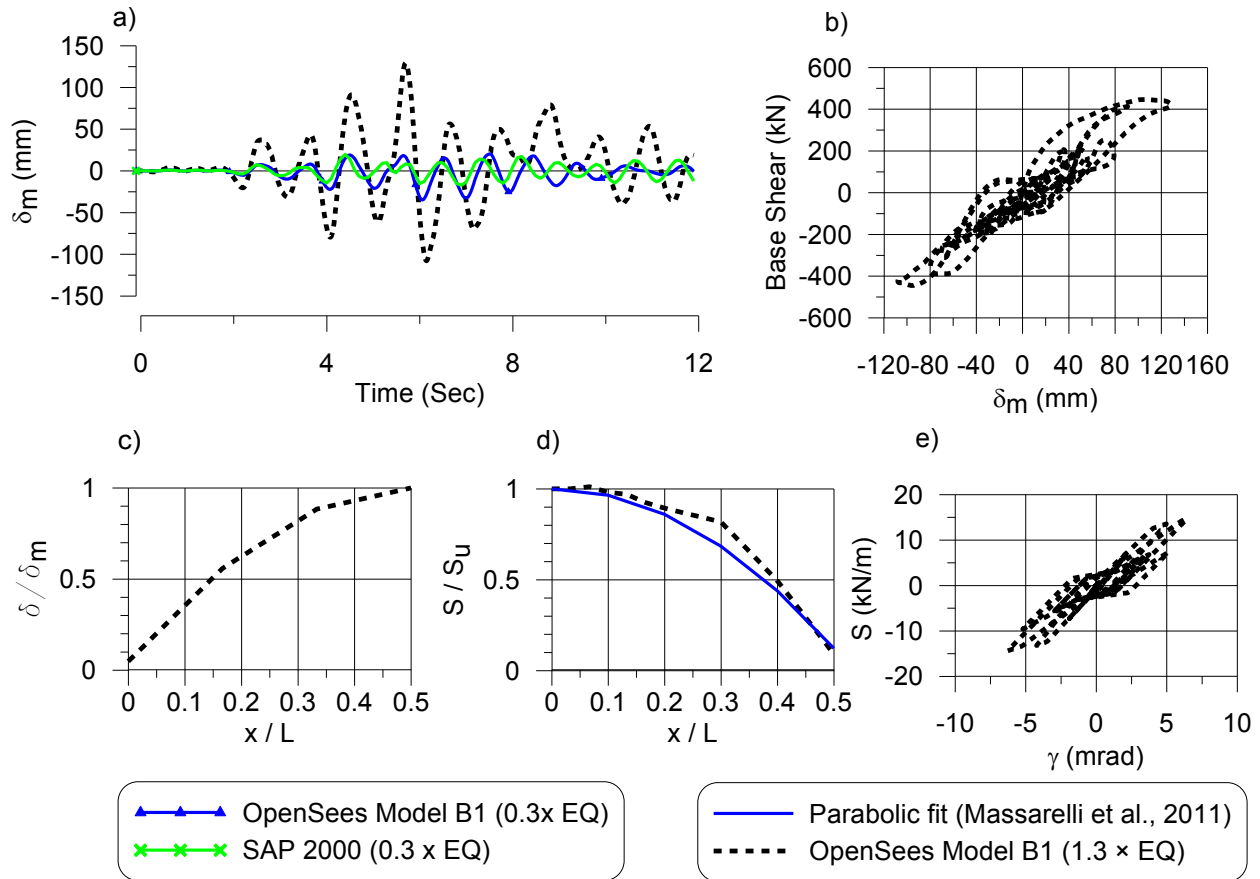
Figure 4.10 – Building response for Design 2 of BVM0 (30m×60m×7m) building under design level earthquake signal (record no. 0805): a) Displacement time history at mid-span; b) base shear vs. mid-span displacement; c) normalized maximum displacement profile along length; d) normalized shear force distribution along length; e) hysteretic response of diaphragm at the building edge.

Figure 4.10 shows the predicted building responses for the Design 2 BVM0 building with OpenSees Model B1 under the design level earthquake (1.3 × Loma Prieta EQ). The difference in actual periods of BVM0 and BVM1 was not significant. However, due to the period limitation in the design of the BVM0 building the diaphragm was designed for a higher shear force
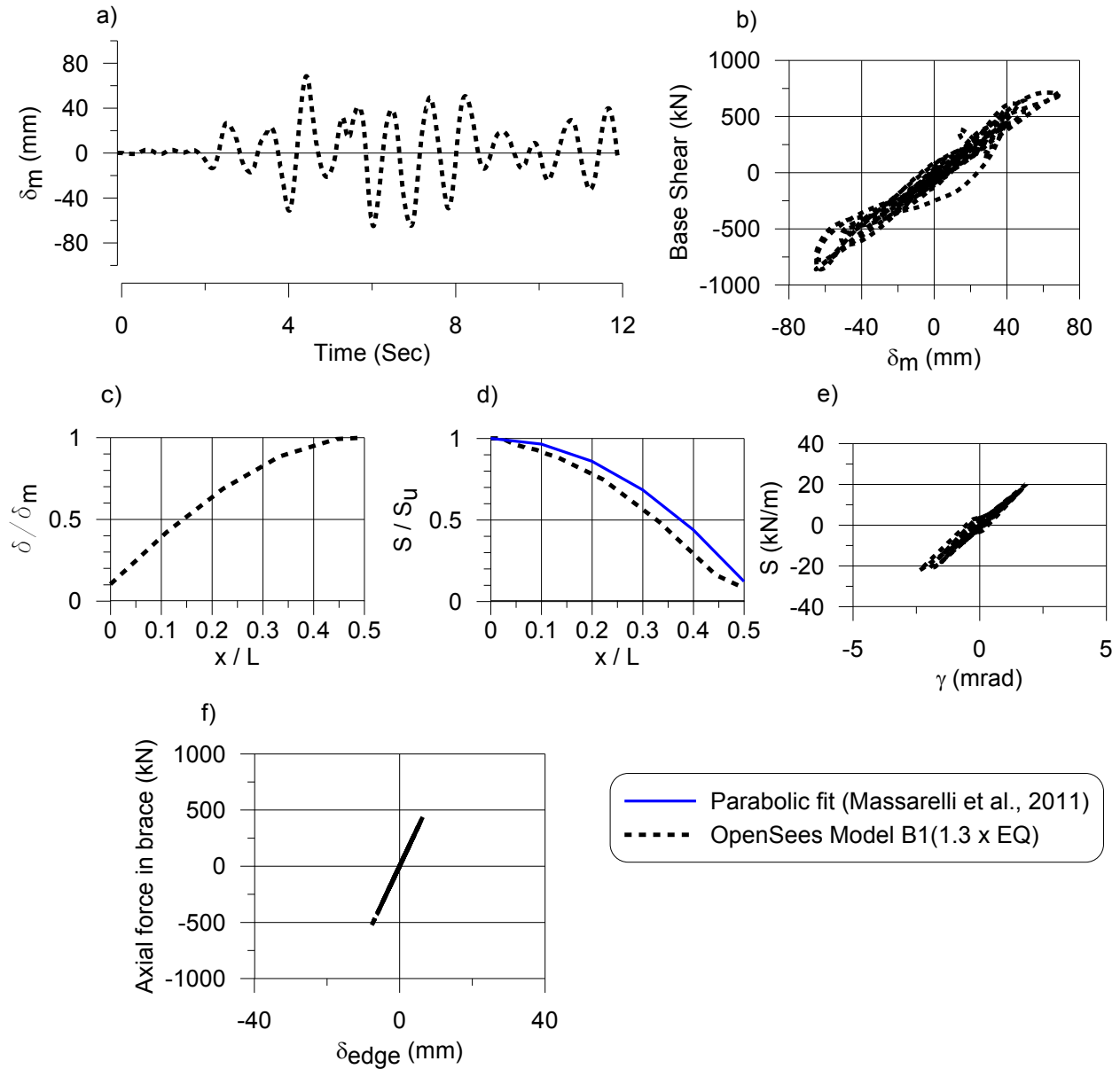
Figure 4.11 – Building response for BVL0 building (40m×90m×8m) under design level
earthquake signal (record no. 0805): a) Displacement time history at mid-span; b) base shear vs.
mid-span displacement; c) normalized maximum displacement profile along length; d)
normalized shear force distribution along length; e) hysteretic response of diaphragm at the
building edge; f) response of diagonal brace

compared with the diaphragm of the BVM1 Design 2 building. This resulted in lower inelastic

shear deformation demand in the diaphragm of the BVM0 building (Figure 4.10e) compared

with the diaphragm of the BVM1 building (Figure 4.9e). Similar results were obtained under the other earthquake signals (Appendix E).

The seismic response of large sized buildings under the design level earthquake signals was also predicted. Figure 4.11 shows the predicted building responses for the Design 2 BVL0 building under the design level earthquake loading (record number 0805). Compared to the response of the medium sized building BVM0, the maximum inelastic mid-span displacement as well as the inelastic shear displacement demand in the roof diaphragm were found lower in the BVL0 building. Similar response was obtained for the BVL1 building where the period was not limited in design. The lower inelastic shear displacement demand in the roof diaphragm for the large sized buildings could be due to increase in the flexibility of the building system.

Even though the design force on the diagonal vertical bracing was control by the proposed upper limit force (Section 3.8) corresponding to $R_dR_o = 2.0$ in many design cases, the axial force demand on the vertical diagonal brace members did not exceed their corresponding probable compression resistance for all the design cases that were designed for Abbotsford and Montreal region. This was mainly because the selected diagonal members had comparatively higher strength than the design force. Probably, when the diagonal braces are expected to go into the inelastic range of behaviour as could have been the case for the buildings studied, integrating a non-linear brace model of the CBF to the non-linear diaphragm truss model would be more appropriate to properly predict the entire building inelastic response, including brace buckling and yielding.

4.3.1.2 Results of buildings designed for Montreal (QC)

Figure 4.12 shows the predicted building responses for the Design 1 BMM0 building with OpenSees Model B1 under the design level earthquake (closely matched simulated EQ, No. 24) and under the 0.3×simulated earthquake. The diaphragm remained elastic under the design level earthquake (Figure 4.12e). Figure 4.12a shows the predicted displacement time history response at the end and middle of the roof diaphragm. The maximum predicted displacement at the middle of the roof diaphragm was 42 mm under the closely matched simulated earthquake which was

significantly lower compared to the displacement obtained in the corresponding building that was designed for Abbotsford. The elastic response of the diaphragm and the lower inelastic mid-span displacement demand under the design level ground motion signal compared to the force and the displacement of the BVM0 building was mainly due to the $T_a = 0.35$ s period limitation in design. Similar results were obtained under other design level earthquake signals (Section 4.2). Even though the design base shear was controlled by the upper limit, it was equal to the base shear corresponding to a period of 0.4 s, whereas, the actual fundament period (0.9 s) of the building was significantly longer. In addition, the lower inelastic demand may also be due to the characteristics of the earthquake signal that was selected.
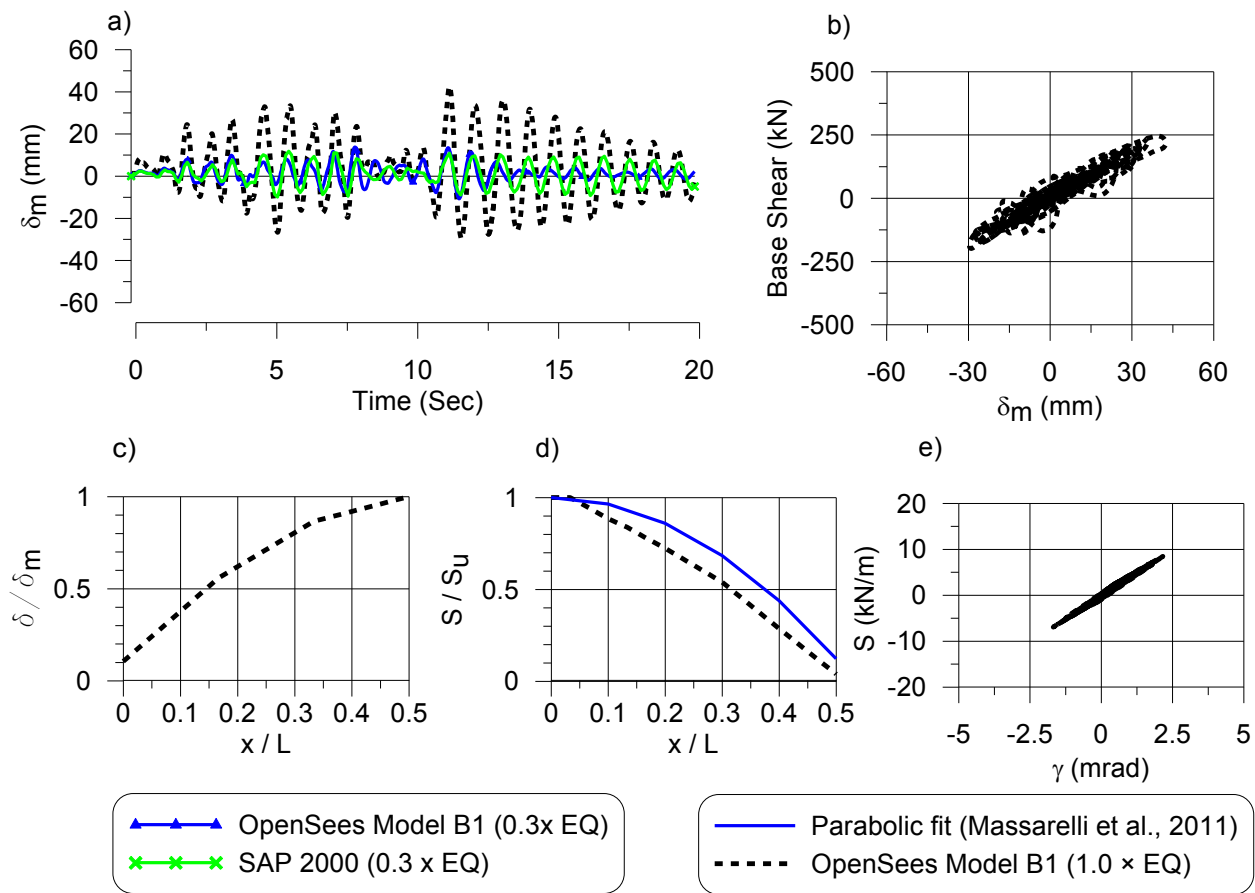
Figure 4.12 – Building response for Design 1 of BMM0 building (30m×60m×7m) under design level earthquake signal (No. 24): a) Displacement time history at mid-span; b) base shear vs. mid-span displacement; c) normalized maximum displacement profile along length; d) normalized shear force distribution along length; e) hysteretic response of diaphragm at the building edge.
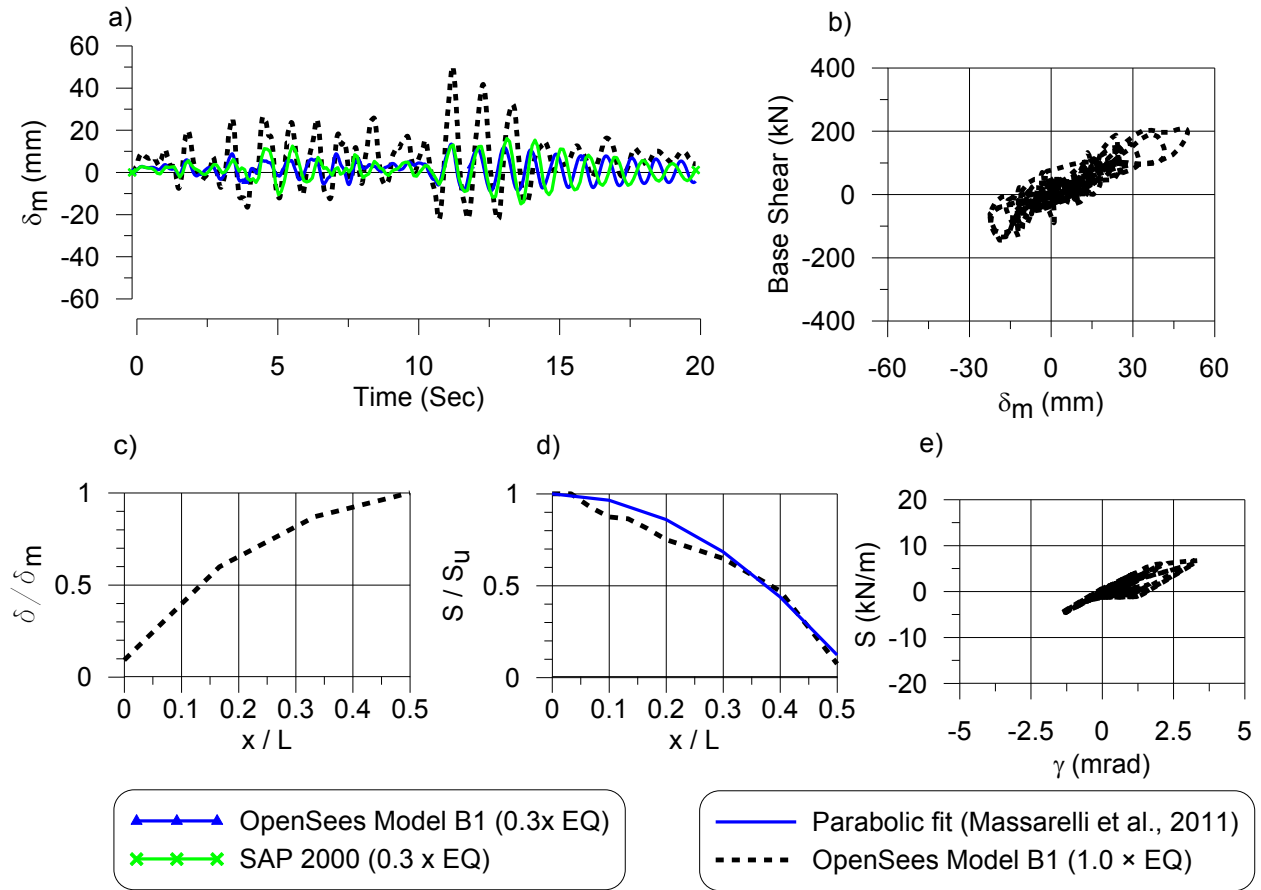
Figure 4.13 – Building response for Design 1 of BMM1(30m×60m×7m) building under design
level earthquake signal (No. 24): a) Displacement time history at mid-span; b) base shear Vs
mid-span displacement; c) normalized maximum displacement profile along length; d)
normalized shear force distribution along length; e) hysteretic response of diaphragm at the
building edge.

The predicted building responses for the Design 1 BMM1 building with OpenSees Model B1
under the design level earthquake (closely matched simulated EQ) and under the 0.3×simulated
earthquake is shown in Figure 4.13 The inelastic displacement demand at mid-span (Figure
4.13a) and the inelastic shear deformation demand at the end of the diaphragm (Figure 4.13e)
were significantly lower than the response of the similar building BVM1 designed for
Abbotsford, BC. Design seismic forces were small for the buildings designed for Montreal. Even
though the 0.76 mm thick, 36/4 nail frame fasteners and 600 mm spaced screw side-laps were
selected for the diaphragm, the factored shear resistance of the diaphragm was comparatively

higher than the design shear force on it (4.8 kN/m vs. 3.4 kN/m in Table 3.9b). . The results under the other earthquake signals were not significantly different. The higher shear resistance of the diaphragm was the reason for the smaller inelastic demand. A study is required to investigate the response of building size.

4.4 Numerical modeling of buildings with CBFs (System A)

A general purpose concentric braced frame model developed by Agüero et al. (2006) in the OpenSees software platform was used to simulate the hysteretic response of the diagonal steel bracing members (Figure 4.14). Force based non-linear beam-column elements with a fibre representation and with Giuffré-Menegotto-Pinto constitutive model (Steel02) were used for the bracing members. The initial out-of-plane imperfection at mid-length of the braces was assumed to be 0.1% of the brace length in the analysis. Uriz et al. (2008) recommended the initial out-of-plane imperfection should be between 0.05% to 0.1% of the brace length. A total of 16 non-linear beam-column elements were used to model a brace member (to obtain the initial out-of-plane imperfection and buckling response) where each element included 4 integration points and a total of 16 fibres to model the cross-section. Rotational zero length spring elements were used at beam column joints (C1), brace ends (C2 and C3) (connection between gusset plate and brace
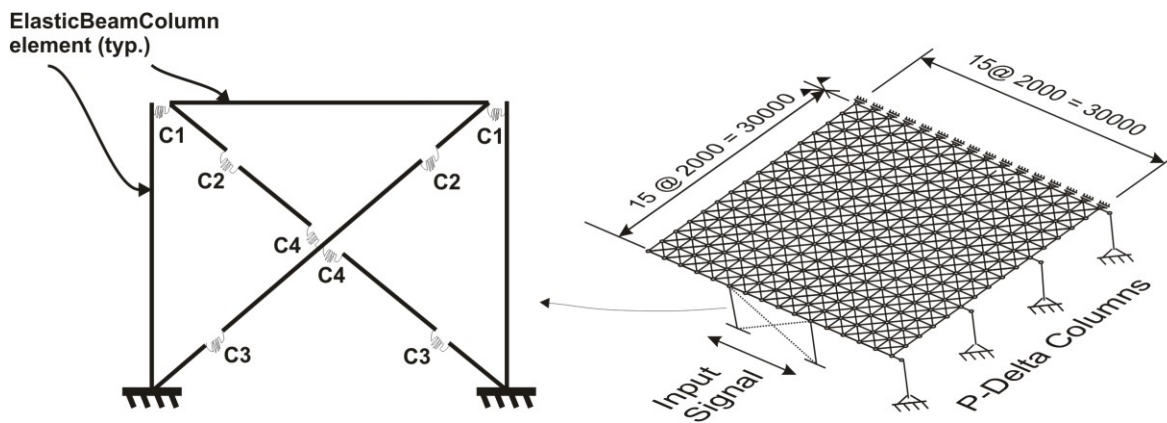
Figure 4.14 – Non-linear OpenSees model of building with CBF as a structural system (OpenSees Model A)

member to reproduce the hysteretic response of the gusset plates) and at the connection between the two braces at the middle (C4). The size of the gusset plates was based on the size of beam and column members as well as the size and material characteristics of the diagonal vertical bracing members. The in-plane flexural stiffness of spring C1 was set zero and other spring elements were considered as infinitely stiff for in-plane bending. The out-of-plane flexural stiffness and torsional stiffness of Springs C1 were set as zero and infinitely large respectively, whereas these values for the C2 and C3 springs were determined based on the size and material characteristics of the gusset plates. Spring C4 was defined as fully rigid in all three rotational axes. Additional details about the model and material parameters can be found in the paper by Agüero et al. (2006).

Designs of the buildings for CBF structural system (System A) are presented in Section 3.7. OpenSees models (OpenSees Model A) were developed for the designed medium and large sized buildings which were located in Abbotsford, BC (Figure 4.14). The CBF OpenSees model developed by Agüero et al. (2006), which was available for use, was integrated with the non linear diaphragm model to develop the OpenSees building model (OpenSees Model A). The Pinching4 material parameters obtained from the calibration of the numerical models of the Layout II diaphragm test specimens were used in the OpenSees building models (Section 2.4.1). The designed buildings were evaluated by exciting the design level earthquakes (Section 4.2) in the N-S direction of the buildings. For the AVM0 and AVL0 buildings, 100% of the SDI predicted shear stiffness was used in the model, whereas 70% of the SDI shear stiffness was used in the model for the AVM1, AVM2 and AVL2 buildings. Since the steel deck panels were parallel to the earthquake loading (Design 2), OpenSees Model A was similar to the OpenSees Model B1 (Figure 4.14).

4.4.1 Results and discussion

The results obtained from the OpneSees Model A under the Loma Prieta earthquake record (record no 0805) are presented in the beginning which will be supplemented with a comparison to the results from the other earthquake records later in this chapter. Moreover, the results obtained under the simulated earthquake signals are presented in Appendix E.
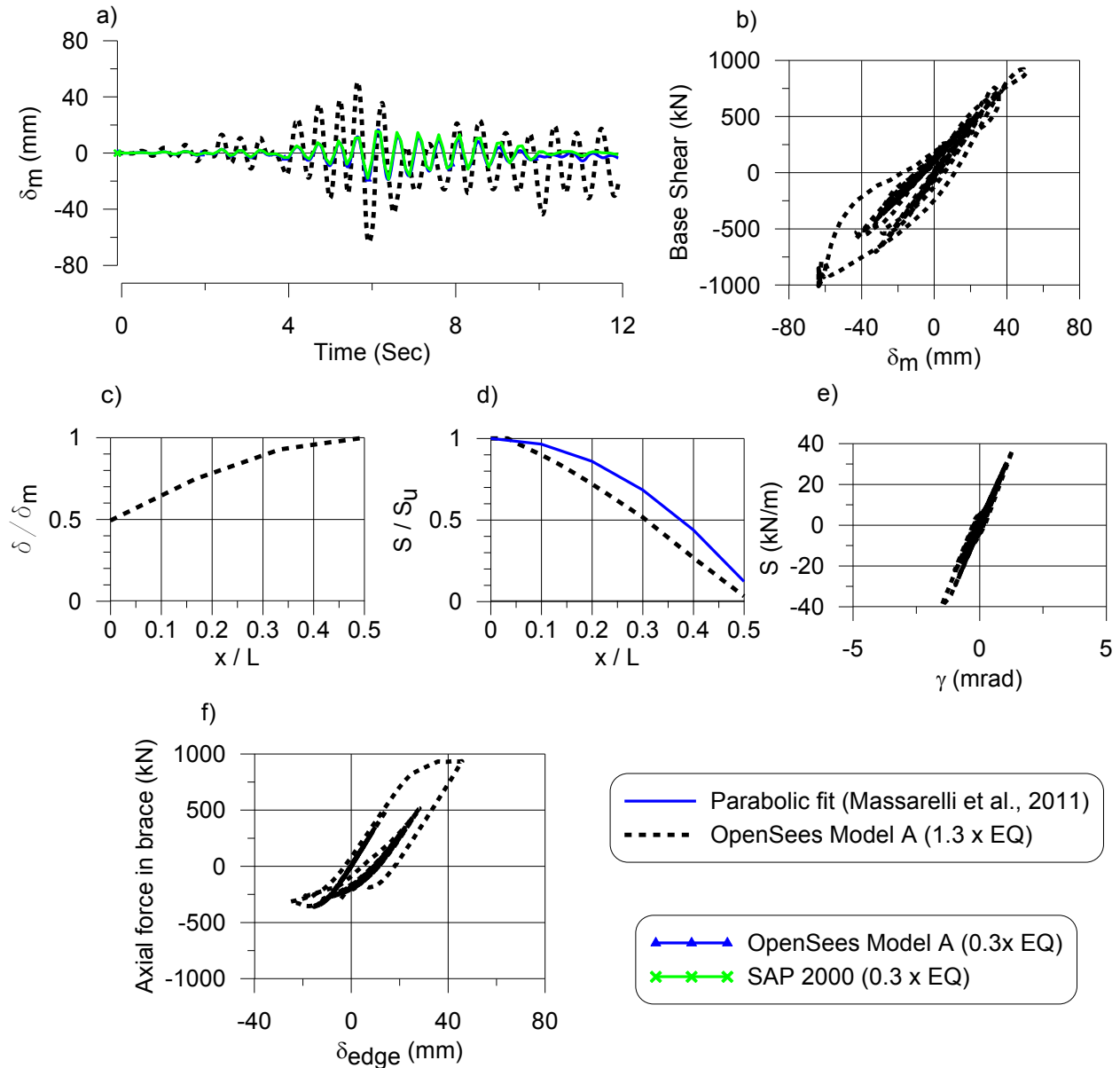
Figure 4.15 – Building response for AVM0 building (30m×60m×7m) under design level earthquake signal (record no. 0805): a) Displacement time history at mid-span; b) base shear vs. mid-span displacement; c) normalized maximum displacement profile along length; d) normalized shear force distribution along length; e) hysteretic response of diaphragm at the building edge and f) hysteretic response of a diagonal brace member.

The OpenSees Model A provided the identical fundamental periods of vibration as obtained by the SAP 2000 models for the medium and large sized buildings. Figure 4.15 shows the predicted building responses for the AVM0 building (30m×60m×7m) with the OpenSees Model A. Figure

4.15a shows the mid-span displacement time history under the elastic as well as design level signals. The mid-span displacement time history under the elastic earthquake signal obtained from SAP 2000 (Figure 4.15a) matches well with the results obtained from the OpenSees models. The displacement under the design level ground motion at the mid-span of the building for the structural system A was significantly smaller than that of the structural system B where the diaphragm was designed as a weak element in the SFRS. Due to the stiffness degradation of the steel roof diaphragm in structural system B, the displacement demand in this system could be higher than the structural system A. Figure 4.15b shows the predicted base shear (for one side of the building) vs. the mid-span displacement. Figures 4.15c and 4.15d show the normalized maximum displacement profile and the shear force distribution on the diaphragm at the occurrence of maximum shear force at the end of diaphragm along the length of building. The maximum inelastic displacement at the building edge was about 50% of the maximum mid-span displacement (Figure 4.15c). The parabolic shear profile obtained from the diaphragm tests (Massarelli et al., 2011) is also shown in Figure 4.15d. Figure 4.15e shows the shear response of the diaphragm at the end of the building which was nearly elastic. In the design of the diaphragm of the building, the design shear force was controlled by that corresponding to the base shear determined with R_dR_o of 2.0. Due to this, the maximum shear force demand on the diaphragm was more than its factored shear resistance. The maximum shear displacement demand on diaphragm under the design level earthquake signal was well below the limit (0.01 rad.) suggested by Essa et al. (2001). The maximum shear force on the diaphragm was 40 kN/m under the design level earthquake, whereas 28.4 kN/m was the factored shear resistance of the diaphragm. The nominal shear strength (47.3 kN/m) determined using SDI method was used in the numerical model. Similar results were also found under the other earthquake signals.

Figure 4.16 shows the predicted building responses for the AVM1 building with the OpenSees Model A. The structural design and details of the AVM1 building were similar to the AVM0 building. However the use of 70% of the SDI predicted stiffness for the AVM1 building in the model decreased the force demand in the diaphragm (Figure 4.16e) and in the vertical brace member (Figure 4.16f) slightly due to the increase in the fundamental period of vibration from 0.49 s to 0.52 s. Comparable to the shear force demand on the diaphragm of AVM0 building, the maximum shear force demand on the diaphragm of AVM1 building was more than its factored
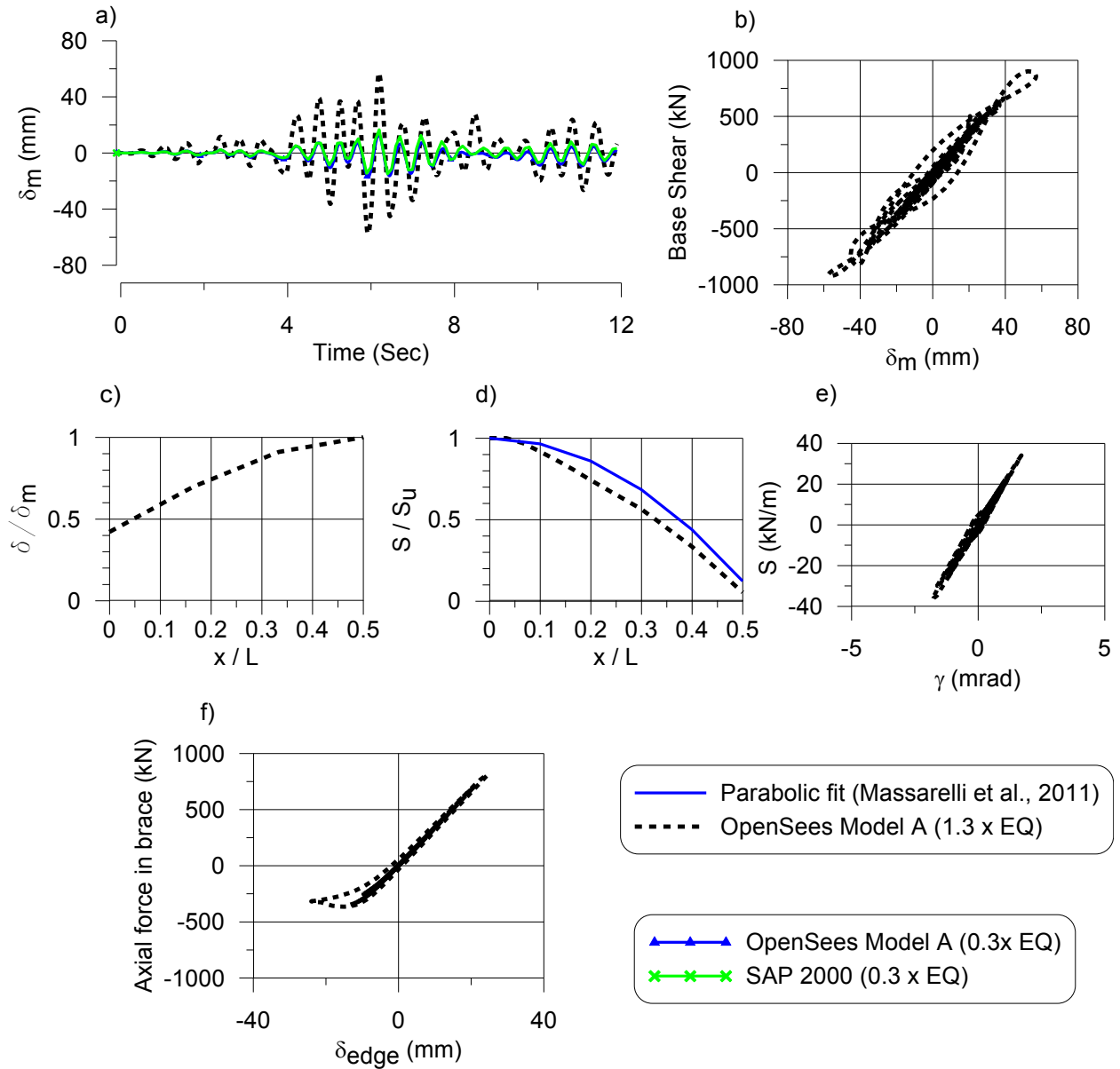
Figure 4.16 – Building response for AVM1(30m×60m×7m) building under design level earthquake signal (record no. 0805): a) Displacement time history at mid-span; b) base shear vs. mid-span displacement; c) normalized maximum displacement profile along length; d) normalized shear force distribution along length; e) hysteretic response of diaphragm at the building edge and f) hysteretic response of a diagonal brace member.

shear resistance. Figure 4.16e shows the shear response of the diaphragm at the end of the building. The maximum shear displacement demand on diaphragm was well below the limit (0.01 rad.) suggested by Essa et al. (2001). The inelastic displacement demand on the vertical
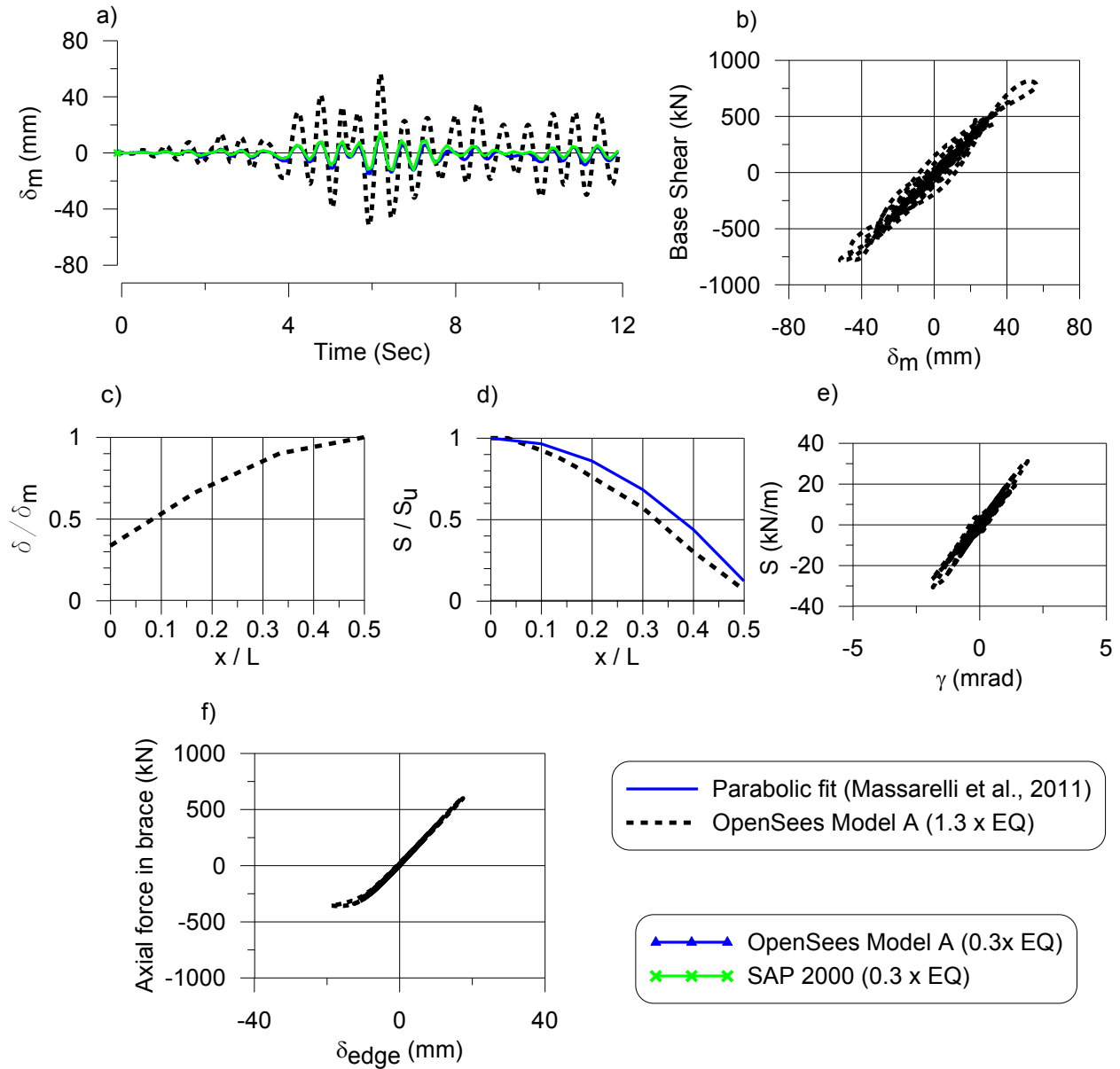
Figure 4.17 – Building response for AVM2 building (30m×60m×7m) under design level earthquake signal (record no. 0805): a) Displacement time history at mid-span; b) base shear vs. mid-span displacement; c) normalized maximum displacement profile along length; d) normalized shear force distribution along length; e) hysteretic response of diaphragm at the building edge and f) hysteretic response of a diagonal brace member.

bracing member reduced compared to the demand in the AVM0 building (Figure 4.16f). The maximum displacement demand at the mid-span under the design level earthquake was not significantly increased (Figure 4.16a). The maximum displacement at the building edge was

about 40% of the maximum mid-span displacement (Figure 4.16c). Again, similar results were obtained under the other earthquake signals.

Figure 4.17 shows the predicted building responses for the AVM2 building with the OpenSees Model A. The structural design and details of the AVM2 building, except the design of the diaphragm, were similar to the AVM0 and AVM1 buildings. Because of the use of an unlimited period in the strength design of the AVM2 building the design shear force on the diaphragm of the AVM2 building was smaller compared to that on the diaphragm of the AVM0 and AVM1 buildings. It should be noted that the use of an unlimited period in design did not increase the maximum displacement demand at mid-span due to the decrease in the lateral forces (Figure 4.17a and 4.17b). This indicates that the analytically predicted fundamental period of vibration could be used in the design of such single-storey steel buildings. The maximum displacement at the building edge under the design level earthquake was about 33% of the maximum mid-span displacement (Figure 4.17c). Figure 4.17e shows the shear response of the diaphragm at the end of the building. The maximum shear displacement demand on diaphragm was well below the limit (0.01 rad.) suggested by Essa et al. (2001). Similar to the shear force demand on the diaphragm of the AVM0 and AVM1 buildings, the maximum shear force demand on the diaphragm of the AVM2 building was also more than its factored shear resistance. Similar results were obtained under the other earthquake signals (Appendix E).

The response obtained for the large sized buildings (AVL0 and AVL2), which were designed for the Abbotsford region, were not considerably different from that of the medium sized buildings. Figure 4.18 shows the predicted building responses for the Design 2 AVL0 building under design level earthquake loading (record number 0805). The roof diaphragm remains mainly elastic under design level earthquake signals. The shear force on the diaphragm was higher than in the corresponding medium sized buildings as expected. The maximum mid-span displacement was found higher in the large sized buildings; however, the values were still significantly lower than the drift limit provided by NBCC.

The inelastic demand on the vertical brace was found to decrease as the flexibility of the diaphragm increases (Figures 4.15f, 4.16f and 4.17f). This may be due to the influence of the

ratio of the stiffness of the diaphragm to that of the bracing bent. Further study is needed to understand this behaviour.
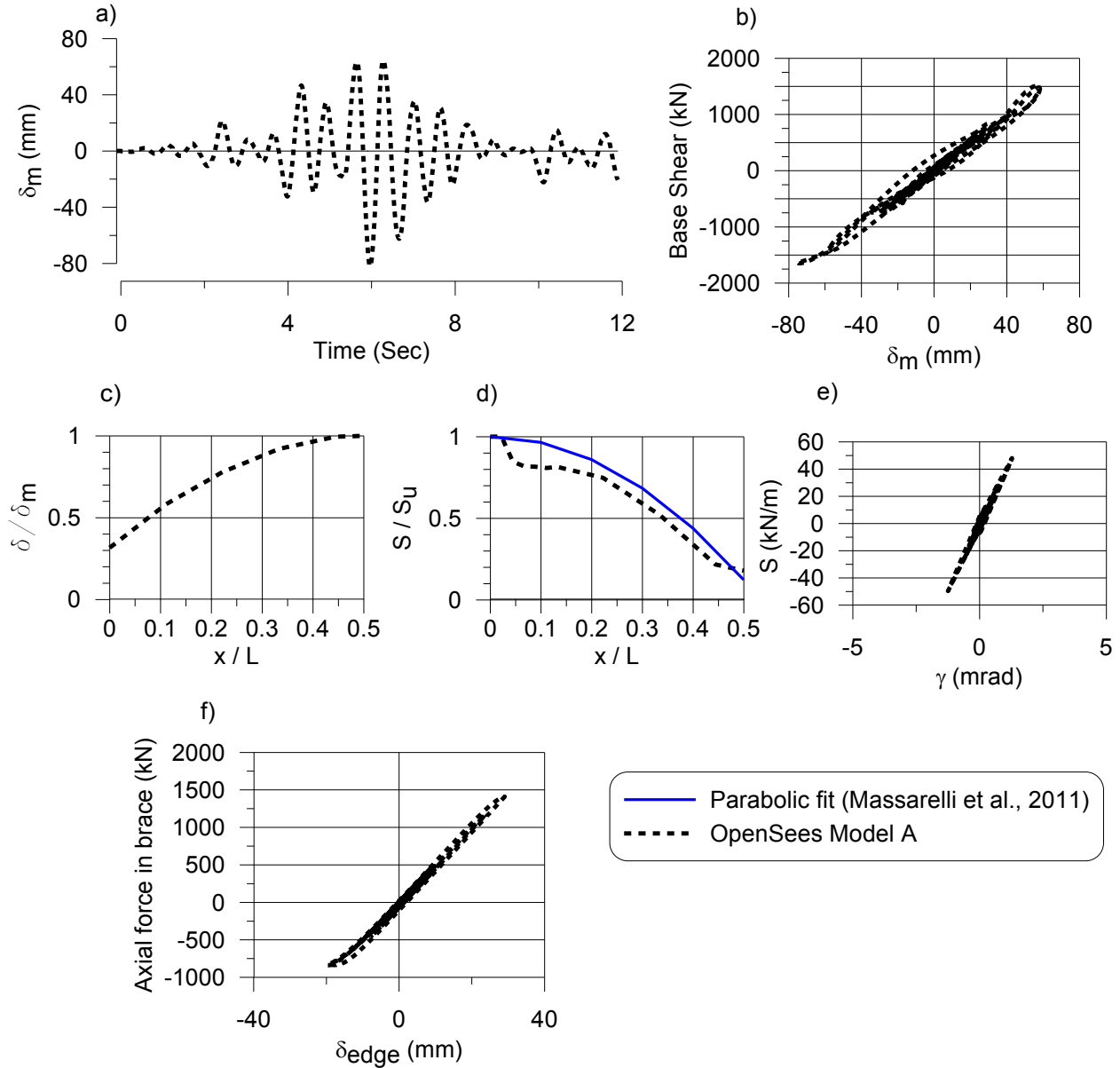
Figure 4.18 – Building response for AVL0 (40m×90m×8m) building under design level earthquake signal (record no. 0805): a) Displacement time history at mid-span; b) base shear vs. mid-span displacement; c) normalized maximum displacement profile along length; d) normalized shear force distribution along length; e) hysteretic response of diaphragm at the building edge and f) hysteretic response of a diagonal brace member.

4.5 Numerical modeling of buildings with EBF structural system (System C)

An eccentric braced frame model developed by Koboevic et al. (2011) in the OpenSees software platform was used to simulate the hysteretic response of the EBF structural system (Figure 4.19). The shear response of the link beam was captured by a use of a single spring in the vertical direction with inelastic behaviour described using the Giuffré-Menegotto-Pinto (Steel02) hysteretic material. The properties of the link beam element used in the study were determined by calibration against data from 11 cyclic tests on short shear links by Okazaki et al. (2005). The ratio of elongation of the zero length spring element to the length of the link beam represents the shear strain of the link beam. The expected yield shear strength of the link element was given to a zeroLength spring element. Additional details about the model and material parameters can be found in Koboevic et al. (2011).
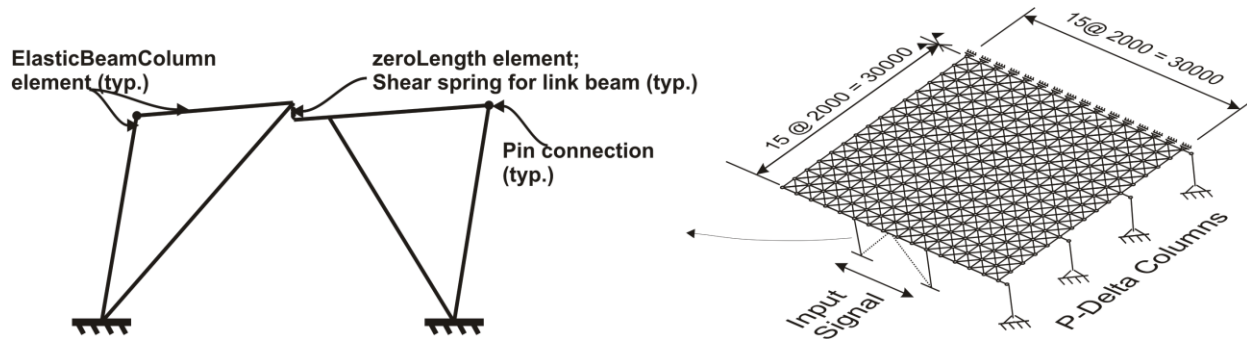
Figure 4.19 – Non-linear OpenSees model of building with EBF as a structural system (OpenSees Model C)

Designs of the buildings for EBF structural system (System C) are presented in the Section 3.9. OpenSees models (OpenSees Model C) were developed for the designed medium and large sized buildings which were located at Abbotsford, BC (Figure 4.19). The EBF OpenSees model developed by Koboevic et al. (2011) was integrated with the non linear diaphragm model to develop the OpenSees building model. The Pinching4 material parameters obtained from the calibration of the numerical models of the Phase I to III diaphragm test specimens were used in the OpenSees building models (Section 2.4.1). The designed buildings were evaluated by exciting the model with the design level earthquakes (Section 4.2) in the N-S direction of the buildings. For all the design cases of this structural system 70% of the SDI predicted shear

stiffness was used in the models. Since the steel deck panels were parallel to the earthquake loading (Design 2), the mesh size of the OpenSees Model C for the diaphragm modeling was similar to the OpenSees Model B1.

4.5.1 Results and discussion

Figure 4.20 shows the predicted building responses for the CVM0 building with OpenSees Model C under the design level earthquake (record no. 0805). Figure 4.20a shows the mid-span displacement time history under the elastic as well as the design level earthquake signals. The mid-span displacement time history under the elastic earthquake signal obtained from SAP 2000 is also plotted in Figure 4.20a; it matches well with the results obtained from the OpenSees model. Figure 4.20b shows the predicted base shear (for one side of the building) vs. the mid-span displacement. The maximum base shear for the structural system C is about half of the base shear obtained in structural system A. Figures 4.20c and 4.20d show the normalized maximum displacement profile and the shear force distribution on the diaphragm at the occurrence of maximum shear force at the edge of the building. The maximum displacement at the building edge under the design level ground motion is about 72% of the maximum mid-span displacement. This is due to the higher flexibility and greater inelastic deformations of the EBF system compared to the CBF. The parabolic shear profile obtained from the diaphragm tests (Massarelli et al., 2011) is also shown in Figure 4.20d. Figure 4.20e shows the shear response of the diaphragm at the end of building. The maximum shear displacement demand on diaphragm was well below the limit (0.01 rad.) suggested by Essa et al. (2001).Similar results were obtained under the other earthquake signals (Appendix E). The maximum shear force demand on the diaphragm (17.4kN/m) is slightly above the factored shear resistance of the diaphragm ($0.6S_n$ = 14 kN/m). The reason could be as follows: when the force on the diaphragm was within the elastic limit, the shear force at the middle (over the depth) of the diaphragm was about 16% higher than the force towards the edge (over the depth) of the diaphragm (Figure 2.8e). The predicted shear response of the link beam is shown in Figure 4.20f. The maximum shear rotation of the link beam was slightly over the 0.08 radian which is the limit specified in the CSA S16

Standard (2009) for link beams designed to yield in shear, which was the case here. But for most of the other earthquake records, the shear rotation was below the 0.08 radian. To study the
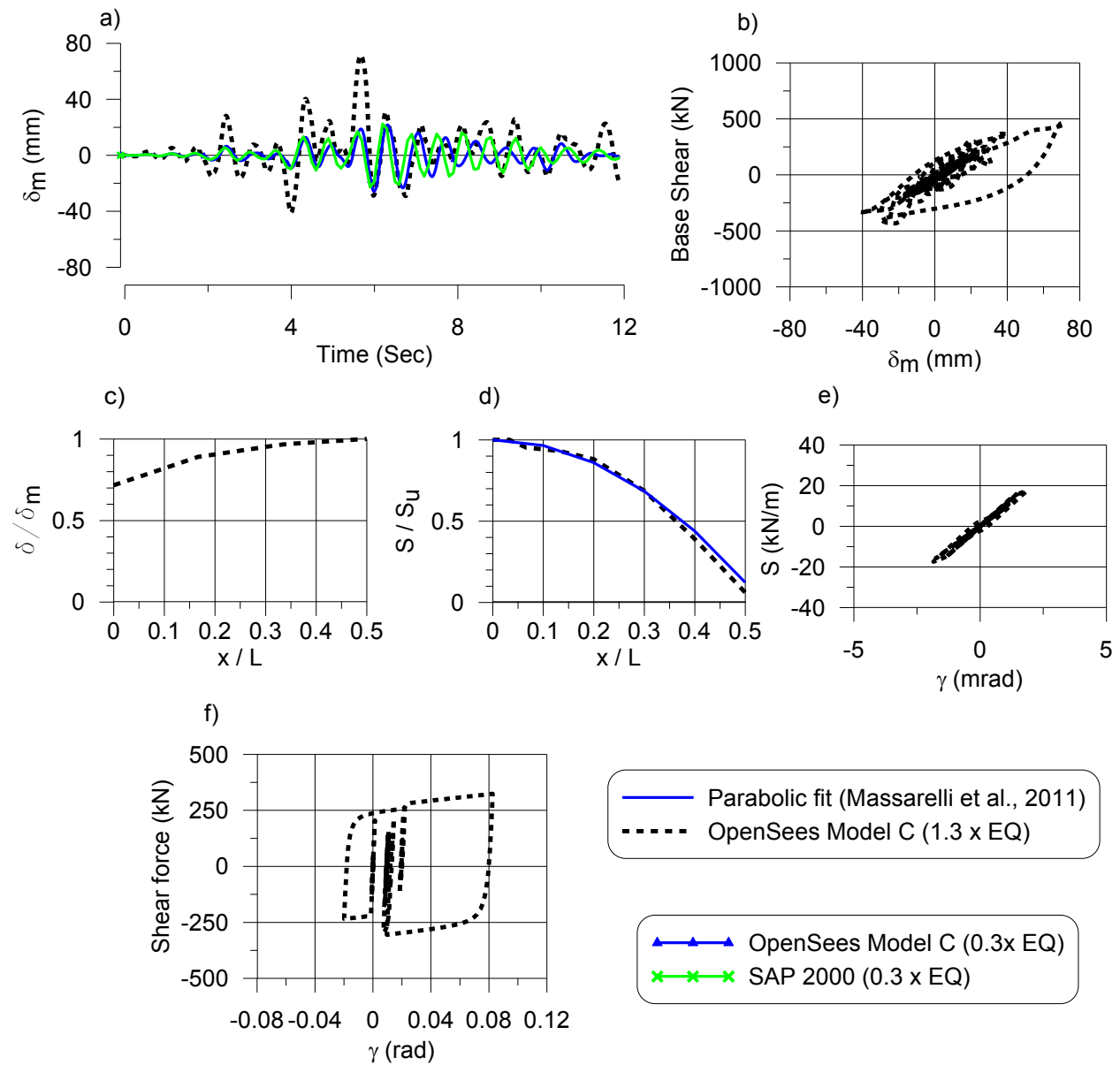
Figure 4.20 – Building response for CVM0 building (30m×60m×7m) under design level earthquake signal (record no. 0805): a) Displacement time history at mid-span; b) base shear vs. mid-span displacement; c) normalized maximum displacement profile along length; d) normalized shear force distribution along length; e) hysteretic response of diaphragm at the building edge and f) hysteretic response of a link beam.

influence of diaphragm flexibility on the inelastic demand on the link beam, an analysis was also done using the SDI predicted shear stiffness G' for the diaphragm in the CVM0 building instead of using 70% of the SDI predicted stiffness. The analysis results showed that the maximum mid-span displacement and the inelastic demand on the link beam could be decreased if the stiffness of the diaphragm were increased (Figure 4.21).
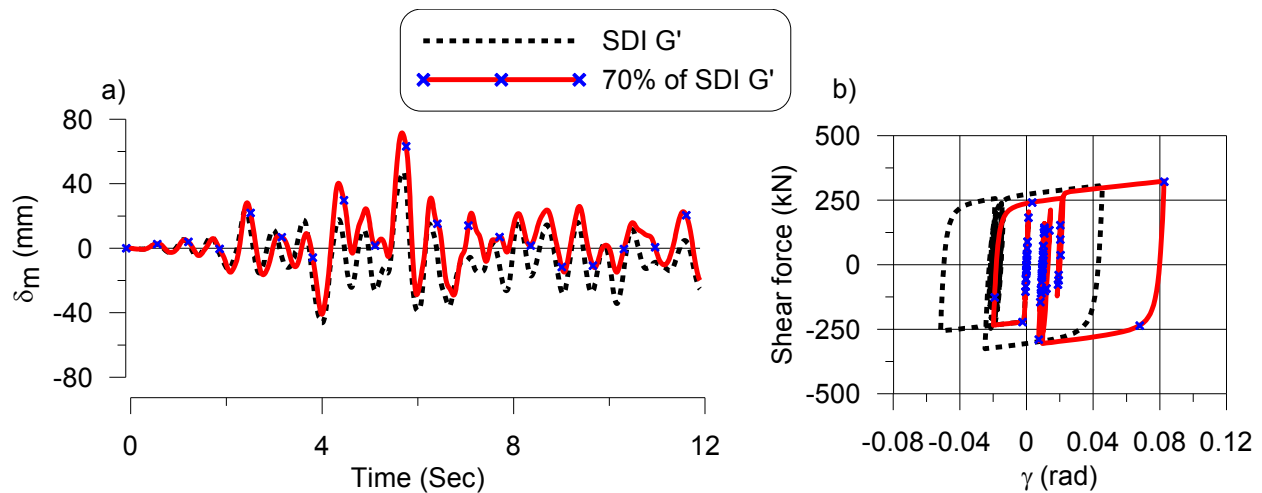
Figure 4.21 – Building response of CVM0 building (30m×60m×7m) under under design level earthquake signal (record no. 0805): a) Displacement time history at mid-span;   b) hysteretic response of a link beam.

Figure 4.22 shows the predicted building responses for the CVM1 building with OpenSees Model C under the same design level earthquake (record no. 0805). The maximum displacement at the mid-span did not increase in the CVM1 building even though the CVM1 building was more flexible than CVM0 building (Figure 4.22a). Similar responses were obtained under the other earthquake signals. The maximum base shear in the CVM1 building was lower to some extent than in the CVM0 building (Figure 4.22b). The fundamental periods of the CVM0 and CVM1 building were 0.64 s and 0.69 s, respectively.   Similar response to the CVM0 building was obtained for the maximum displacement profile and shear force distribution along the length of the diaphragm as well as for the shear response of the diaphragm at the end of building (Figures 4.22c to 4.22e). The maximum inelastic shear link rotation of the link beam was slightly

greater in the CVM1 building compared to that in the CVM0 building (Figure 4.22f).But this was not the case under all the other earthquake records.
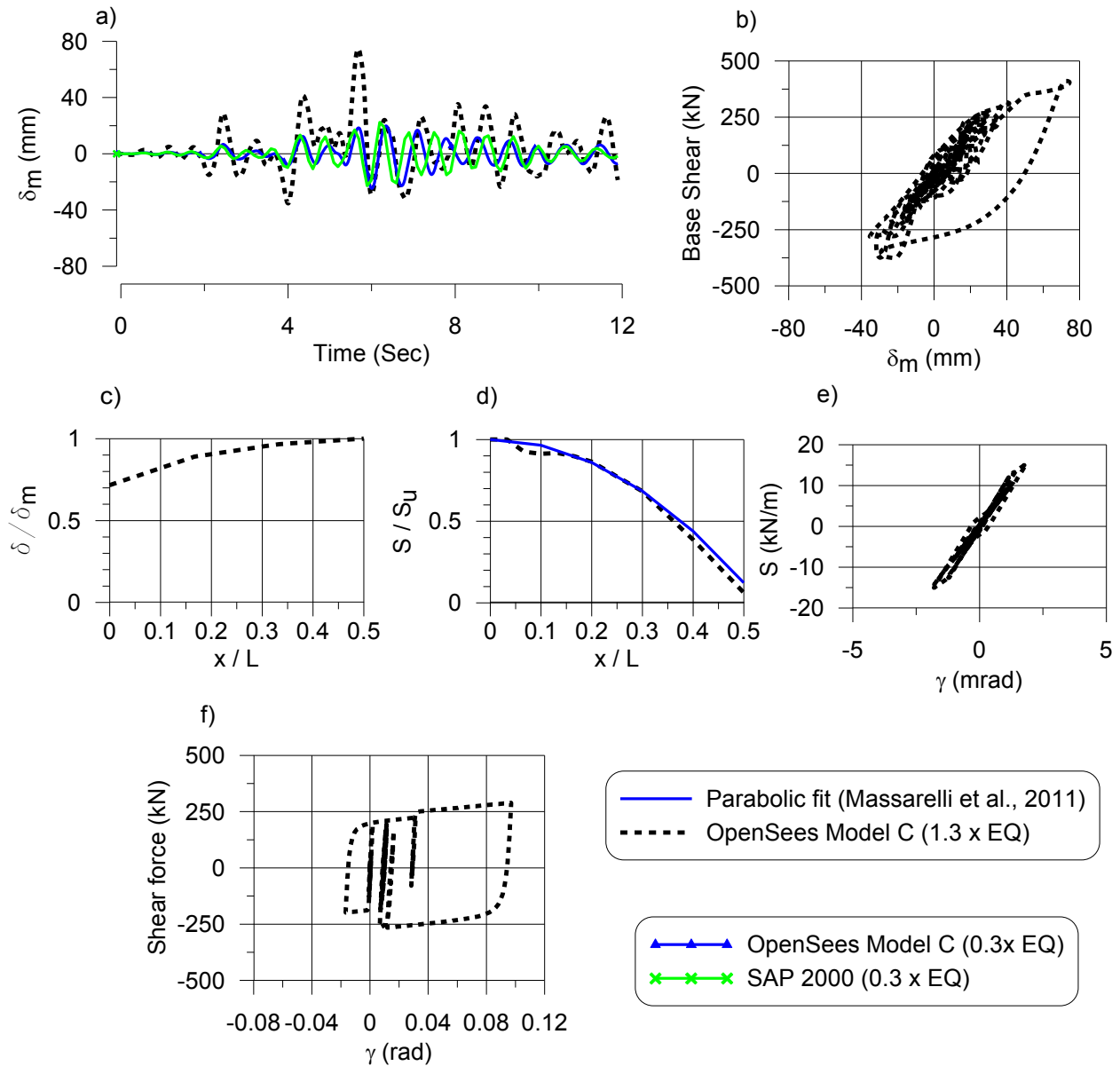
Figure 4.22 – Building response for CVM1 building (30m×60m×7m) under design level earthquake signal (record no. 0805): a) Displacement time history at mid-span; b) base shear vs. mid-span displacement; c) normalized maximum displacement profile along length; d) normalized shear force distribution along length; e) hysteretic response of diaphragm at the building edge and f) hysteretic response of a link beam.

Similar response was obtained for the large sized buildings (CVL0 and CVL1) which were designed for Abbotsford region. Figure 4.23 shows the predicted building responses for the Design 2 CVL0 building under design level earthquake loading (record number 0805). The roof
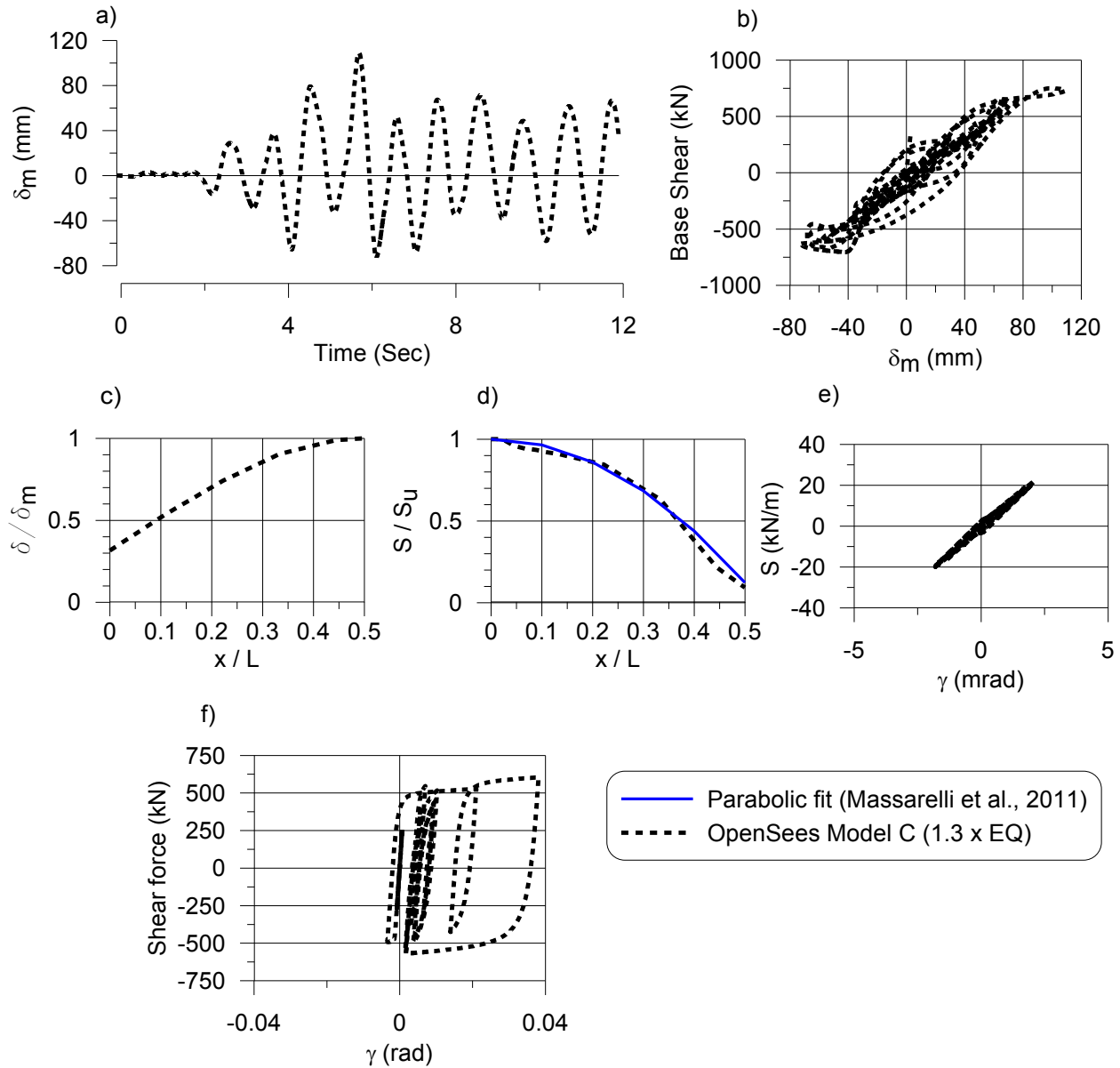
Figure 4.23 – Building response for CVL0 building (40m×90m×8m) under design level earthquake signal (record no. 0805): a) Displacement time history at mid-span; b) base shear vs. mid-span displacement; c) normalized maximum displacement profile along length; d) normalized shear force distribution along length; e) hysteretic response of diaphragm at the building edge and f) hysteretic response of a link beam.

diaphragm remains mainly elastic under design level earthquake signals. The maximum mid span displacement was found higher in the large sized buildings; however, the values were still significantly lower than the drift limit provided by NBCC. The deformation profile and shear profile along the length are similar to that of corresponding medium sized buildings. Similar results were obtained under the other earthquake signals (Appendix E).

4.6 Numerical modeling of buildings designed with CC type (System D)

Design of the buildings for the Conventional Construction type with CBF tension/compression structural system (System D) are presented in Section 3.10. OpenSees models were developed for the designed medium and large sized buildings which were located in Abbotsford, BC (Figure 4.14). The models were similar to the OpenSees Model A where the CBF OpenSees model developed by Agüero et al. (2006) was integrated with the non linear diaphragm model to develop full building model. The designed buildings were evaluated by applying the design level earthquakes (Section 4.2) in the N-S direction of the buildings.

4.6.1 Results and discussion

The predicted responses for the DVM0 building with OpenSees Model A under the design level earthquake are shown in Figure 4.24. The mid-span displacement time history under the elastic as well as inelastic earthquake signals is shown in Figure 4.24a. The time history result at the mid-span obtained from SAP 2000 under the elastic earthquake signal is also plotted in Figure 4.24a; it matches well with the results obtained from the OpenSees model. Figure 4.24b shows the predicted base shear vs. the mid-span displacement. The maximum base shear for the DVM0 building was similar to that obtained in AVM0 building. Figures 4.24c and 4.24d show the normalized maximum displacement profile and the shear force distribution on the diaphragm at the occurrence of maximum shear force at the edge of the building. The maximum displacement at the building edge under the design level ground motion was about 20% of the maximum mid-span displacement. Compared to the structural system A in which diagonal vertical braces are designed as fuse elements, the structural system D has a stiffer and a stronger brace system. On

the other hand, the diaphragms in this system are either weaker or comparatively of equal strength to that of structural system A. Hence, in the structural system D, the diaphragm experienced significant inelastic deformations and the braces remained elastic under the design
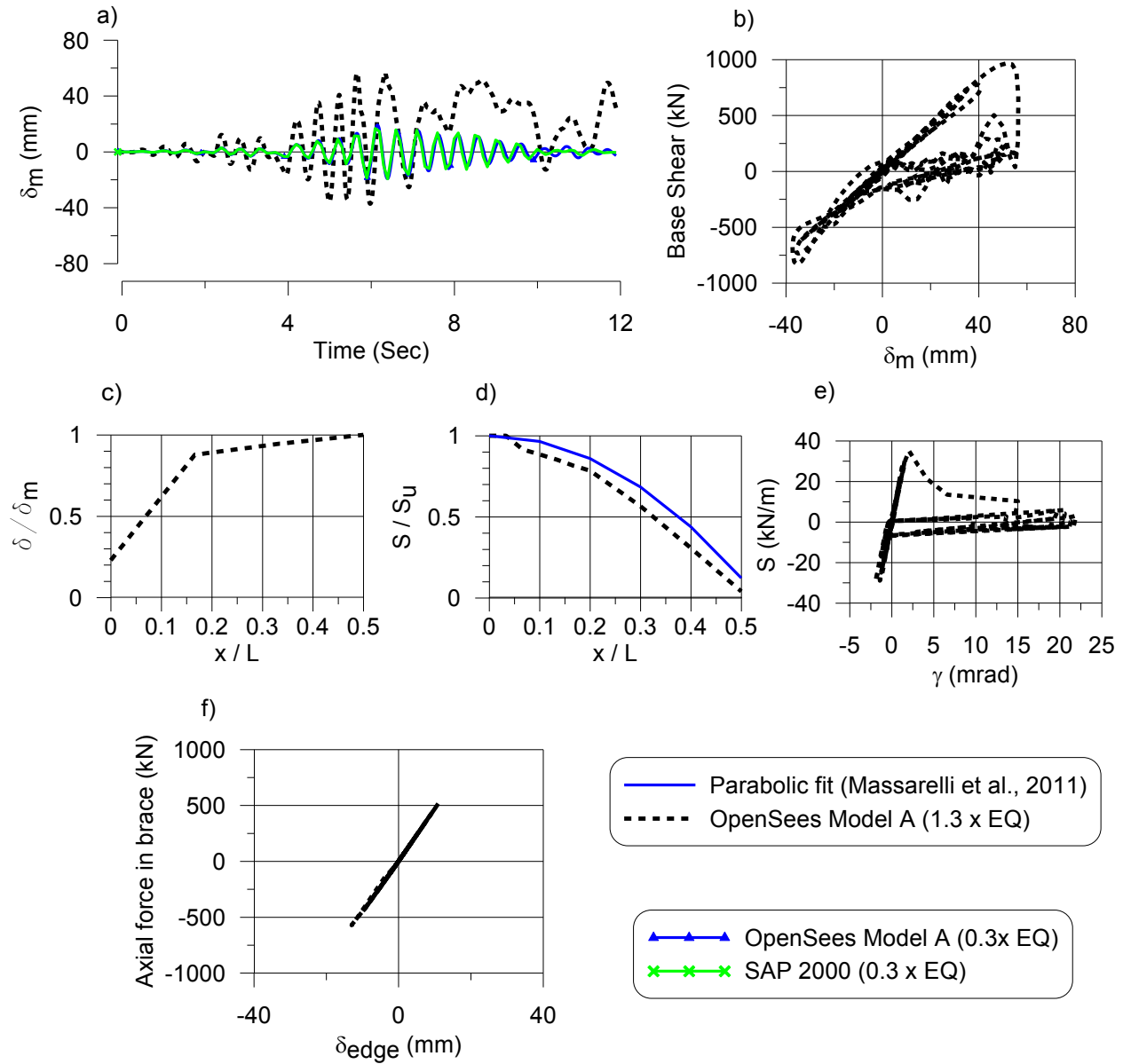
Figure 4.24 – Building response for DVM0 building (30m×60m×7m) under design level earthquake signal (record no. 0805): a) Displacement time history at mid-span; b) base shear vs. mid-span displacement; c) normalized maximum displacement profile along length; d) normalized shear force distribution along length; e) hysteretic response of diaphragm at the building edge and f) response of a diagonal brace member.

level earthquake loading. Figure 4.24e shows the shear response of the diaphragm at the end of building. The inelastic demand on the diaphragm was concentrated at the edge of the building (Figure 4.24c). The numerical model predicted significant strength degradation which could be
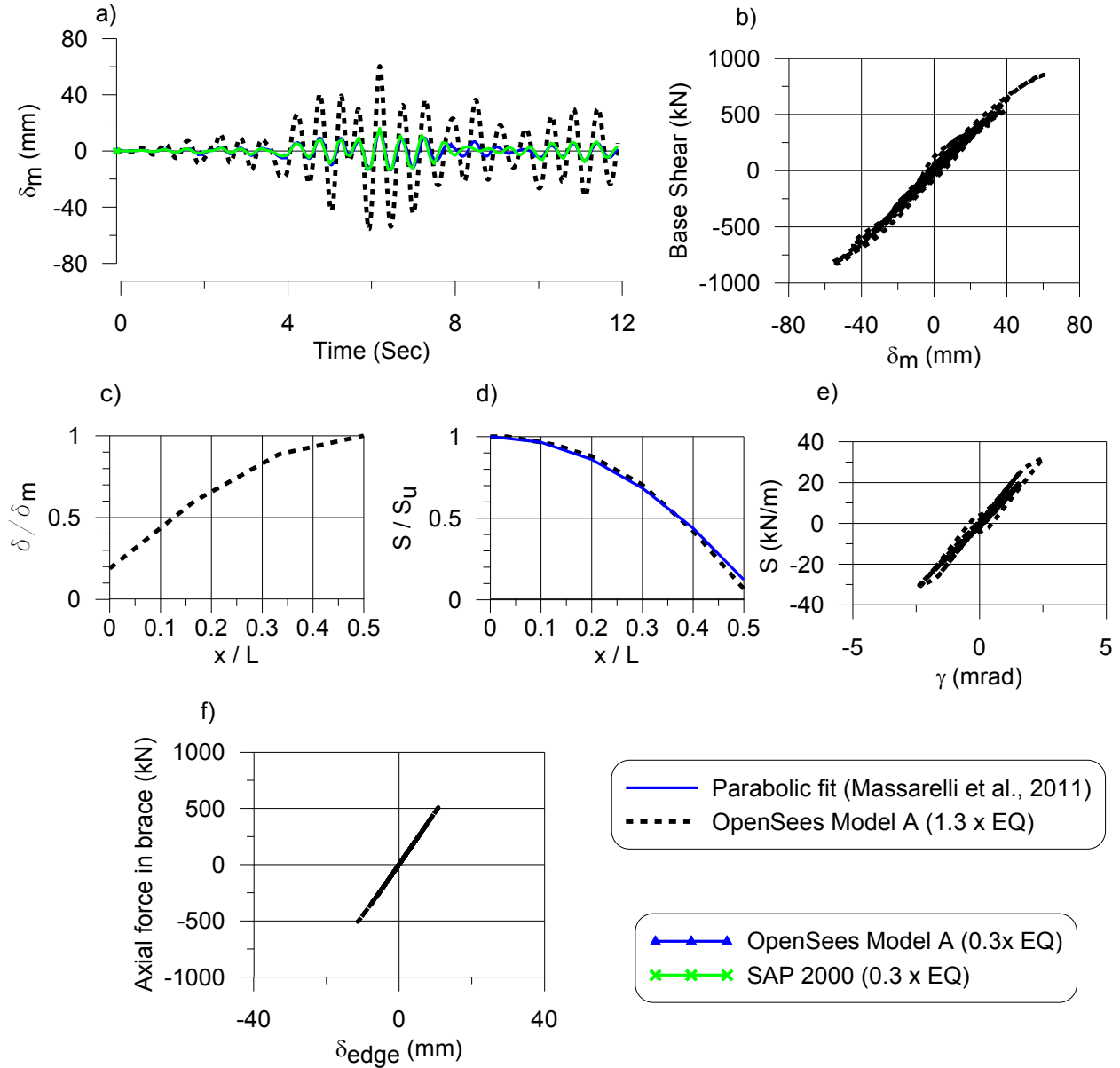
Figure 4.25 – Building response for DVM1 building (30m×60m×7m) under design level earthquake signal (record no. 0805): a) Displacement time history at mid-span; b) base shear vs. mid-span displacement; c) normalized maximum displacement profile along length; d) normalized shear force distribution along length; e) hysteretic response of diaphragm at the building edge and f) response of a diagonal brace member.

interpreted as a complete failure at these locations. Further, the diagonal brace remained elastic under the design level earthquake loading (Figure 4.24f). Similar results were also obtained under the other earthquake signals (Apendix E).
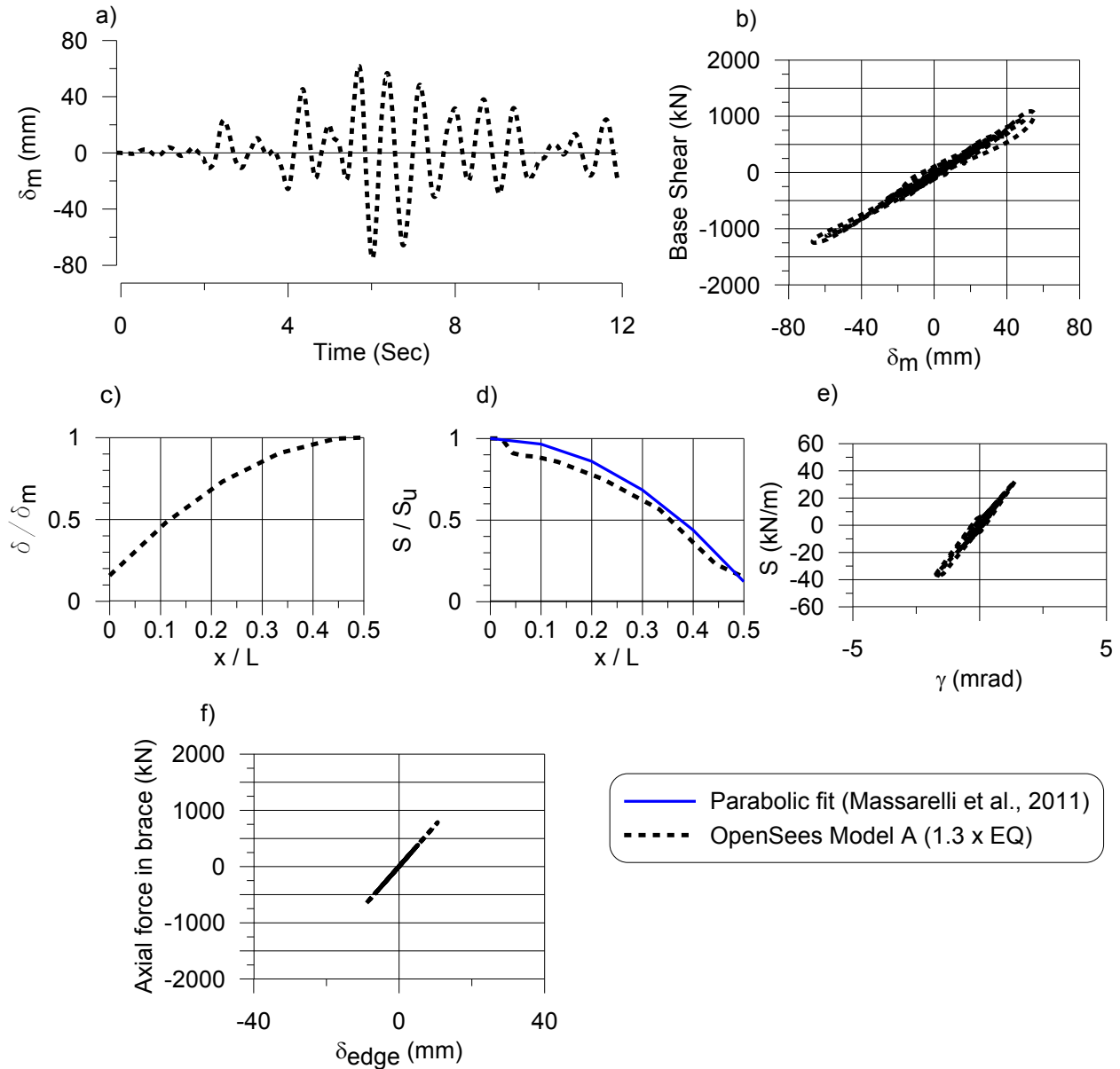
Figure 4.26 – Building response for DVL2 building (40m×90m×8m) under design level earthquake signal (record no. 0805): a) Displacement time history at mid-span; b) base shear vs. mid-span displacement; c) normalized maximum displacement profile along length; d) normalized shear force distribution along length; e) hysteretic response of diaphragm at the building edge and f) response of a diagonal brace member.

Figure 4.25 shows the predicted building responses for the DVM1 building with OpenSees Model A under the design level earthquake ($1.3 \times$ Loma Prieta EQ). Use of 70% of the SDI stiffness in the model did not significantly increase the maximum displacement demand at the mid-span as compared to that of the DVM0 building where 100% of SDI stiffness was used in the model (Figure 4.25a). Analysis using series of earthquake signal shows that the diaphragm could go into inelastic region. However, the model provided a near elastic response for the diaphragm under design level Loma Prieta earthquake signal (Figure 4.25e). The maximum shear force demand on the diaphragm was higher than the factored shear resistance (32kN/m vs 25kN/m). The nominal shear resistance (SDI value) of 41.6 kN/m was used in the model.

Similar response was obtained for the large sized buildings (DVL0 and DVL1) that were designed for Abbotsford. Figure 4.26 shows the predicted building responses under design level earthquake loading (record number 0805) for the Design 2 DVL2 building in which the period of vibration was not limited in design. The diagonal brace remained elastic (Figure 4.26 f) whereas the roof diaphragm went into inelastic region of behaviour (Figure 4.26e) under the design level earthquake signals. Analysis showed that similar response could be obtained under the other earthquake signals. The maximum mid-span displacement was found slightly higher in the large sized buildings than in the corresponding medium sized buildings; however, the values were still significantly lower than the drift limit provided by NBCC. The deformation profile and shear profile along the length are similar to that of corresponding medium sized buildings.

4.7 Comparison of maximum inelastic mid-span displacement

Table 4.4 and 4.5 show the predicted maximum inelastic mid-span displacement using the elastic SAP 2000 models and the inelastic OpenSees models for the designed medium sized (30m×60m×7m) and large sized (30m×60m×7m) buildings respectively. The lateral loads calculated by using the equivalent static method (NBCC, 2010) were used to determine the elastic displacements in the SAP models. The actual building periods were used to calculate these displacements as permitted in the NBCC. The maximum inelastic displacements at mid-span are generally estimated by multiplying the total elastic displacement (Δ) with $R_d R_o$ of the structural system (Method A). One could also use Method B where only the edge displacement

126

or diaphragm displacement is multiplied with the R_dR_o factor depending upon the structural system. Under the design level earthquake loading, it could be expected that the diaphragms would remain elastic in structural system A and C. Whereas, for the structural system B and D, it could be expected that the vertical brace would remain elastic under the design level earthquake loading. Method A will always give higher values than Method B.

Table 4.4– Maximum inelastic mid-span lateral displacement of medium sized buildings

Structural system	R_dR_o	Design Case	Mid-span inelastic displacement (mm)		OpenSees Model (Avg.)	OpenSees Model (Standard Dev.)
			SAP Model			
			Method A*	Method B†		
A	3.9	AVM0	41.3	26.8	49	9.0
		AVM1	49.1	29.4	50	6.8
		AVM2	51.5	29.4	51	6.6
B	3.8	BVM0	91.6	82.3	91	14.6
		BVM1_Design 1	92.0	81.3	87	19.1
		BVM1_Design 2	93.8	83.2	106	24.2
		BMM0	43.3	38.3	44	11.5
		BMM1	42.9	36.8	44	7.0
C	6.0	CVM0	72.6	35.6	55	9.0
		CVM1	80.4	42.9	56	11.5
D	2.0	DVM0	45.6	36.8	62	21.2
		DVM1	52.2	43.7	56	9.2
		DVM2	51.5	43.1	56	9.2

*Method A: ΔR_dR_o , †Method B: $\Delta_bR_dR_o + \Delta_d$ or $\Delta_dR_dR_o + \Delta_b$

Where,

Δ - Total elastic deformation at mid-span

Δ_b - Elastic deformation at building edge,

Δ_d - Elastic deformation of diaphragm at mid-span relative to the building edge,

The predicted maximum inelastic displacement (average considering all the other earthquake signals) from the OpenSees models were closer to the corresponding values determined with SAP models "Method A" for almost all the structural systems. Further, as can be seen on the Table 4.4 and 4.5, the use of an unlimited period of vibration in design did not significantly

increase the maximum displacement demand at mid-span due to the decrease in the lateral forces. This indicates that analytically predicted fundamental periods could be used in the design of such single-storey steel buildings.

Table 4.5– Maximum inelastic mid-span lateral displacement of large sized buildings

| Structural system | R_dR_o | Design Case | Mid-span inelastic displacement (mm) | | OpenSees Model (Avg.) | OpenSees Model (Standard Dev.) |
| | | | SAP Model | | | |
			Method A*	Method B†		
A	3.9	AVL0	72.2	45.4	73	17.9
		AVL2	84.6	39.8	72	16.0
B	3.8	BVL0	88.7	75.9	56	9.1
		BVL1	146.2	130.8	95	39.4
C	6	CVL0	99	42.5	87	13.3
		CVL1	108	54	88	13.2
D	2	DVL0	71	60.9	71	16.4
		DVL2	65.1	56	78	20.0

*Method A: ΔR_dR_o , †Method B: $\Delta_b R_dR_o + \Delta_d$ or $\Delta_d R_dR_o + \Delta_b$

4.8 Summary and conclusion on numerical modeling of buildings

Non-linear OpenSees building models were developed for the single-storey steel buildings which were designed for the four structural systems under different design considerations. The calibrated Pinching4 material modeling parameters obtained from the numerical modeling of the Phase I to III test specimens were used in the OpenSees building models to assess the inelastic deformation demand within the diaphragm. The calculated SDI nominal shear strength of the diaphragm (S_n) and either 70% or 100% of the SDI shear stiffness (G'), depending upon the design case, were used in the models. The historical earthquake records and simulated earthquake signals provided by Atkinson (2009) were used in the analysis. For all the structural systems, the OpenSees models provided the same fundamental period of vibration as obtained by the corresponding SAP 2000 building models. Further, the maximum displacement demand at mid-span was not notably affected by the use of an unlimited period in design in all four

structural systems due to the associated decrease in the lateral forces. This indicates that analytically predicted fundamental periods could be used in the design of such single-storey steel buildings.

4.8.1   Structural System B

The non linear diaphragm model was used with an elastic vertical bracing system to develop the OpenSees model for the buildings designed with the inelastic diaphragm structural system (System B). The response of the buildings was evaluated under the design level earthquake signals.

Two types of models "Model B1 and Model B2" were developed for design case BVM1 (System B), for which a mesh size of 2m by 2m and 2m by 10m were used, respectively. The 2m by 10m mesh size was selected in Model B2 to study the applicability of the strip model. The predicted responses using the OpenSees Model B1 and B2 were identical for the Design 1 (Layout I diaphragm) buildings. This showed that a strip model "Model B2" can be used for modeling a large building when the steel deck panels are perpendicular to the loading direction, which could save both time and effort in modeling. However, for the Design 2 (Layout II diaphragm) buildings, when the deck panels were oriented parallel to the seismic loading, the OpenSees Model B2 did not provide an identical response in comparison with the OpenSees Model B1 and hence may not be appropriate for the non linear analysis. The difference in inelastic demand between Model B1 and Model B2 for the Design 2 buildings could be because of an influence of the joist members which run perpendicular to the direction of excitation.

As expected, a higher concentration of inelastic demand at the end of the diaphragm was found in the Design 2 building compared to the Design 1 building under the design level earthquake. For these structures, the maximum displacement at the edge of the building was below 10% of the maximum displacement at the mid-span, which demonstrated that the flexibility of the diaphragm played an important role in the overall response of the structure. Furthermore, the maximum displacement demand at the mid-span of the buildings was significantly lower for the buildings that were designed for Montreal compared to the buildings designed for Abbotsford.

129

The lower inelastic demand for the buildings that were designed for the Montreal region could be due to the nature of eastern Canada ground motion.

The plastic shear deformation demand under the design level earthquake loading for the steel deck diaphragms in the structural system B with Design 2 consideration was greater than 0.01 radian. When the period was limited to the code provision, the inelastic shear deformation in the diaphragm was notably lower because of the higher design shear force for the diaphragm. However, analysis shows that the shear deformation in the diaphragm could be greater than 0.01 radian even though the design period was limited as of the NBCC provision. Essa et al. (2001) recommended to limit the plastic shear deformation to 0.01 radian for the diaphragms with nail deck to frame fasteners and screw side-lap fasteners in order to maintain the shear strength of a diaphragm at greater than 80% of its ultimate capacity. Almost complete shear failure of the diaphragm occurred at the edge of the Design 2 building which demonstrated that the use of $R_d =$ 2.0 in the design of this type of buildings might not be appropriate. A study is needed to develop an appropriate R_d value for the design of the buildings with this type of structural system.

4.8.2 Structural System A

A non-linear concentric braced frame model in the OpenSees software platform, developed by Agüero et al. (2006) to simulate the hysteretic response of the vertical bracing member, was incorporated in the OpenSees models for the buildings with the CBF structural systems (System A). The response of the buildings was evaluated under the design level earthquake signals.

The inelastic displacement at the mid-span of the medium sized building for structural system A was considerably smaller than that of structural system B. The maximum inelastic displacement at the building edge for the medium sized buildings was about 50% of the maximum mid-span displacement. This value was decreased approximately to 35% for large sized buildings. The drift demand at the building edge was found to decrease as the flexibility of the diaphragm was increased. For all the design cases of structural system A, the design shear force on the diaphragms was controlled by the base shear determined with R_dR_o of 2.0. Due to this (most probably), the maximum shear force demand on the diaphragm was more than its factored shear

resistance. However, the maximum shear displacement demand on diaphragm was well below the limit (0.01 rad.) suggested by Essa et al. (2001). This indicated that the upper limit on the diaphragm force when carrying out capacity design calculations could correspond to that obtained with $R_dR_o = 2$. Further, the shear force demand on the diaphragm decreased when the flexibility of the diaphragm was increased. The inelastic deformation demand on the vertical brace was also found to decrease as the flexibility of the diaphragm increases. This may be due to the influence of the ratio of the stiffness of the diaphragm to that of the bracing bent. Further study is needed to understand this behaviour.

4.8.3 Structural System C

For the buildings with an EBF structural system (System C), the non-linear OpenSees EBF model developed by Koboevic et al. (2011) was integrated with the non-linear OpenSees diaphragm models. The response of the buildings (both sizes) was evaluated under the design level earthquake signals.

Due to the inherent greater flexibility of EBFs vs. CBFs (e.g., $T_{N-S} = 0.69$ s instead of 0.54 s for the CMV1 and AVM2 buildings) and the higher force modification factors specified for Type D EBFs vs. Type MD CBFs ($R_dR_o = 6.0$ instead of 3.9), the maximum base shear for the buildings (with or without period limitation) of the structural system C was about half of the base shear obtained in the corresponding building of the structural system A. This demonstrated that system C could be a better option than the system A. Further, the maximum displacement at the mid-span did not increase notably in the buildings where period of vibration was not limited in design. This suggests that period limitation could be exploited in the design of such buildings. The maximum displacement at the edge of the building was comparatively higher in the EBF system than in the CBF system due to higher flexibility and inelastic deformations of the EBF system. The design of diaphragm of buildings for this system was not controlled by the force corresponding to $R_dR_o = 2.0$. The maximum shear force on the diaphragm was slightly above the factored shear resistance of the diaphragm. The reason could be as follows: when the force on the diaphragm was within the elastic limit, the shear force at the middle (over the depth) of the diaphragm was about 16% higher than the force towards the edge (over the depth) of the

diaphragm. The maximum shear displacement demand on diaphragm was well below the limit (0.01 rad.) suggested by Essa et al. (2001). Although the design of diaphragm of buildings for this system was not controlled by the force corresponding to $R_dR_o = 2.0$, it is likely that the diaphragm could be designed for this force whenever it controls the design.

Analysis shows that the maximum inelastic shear link rotation of the link beam could be slightly over 0.08 radian in the buildings with EBF structural system; which is the limit specified in the CSA S16 Standard (2009) for link beams yielding in shear. Further, the maximum inelastic shear link rotation of the link beam was slightly greater in the buildings where the period of vibration was not limited in design. Analysis that was done using the SDI predicted shear stiffness for the diaphragm in the CVM0 building, instead of using 70% of the SDI predicted stiffness, showed that the maximum mid-span displacement and the inelastic demand on the link beam could be decreased if the stiffness of the diaphragm were increased.

4.8.4 Structural System D

The models in the structural system D were similar to the OpenSees Model A where the CBF OpenSees model developed by Agüero et al. (2006) was integrated with the non linear diaphragm model to develop the OpenSees building model. The designed buildings were evaluated by exciting the design level earthquake signals in the N-S direction of the buildings.

Compared to the structural system A in which diagonal vertical braces are designed as fuse elements, the structural system D has a stiffer and a stronger brace system. On the other hand, the diaphragms in this system are either weaker or comparatively of equal strength to that of structural system A. Hence, in the structural system D, the diaphragm experienced significant inelastic deformations and the braces remained elastic under the design level earthquake loading. The inelastic demand on the diaphragm was concentrated at the edge of the building (Design 2 building). Analysis shows that the inelastic demand on diaphragm could be significantly higher than the limit (0.01 rad.) suggested by Essa et al. (2001). The prediction of such failure was the motivation for the development of the OpenSees diaphragm model with strength degradation.

Chapter 5 – Conclusions and Recommendations

5.1 Summary

The general objective of the study was to improve knowledge of the flexibility and ductility characteristics of steel deck roof diaphragms and to incorporate this information into the design of single-storey steel buildings. The influence of the diaphragm flexibility on the overall period of vibration of a building was first investigated. A design approach in which the steel roof diaphragm acts as a ductile fuse element in the SFRS was also evaluated. This design approach, at present, is not permitted by the NBCC or CSA S16.

Nineteen large-scale roof diaphragm specimens were tested in a complementary study. This three phase test program involved a rectangular (7.31 m × 21.02 m) test frame on which common steel deck configurations were constructed. The tests were performed at various amplitudes of loading to measure the response of the diaphragm. The information obtained from these tests was used in the development and calibration of a deep horizontal plane truss diaphragm model using the OpenSees software platform. The model was proven capable of predicting the elastic and inelastic dynamic responses of the steel deck diaphragm test specimens.

Further, detailed design of representative medium sized (30 m × 60 m × 7 m) and a large sized (40 m × 90 m × 8 m) single-storey steel buildings was carried out. These buildings were designed with four types of structural system, within which, different design cases such as with and without period limitation as well as with reduced SDI shear stiffness of the diaphragm were considered. The designed buildings were modelled elastically in SAP 2000 in order to verify the initial assumption of fundamental period of vibration and drift limit specified by 2010 NBCC. Moreover, OpenSees non-linear building models were developed for the designed buildings by integrating non-linear brace models with the non-linear diaphragm models. Non-linear dynamic time history analyses were performed on the designed buildings using the corresponding OpenSees building model. The response of the buildings was evaluated under a series of design level earthquake signals to gain an understanding of the behaviour and how it would be affected by the different design approaches that were implemented.

133

5.2 Conclusion

5.2.1 Numerical modeling of roof diaphragm test specimens

The inelastic response of the dynamic diaphragm test specimens was simulated by using the OpenSees platform and the Pinching4 material models in a truss based configuration. Material parameters and mesh sizes were proposed. These parameters were further validated with the results obtained from past reversed cyclic tests of cantilever diaphragm specimens. The models provided good matching of elastic and inelastic response with the test results when the measured stiffness of the test specimens was used. Since the measured stiffness of the test specimens having nail or weld frame fasteners and screw side-lap connections was about 70% of the SDI stiffness, using such a value in the model provided an adequate match with the test response.

When the test specimens were connected to the underlying frame members only at alternate flutes of the deck (36/4 pattern), it was found necessary to incorporate a change in shear stiffness over the span length of the diaphragm in order for the model to match with the measured displacement profile. Use of a uniform shear stiffness over the span length in the model provided an adequate match with the test results when all the flutes of the test specimens were connected to the frame. However, the overall response, i.e., shear force at the end and displacement at mid-span, matched well for both the alternate and all flutes connected test specimens when uniform stiffness over the span length was used in the models. Since only the maximum shear force and maximum displacement are generally considered in the design of single-storey steel buildings, uniform stiffness over the span length could be used in analysis provided the diaphragm configuration does not change over the span length.

5.2.2 Design of single-storey steel buildings

The fundamental period of vibration of single-storey steel buildings with flexible roof diaphragms determined with the numerical models was significantly longer than the limit provided by the 2010 NBCC for all four structural systems. In contrast, the use of a rigid assumption for the roof diaphragm in the SAP models resulted in a period of vibration close to the limit provided by the NBCC. This clearly shows the impact of diaphragm flexibility in the

determination of fundamental period of vibration which is not considered by the NBCC recommended expression for such single-storey steel buildings.

The upper limit of the seismic base shear would control the design for the representative medium and large sized buildings whenever the period of vibration was limited in design as specified in the NBCC. It was found that the seismic design forces can decrease significantly when the period obtained by the numerical model is used for design. Particularly, in the buildings with the inelastic diaphragm structural system (system B), the design forces on the diaphragm can be decreased to 1/3 of the design forces with structural system A or D. This was mainly because the diaphragm itself acts as a fuse element in this structural system, and does not need to be capacity protected as is required when the braces are specified to dissipate seismic energy through inelastic action. Further, due to the lower design forces, the diaphragm in this system was more flexible, because it was either thinner or had fewer connectors, which helped to increase the fundamental period and to reduce the design seismic forces. On the other hand, due to the capacity design approach, diaphragms in structural system A and C must be configured to carry the probable resistance of the diagonal braces (CBF) or link beams (EBF), respectively. In particular, a thicker deck panel along with a more closely spaced fastener pattern was required for the diaphragm of the CBF structural system A compared to all other systems due to the larger design shear forces. This effect was less pronounced in for the diaphragm of buildings with the EBF structural system as those could be designed for a lower shear force compared to the diaphragms of buildings with structural system A or D because of the higher seismic force reduction R-factors specified in the NBCC, the lower system overstrength and the higher flexibility of the EBF system. Moreover, the NBCC listed seismic drift limit and the P-Δ effects were found to be not critical in the design of the single-storey buildings with the four structural systems.

5.2.3 Behaviour of single-storey steel buildings as obtained from OpenSees models

The maximum displacement demand at mid-span was not notably affected by the use of an unlimited period in design in all four structural systems due to the associated decrease in the lateral forces. This demonstrated that the analytically predicted fundamental period of vibration

could be used in the design of such single-storey steel buildings. This finding leads to the recommendation to revise the expression given in 2010 NBCC for the fundamental period of vibration as well as for the period limitation. The predicted maximum inelastic displacements from the OpenSees models were, on average, closer to the corresponding values determined with elastic SAP models "Method A" in which the total displacement was amplified by the factor R_dR_o, irrespective of whether the diaphragm or braced bay was expected to undergo inelastic deformations.

The design of diaphragms in the buildings of structural system A and C was slightly modified compared to current code requirements; an upper limit corresponding to $R_dR_o = 2.0$ was used for the design of the diaphragms instead of using $R_dR_o = 1.3$ that is currently specified in CSA S16-09. The upper limit corresponding to $R_dR_o = 2.0$ controlled the design of the diaphragm in all the design cases of structural system A, whereas it did not control the design for structural system C. The maximum shear displacement demand on the diaphragms under the design level earthquake signal was well below the limit (0.01 rad.) suggested by Essa et al. (2001) in both the buildings of structural system A and C. This indicated that the diaphragms in these structural system could be designed for the force corresponding to the upper limit with $R_dR_o = 2$ when carrying out capacity calculations for the SFRS.

Compared to the different structural systems, the buildings designed with an EBF structural system were found most promising in terms of the relative capacity force on the steel deck diaphragm and the building response. Further, from the analysis of these buildings, it was found that the inelastic shear rotation of the link beam as given by the CSA S16 Standard could be more critical than the overall drift limit. The mid-span drift demand was much lower than the overall drift limit, whereas the inelastic shear link rotation demand on the link beam was at the limiting level.

The inelastic rotational demand in the link beam was found to increase as the flexibility of the diaphragm was increased. In contrast, the inelastic deformation demand on the vertical braces in the buildings of structural system A was found to decrease as the flexibility of the diaphragm was increased. This dissimilar effect of diaphragm flexibility on the inelastic deformation demand may be due to differences in relative stiffness between the diaphragm and the braces in

136

these two lateral systems when the fuse elements enter into the inelastic range of behaviour. Further study is required to better understand this behaviour.

The inelastic shear deformation demand at the end of the diaphragms in the structural system B buildings was much more highly concentrated when the deck panels were parallel to the loading direction (Design 2) compared with the buildings with the panels oriented in the opposite orthogonal direction (Design 1). Similar damage concentration at the end of the diaphragm was observed in the dynamic tests of the Layout II diaphragm specimens. In these specimens, the side-laps of deck panels were parallel to the loading direction. The damage concentrated at the side-lap located near the edge of diaphragm. Under the design level earthquake loading, the inelastic shear deformation demand of the steel deck diaphragm in the structural system B with Design 2 consideration reached approximately two times the limit (0.01 radian) recommended by Essa et al. (2001). Such higher inelastic deformation was distributed mainly over a 7% " 2 m length" of the diaphragm span from the end after which there was drastic decrease in the deformation demand. A study should be carried out by using a lower value of R_d in the design of such buildings instead of the 2.0 that was assumed for design herein. In Design 1 building, the inelastic deformation demand was approximately in the range of 0.006 radian to 0.008 radian, and was distributed up to 20% of the diaphragm span from the end. Further, for the Montreal region, it was found that the maximum inelastic mid-span displacement demand of such buildings was lower. This could be due to the effect of the frequency content of the earthquake ground motions that are expected in eastern North America.

In the buildings with a Type CC structural system it was observed that the diaphragm could go into the inelastic region while the brace would remain mainly elastic under the design level earthquake loading. Significant strength degradation and concentration of inelastic demand in the diaphragm were observed in this structural system, which shows that the diaphragm may need to be designed corresponding to the elastic seismic force.

In terms of mesh sizing, the numerical analyses showed that a strip model could be used for modeling of the roof diaphragm in a large building when the steel deck is laid perpendicular to the loading direction (Design 1 buildings), which could save both time and effort in modeling. However, such models may not provide an identical response compared with the fine mesh

OpenSees models that incorporate a strip mesh pattern for the Design 2 buildings (deck parallel to loading direction) may not be appropriate. This could be because of an influence of the joist members which run perpendicular to the direction of excitation. A smaller diaphragm mesh size, joist spacing by joist spacing, is recommended for the analysis of Design 2 buildings.

5.3 Recommendation for further study

For the recommendation of the use of the analytical period in design, incremental dynamic analysis along with a study of the probability of failure of such designed buildings, through the development of fragility curves, are also required. A similar study is also needed on the design and evaluation of the buildings with ductile diaphragm (System B) to evaluate the ductility related seismic force reduction factor. Moreover, field measurements of the fundamental period of vibration of buildings using forced vibration techniques in addition to ambient vibration could be carried out to justify the elongated periods of vibration obtained from the numerical simulations.

It was found that the steel roof diaphragms along with other structural members of the SFRS are penalized significantly in the CBF structural system (System A) due to the probable tension resistance of the diagonal brace. More economical diaphragms could be obtained if the tension and compression brace capacity were comparable.

When the design of perimeter beams and braced frame members is controlled by the cut-off forces corresponding to $R_dR_o=2$ in the structural system B, these members may go into the inelastic region to some extent under the design level earthquake. Hence the building model for this structural system could be improved by using non-linear elements for these members.

In some of the dynamic diaphragm tests, mainly in thicker deck diaphragms and layout II diaphragm specimens, the inelastic demand was concentrated at one side of the specimen. This study can be extended to capture this response by modeling the full diaphragm specimen and allowing a slight difference in strength at the two edges of the diaphragm. This can further help to identify the sensitivity of inelastic demand to the lack of symmetry in the constructed structure. Furthermore, a study can be done to predict the building behaviour and inelastic

demand in fuse elements, as the buildings may exhibit torsional response under such condition. With regards to modeling the steel roof deck diaphragms, a study could also be done to incorporate the panel effect, which was observed in the dynamic tests, in the numerical model.

References

Adams, J. (1989)."Seismicity and Seismotectonics of Southeastern Canada". In "Earthquake Hazards and the Design of Constructed Facilities in the Eastern United States", Annals of the New York Academy of Sciences, Volume 558,:40-53.

Aguero, A., Izvernari, C., and Tremblay, R. (2006). "Modelling of the Seismic Response of Concentrically Braced Steel Frames using the OpenSees Analysis Environment." *Int. J. of Advanced Steel Construction*, 2, 3, 242-274.

Allahabadi, R., and Powell, G. H. (1988). "DRAIN-2DX". Berkeley, CA: Earthquake Engineering Research Center, University of California.

Atkinson, G. M. (2009). "Earthquake Time Histories Compatible with the 2005 NBCC Uniform Hazard Spectrum." *Canadian Journal of Civil Engineering*.

Canadian Institute of Steel Construction. (2010). "Handbook of Steel Construction", 10th Edition. Willowdale, ON: Canadian Institute of Steel Construction.

Canadian Sheet Steel Building Institute. (2006). "CSSBI B13-06: Design of Steel Deck Diaphragms", 3rd Edition. Cambridge, ON.

Canadian Sheet Steel Building Institute. (2007). "Sheet Steel Fact Sheet, SSF 9: Alternative Design Methods for Steel Deck Diaphragms". Cambridge, ON.

Canadian Standards Association. (1994). CSA-S16: "Limit States Design of Steel Structures". Rexdale, ON: Canadian Standards Association.

Canadian Standards Association. (2007). CSA-S136: "North American specification for the design of cold-formed steel structural members". Mississauga, ON: Canadian Standards Association.

Canadian Standards Association. (2009). CSA-S16: "Limit States Design of Steel Structures". Mississauga, ON: Canadian Standards Association.

Canam Group Inc., (2008a). "Joist Catalogue", Canada.

Canam Group Inc., (2008b). "Steel Deck", Canada.

Carr, A. J. (2004). "Ruaumoko - Dynamic Analysis of 2-Dimensional Inelastic Structures". Christchurch, New Zealand: University of Canterbury.

CSI. (2000). SAP 2000: "Integrated Software for Structural Analysis & Design", Version 10. Computers and Structures, Inc., Berkeley, CA.

CSI. (2010). SAP2000: "Integrated Software for Structural Analysis and Design", Version 14. Berkeley, CA: Computers and Structures, Inc.

Davies, J. M. (2006). "Developments in Stressed Skin Design." *Thin-Walled Structures*, Vol. 44, 1250–1260.

Davies, J. M., and Bryan, E. R. (1982). "Manual of Stressed Skin Diaphragm Design". St. Albans, Hertfordshire, England: Granada Publishing Ltd.

EERF. (2008). " In-plane monotonic and cyclic testing of steel roof deck diaphragms with nailed and welded connections" Earthquake Engineering Research Facility, University of British Columbia , Project No.: EERF 08-06

Essa, H. S., Tremblay, R., and Rogers, C. A. (2001). Report No. EPM/CGS-2001-11: "Inelastic Seismic Behaviour of Steel Deck Roof Diaphragms Under Quasi-Static Cyclic Loading". École Polytechnique de Montréal, Montreal, QC.

FEMA, "Effects of Strength and Stiffness Degradation on Seismic Response (ATC- 62 Project)," FEMA P440A, Federal Emergency Management Agency, Washington D.C., 2009.

Franquet, J. (2010). "Seismic design repair and retrofit strategies for steel roof deck diaphragms". Master of Engineering thesis. McGill University, Montreal, QC.

Franquet, J., Massarelli, R., Shrestha, K., Tremblay, R., and Rogers, C. A. (2010). "Dynamic Tests of 0.76 and 0.91 mm Steel Deck Diaphragms for Single-Storey Buildings." Paper

presented at the *9th US National and 10th Canadian Conference on Earthquake Engineering*, Toronto, ON.

Heidebrecht, A. C. (2003). "Overview of Seismic Provisions of the Proposed 2005 Edition of the National Building Code of Canada." *Canadian Journal of Civil Engineering*, Vol. 30, 241-254.

Humar, J., and Mahgoub, M. A. (2003). "Determination of Seismic Design Forces by Equivalent Static Load Method." *Canadian Journal of Civil Engineering*, Vol. 30, 287-307.

Humar, J., Yavari, S., and Saatcioglu, M. (2003). "Design for Forces Induced by Seismic Torsion." *Canadian Journal of Civil Engineering*, Vol. 30, 328-337.

Jin J, El-Tawil S. (2003). Inelastic cyclic model for steel braces. Journal of Engineering Mechanics, ASCE, 129(5): 548–557.

Koboevic,S., Rozon, J. and Tremblay,R. (2011). "Seismic performance of low-to-moderate height eccentrically braced steel frames designed for North-American seismic conditions." *Journal of Structural Engineering*, American Society of Civil Engineers. (in press)

Lamarche, C.-P., Proulx, J., and Paultre, P. (2004). "An Experimental Investigation of the Dynamic Characteristics of Low Rise Steel Structures." Paper presented at the *5th Structural Specialty Conference of the Canadian Society for Civil Engineering*, Saskatoon, SK.

Lamarche, C.-P., Proulx, J., Paultre, P., Turek, M., Ventura, C. E., Le, T. P., et al. (2009). "Toward a better understanding of the dynamic characteristics of single-storey braced steel frame buildings in Canada." *Canadian Journal of Civil Engineering*, Vol. 36, 969-979.

Léger, P., Tayebi, A. K., Paultre, P. (1993). "Spectrum-compatible Accelerograms for Inelastic Seismic Analysis of Short-period Structures located in eastern Canada." *Canadian Journal of Civil Engineering*, Vol. 20, 951-968.

Luttrell, L. D. (1981)." Steel Deck Diaphragm Design Manual", 1st Edition. Steel Deck Institute.

Luttrell, L. D. (2004). "Diaphragm Design Manual", 3rd Edition. Fox River Grove, IL: Steel Deck Institute.

Mansour, N., Shen, Y., Christopoulos, C., & Tremblay, R. (2008). "Experimental evaluation of nonlinear replaceable links in eccentrically braced frames and moment resisting frames." Paper presented at the *14th World Conference on Earthquake Engineering*, Beijing, China.

Martin, E. (2002). "Inelastic Response of Steel Roof Deck Diaphragms Undeeer Simulated Dynamically Applied Seismic Loading". Master of Applied Science thesis. École Polytechnique de Montréal, Montreal, QC.

Massarelli, R. (2010). "Dynamic Behaviour and Inelastic Performance of Steel Roof Deck Diaphragms". Master of Engineering, thesis, McGill University, Montreal, QC.

Massarelli, R., Franquet, J., Shresta, K., Tremblay, R., and Rogers, C. (2011). "Dynamic Seismic Response of Large Scale Steel Deck Diaphragms". J. Constr. Steel Research (submitted).

Mastrogiuseppe, S. (2006). "Numerical Linear Elastic Investigation of Steel Roof Deck Diaphragm Behaviour Accounting for the Contribution of Non-structural Components". M. Eng. thesis. McGill University, Montreal, QC, Canada.

Mastrogiuseppe, S., Rogers, C.A., Nedisan, C.D., Tremblay, R., (2008). "Influence of non-structural components on roof diaphragm stiffness and fundamental periods of single-storey steel buildings." *Journal of Constructional Steel Research*, 64(2), 214-227.

Mazzoni, S., McKenna, F., Scott, M.H., and Fenves, G.L. (2009). "Open System for Earthquake Engineering Simulation". User Command-Language Manual. *Pacific Earthquake Engineering Research Center*, University of California, Berkeley, Berkeley, CA. http://opensees.berkeley.edu/OpenSees/manuals/usermanual/index.html

McKenna, F. (1997). "Object-oriented finite-element programming: Frameworks for analysis, algorithms, and parallel computing." Ph.D. thesis, Univ. of California, Berkeley, Calif.

Medhekar, M. S., and Kennedy, D. J. L. (1999). "Seismic Evaluation of Single-Storey Steel Buildings." *Canadian Journal of Civil Engineering*, Vol. 26, 379-394.

Medhekar, M. S.(1997). "Seismic evaluation of steel buildings with concentrically braced frames". Ph.D. Thesis, Dept. of Civil and Environmental Engineering, University of Alberta, Edmonton, AB, Canada.

Mitchell, D., Tremblay, R., Karacabeyli, E., Paultre, P., Saatcioglu, M., and Anderson, D. L. (2003). "Seismic Force Modification Factors for the Proposed 2005 Edition of the National Building Code of Canada." *Canadian Journal of Civil Engineering*, Vol. 30, 308-327.

National Research Council of Canada (1990). "National building code of Canada 1990", 10th Edition. Ottawa, ON.

National Research Council of Canada. (1995). "National Building Code of Canada 1995", 11th Edition. Ottawa, ON.

National Research Council of Canada. (2010a). "National Building Code of Canada 2010", Ottawa, ON.

National Research Council of Canada. (2010b). "User's Guide – NBC 2010 Structural Commentaries (Part 4 of Division B)", Ottawa, On, Canada.

National Research Council of Canada. (2005). "User's Guide – NBC 2005 Structural Commentaries (Part 4 of Division B)", Ottawa, On, Canada.

Okazaki, T., Arce, G., Ryu, H., and Engelhardt, M. 2005. Experimental study of local buckling, overstrength, and fracture of links in eccentrically braced frames. ASCE J. of Struct. Eng. 131(10): 1526-1535.

Paultre, P., Proulx, J., Ventura, C., Tremblay, R., Rogers, C., Lamarche, C.-P., Turek, M. (2004). "Experimental Investigation of Low-Rise Steel Buildings for Efficient Seismic Design." *13th World Conference on Earthquake Engineering*, Canadian Association for Earthquake Engineering (CAEE), paper 2919.

Rainer, J.H., Jablonsky, A.M., Law, K.T., and Allen, D.E. (1990). "The San Francisco area earthquake of 1989 and implication for the Greater Vancouver area." *Canadian Journal of Civil Engineering*, 17(5): 798-812.

Risk Engineering, Inc. (2001). Technical basis for revision of regulatory guidance on design ground motions: hazard- and risk-consistent ground motion spectra guidelines, US Nuc. Reg. Comm. Rept. NUREG/CR-6728, October.

Rogers, C. A., and Tremblay, R. (2003a). "Inelastic Seismic Response of Frame Fasteners for Steel Roof Deck Diaphragms." *Journal of Structural Engineering*, Vol. 129, No. 12, 1647-1657.

Rogers, C. A., and Tremblay, R. (2003b). "Inelastic Seismic Response of Side Lap Fasteners for Steel Roof Deck Diaphragms." *Journal of Structural Engineering*, Vol. 129, No. 12, 1637-1646.

Rogers, C. A., and Tremblay, R. (2010). "Impact of Diaphragm Behaviour on the Seismic Design of Low-Rise Steel Buildings." *AISC Engineering Journal*, Vol. 47, No. 1, 21-36.

Rogers, C.A., Tremblay, R., (2000). "Inelastic seismic response of frame and sidelap fasteners for steel roof decks". Research Report No. EPM/CGS-2000-09, Department of Civil, Geological and Mining Engineering, École Polytechnique de Montréal, Montréal, QC, Canada.

Rogers, C.A., Tremblay, R., Yang, W., Martin, E., (2004). "Ductile Design of Steel Roof Deck Diaphragms for Earthquake Resistance." *13th World Conference on Earthquake Engineering*, Vancouver, Canada, Paper No. 1997.

Shrestha, K., Franquet, J., Rogers, C. A., and Tremblay, R. (2009). "OpenSees modeling of the inelastic seismic response of steel roof deck diaphragms." Paper presented at the *6th International Conference - Behaviour of Steel Structures in Seismic Areas (STESSA)*, Philadelphia, PA.

Stewart, W.G. (1987). "The seismic design of plywood sheated shear walls". Ph.D thesis, Department of Civil Engineering, Christchurch, New Zealand.

Tremblay R., Nedisan C., Lamarche C.-P. and Rogers C.A. (2008a). "Periods of Vibration of A Low-Rise Building with A Flexible Steel Roof Deck Diaphragm." 5th *International Conference on Thin-Walled Structures*, Brisbane, Australia

Tremblay, R., and Stiemer, S. S. (1996). "Seismic Behaviour of Single-Storey Steel Structures with a Flexible Roof Diaphragm." *Canadian Journal of Civil Engineering*, Vol. 23, 49-62.

Tremblay, R., Berair, T., and Filiatrault, A. (2000). "Experimental Behaviour of Low-Rise Steel Buildings with Flexible Roof Diaphragms." Paper presented at the *12th World Conference on Earthquake Engineering*, Auckland, New Zealand, Paper No. 2567.

Tremblay, R., Rogers, C.A., (2005). "Impact of capacity design provisions and period limits on the seismic design of low-rise steel buildings." *International Journal of Steel Structures*, 5(1), 1-22.

Tremblay, R., Rogers, C.A., Franquet, J., Lamarche, C.-P., Nedisan, C., and Massarelli, R. (2011). "Large Scale Dynamic and Seismic Testing of Steel Deck Diaphragm for Low-Rise Buildings". J. Constr. Steel Research (submitted)

Tremblay, R., Rogers, C.A., Lamarche, C.-P., Nedisan, J., Franquet, J., Massarelli, R. and Shrestha, K (2008b). " Dynamic seismic testing of large size steel deck diaphragm for low-rise building applications." *14th World Conference on Earthquake Engineering*, October 12-17, 2008, Beijing, China.

Tremblay, R., Rogers, C.A., Martin, E., Yang, W., (2004). "Analysis, testing and design of steel roof deck diaphragms for ductile earthquake resistance." *Journal of Earthquake Engineering*, 8(5), 775-816.

Tremblay, R., Rogers, C.A., Nedisan, C., (2002). "Use of Uniform Hazard Spectrum and Computed Period in the Seismic Design of Single-Story Steel Structures." *7th U.S. National Conference on Earthquake Engineering*, Boston, USA, Paper No. 195.

Tremblay, R., Rogers, C.A., Nedisan, C. (2003). "Seismic Torsional Response of Single-Storey Steel Structures With Flexible Roof Diaphragms." *Advances in Structures*, Vols 1 and 2, p. 1299-1305.

Tri-Services Technical Manual. (1973). "Seismic Design for Buildings", TM 5-809-10/NAVFAC P-355/AFM 88-3, Chap. 13, Departments of the Army, Navy and Air Force, USA.

Tri-Services Technical Manual. (1982). "Seismic Design for Buildings". Departments of the Army, Navy and Air Force, Philadelphia, PA: US Government Printing Office.

Uriz, P. (2005). Towards earthquake resistant design of concentrically braced steel structures, PhD Dissertation, University of California, Berkeley.

Uriz, P., F.C. Filippou and S.A. Mahin (2008). "Model for Cyclic Inelastic Buckling of Steel Braces." *Journal of Structural Engineering*, American Society of Civil Engineers, Vol. 134, No. 4, pp. 619-628.

USACE. (1998). "Seismic design for Buildings", Technical Instructions TI-809-04, US Army Corps of Engineers (USACE), Engineering Division, Washington, DC.

Yang, W. (2003). "Inelastic Seismic Response of Steel Roof Deck Diaphragms Including Effects of Non-Structural Components and End Laps". Master of Applied Science thesis. École Polytechnique de Montréal, Montreal, QC.

Appendix A:

Example OpenSees script for non-linear modeling of diaphragm test specimens (Specimen 6)

#Hysteretic Modelling of Diaphragm, TEST 6
#Unit kN, mm, Sec
Start of model generation

Create ModelBuilder (with two-dimensions and 3 DOF/node)
model BasicBuilder -ndm 2 -ndf 3

Create nodes & add to Domain - command: node nodeId xCrd yCrd Mass in x Direc, Mass in Y Direc, Mass in rotional direc

node	1	0	0	-mass	0	5.02E-05	0
node	2	875.8	0	-mass	0	5.46E-05	0
node	3	1751.6	0	-mass	0	1.30E-04	0
node	4	2627.4	0	-mass	0	5.46E-05	0
node	5	3503.2	0	-mass	0	1.30E-04	0
node	6	4379	0	-mass	0	5.46E-05	0
node	7	5254.8	0	-mass	0	1.30E-04	0
node	8	6130.6	0	-mass	0	5.46E-05	0
node	9	7006.4	0	-mass	0	1.30E-04	0
node	10	7882.2	0	-mass	0	5.46E-05	0
node	11	8758	0	-mass	0	1.30E-05	0
node	12	9633.8	0	-mass	0	5.46E-05	0
node	13	10509.6	0	-mass	0	6.52E-05	0
node	14	0	914	-mass	0	5.68E-05	0
node	15	875.8	914	-mass	0	2.19E-05	0
node	16	1751.6	914	-mass	0	1.74E-04	0
node	17	2627.4	914	-mass	0	2.19E-05	0
node	18	3503.2	914	-mass	0	1.74E-04	0
node	19	4379	914	-mass	0	2.19E-05	0
node	20	5254.8	914	-mass	0	1.74E-04	0
node	21	6130.6	914	-mass	0	2.19E-05	0
node	22	7006.4	914	-mass	0	1.74E-04	0
node	23	7882.2	914	-mass	0	2.19E-05	0
node	24	8758	914	-mass	0	1.73E-04	0
node	25	9633.8	914	-mass	0	2.19E-05	0
node	26	10509.6	914	-mass	0	8.68E-05	0
node	27	0	1828	-mass	0	5.68E-05	0
node	28	875.8	1828	-mass	0	2.19E-05	0
node	29	1751.6	1828	-mass	0	1.74E-04	0
node	30	2627.4	1828	-mass	0	2.19E-05	0
node	31	3503.2	1828	-mass	0	1.74E-04	0
node	32	4379	1828	-mass	0	2.19E-05	0
node	33	5254.8	1828	-mass	0	1.74E-04	0
node	34	6130.6	1828	-mass	0	2.19E-05	0
node	35	7006.4	1828	-mass	0	1.74E-04	0
node	36	7882.2	1828	-mass	0	2.19E-05	0
node	37	8758	1828	-mass	0	1.73E-04	0
node	38	9633.8	1828	-mass	0	2.19E-05	0
node	39	10509.6	1828	-mass	0	8.68E-05	0
node	40	0	2742	-mass	0	5.68E-05	0
node	41	875.8	2742	-mass	0	2.19E-05	0
node	42	1751.6	2742	-mass	0	1.74E-04	0
node	43	2627.4	2742	-mass	0	2.19E-05	0
node	44	3503.2	2742	-mass	0	1.74E-04	0
node	45	4379	2742	-mass	0	2.19E-05	0
node	46	5254.8	2742	-mass	0	1.74E-04	0

node	47	6130.6	2742	-mass	0	2.19E-05	0
node	48	7006.4	2742	-mass	0	1.74E-04	0
node	49	7882.2	2742	-mass	0	2.19E-05	0
node	50	8758	2742	-mass	0	1.73E-04	0
node	51	9633.8	2742	-mass	0	2.19E-05	0
node	52	10509.6	2742	-mass	0	8.68E-05	0
node	53	0	3656	-mass	0	5.68E-05	0
node	54	875.8	3656	-mass	0	2.19E-05	0
node	55	1751.6	3656	-mass	0	1.74E-04	0
node	56	2627.4	3656	-mass	0	2.19E-05	0
node	57	3503.2	3656	-mass	0	1.74E-04	0
node	58	4379	3656	-mass	0	2.19E-05	0
node	59	5254.8	3656	-mass	0	1.74E-04	0
node	60	6130.6	3656	-mass	0	2.19E-05	0
node	61	7006.4	3656	-mass	0	1.74E-04	0
node	62	7882.2	3656	-mass	0	2.19E-05	0
node	63	8758	3656	-mass	0	1.73E-04	0
node	64	9633.8	3656	-mass	0	2.19E-05	0
node	65	10509.6	3656	-mass	0	8.68E-05	0
node	66	0	4570	-mass	0	5.68E-05	0
node	67	875.8	4570	-mass	0	2.19E-05	0
node	68	1751.6	4570	-mass	0	1.74E-04	0
node	69	2627.4	4570	-mass	0	2.19E-05	0
node	70	3503.2	4570	-mass	0	1.74E-04	0
node	71	4379	4570	-mass	0	2.19E-05	0
node	72	5254.8	4570	-mass	0	1.74E-04	0
node	73	6130.6	4570	-mass	0	2.19E-05	0
node	74	7006.4	4570	-mass	0	1.74E-04	0
node	75	7882.2	4570	-mass	0	2.19E-05	0
node	76	8758	4570	-mass	0	1.73E-04	0
node	77	9633.8	4570	-mass	0	2.19E-05	0
node	78	10509.6	4570	-mass	0	8.68E-05	0
node	79	0	5484	-mass	0	5.68E-05	0
node	80	875.8	5484	-mass	0	2.19E-05	0
node	81	1751.6	5484	-mass	0	1.74E-04	0
node	82	2627.4	5484	-mass	0	2.19E-05	0
node	83	3503.2	5484	-mass	0	1.74E-04	0
node	84	4379	5484	-mass	0	2.19E-05	0
node	85	5254.8	5484	-mass	0	1.74E-04	0
node	86	6130.6	5484	-mass	0	2.19E-05	0
node	87	7006.4	5484	-mass	0	1.74E-04	0
node	88	7882.2	5484	-mass	0	2.19E-05	0
node	89	8758	5484	-mass	0	1.73E-04	0
node	90	9633.8	5484	-mass	0	2.19E-05	0
node	91	10509.6	5484	-mass	0	8.68E-05	0
node	92	0	6398	-mass	0	5.68E-05	0
node	93	875.8	6398	-mass	0	2.19E-05	0
node	94	1751.6	6398	-mass	0	1.74E-04	0
node	95	2627.4	6398	-mass	0	2.19E-05	0
node	96	3503.2	6398	-mass	0	1.74E-04	0
node	97	4379	6398	-mass	0	2.19E-05	0
node	98	5254.8	6398	-mass	0	1.74E-04	0
node	99	6130.6	6398	-mass	0	2.19E-05	0
node	100	7006.4	6398	-mass	0	1.74E-04	0
node	101	7882.2	6398	-mass	0	2.19E-05	0
node	102	8758	6398	-mass	0	1.73E-04	0

node	103	9633.8	6398	-mass	0	2.19E-05	0
node	104	10509.6	6398	-mass	0	8.68E-05	0
node	105	0	7312	-mass	0	5.02E-05	0
node	106	875.8	7312	-mass	0	5.46E-05	0
node	107	1751.6	7312	-mass	0	1.30E-04	0
node	108	2627.4	7312	-mass	0	5.46E-05	0
node	109	3503.2	7312	-mass	0	1.30E-04	0
node	110	4379	7312	-mass	0	5.46E-05	0
node	111	5254.8	7312	-mass	0	1.30E-04	0
node	112	6130.6	7312	-mass	0	5.46E-05	0
node	113	7006.4	7312	-mass	0	1.30E-04	0
node	114	7882.2	7312	-mass	0	5.46E-05	0
node	115	8758	7312	-mass	0	1.30E-04	0
node	116	9633.8	7312	-mass	0	5.46E-05	0
node	117	10509.6	7312	-mass	0	6.52E-05	0
node	118	0	8063				

impose the translational displacements in y direction of node 1 to be the same as those of node 53.

equalDOF	53	1	2
equalDOF	54	2	2
equalDOF	55	3	2
equalDOF	56	4	2
equalDOF	57	5	2
equalDOF	58	6	2
equalDOF	59	7	2
equalDOF	60	8	2
equalDOF	61	9	2
equalDOF	62	10	2
equalDOF	63	11	2
equalDOF	64	12	2
equalDOF	65	13	2
equalDOF	53	14	2
equalDOF	54	15	2
equalDOF	55	16	2
equalDOF	56	17	2
equalDOF	57	18	2
equalDOF	58	19	2
equalDOF	59	20	2
equalDOF	60	21	2
equalDOF	61	22	2
equalDOF	62	23	2
equalDOF	63	24	2
equalDOF	64	25	2
equalDOF	65	26	2
equalDOF	53	27	2
equalDOF	54	28	2
equalDOF	55	29	2
equalDOF	56	30	2
equalDOF	57	31	2
equalDOF	58	32	2
equalDOF	59	33	2
equalDOF	60	34	2
equalDOF	61	35	2
equalDOF	62	36	2

equalDOF	63	37	2
equalDOF	64	38	2
equalDOF	65	39	2
equalDOF	53	40	2
equalDOF	54	41	2
equalDOF	55	42	2
equalDOF	56	43	2
equalDOF	57	44	2
equalDOF	58	45	2
equalDOF	59	46	2
equalDOF	60	47	2
equalDOF	61	48	2
equalDOF	62	49	2
equalDOF	63	50	2
equalDOF	64	51	2
equalDOF	65	52	2
equalDOF	53	66	2
equalDOF	54	67	2
equalDOF	55	68	2
equalDOF	56	69	2
equalDOF	57	70	2
equalDOF	58	71	2
equalDOF	59	72	2
equalDOF	60	73	2
equalDOF	61	74	2
equalDOF	62	75	2
equalDOF	63	76	2
equalDOF	64	77	2
equalDOF	65	78	2
equalDOF	53	79	2
equalDOF	54	80	2
equalDOF	55	81	2
equalDOF	56	82	2
equalDOF	57	83	2
equalDOF	58	84	2
equalDOF	59	85	2
equalDOF	60	86	2
equalDOF	61	87	2
equalDOF	62	88	2
equalDOF	63	89	2
equalDOF	64	90	2
equalDOF	65	91	2
equalDOF	53	92	2
equalDOF	54	93	2
equalDOF	55	94	2
equalDOF	56	95	2
equalDOF	57	96	2
equalDOF	58	97	2
equalDOF	59	98	2
equalDOF	60	99	2
equalDOF	61	100	2
equalDOF	62	101	2
equalDOF	63	102	2
equalDOF	64	103	2
equalDOF	65	104	2
equalDOF	53	105	2

```
equalDOF     54     106     2
equalDOF     55     107     2
equalDOF     56     108     2
equalDOF     57     109     2
equalDOF     58     110     2
equalDOF     59     111     2
equalDOF     60     112     2
equalDOF     61     113     2
equalDOF     62     114     2
equalDOF     63     115     2
equalDOF     64     116     2
equalDOF     65     117     2
```

#Set the boundary conditions - command: fix nodeID xResrnt? yRestrnt? Rotation?

```
fix     13     1     0     0
fix     15     0     0     1;#rotation fixed at intersection of truss elements only
fix     16     0     0     0
fix     17     0     0     1
fix     18     0     0     0
fix     19     0     0     1
fix     20     0     0     0
fix     21     0     0     1
fix     22     0     0     0
fix     23     0     0     1
fix     24     0     0     0
fix     25     0     0     1
fix     26     1     0     0
fix     27     0     0     0
fix     28     0     0     1
fix     29     0     0     0
fix     30     0     0     1
fix     31     0     0     0
fix     32     0     0     1
fix     33     0     0     0
fix     34     0     0     1
fix     35     0     0     0
fix     36     0     0     1
fix     37     0     0     0
fix     38     0     0     1
fix     39     1     0     0
fix     40     0     0     0
fix     41     0     0     1
fix     42     0     0     0
fix     43     0     0     1
fix     44     0     0     0
fix     45     0     0     1
fix     46     0     0     0
fix     47     0     0     1
fix     48     0     0     0
fix     49     0     0     1
fix     50     0     0     0
fix     51     0     0     1
fix     52     1     0     0
fix     53     0     0     0
fix     54     0     0     1
```

fix	55	0	0	0
fix	56	0	0	1
fix	57	0	0	0
fix	58	0	0	1
fix	59	0	0	0
fix	60	0	0	1
fix	61	0	0	0
fix	62	0	0	1
fix	63	0	0	0
fix	64	0	0	1
fix	65	1	0	0
fix	66	0	0	0
fix	67	0	0	1
fix	68	0	0	0
fix	69	0	0	1
fix	70	0	0	0
fix	71	0	0	1
fix	72	0	0	0
fix	73	0	0	1
fix	74	0	0	0
fix	75	0	0	1
fix	76	0	0	0
fix	77	0	0	1
fix	78	1	0	0
fix	79	0	0	0
fix	80	0	0	1
fix	81	0	0	0
fix	82	0	0	1
fix	83	0	0	0
fix	84	0	0	1
fix	85	0	0	0
fix	86	0	0	1
fix	87	0	0	0
fix	88	0	0	1
fix	89	0	0	0
fix	90	0	0	1
fix	91	1	0	0
fix	92	0	0	0
fix	93	0	0	1
fix	94	0	0	0
fix	95	0	0	1
fix	96	0	0	0
fix	97	0	0	1
fix	98	0	0	0
fix	99	0	0	1
fix	100	0	0	0
fix	101	0	0	1
fix	102	0	0	0
fix	103	0	0	1
fix	104	1	0	0
fix	105	0	0	0
fix	106	0	0	0
fix	107	0	0	0
fix	108	0	0	0
fix	109	0	0	0
fix	110	0	0	0

```
fix      111     0       0       0
fix      112     0       0       0
fix      113     0       0       0
fix      114     0       0       0
fix      115     0       0       0
fix      116     0       0       0
fix      117     1       0       0
fix      118     1       1       1
```

Define Geometric transformation
geomTransf Linear 1;

Define elements
#element elasticBeamColumn $eleTag $iNode $jNode $A $E $Iz $transfTag

element elasticBeamColumn	1 1 2	6236	200	5.70E+06	1 ;# W360x39 + HSS 102x102x4.8
element elasticBeamColumn	2	2	3	6236	200	5.70E+06	1
element elasticBeamColumn	3	3	4	6236	200	5.70E+06	1
element elasticBeamColumn	4	4	5	6236	200	5.70E+06	1
element elasticBeamColumn	5	5	6	6236	200	5.70E+06	1
element elasticBeamColumn	6	6	7	6236	200	5.70E+06	1
element elasticBeamColumn	7	7	8	6236	200	5.70E+06	1
element elasticBeamColumn	8	8	9	6236	200	5.70E+06	1
element elasticBeamColumn	9	9	10	6236	200	5.70E+06	1
element elasticBeamColumn	10	10	11	6236	200	5.70E+06	1
element elasticBeamColumn	11	11	12	6236	200	5.70E+06	1
element elasticBeamColumn	12	12	13	6236	200	5.70E+06	1
element elasticBeamColumn	13	105	106	6236	200	5.70E+06	1
element elasticBeamColumn	14	106	107	6236	200	5.70E+06	1
element elasticBeamColumn	15	107	108	6236	200	5.70E+06	1
element elasticBeamColumn	16	108	109	6236	200	5.70E+06	1
element elasticBeamColumn	17	109	110	6236	200	5.70E+06	1
element elasticBeamColumn	18	110	111	6236	200	5.70E+06	1
element elasticBeamColumn	19	111	112	6236	200	5.70E+06	1
element elasticBeamColumn	20	112	113	6236	200	5.70E+06	1
element elasticBeamColumn	21	113	114	6236	200	5.70E+06	1
element elasticBeamColumn	22	114	115	6236	200	5.70E+06	1
element elasticBeamColumn	23	115	116	6236	200	5.70E+06	1
element elasticBeamColumn	24	116	117	6236	200	5.70E+06	1
element elasticBeamColumn	25	1	14	6275	200	5.70E+06	1
element elasticBeamColumn	26	14	27	6275	200	5.70E+06	1
element elasticBeamColumn	27	27	40	6275	200	5.70E+06	1
element elasticBeamColumn	28	40	53	6275	200	5.70E+06	1
element elasticBeamColumn	29	53	66	6275	200	5.70E+06	1
element elasticBeamColumn	30	66	79	6275	200	5.70E+06	1
element elasticBeamColumn	31	79	92	6275	200	5.70E+06	1
element elasticBeamColumn	32	92	105	6275	200	5.70E+06	1
element elasticBeamColumn	141	3	16	997	200	1.08E+06	1; #Joist top
element elasticBeamColumn	142	16	29	997	200	1.08E+06	1
element elasticBeamColumn	143	29	42	997	200	1.08E+06	1
element elasticBeamColumn	144	42	55	997	200	1.08E+06	1
element elasticBeamColumn	145	55	68	997	200	1.08E+06	1

element elasticBeamColumn	146	68	81	997	200	1.08E+06	1
element elasticBeamColumn	147	81	94	997	200	1.08E+06	1
element elasticBeamColumn	148	94	107	997	200	1.08E+06	1
element elasticBeamColumn	149	5	18	997	200	1.08E+06	1
element elasticBeamColumn	150	18	31	997	200	1.08E+06	1
element elasticBeamColumn	151	31	44	997	200	1.08E+06	1
element elasticBeamColumn	152	44	57	997	200	1.08E+06	1
element elasticBeamColumn	153	57	70	997	200	1.08E+06	1
element elasticBeamColumn	154	70	83	997	200	1.08E+06	1
element elasticBeamColumn	155	83	96	997	200	1.08E+06	1
element elasticBeamColumn	156	96	109	997	200	1.08E+06	1
element elasticBeamColumn	157	7	20	997	200	1.08E+06	1
element elasticBeamColumn	158	20	33	997	200	1.08E+06	1
element elasticBeamColumn	159	33	46	997	200	1.08E+06	1
element elasticBeamColumn	160	46	59	997	200	1.08E+06	1
element elasticBeamColumn	161	59	72	997	200	1.08E+06	1
element elasticBeamColumn	162	72	85	997	200	1.08E+06	1
element elasticBeamColumn	163	85	98	997	200	1.08E+06	1
element elasticBeamColumn	164	98	111	997	200	1.08E+06	1
element elasticBeamColumn	165	9	22	997	200	1.08E+06	1
element elasticBeamColumn	166	22	35	997	200	1.08E+06	1
element elasticBeamColumn	167	35	48	997	200	1.08E+06	1
element elasticBeamColumn	168	48	61	997	200	1.08E+06	1
element elasticBeamColumn	169	61	74	997	200	1.08E+06	1
element elasticBeamColumn	170	74	87	997	200	1.08E+06	1
element elasticBeamColumn	171	87	100	997	200	1.08E+06	1
element elasticBeamColumn	172	100	113	997	200	1.08E+06	1
element elasticBeamColumn	173	11	24	997	200	1.08E+06	1
element elasticBeamColumn	174	24	37	997	200	1.08E+06	1
element elasticBeamColumn	175	37	50	997	200	1.08E+06	1
element elasticBeamColumn	176	50	63	997	200	1.08E+06	1
element elasticBeamColumn	177	63	76	997	200	1.08E+06	1
element elasticBeamColumn	178	76	89	997	200	1.08E+06	1
element elasticBeamColumn	179	89	102	997	200	1.08E+06	1
element elasticBeamColumn	180	102	115	997	200	1.08E+06	1
element elasticBeamColumn	181	13	26	499	200	5.40E+05	1; #Joist top
element elasticBeamColumn	182	26	39	499	200	5.40E+05	1
element elasticBeamColumn	183	39	52	499	200	5.40E+05	1
element elasticBeamColumn	184	52	65	499	200	5.40E+05	1
element elasticBeamColumn	185	65	78	499	200	5.40E+05	1
element elasticBeamColumn	186	78	91	499	200	5.40E+05	1
element elasticBeamColumn	187	91	104	499	200	5.40E+05	1
element elasticBeamColumn	188	104	117	499	200	5.40E+05	1

```
# --------------
# Define materials for truss elements parallel to longitudinal direction of deck panels
set E 200
# Create Elastic material prototype - command: uniaxialMaterial Elastic matID E
uniaxialMaterial Elastic 1 $E
# Create truss elements - command: element truss trussID node1 node2 Area matID

element truss     45     14     15     926.44          1; # Area .76*1219=926.44  mm2
element truss     46     15     16     926.44          1
```

element truss	47	16	17	926.44	1
element truss	48	17	18	926.44	1
element truss	49	18	19	926.44	1
element truss	50	19	20	926.44	1
element truss	51	20	21	926.44	1
element truss	52	21	22	926.44	1
element truss	53	22	23	926.44	1
element truss	54	23	24	926.44	1
element truss	55	24	25	926.44	1
element truss	56	25	26	926.44	1
element truss	57	27	28	926.44	1
element truss	58	28	29	926.44	1
element truss	59	29	30	926.44	1
element truss	60	30	31	926.44	1
element truss	61	31	32	926.44	1
element truss	62	32	33	926.44	1
element truss	63	33	34	926.44	1
element truss	64	34	35	926.44	1
element truss	65	35	36	926.44	1
element truss	66	36	37	926.44	1
element truss	67	37	38	926.44	1
element truss	68	38	39	926.44	1
element truss	69	40	41	926.44	1
element truss	70	41	42	926.44	1
element truss	71	42	43	926.44	1
element truss	72	43	44	926.44	1
element truss	73	44	45	926.44	1
element truss	74	45	46	926.44	1
element truss	75	46	47	926.44	1
element truss	76	47	48	926.44	1
element truss	77	48	49	926.44	1
element truss	78	49	50	926.44	1
element truss	79	50	51	926.44	1
element truss	80	51	52	926.44	1
element truss	81	53	54	926.44	1
element truss	82	54	55	926.44	1
element truss	83	55	56	926.44	1
element truss	84	56	57	926.44	1
element truss	85	57	58	926.44	1
element truss	86	58	59	926.44	1
element truss	87	59	60	926.44	1
element truss	88	60	61	926.44	1
element truss	89	61	62	926.44	1
element truss	90	62	63	926.44	1
element truss	91	63	64	926.44	1
element truss	92	64	65	926.44	1
element truss	93	66	67	926.44	1
element truss	94	67	68	926.44	1
element truss	95	68	69	926.44	1
element truss	96	69	70	926.44	1
element truss	97	70	71	926.44	1
element truss	98	71	72	926.44	1
element truss	99	72	73	926.44	1
element truss	100	73	74	926.44	1
element truss	101	74	75	926.44	1
element truss	102	75	76	926.44	1

element truss	103	76	77	926.44	1
element truss	104	77	78	926.44	1
element truss	105	79	80	926.44	1
element truss	106	80	81	926.44	1
element truss	107	81	82	926.44	1
element truss	108	82	83	926.44	1
element truss	109	83	84	926.44	1
element truss	110	84	85	926.44	1
element truss	111	85	86	926.44	1
element truss	112	86	87	926.44	1
element truss	113	87	88	926.44	1
element truss	114	88	89	926.44	1
element truss	115	89	90	926.44	1
element truss	116	90	91	926.44	1
element truss	117	92	93	926.44	1
element truss	118	93	94	926.44	1
element truss	119	94	95	926.44	1
element truss	120	95	96	926.44	1
element truss	121	96	97	926.44	1
element truss	122	97	98	926.44	1
element truss	123	98	99	926.44	1
element truss	124	99	100	926.44	1
element truss	125	100	101	926.44	1
element truss	126	101	102	926.44	1
element truss	127	102	103	926.44	1
element truss	128	103	104	926.44	1
element truss	33	1	2	463.22	1
element truss	34	2	3	463.22	1
element truss	35	3	4	463.22	1
element truss	36	4	5	463.22	1
element truss	37	5	6	463.22	1
element truss	38	6	7	463.22	1
element truss	39	7	8	463.22	1
element truss	40	8	9	463.22	1
element truss	41	9	10	463.22	1
element truss	42	10	11	463.22	1
element truss	43	11	12	463.22	1
element truss	44	12	13	463.22	1
element truss	129	105	106	463.22	1
element truss	130	106	107	463.22	1
element truss	131	107	108	463.22	1
element truss	132	108	109	463.22	1
element truss	133	109	110	463.22	1
element truss	134	110	111	463.22	1
element truss	135	111	112	463.22	1
element truss	136	112	113	463.22	1
element truss	137	113	114	463.22	1
element truss	138	114	115	463.22	1
element truss	139	115	116	463.22	1
element truss	140	116	117	463.22	1
element truss	381	105	118	1.00E+10	1;#Stiff truss element

```
#Hysteretic material Pinching4
set Sn 32.3 ; # Shear strength of Diaphragm in kN/m
set diagonalLength 1266; # Length in mm
set Fu [expr ($diagonalLength*$Sn/2/1000)]
set Gprime 10.7;  #Shear stiffness of diaphragm kN/mm
set Area [expr $Gprime*$diagonalLength/$E]
set ultimateStress2 [expr $Fu/$Area]
set ultimateStrain2 [expr $ultimateStress2/80]
set Stress1 [expr $ultimateStress2*0.71]
set Strain1 [expr $Stress1/$E]
set Stress3 [expr $ultimateStress2*0.88]
set Strain3 [expr $Stress3/55]
set Stress4 [expr $ultimateStress2*0.07]
set Strain4 [expr $Stress4/0.6]

uniaxialMaterial Pinching4 7 $Stress1 $Strain1 $ultimateStress2 $ultimateStrain2 $Stress3 $Strain3 $Stress4
$Strain4 -$Stress1 -$Strain1 -$ultimateStress2 -$ultimateStrain2 -$Stress3 -$Strain3 -$Stress4 -$Strain4  0.16 0.22
0.16   0.16 0.22 0.16  0.8 0.8 0.3 0.2 0.3  0.2 1.0 0.4 0.7 1.0  0.0 0.0 0.0 0.0 0.0 2.0 energy;
```

element truss	189	1	15	$Area	7 ; #A= (Kxx*L)/E Kxx = G'=10.7
element truss	190	2	16	$Area	7
element truss	191	3	17	$Area	7
element truss	192	4	18	$Area	7
element truss	193	5	19	$Area	7
element truss	194	6	20	$Area	7
element truss	195	7	21	$Area	7
element truss	196	8	22	$Area	7
element truss	197	9	23	$Area	7
element truss	198	10	24	$Area	7
element truss	199	11	25	$Area	7
element truss	200	12	26	$Area	7
element truss	201	14	28	$Area	7
element truss	202	15	29	$Area	7
element truss	203	16	30	$Area	7
element truss	204	17	31	$Area	7
element truss	205	18	32	$Area	7
element truss	206	19	33	$Area	7
element truss	207	20	34	$Area	7
element truss	208	21	35	$Area	7
element truss	209	22	36	$Area	7
element truss	210	23	37	$Area	7
element truss	211	24	38	$Area	7
element truss	212	25	39	$Area	7
element truss	213	27	41	$Area	7
element truss	214	28	42	$Area	7
element truss	215	29	43	$Area	7
element truss	216	30	44	$Area	7
element truss	217	31	45	$Area	7
element truss	218	32	46	$Area	7
element truss	219	33	47	$Area	7
element truss	220	34	48	$Area	7
element truss	221	35	49	$Area	7
element truss	222	36	50	$Area	7
element truss	223	37	51	$Area	7
element truss	224	38	52	$Area	7
element truss	225	40	54	$Area	7

element truss	226	41	55	$Area	7
element truss	227	42	56	$Area	7
element truss	228	43	57	$Area	7
element truss	229	44	58	$Area	7
element truss	230	45	59	$Area	7
element truss	231	46	60	$Area	7
element truss	232	47	61	$Area	7
element truss	233	48	62	$Area	7
element truss	234	49	63	$Area	7
element truss	235	50	64	$Area	7
element truss	236	51	65	$Area	7
element truss	237	53	67	$Area	7
element truss	238	54	68	$Area	7
element truss	239	55	69	$Area	7
element truss	240	56	70	$Area	7
element truss	241	57	71	$Area	7
element truss	242	58	72	$Area	7
element truss	243	59	73	$Area	7
element truss	244	60	74	$Area	7
element truss	245	61	75	$Area	7
element truss	246	62	76	$Area	7
element truss	247	63	77	$Area	7
element truss	248	64	78	$Area	7
element truss	249	66	80	$Area	7
element truss	250	67	81	$Area	7
element truss	251	68	82	$Area	7
element truss	252	69	83	$Area	7
element truss	253	70	84	$Area	7
element truss	254	71	85	$Area	7
element truss	255	72	86	$Area	7
element truss	256	73	87	$Area	7
element truss	257	74	88	$Area	7
element truss	258	75	89	$Area	7
element truss	259	76	90	$Area	7
element truss	260	77	91	$Area	7
element truss	261	79	93	$Area	7
element truss	262	80	94	$Area	7
element truss	263	81	95	$Area	7
element truss	264	82	96	$Area	7
element truss	265	83	97	$Area	7
element truss	266	84	98	$Area	7
element truss	267	85	99	$Area	7
element truss	268	86	100	$Area	7
element truss	269	87	101	$Area	7
element truss	270	88	102	$Area	7
element truss	271	89	103	$Area	7
element truss	272	90	104	$Area	7
element truss	273	92	106	$Area	7
element truss	274	93	107	$Area	7
element truss	275	94	108	$Area	7
element truss	276	95	109	$Area	7
element truss	277	96	110	$Area	7
element truss	278	97	111	$Area	7
element truss	279	98	112	$Area	7
element truss	280	99	113	$Area	7
element truss	281	100	114	$Area	7

element truss	282	101	115	$Area	7
element truss	283	102	116	$Area	7
element truss	284	103	117	$Area	7
element truss	285	2	14	$Area	7
element truss	286	3	15	$Area	7
element truss	287	4	16	$Area	7
element truss	288	5	17	$Area	7
element truss	289	6	18	$Area	7
element truss	290	7	19	$Area	7
element truss	291	8	20	$Area	7
element truss	292	9	21	$Area	7
element truss	293	10	22	$Area	7
element truss	294	11	23	$Area	7
element truss	295	12	24	$Area	7
element truss	296	13	25	$Area	7
element truss	297	15	27	$Area	7
element truss	298	16	28	$Area	7
element truss	299	17	29	$Area	7
element truss	300	18	30	$Area	7
element truss	301	19	31	$Area	7
element truss	302	20	32	$Area	7
element truss	303	21	33	$Area	7
element truss	304	22	34	$Area	7
element truss	305	23	35	$Area	7
element truss	306	24	36	$Area	7
element truss	307	25	37	$Area	7
element truss	308	26	38	$Area	7
element truss	309	28	40	$Area	7
element truss	310	29	41	$Area	7
element truss	311	30	42	$Area	7
element truss	312	31	43	$Area	7
element truss	313	32	44	$Area	7
element truss	314	33	45	$Area	7
element truss	315	34	46	$Area	7
element truss	316	35	47	$Area	7
element truss	317	36	48	$Area	7
element truss	318	37	49	$Area	7
element truss	319	38	50	$Area	7
element truss	320	39	51	$Area	7
element truss	321	41	53	$Area	7
element truss	322	42	54	$Area	7
element truss	323	43	55	$Area	7
element truss	324	44	56	$Area	7
element truss	325	45	57	$Area	7
element truss	326	46	58	$Area	7
element truss	327	47	59	$Area	7
element truss	328	48	60	$Area	7
element truss	329	49	61	$Area	7
element truss	330	50	62	$Area	7
element truss	331	51	63	$Area	7
element truss	332	52	64	$Area	7
element truss	333	54	66	$Area	7
element truss	334	55	67	$Area	7
element truss	335	56	68	$Area	7
element truss	336	57	69	$Area	7
element truss	337	58	70	$Area	7

```
element truss     338    59    71    $Area    7
element truss     339    60    72    $Area    7
element truss     340    61    73    $Area    7
element truss     341    62    74    $Area    7
element truss     342    63    75    $Area    7
element truss     343    64    76    $Area    7
element truss     344    65    77    $Area    7
element truss     345    67    79    $Area    7
element truss     346    68    80    $Area    7
element truss     347    69    81    $Area    7
element truss     348    70    82    $Area    7
element truss     349    71    83    $Area    7
element truss     350    72    84    $Area    7
element truss     351    73    85    $Area    7
element truss     352    74    86    $Area    7
element truss     353    75    87    $Area    7
element truss     354    76    88    $Area    7
element truss     355    77    89    $Area    7
element truss     356    78    90    $Area    7
element truss     357    80    92    $Area    7
element truss     358    81    93    $Area    7
element truss     359    82    94    $Area    7
element truss     360    83    95    $Area    7
element truss     361    84    96    $Area    7
element truss     362    85    97    $Area    7
element truss     363    86    98    $Area    7
element truss     364    87    99    $Area    7
element truss     365    88    100   $Area    7
element truss     366    89    101   $Area    7
element truss     367    90    102   $Area    7
element truss     368    91    103   $Area    7
element truss     369    93    105   $Area    7
element truss     370    94    106   $Area    7
element truss     371    95    107   $Area    7
element truss     372    96    108   $Area    7
element truss     373    97    109   $Area    7
element truss     374    98    110   $Area    7
element truss     375    99    111   $Area    7
element truss     376    100   112   $Area    7
element truss     377    101   113   $Area    7
element truss     378    102   114   $Area    7
element truss     379    103   115   $Area    7
element truss     380    104   116   $Area    7
```

Define loads

Create a Plain load pattern with a linear TimeSeries

pattern Plain 1 "Linear" {

Create the nodal load - command: load nodeID xForce yForce

load 65 0 0 0
}

```
#------------------------------------
# Define earthquake excitation
# Set up the acceleration records for EQ parallel to Short side
set AmpFac 1.0
set g [ expr $AmpFac*9810]; # Gravitational constant
#set FN "Path -filePath DIA6_SS1_120.txt -dt 0.01 -factor $g"
set FN "Path -filePath Dia6_Inelastic.txt -dt 0.01 -factor $g"; #
pattern UniformExcitation 2 2 -accel $FN ;  # creates uniform excitation with IDtag 2 in direction 2
#-------------------------------

set Type_analysis 1;# #Put  1 for inelastic response data to record, Put 2 so as not to record unnecessary data when
running elastic analysis

## Define damping##
set xDamp 0.03; # damping ratio
set MpropSwitch 1.0;
set KcurrSwitch 0.0;
set KcommSwitch 1.0;
set KinitSwitch 0.0;
set nEigenI 1; # mode 1
set nEigenJ 2; # mode 3
set lambdaN [eigen [expr $nEigenJ]]; # eigenvalue analysis for nEigenJ modes
set lambdaI [lindex $lambdaN [expr $nEigenI-1]]; # eigenvalue mode i
set lambdaJ [lindex $lambdaN [expr $nEigenJ-1]]; # eigenvalue mode j
set omegaI [expr pow($lambdaI,0.5)];
set omegaJ [expr pow($lambdaJ,0.5)];
set alphaM [expr $MpropSwitch*$xDamp*(2*$omegaI*$omegaJ)/($omegaI+$omegaJ)]; # M-prop. damping; D =
alphaM*M
set betaKcurr [expr $KcurrSwitch*2.*$xDamp/($omegaI+$omegaJ)]; # current-K; +beatKcurr*KCurrent
set betaKcomm [expr $KcommSwitch*2.*$xDamp/($omegaI+$omegaJ)]; # last-committed K;
+betaKcomm*KlastCommitt
set betaKinit [expr $KinitSwitch*2.*$xDamp/($omegaI+$omegaJ)]; # initial-K; +beatKinit*Kini
rayleigh $alphaM $betaKcurr $betaKinit $betaKcomm; # RAYLEIGH damping


# ---------------------------
# Start of Analysis
# Create the convergence test

set DtAnalysis [expr 0.01];#time-step Dt for lateral analysis
set TmaxAnalysis [expr 10.];
constraints Transformation ;
numberer RCM
system BandSPD
set Tol 1.e-10; # Convergence Test: tolerance
set maxNumIter 20; # Convergence Test: maximum number of iterations that will be performed before "failure to
converge" is returned
set printFlag 0; # Convergence Test: flag used to print information on convergence (optional) # 1: print information
on each step;
set TestType EnergyIncr; # Convergence-test type
test $TestType $Tol $maxNumIter $printFlag;
set algorithmType Newton
algorithm $algorithmType;
set NewmarkGamma 0.5; # Newmark-integrator gamma parameter
set NewmarkBeta 0.25; # Newmark-integrator beta parameter
integrator Newmark $NewmarkGamma $NewmarkBeta
```

analysis Transient

End of analysis generation

----
recorder Node -file node65_elastic_test.out -time -node 65 -dof 2 disp
recorder Element -file ele381ocalforce_elastic_force.out -time -ele 381 localForce
#
##
if {$Type_analysis == 1} {

recorder Node -file node2.out -time -node 2 -dof 2 disp
recorder Node -file node55.out -time -node 55 -dof 2 disp
recorder Node -file node57.out -time -node 57 -dof 2 disp
recorder Node -file node59.out -time -node 59 -dof 2 disp
recorder Node -file node61.out -time -node 61 -dof 2 disp
recorder Node -file node63.out -time -node 63 -dof 2 disp
recorder Node -file node65.out -time -node 65 -dof 2 disp

recorder Element -file ele225localforce.out -time -ele 225 localForce
recorder Element -file ele225localdisp.out -time -ele 225 deformation
recorder Element -file ele226localforce.out -time -ele 226 localForce
recorder Element -file ele226localdisp.out -time -ele 226 deformation
recorder Element -file ele227localforce.out -time -ele 227 localForce
recorder Element -file ele227localdisp.out -time -ele 227 deformation
recorder Element -file ele228localforce.out -time -ele 228 localForce
recorder Element -file ele228localdisp.out -time -ele 228 deformation
recorder Element -file ele229localforce.out -time -ele 229 localForce
recorder Element -file ele229localdisp.out -time -ele 229 deformation
recorder Element -file ele230localforce.out -time -ele 230 localForce
recorder Element -file ele230localdisp.out -time -ele 230 deformation
recorder Element -file ele231ocalforce.out -time -ele 231 localForce
recorder Element -file ele231localdisp.out -time -ele 231 deformation
recorder Element -file ele232localforce.out -time -ele 232 localForce
recorder Element -file ele232localdisp.out -time -ele 232 deformation
recorder Element -file ele233localforce.out -time -ele 233 localForce
recorder Element -file ele233localdisp.out -time -ele 233 deformation
recorder Element -file ele234ocalforce.out -time -ele 234 localForce
recorder Element -file ele234ocaldisp.out -time -ele 234 deformation
recorder Element -file ele235Localforce.out -time -ele 235 localForce
recorder Element -file ele235Localdisp.out -time -ele 235 deformation
recorder Element -file ele236Localforce.out -time -ele 236 localForce
recorder Element -file ele236Localdisp.out -time -ele 236 deformation
recorder Element -file ele381ocalforce.out -time -ele 381 localForce
}
#Fundamental period of vibration
set lambda1 [eigen 1]
set omega1 [expr pow($lambda1,0.5)]
set PI 3.142857
set Tperiod1 [expr 2*$PI/$omega1]; # period (s)
puts $Tperiod1

set Nsteps [expr int($TmaxAnalysis/$DtAnalysis)];
set ok [analyze $Nsteps $DtAnalysis]; # actually perform analysis; returns ok=0 if analysis was successful
if {$ok != 0} { ; # if analysis was not successful.

164

```
# change some analysis parameters to achieve convergence
# performance is slower inside this loop
# Time-controlled analysis
set ok 0;
set controlTime [getTime];
while {$controlTime < $TmaxAnalysis && $ok == 0} {
set ok [analyze 1 $DtAnalysis]
set controlTime [getTime]
set ok [analyze 1 $DtAnalysis]
if {$ok != 0} {
puts "Trying Newton with Initial Tangent .."
test NormDispIncr $Tol 1000 0
algorithm Newton -initial
set ok [analyze 1 $DtAnalysis]
test $TestType $Tol $maxNumIter 0
algorithm $algorithmType
}
if {$ok != 0} {
puts "Trying Broyden .."
algorithm Broyden 8
set ok [analyze 1 $DtAnalysis]
algorithm $algorithmType
}
if {$ok != 0} {
puts "Trying NewtonWithLineSearch .."
algorithm NewtonLineSearch .8
set ok [analyze 1 $DtAnalysis]
algorithm $algorithmType
}
}
}; # end if ok !0

puts "Ground Motion Done. End Time: [getTime]"
```

Appendix B:

Test results and numerical prediction using OpenSees truss model for all the new diaphragm test specimens
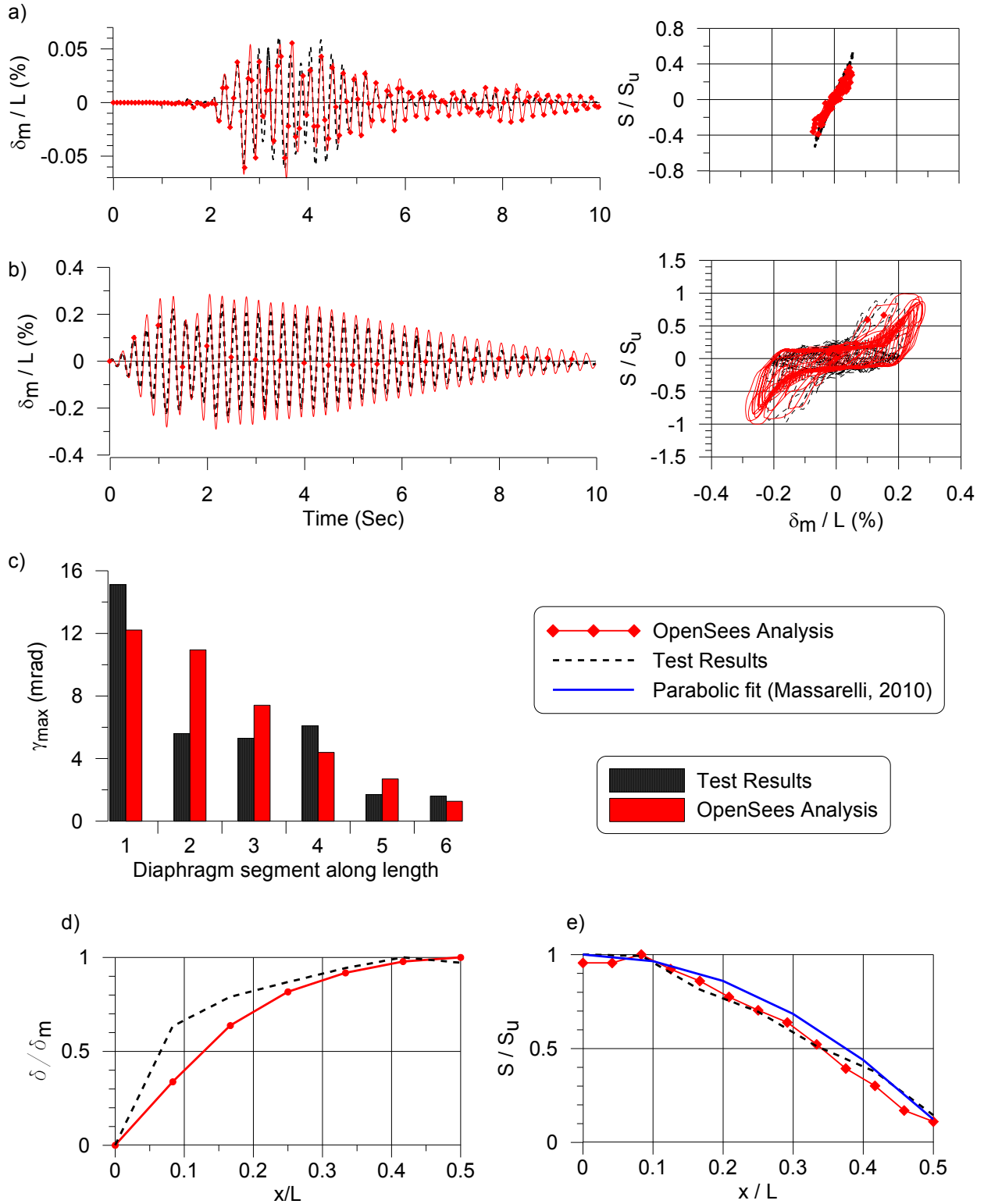
Specimen 1: under elastic loading signal (1.6 x SS1), a) Time history and hysteretic responses; under inelastic loading signal; b) Time history and hysteretic responses, c) maximum shear deformation along length, d) and e) displacement and shear force along length at the occurrence of maximum shear force at end.
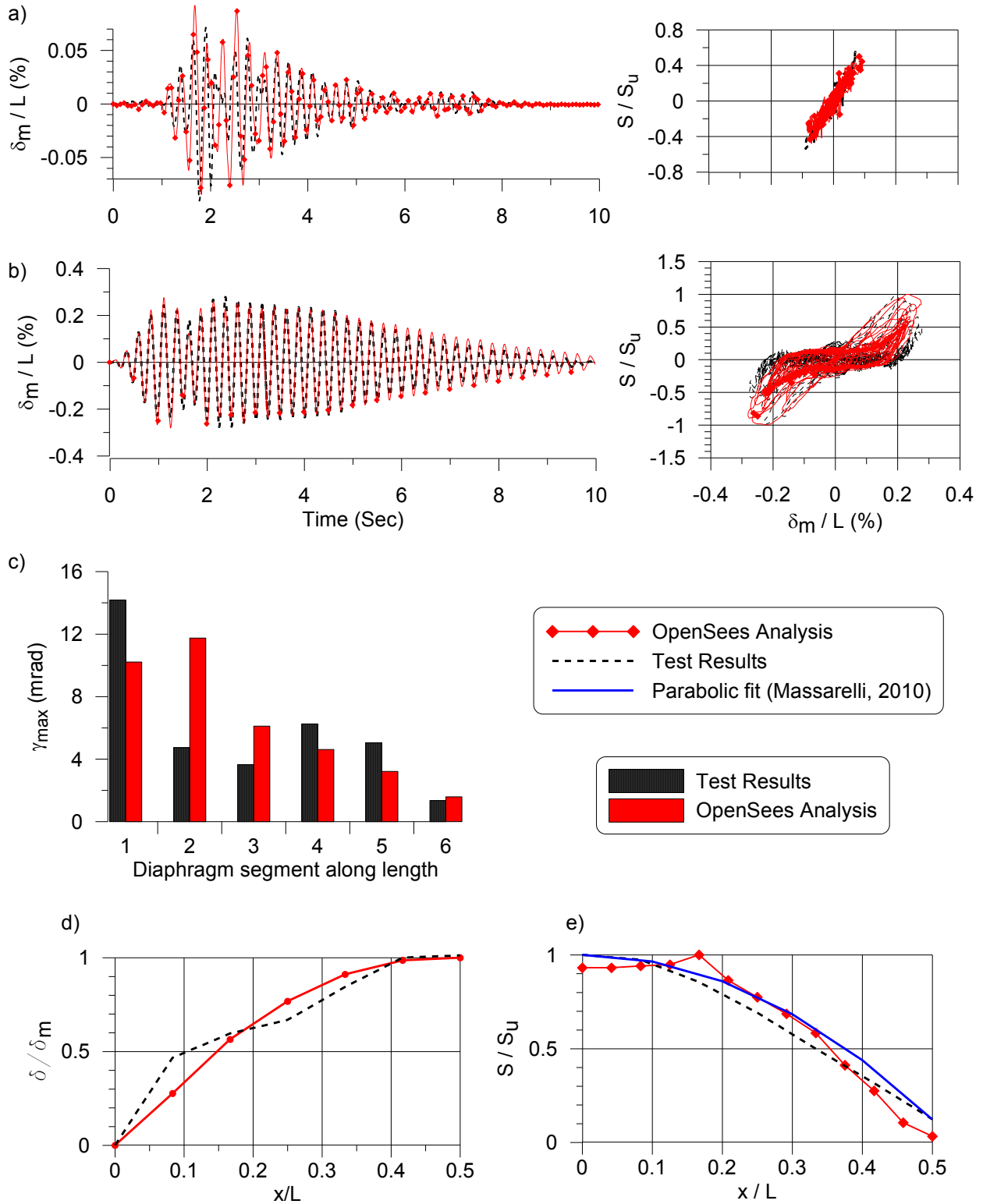
Specimen 2: under elastic loading signal (1.6 x SS1), a) Time history and hysteretic responses; under inelastic loading signal; b) Time history and hysteretic responses, c) maximum shear deformation along length, d) and e) displacement and shear force along length at the occurrence of maximum shear force at end.
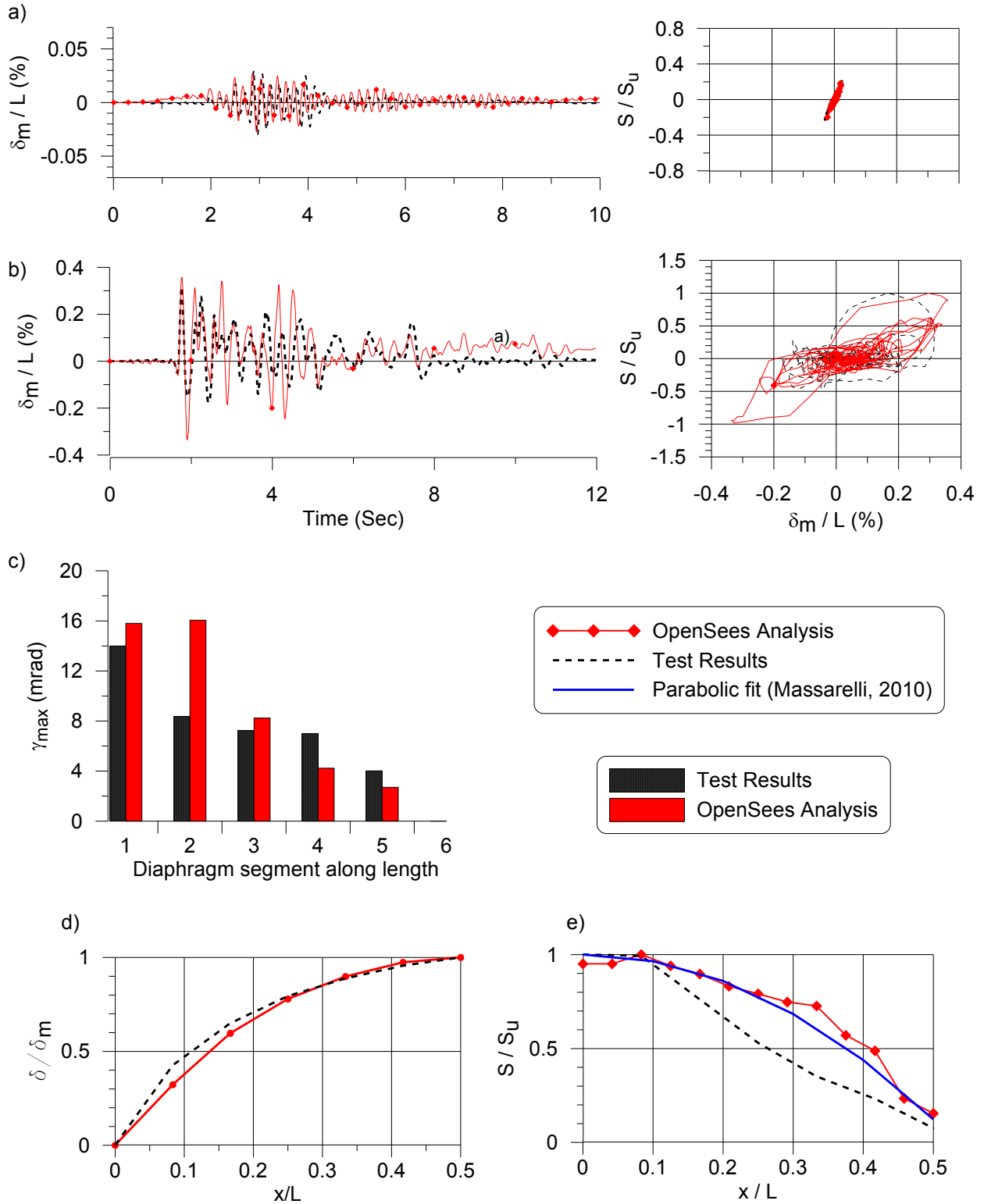
Specimen 3: under elastic loading signal (0.8 x SS1), a) Time history and hysteretic responses; under inelastic loading signal; b) Time history and hysteretic responses, c) maximum shear deformation along length, d) and e) displacement and shear force along length at the occurrence of maximum shear force at end.
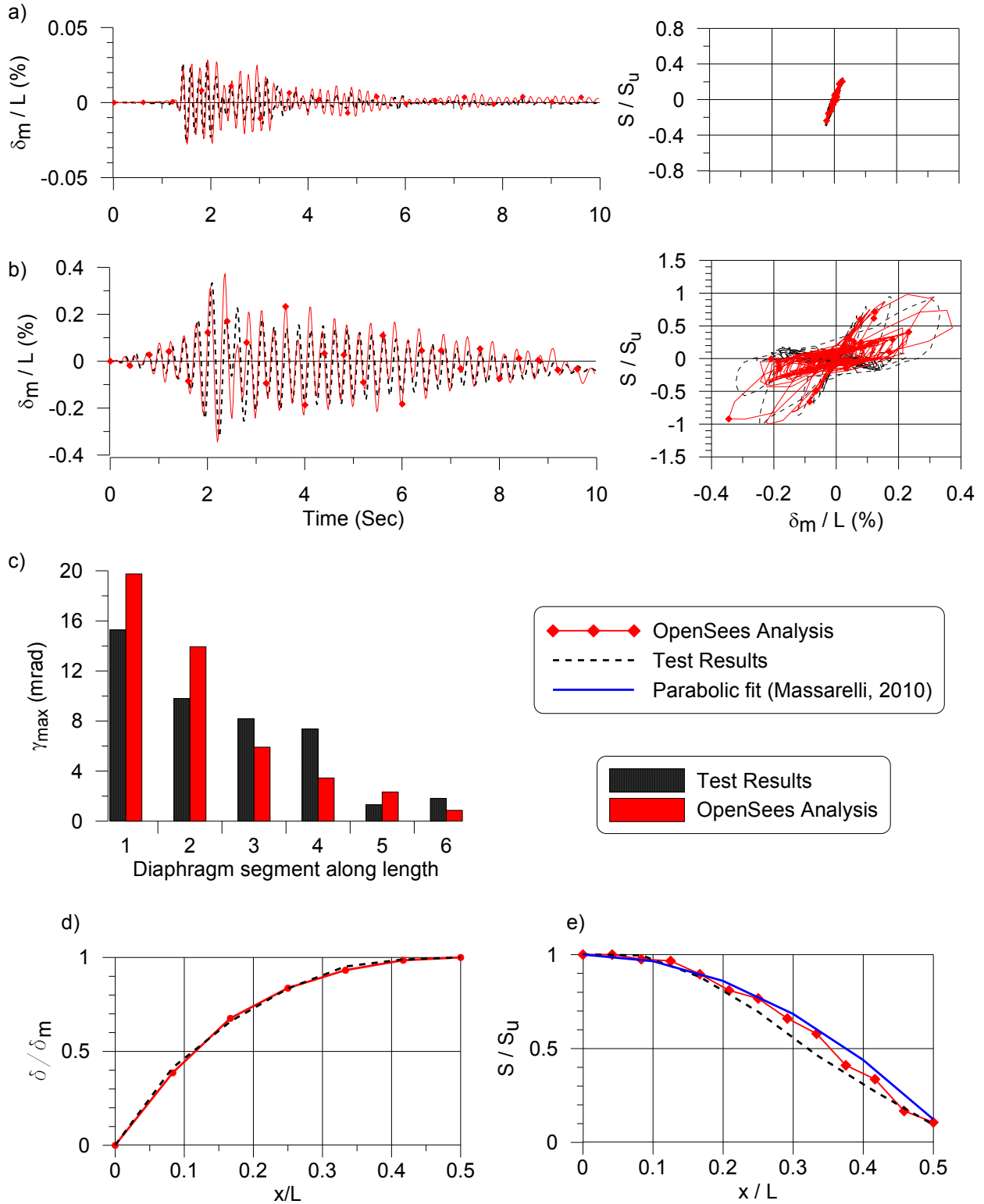
Specimen 4: under elastic loading signal (2.0 x SS3), a) Time history and hysteretic responses; under inelastic loading signal; b) Time history and hysteretic responses, c) maximum shear deformation along length, d) and e) displacement and shear force along length at the occurrence of maximum shear force at end.
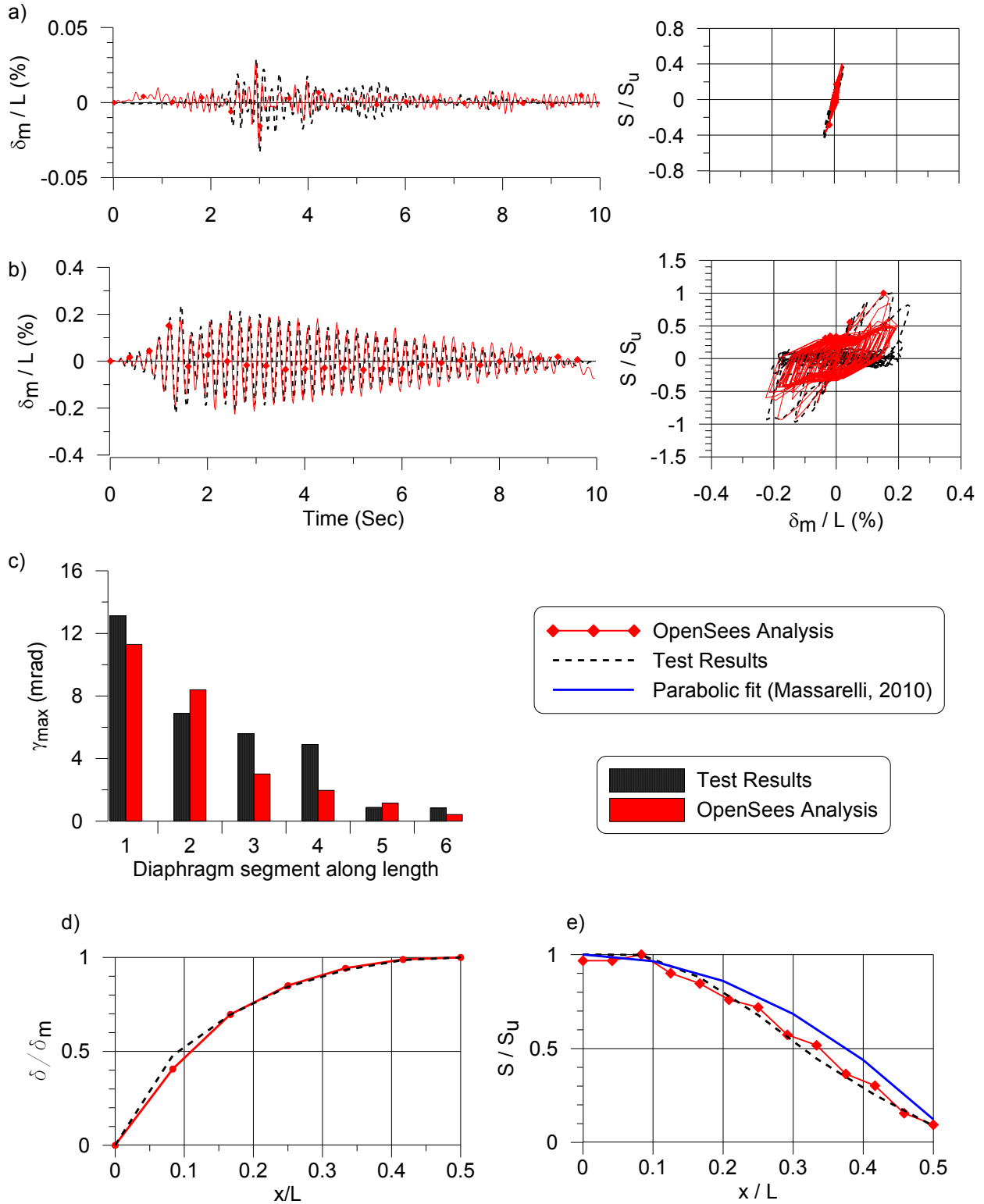
Specimen 5: under elastic loading signal (1.2 x SS1), a) Time history and hysteretic responses; under inelastic loading signal; b) Time history and hysteretic responses, c) maximum shear deformation along length, d) and e) displacement and shear force along length at the occurrence of maximum shear force at end.
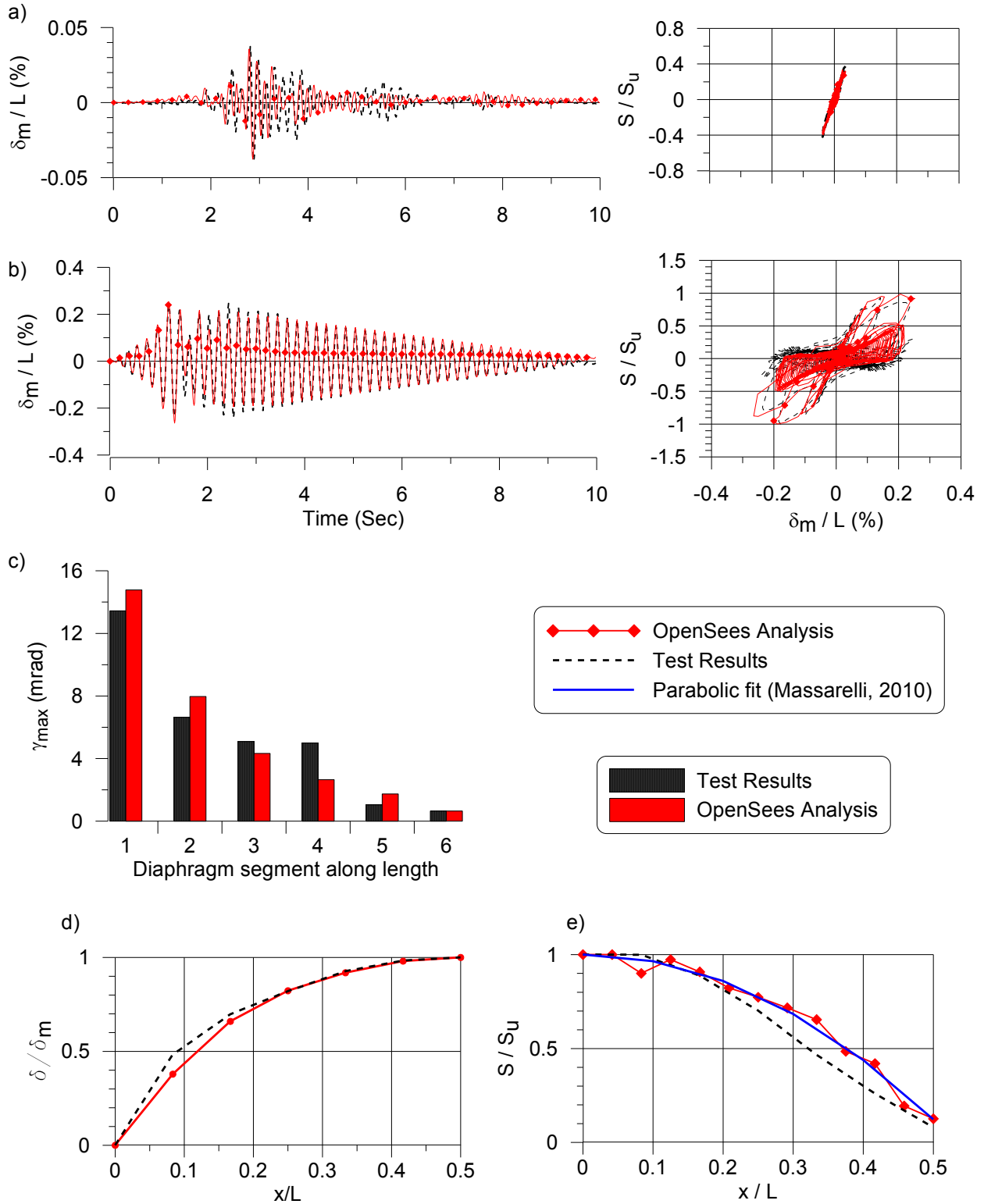
Specimen 6: under elastic loading signal (1.2 x SS1), a) Time history and hysteretic responses; under inelastic loading signal; b) Time history and hysteretic responses, c) maximum shear deformation along length, d) and e) displacement and shear force along length at the occurrence of maximum shear force at end.
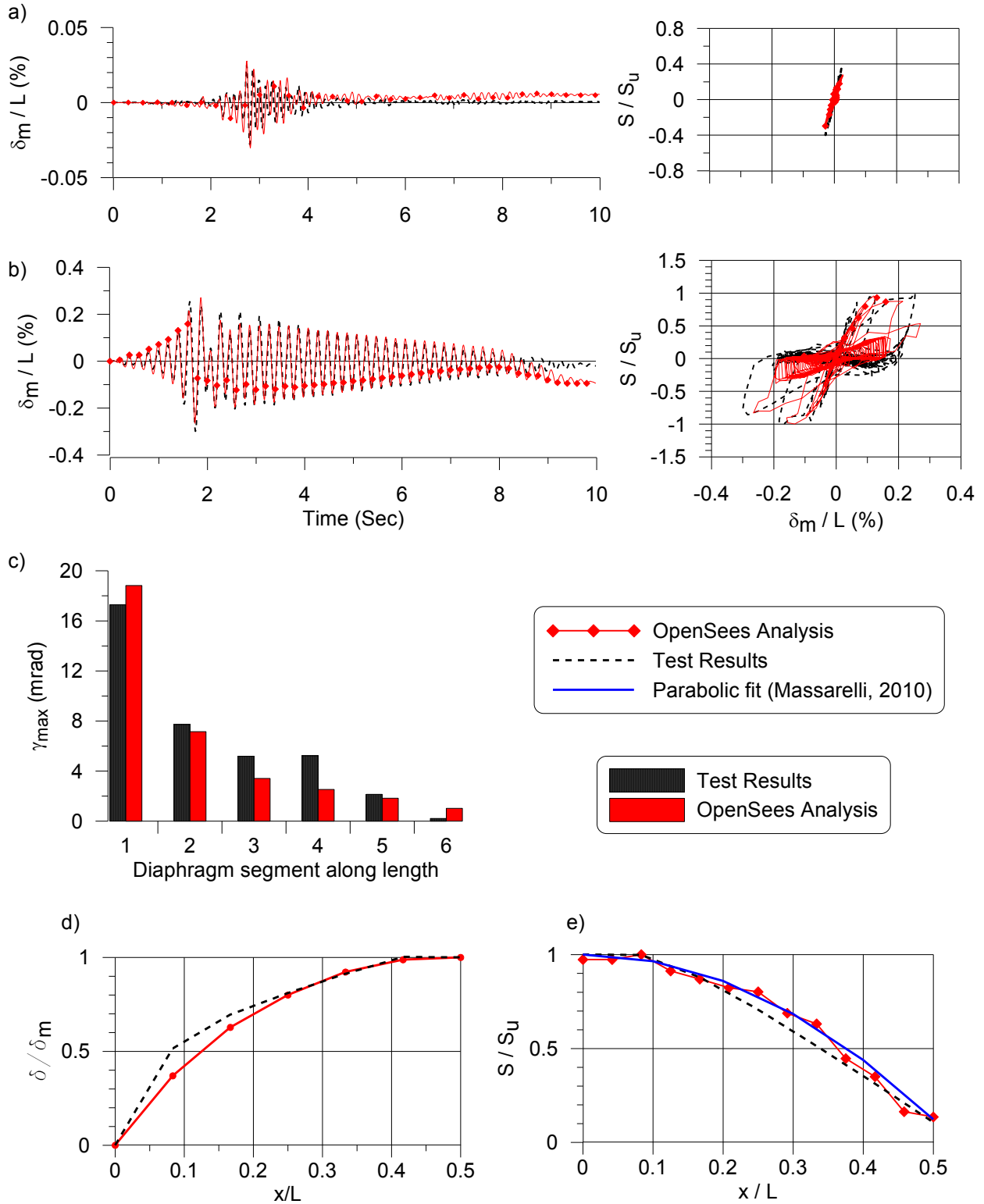
Specimen 7: under elastic loading signal (0.8 x SS1), a) Time history and hysteretic responses; under inelastic loading signal; b) Time history and hysteretic responses, c) maximum shear deformation along length, d) and e) displacement and shear force along length at the occurrence of maximum shear force at end.
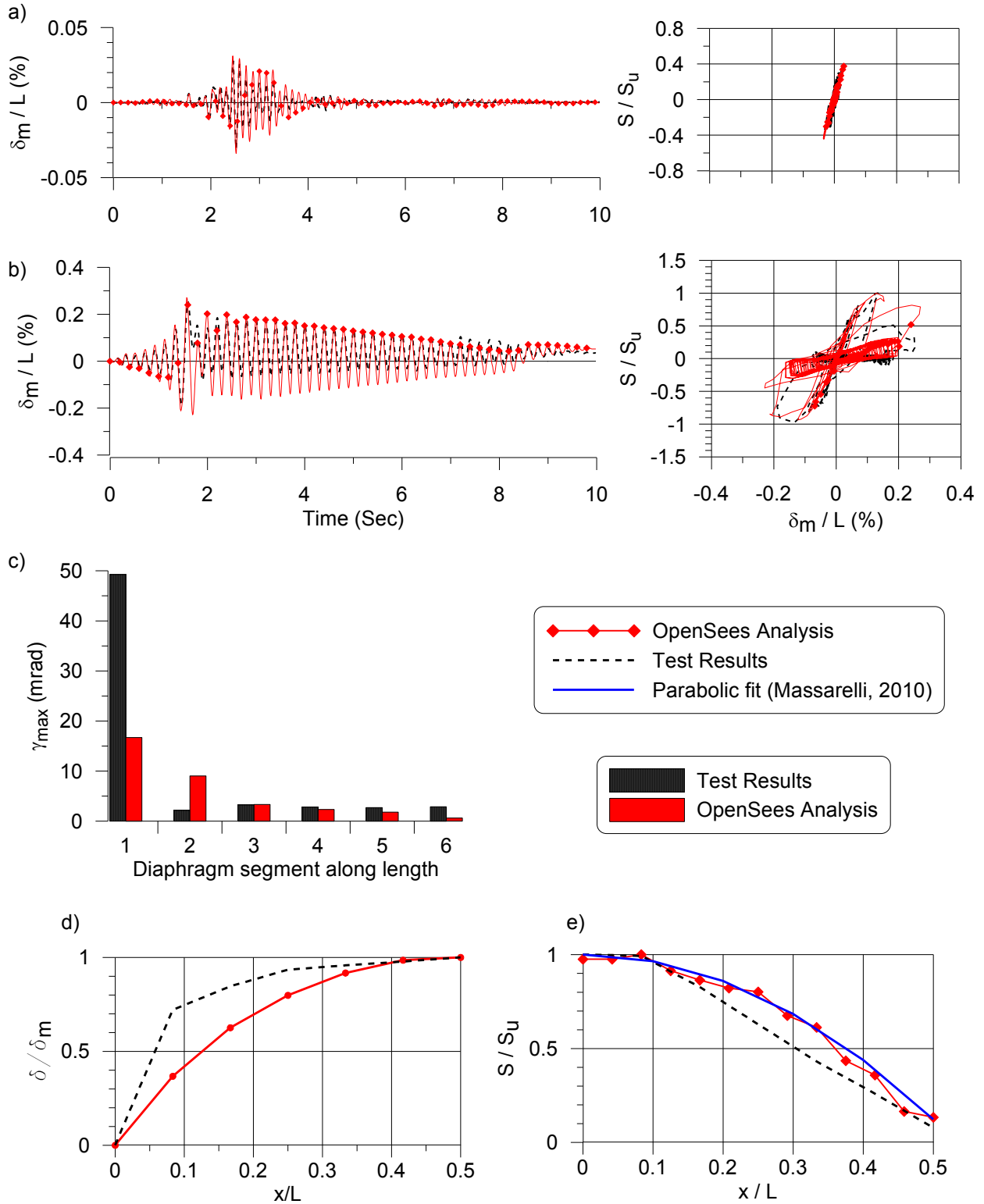
Specimen 8: under elastic loading signal (0.9 x SS1), a) Time history and hysteretic responses; under inelastic loading signal; b) Time history and hysteretic responses, c) maximum shear deformation along length, d) and e) displacement and shear force along length at the occurrence of maximum shear force at end.
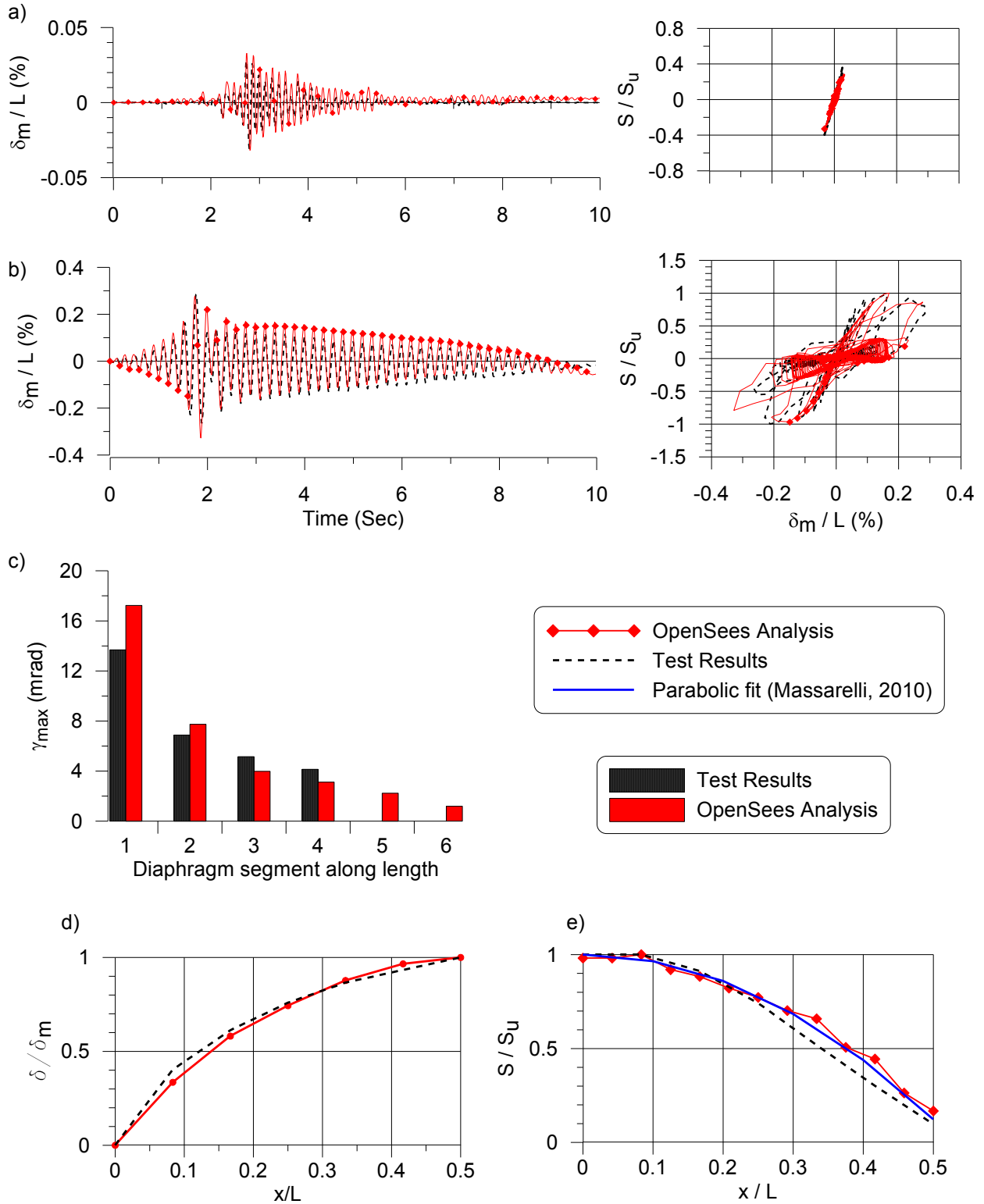
Specimen 9: under elastic loading signal (0.9 x SS1), a) Time history and hysteretic responses; under inelastic loading signal; b) Time history and hysteretic responses, c) maximum shear deformation along length, d) and e) displacement and shear force along length at the occurrence of maximum shear force at end.
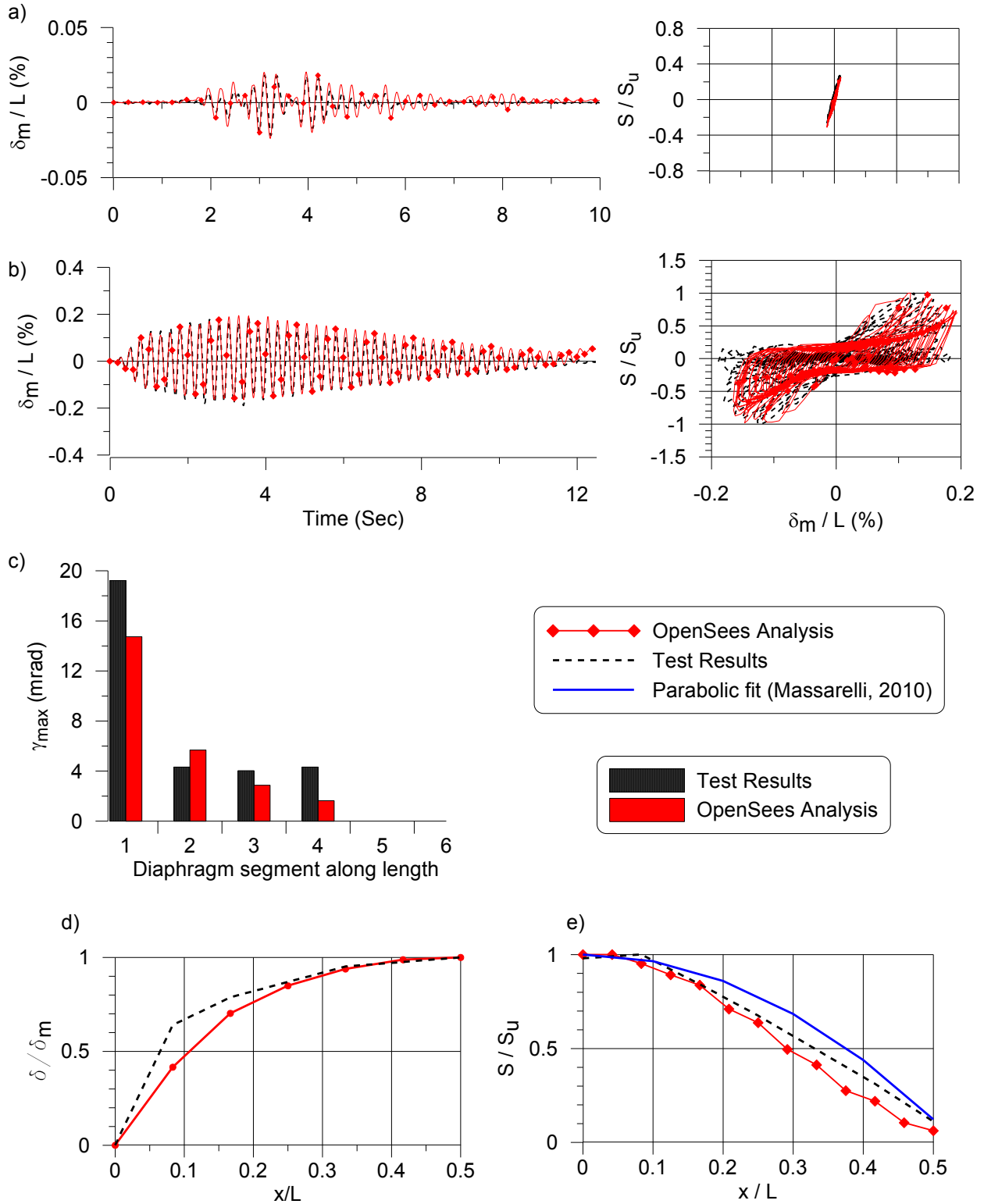
Specimen 10: under elastic loading signal (0.7 x SS1), a) Time history and hysteretic responses; under inelastic loading signal; b) Time history and hysteretic responses, c) maximum shear deformation along length, d) and e) displacement and shear force along length at the occurrence of maximum shear force at end.
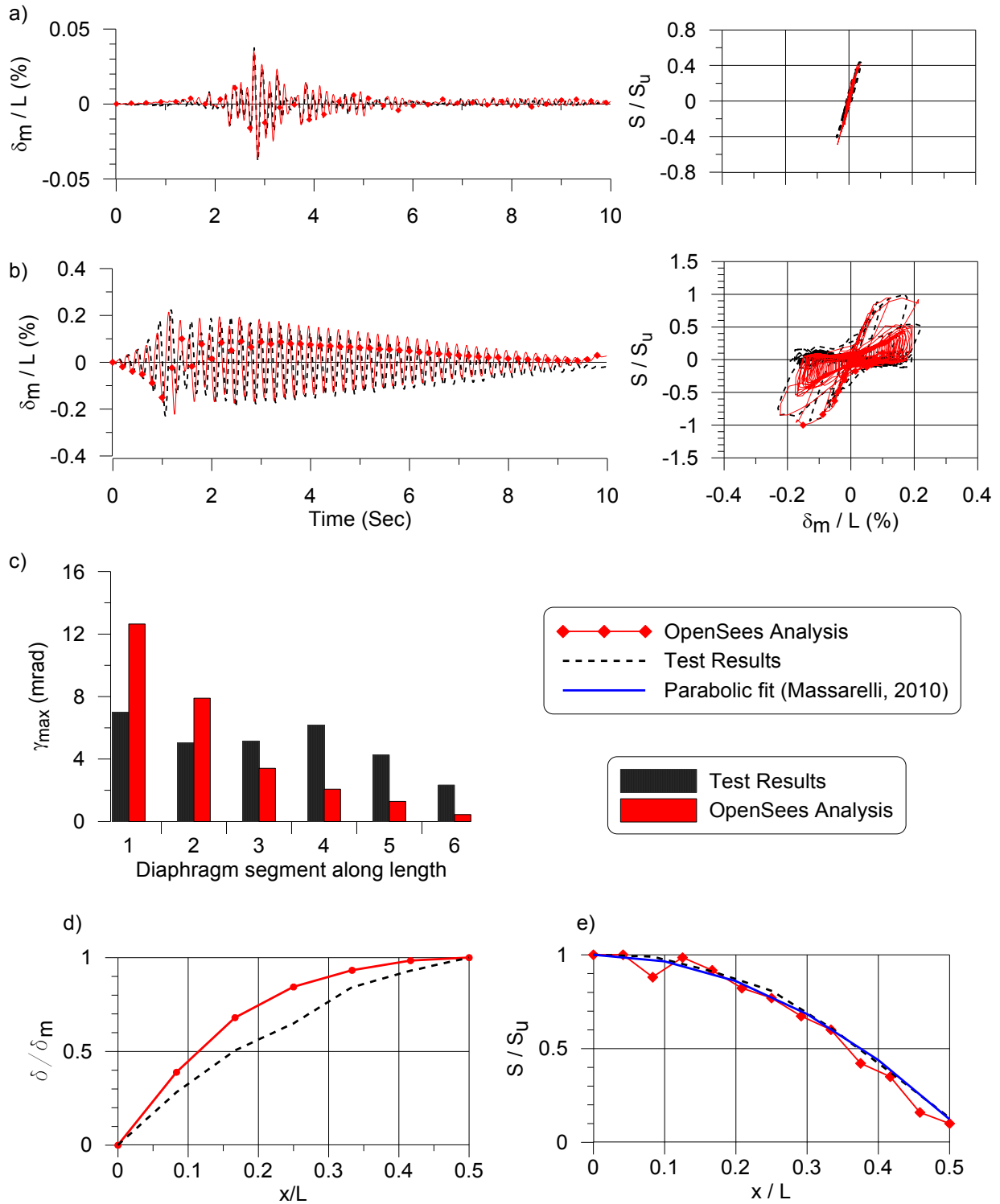
Specimen 11: under elastic loading signal (1.1 x SS1), a) Time history and hysteretic responses; under inelastic loading signal; b) Time history and hysteretic responses, c) maximum shear deformation along length, d) and e) displacement and shear force along length at the occurrence of maximum shear force at end.
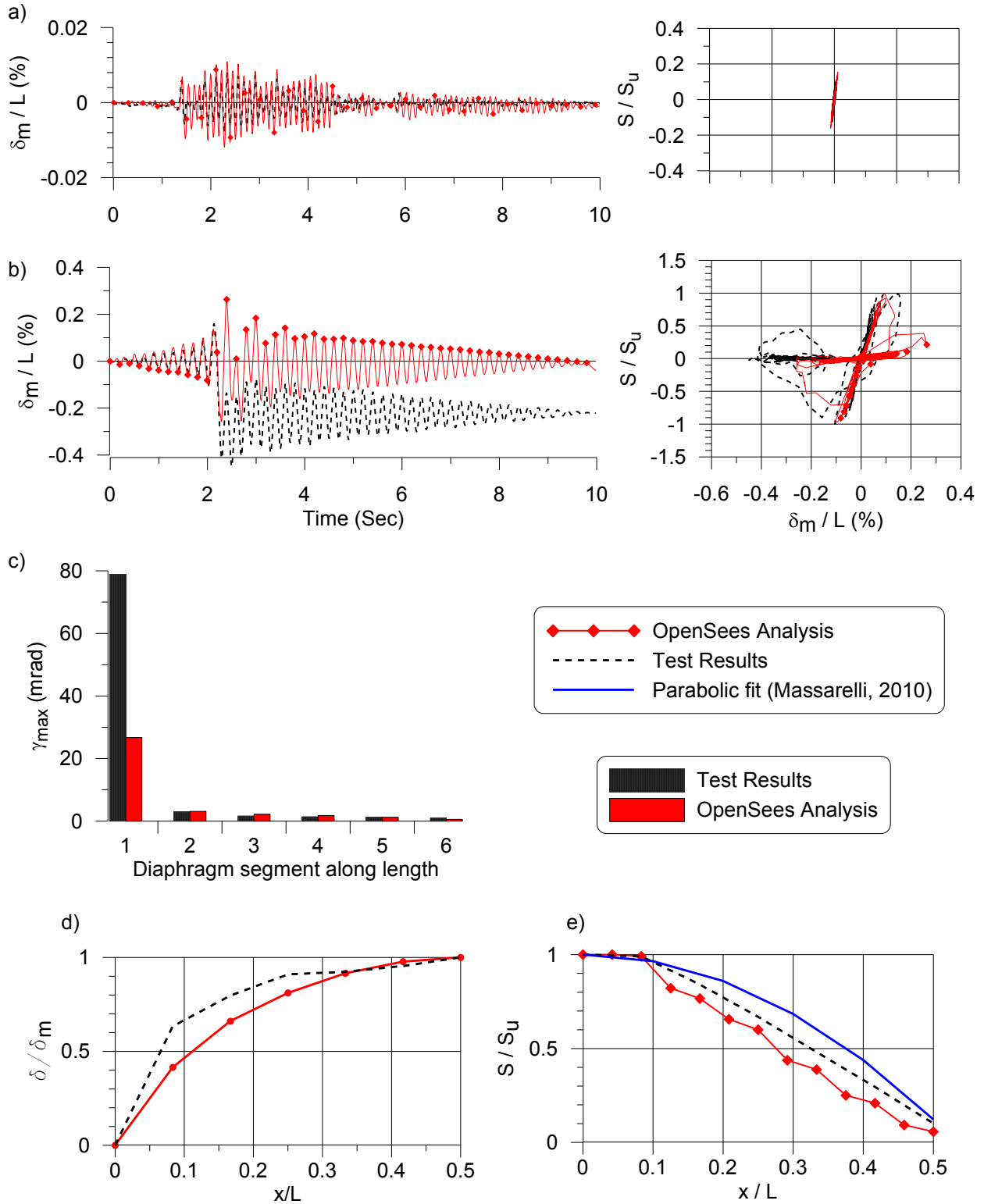
Specimen 12: under elastic loading signal (1.6 x SS3), a) Time history and hysteretic responses; under inelastic loading signal; b) Time history and hysteretic responses, c) maximum shear deformation along length, d) and e) displacement and shear force along length at the occurrence of maximum shear force at end.
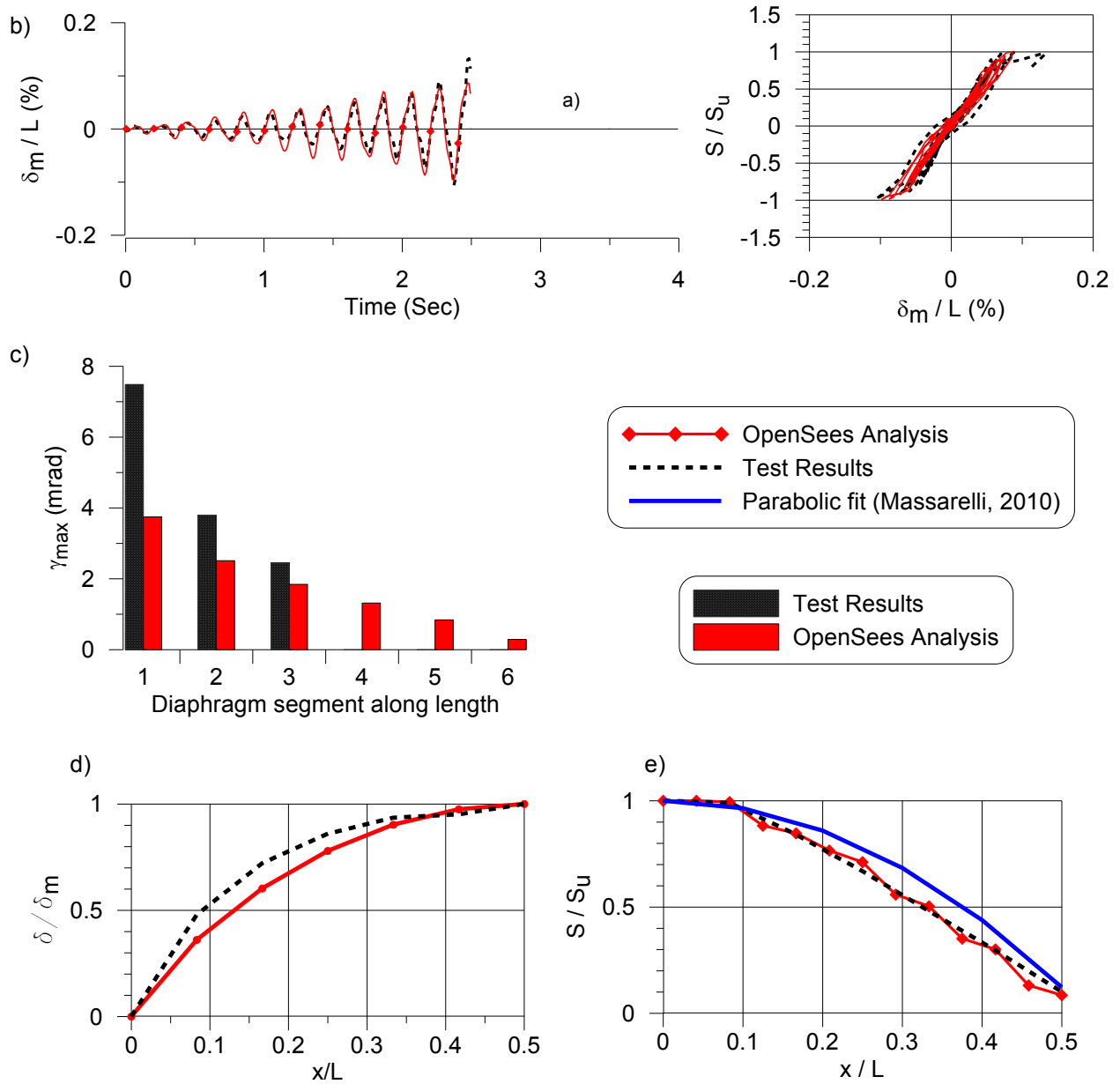
Specimen 13: under inelastic loading signal; a) Time history and hysteretic responses, b) maximum shear deformation along length, c) and d) displacement and shear force along length at the occurrence of maximum shear force at end.
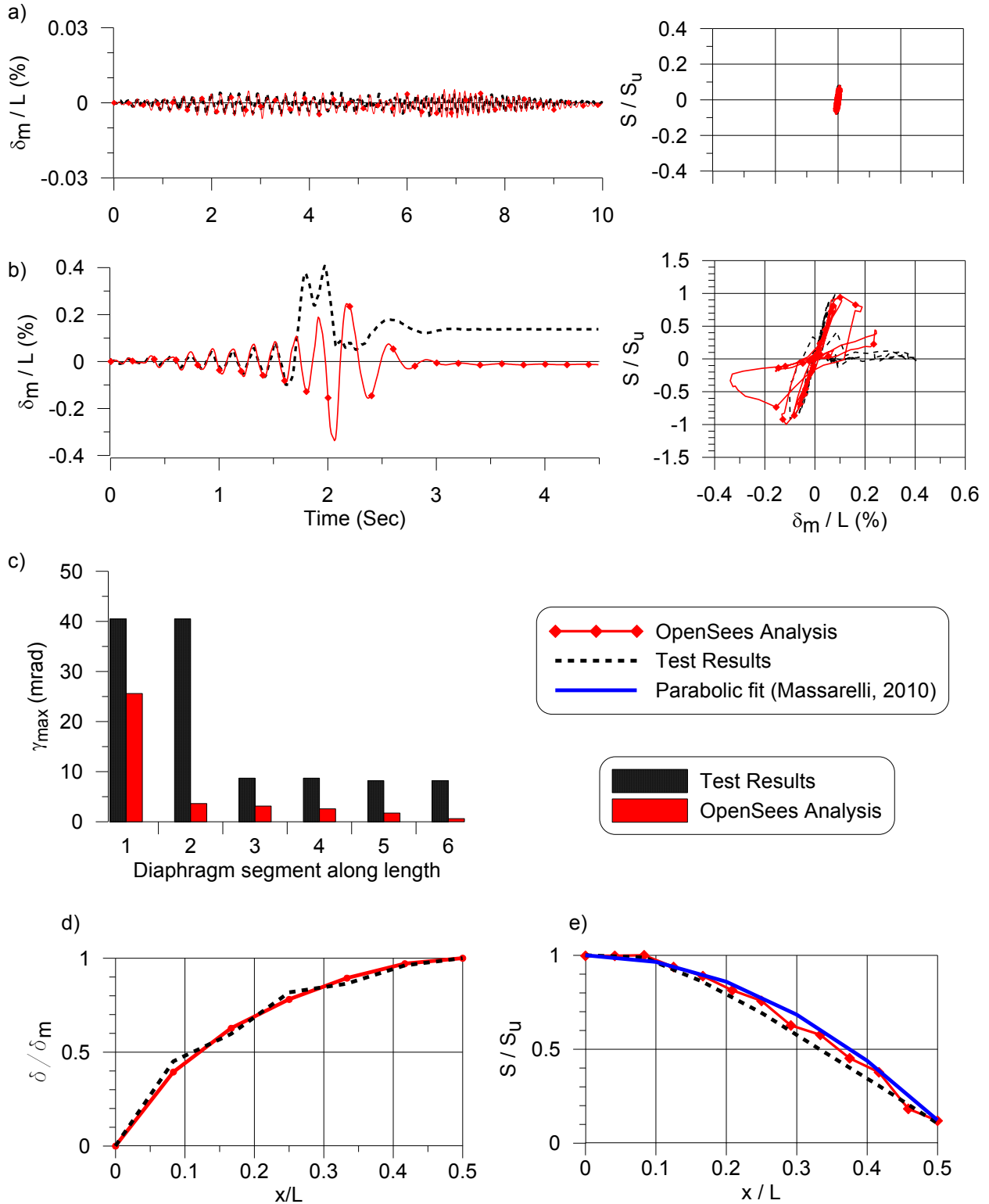
Specimen 14: under elastic loading signal (0.05 x SS2), a) Time history and hysteretic responses; under inelastic loading signal; b) Time history and hysteretic responses, c) maximum shear deformation along length, d) and e) displacement and shear force along length at the occurrence of maximum shear force at end.
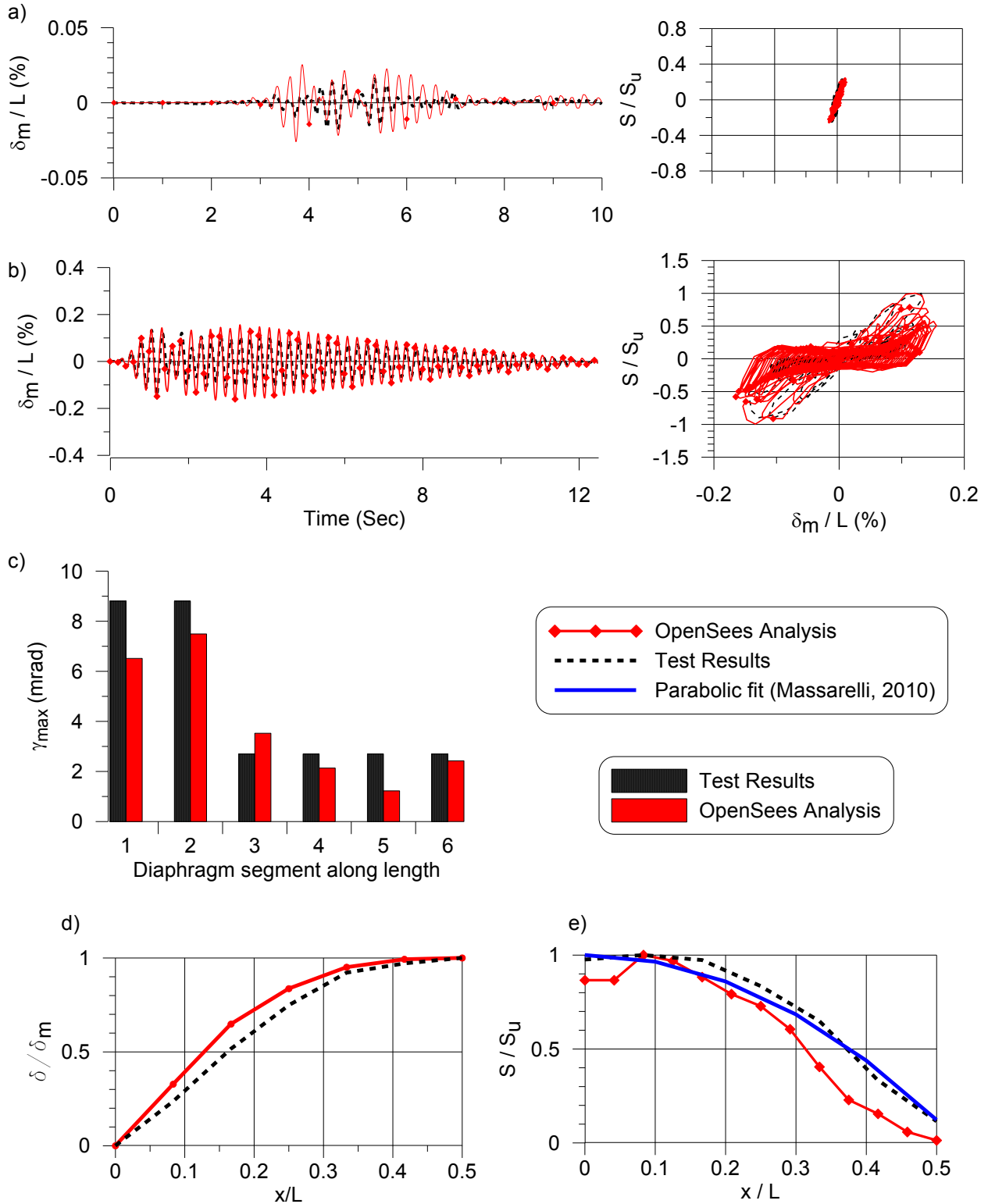
Specimen 15: under elastic loading signal (0.8 x SS1), a) Time history and hysteretic responses; under inelastic loading signal; b) Time history and hysteretic responses, c) maximum shear deformation along length, d) and e) displacement and shear force along length at the occurrence of maximum shear force at end.

a)

b)

c)

d)

e)
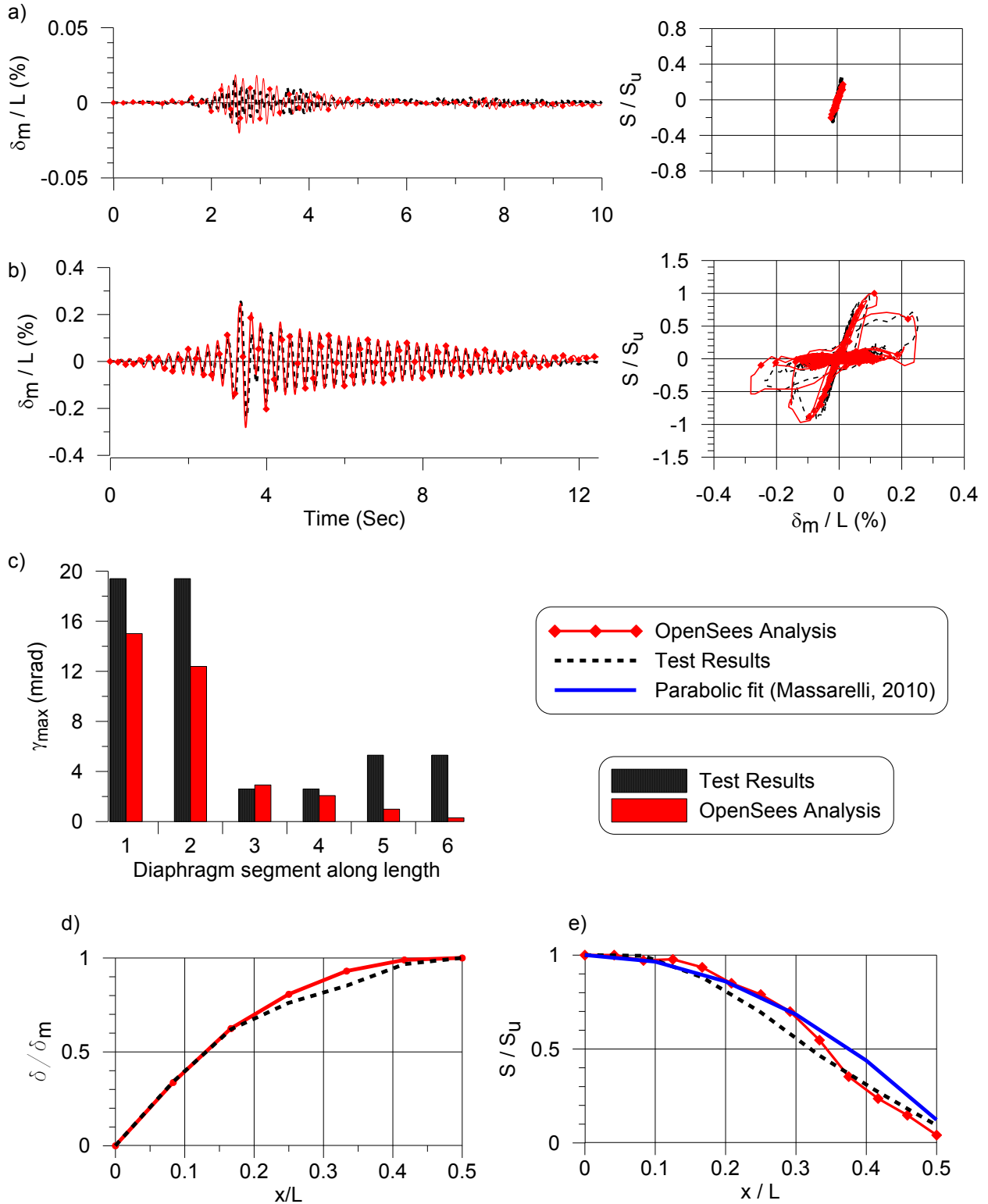
Specimen 16: under elastic loading signal (0.8 x SS1), a) Time history and hysteretic responses; under inelastic loading signal; b) Time history and hysteretic responses, c) maximum shear deformation along length, d) and e) displacement and shear force along length at the occurrence of maximum shear force at end.
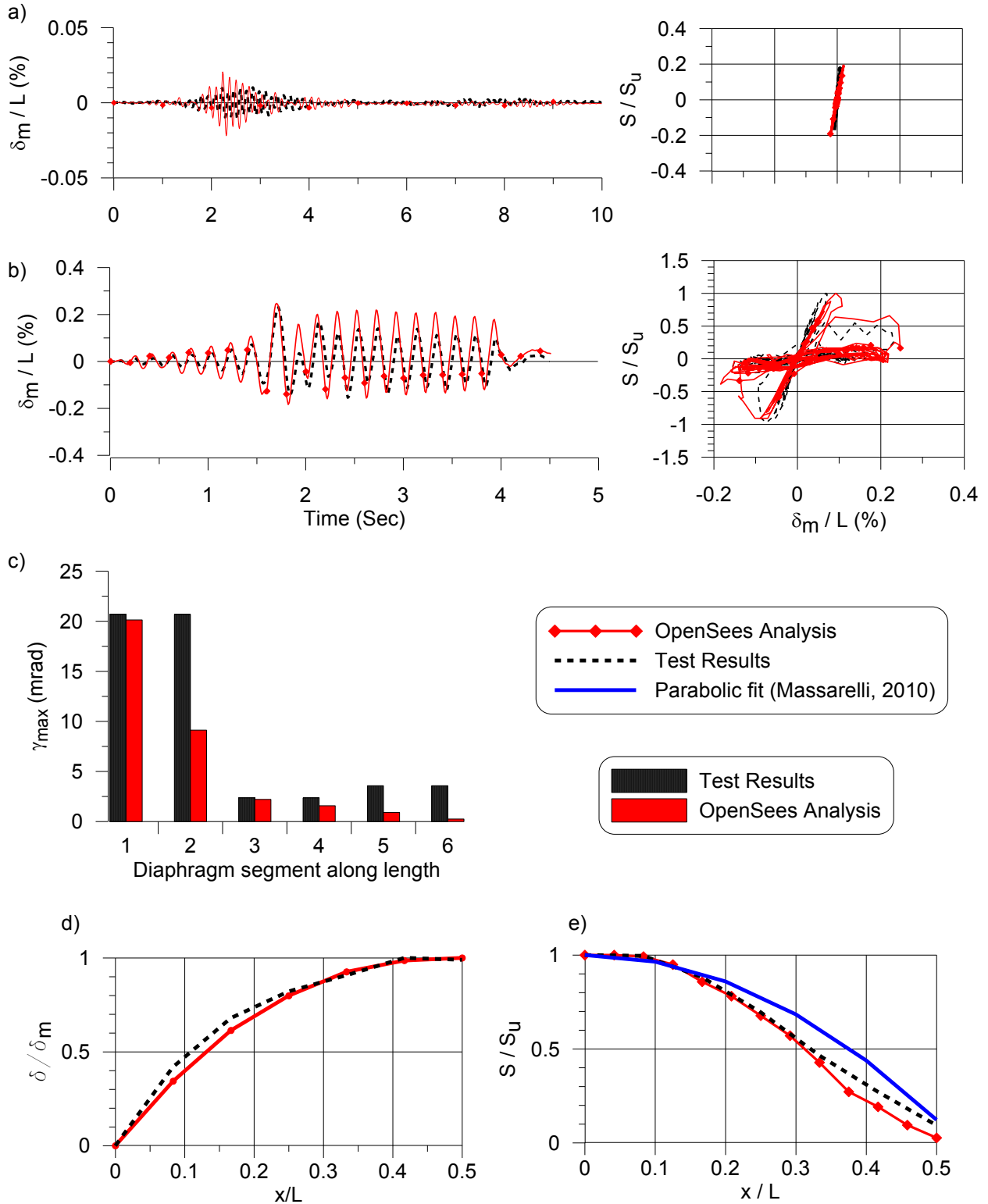
Specimen 17: under elastic loading signal (0.8 x SS1), a) Time history and hysteretic responses; under inelastic loading signal; b) Time history and hysteretic responses, c) maximum shear deformation along length, d) and e) displacement and shear force along length at the occurrence of maximum shear force at end.
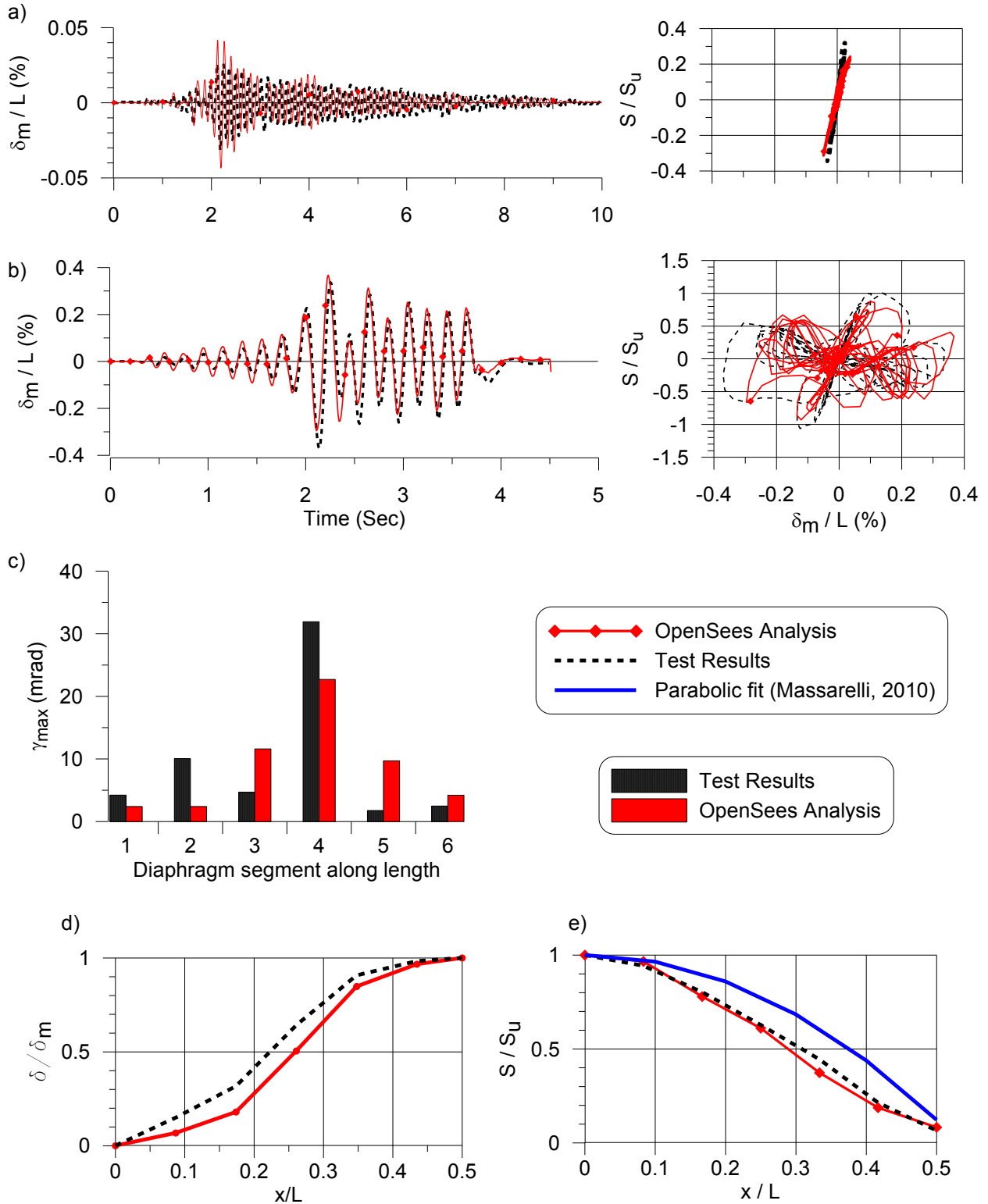
Specimen 18: under elastic loading signal (1.0 x SS1), a) Time history and hysteretic responses; under inelastic loading signal; b) Time history and hysteretic responses, c) maximum shear deformation along length, d) and e) displacement and shear force along length at the occurrence of maximum shear force at end.
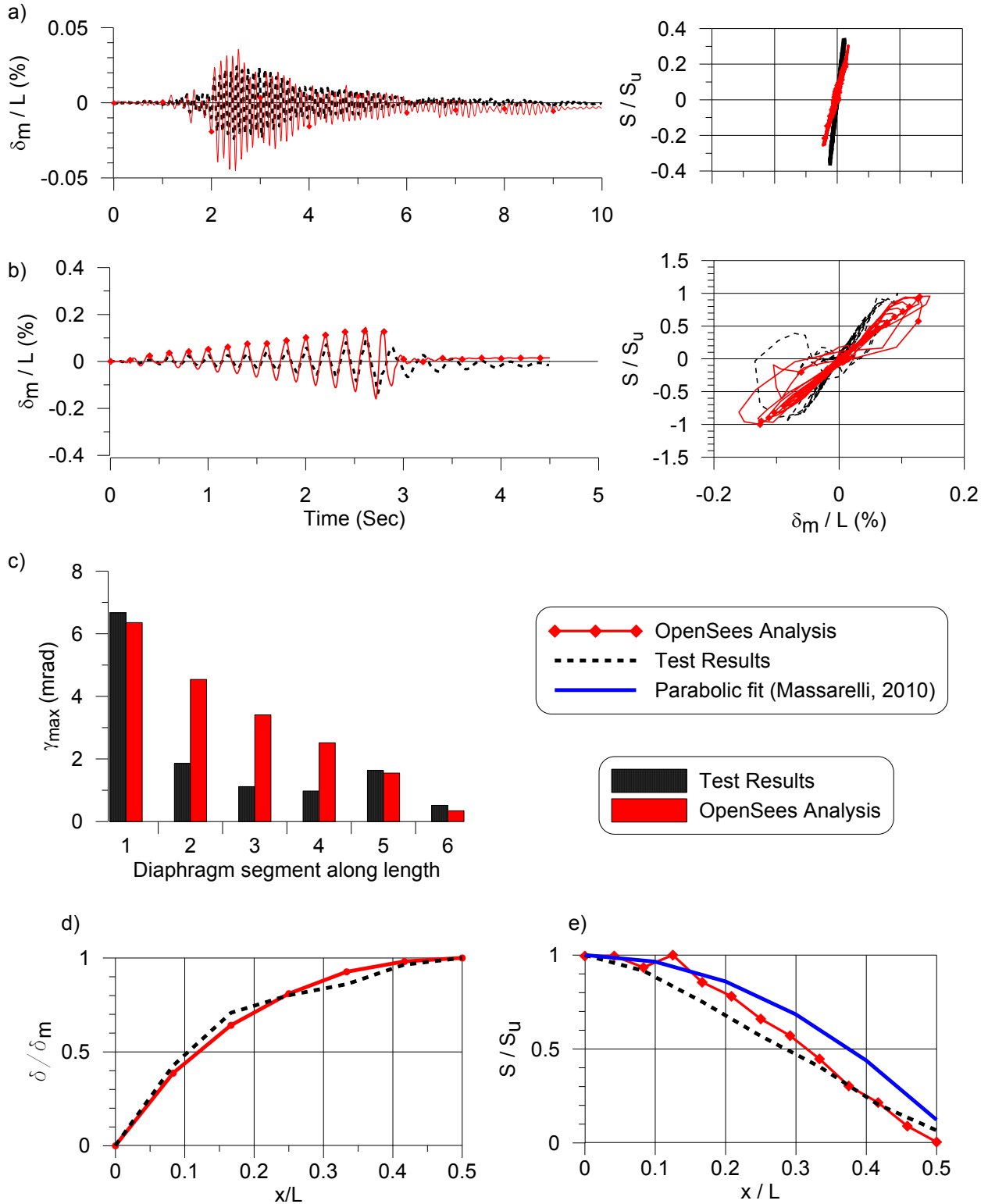
Specimen 19: under elastic loading signal (1.0 x SS1), a) Time history and hysteretic responses; under inelastic loading signal; b) Time history and hysteretic responses, c) maximum shear deformation along length, d) and e) displacement and shear force along length at the occurrence of maximum shear force at end.

Appendix C:

Design of a single-storey steel building with an inelastic diaphragm structural system (Design Case BVM0)

Snow Loads (NBCC, 2010)					
Location	Abbotsford, BC				
Ground snow load (Appendix C)	S_s =	2.0	kPa	Length l =	60	m
Associated rain load (Appendix C)	S_r =	0.3	kPa	Width w =	30	m
Importance factor for snow load (A-3)	I_s =	1.0		l_c =	45.0	m
Basic roof snow load factor(G-3)	C_b =	0.8		$l_c \geq 70m$?	No	
Wind exposer factor (G-3)	C_w =	1.0		C_b =	0.8	
Roof Slope factor (G-4)	C_s =	1.0				
Shape factor (G-4)	C_a =	1.0				
Specified snow load	**S =**	**1.90**	**kPa**			
Considering snow accumulation due to HVAC units (Commentary G, Figure G-8)						
Average Unit Weight of snow γ =	3.0	kN/m^3				
HVAC height =	2.0	m	$3S_s/\gamma$ =	2.00		
HVAC width =	3.0	m	b> $3S_s/\gamma$ so cannot ignore snow loads			
HVAC length =	3.0	m				
x_d =	4.00	m				
h' =	1.73	m				
$C_a(0)$ =	2.51	<	$0.8/C_b$ =	1.0	No	
		>	$2/C_b$ =	2.5	Yes	
$C_a(0)$ =	2.500					
	=	x_d	$x_d < x < 10h'$	> 10h'		
x =	0.00	4.00		17.33		
C_w =	1.0	1.0	1.0	1.0		
C_s =	1.0	1.0	1.0	1.0		
C_a =	2.5	1.0	1.0	1.0		
Max snow adjacent to HVAC =	4.30	kPa				
Snow at distance x_d =	1.90	kPa				
Additional weight of snow within distance x_d =	14.40	kN				
Weight of snow for 1 HVAC =	57.6	kN				
Weight of snow for 4 HVACs =	230.4	kN				
UDL over roof from snow accumulation =	**0.13**	**kPa**				

Wind Loads (NBCC 2010)

Location	Abbotsford, BC							

N-S wind loads

			Pressure zone	normal	high		Zone	p	
I_w =	1		Pressure zone	normal	high		Zone	p	
$q_{1/50}$ =	0.44	kPa	Coefficient	C_pC_g	C_pC_g		1	0.307	kPa
$q_{1/10}$ =	0.34	kPa	Windward	0.75	1.15		1E	0.471	kPa
Width w =	30.0	m	Leeward	-0.55	-0.80		4	-0.225	kPa
Length l =	60	m	Roof	-1.3	-2.0		4E	-0.328	kPa
Height h =	7	m					2	-0.533	kPa
C_e =	0.93		R_{Left} =	61.2	kN		2E	-0.819	kPa
z =	2.8	m	R_{Right} =	56.2	kN				
y =	6.0	m							

N-S wind load for serviceability limit (Calculated with importance factor of 0.75)

		Wind Dir	Lee ward
Total load	kN	51.0	-37.1
UDL	kN/m	0.8	-0.6

E-W wind loads

Pressure zone	normal	high		Zone	p	
coefficient	C_pC_g	C_pC_g		5	0.307	kPa
windward	0.75	1.15		5E	0.471	kPa
leeward	-0.55	-0.80		6	-0.225	kPa
roof	-1.3	-2.0		6E	-0.328	kPa
N-S wall	-0.85	-0.9		2	-0.533	kPa
				2E	-0.819	kPa
R_{Left} =	18.3	kN		1	-0.348	kPa
R_{Right} =	16.8	kN		1E	-0.369	kPa

Earthquake Load (NBCC, 2010)

Location   Abbotsford, BC

			T (Sec.)	0	0.2	0.5	1	2	4	5
$S_a(0.2)$ =	0.990	g								
$S_a(0.5)$ =	0.660	g	S(T) (g)	0.990	0.990	0.660	0.320	0.170	0.085	0.085
$S_a(1.0)$ =	0.320	g								
$S_a(2.0)$ =	0.170	g	T_a =	0.175	sec	*Static Analysis permitted*				
Site Class =	C		$2 \times T_a$ =	0.350	sec	*when $I_E F_a S_a(0.2) < 0.35$*				
F_a =	1.0		$S(2T_a)$ =	**0.825**	g	*Regular Structure h<60 and Ta <2.0 Sec*				
F_v =	1.0									
I_E =	1.0		$S_a(0.2)/S_a(2.0)$ =		5.8	$S_a(0.2)/S_a(2.0) < 8.0$				
$I_E F_a S_a(0.2)$ =	0.99		M_v =		1.00		J =	1.00		
R_d =	2.0									
R_o =	1.9									

$R_d R_o$ =	3.8		Base Shear for drift calculation				
W =	3255.2	kN	From Sap Model T_a=			0.84 sec	$S(T_a)$ = **0.430** g
V =	706.7	kN	Base Shear for Drift =			367.3 kN	
V ≥	145.6	kN	Maximum base shear =			367.3 kN	
V ≤	565.4	kN	Base Shear for drift in the model =			367.3 kN	
V =	**565.4**	**kN**					

N-S Earthquake Loads			E-W Earthquake Loads			Upper limit lateral force on brace		
D_{nx} =	60	m	D_{nx} =	30	m			
$0.10 \times D_{nx}$ =	6.0	m	$0.10 \times D_{nx}$ =	3.0	m	$R_d R_o$ =	2	
F_x =	565.4	kN	F_x =	565.4	kN	V=	1342.8	kN
V_{brace} =	**339.2**	**kN**	V_{brace} =	**339.2**	**kN**	V_{brace} =	**805.7**	kN

Member Designs								
Building Dimensions								
Width w =	30	m		E-W Interior bay width =	10	m		
Length l =	60	m		N-S Interior bay width =	10	m		
Height h=	7.0	m		E-W Exterior bay width =	5	m		
Roof area =	1800	m^2		N-S Exterior bay width =	5	m		
Wall perimeter =	180	m						
Loads								
Roofing Materials and Equipment								
HVAC units, lighting, fans, and sprinkler systems etc =			0.10	kPa				
Walkways, roof ballast/membrane/insulation and joists =			1.00	kPa				
		Deck thickness =	0.76	mm				
		Steel deck load =	0.08	kPa				
Wall Materials and Cladding								
		Steel sheeting insulation =	0.35	kPa				
Dead, Live, and Snow Loads				**Earthquake and Wind Loads on each building edge**				
	Roof dead load =	1.18	kPa	Earthquake lateral force N-S =		339.2	kN	
	Roof live load =	0.00	kPa	Earthquake lateral force E-W =		339.2	kN	
	Roof snow load =	2.03	kPa	Wind lateral force N-S=		61.2	kN	
Half of perimeter wall load =		220.5	kN	Wind lateral force E-W=		18.3	kN	
Roof Seismic load (without wall) =		3034.7	kN					
Seismic Weight on roof W (with wall)=		3255.2	kN					
P-Δ Effects								
	$R_d\Delta$ =	0.049	m					
	ΣC_f =	3034.7	kN					
Notional Load	V_{Hx} =	15.2	kN					
	V =	565.4	kN					
	U_2 =	1.04	1.00	(Can be neglected if less than 1.1, NBCC 2005 Commentary)				

		$V_{x, N-S}$ =	339.2	kN	(per braced wall)			
		$V_{x, E-W}$ =	339.2	kN	(per braced wall)			
Brace force on N-S side =		*346.8*	kN		q =	5.8	kN/m	
Brace force on E-W side =		346.8	kN		q =	11.6	kN/m	
Diaphragm design force		**q =**	**11.6**	**kN/m**				
Roof Diaphragm for Gravity								
					Resistance from Canam deck catalogue			
Factor load w_f =		4.52	kPa		$w_{f, max}$ =	4.6	kPa	OK
Service load $w_{service}$ =		2.03	kPa		$w_{s, max}$ =	2.6	kPa	OK
					bearing length =	65	mm	Assumed
End reaction $R_{f, end}$ =		3.6	kN/m		$R_{f, end}$ =	12.90	kN	OK
Interior reaction $R_{f, interior}$ =		9.9	kN/m		$R_{f, interior}$ =	16.50	kN	OK
Deck profile =		38 x 914	P-3615					
Number of spans =		5						
Span length =		2.0	m					
Panel length =		10.0	m					
thickness t =		0.76	mm					
F_y =		230	MPa					
Roof Diaphragm fuse								
q =	11.6	kN/m				φ =	0.6	
t =	0.76	mm				S_n =	19.4	kN/m	from SDI
Frame fasteners =	EDNK19 and 22 nails					G' =	6.50	kN/mm	from SDI
side-lap fasteners =	#12 screws					ϕS_n =	11.6	kN/m	Ok
Spacing =	36/4				Probable Diaphragm strength =		21.7	kN/m	
Spacing =	140	mm						
OWSJ								
Joist trib. width =		2.0	m					
Joist length =		10.0	m					

Finding joist top angle from Canam joist catlogue (Lightest section from joist table)							
Service load =					6.41	kN/m	
Select d form Canam table for lightest section					650	mm	
percentage of service load to cause L/360 deflection					83		
Select Double angles from Canam table (for deflection criteria)					1 3/4 X 1 3/4 X 5/32		

Selection of X Braces

E-W side brace

Steel : ASTM A500, Fy = 345 MPa

Probable shear flow 21.7 kN/m

Shear flow length	15	m			Shear flow length	15	m

325.9 θ V_{fx} = 325.9 kN

< <

Cut-off with R_dR_o = 2 C_{fx} = 397.8 kN Cut-off with R_dR_o = 2

402.8 kN 402.8 kN

Brace length L= 12206.6 mm

C_{fx}= **397.8** kN

KL= 5493.0 mm

Select HA152x152x6.4 CSA S16 -09 was followed for design

C_r = 483.3 kN

KL/r = 92.3

N-S side brace

Shear flow length	25	m			Shear flow length	35	m

Beam Force 67.1 kN

543.2 θ V_{fx} = 760.5 kN

Cut-off with R_dR_o = 2 Cut-off with R_dR_o = 2

335.7 kN C_{fx} = 491.7 kN 470.0 kN

Brace length L= 12206.6 mm

C_{fx}= **491.7** kN

KL=	5493.0	mm							
Select	HA152x152x8.0		CSA S16 -09 was followed for design						
C_r =	586.8	kN							
KL/r =	93.4								

Selection of Braced Column Section at E-W side

Force on Column

Due to EQ =			228.1	kN					
Tributary area for perimeter column =			50	m^2					
Due to Live load =			0	kN					
Due to snow load =			101.4	kN					
Due to dead load =			58.9	kN					

Total design load in Column C_f = D+E+0.25S

Total design load in Column C_f =	**312.44**	**kN**		CSA S16 -09 was followed for design					
L =	7000.0	mm	Strong Axis	L_x=		7000.0			
C_f =	312.4	kN	weak axis	L_y=		3500.0	*(Assuming Bracing provided at mid height)*		
k=	1.0								
φ =	0.9								
F_y =	345	MPa							
n=	1.34								
E =	200000	MPa	Select	W200x27	Class 2 or better		M_{ry}	23.6	kNm
Strong Axis	kL/r =	80.2		λ =	1.060		C_r =	590.6	kN
weak axis	kL/r =	112.2		λ =	1.483		C_r =	383.0	kN
C_{ro} =	1052.6	kN	*(At KL = 0)*				C_{ey}=	133045	kN
Controlling C_r =	**383.0**	**kN**	*OK*				C_{ex}=	1040167	kN
U_{1y}=	0.6						ω_{1y}=	0.6	
U_{1x}=	0.6								
β =	0.85								
M_{fy}=	2.8	kNm	corresponding to 1% drift with cantilever column assumption						
M_{fx}=	0.0	kNm							
	Cross section strength								
	$\dfrac{C_f}{C_{r0}}$	+	$\dfrac{\beta M_{fy}}{M_{ry}}$	<	1				
		0.40	≤	1	OK				

	Overall Member Strength									
	$\dfrac{C_f}{C_r}$	+	$\dfrac{\beta\, U_{1y}\, M_{fy}}{M_{ry}}$	<	1					
		0.88	≤	1	OK					

Selection of Braced Column Section at N-S side

Force on Column

due to EQ E =	282.0	kN			
Tributary area for perimeter column A=	50	m^2			
Due to Live load L=	0	kN			
Due to snow laod S=	101.4	kN			
Due to dead load D=	58.9	kN			

Total design load in Column C_f = D+E+0.25S

Total design load in Column C_f =   **366.28**   **kN**   CSA S16 -09 was followed for design

L =	7000.0	mm	Strong Axis		L_x= 7000.0				
C_f =	366.3	kN	weak axis		L_y= 3500.0				
k=	1.0								
φ =	0.9								
F_y =	345	MPa							
n=	1.34								
E =	200000	MPa	Select	W200x27	Class 2 or better		M_{ry}	23.6	kNm
Strong Axis	kL/r = 80.2		λ = 1.060		C_r = 590.6	kN			
weak axis	kL/r = 112.2		λ = 1.483		C_r = 383.0	kN			
C_{ro} =	1052.595	kN	*(At KL = 0)*						
Controlling C_r =	**383.0**	**kN**	OK						
Cey=	133045	kN							
Cex=	1040167	kN							
ω_{1y}=	0.6								
		Cross section strength							

		$\dfrac{C_f}{C_{r0}}$	+	$\dfrac{\beta\, M_{fy}}{M_{ry}}$	<	1		
			0.44	≤	1	OK		

		Overall Member Strength							
		$\dfrac{C_f}{C_r}$	+	$\dfrac{\beta\, U_{1y}\, M_{fy}}{M_{ry}}$	<	1			
			1.0	≤	1	OK			

Selection of braced Beam Section for E-W side

	Total design load in Column Cf = D+E+0.25S								
	Joist spacing =	2	m		CSA S16-09 was followed for design				
	Max moment =	105.4	kNm	**Try a**	**W360x51**	Class 2 or better			
	Compressive Force on beam E =	0.0	kN	Use same as perimeter beams					
	$L =$	10.0	m	$M_{rx} =$	149.0	kNm			
	$C_f =$	0.0	kN	$C_{ro} =$	2002.725	kN	*(At KL = 0)*		
	$M_{fx} =$	105.4	kNm	$C_r =$	**1325.2**	**kN**	OK		
	$k =$	1.0		$\omega_{1x} =$	1	Uniformly distributed load			
	$\phi =$	0.9		$U_{1x} =$	1.000				
	$F_y =$	345	MPa	$\beta =$	0.85				
	$n =$	1.34							
	Cross section strength								
	$\dfrac{C_f}{C_{r0}}$	+	$\dfrac{\beta\, M_{fx}}{M_{rx}}$	<	1				
		0.60	≤	1	OK				
	Overall Member Strength								
	$\dfrac{C_f}{C_r}$	+	$\dfrac{\beta\, U_{1x}\, M_{fx}}{M_{rx}}$	<	1				
		0.60	≤	1	OK				

Selection of braced Beam Section for N-S side								
Total design load in Column Cf = D+E+0.25S								
Beam and joist spacing=	2				CSA S16 -09 was followed for design			
Max moment =	21.1	kNm		**Select**	**W310x39**	Class 2 or better		
Compressive force E =	67.1	kN		Using same section as perimeter beams				
	L =	10000.0	mm	M_{rx} =	305.0	kNm		
	C_f =	67.1	kN	C_{ro} =	1533.87	kN	*(At KL = 0)*	
	M_{fx}=	21.1	kNm	C_r =	906.0	kN	OK	
	k=	1.0		ω_{1x} =	1	Uniformly distributed load		
	ϕ =	0.9		U_{1x}=	1.000			
	F_y =	345	MPa	β =	0.85			
	n=	1.34						
		Cross section strength						
		C_f	+	$\beta\,M_{fx}$	<		1	
		C_{r0}		M_{rx}				
		0.10		$\leq$	1	OK		
		Overall Member Strength						
		C_f	+	$\beta\,U_{1x}\,M_{fx}$	<		1	
		C_r		M_{rx}				
		0.13		$\leq$	1	OK		

Interior Columns								
Load combination:	1.25D + 1.5S + 0.5L							
Loading Area=	100	m2	Select	178x178x6.4		CSA S16 -09 was followed for design		
C_f =	452.0	kN	L =	7000.0	mm			
ϕ =	0.9		(b-4t)/t =	24.03	$\leq$	36.07	OK	Class 3 or better
F_y =	345	MPa	kL/r =	100.6	$\leq$	200	OK	
			C_r =	508.2	kN	OK		

Exterior Columns								
Load combination:	1.25D + 1.5S + 0.4W							
L =	7000.0	mm	Strong Axis		L_x=	7000.0		
Loading Area=	50	m2	weak axis		L_y=	3500.0		
		Wind column trib. width =		5.00	m			
			wind UDL =	0.94	kN/m			
			C_f =	225.8	kN			
		Beam Column Eccentricity e =		0.165	m			
$M_{f\,design}$ =	37.3	kNm						
$M_{f\,end}$ =	37.3	kNm						
$M_{f\,wind}$ =	5.8	kNm						
ϕ =	0.9							
F_y =	345	MPa						
Select	W200x31		CSA S16 -09 was followed for design					
b/t =	6.57	≤	9.15	OK	Class 2 or better			
h/w =	29.6	≤	102.8	OK	Class 2 or better			
C_{ro} =	1242.0	kN						
M_{rx} =	104.0	kNm						
kL_x/r_x =	79.0	≤	200	OK				
kL_y/r_y =	109.4	≤	200	OK				
C_{rx} =	708.0	kN						
C_{ry} =	469.1	kN			M_u =	102.0	kNm	
C_{ex} =	1264.9	kN			M_p =	115.6	kNm	
ω_{1x} =	1.0	uniformly distributed load			$0.67M_p$ =	77.4	kNm	
U_{1x}=	1.22				M_r' =	81.7	kNm	
ω_2 =	1.0	max moment at mid-span						
	Cross Section Strength Check							
	$\dfrac{C_f}{C_{r0}}$	+	$\dfrac{0.85U_{1x}M_f}{M_{rx}}$	=	0.55	≤	1	OK
	Overall In-Plane Member Strength Check							
	$\dfrac{C_f}{C_{rx}}$	+	$\dfrac{0.85U_{1x}M_f}{M_{rx}}$	=	0.69	≤	1	OK

	Lateral Torsional Buckling Stability								
	$\dfrac{C_f}{C_r}$	+	$\dfrac{0.85U_{1x}M_f}{M_r'}$	=	0.95	≤	1	OK	
	Moment Check								
	$\dfrac{M_{fx}}{M_{rx}}$	=	0.36	≤	1	OK			

Exterior Columns

Load combination:	1.25D + 0.5S + 1.4W								
Wind column trib. width =	5.00	m							
wind UDL =	3.30	kN/m							
Beam Column Eccentricity e =	0.165	m							
C_f =	124.4	kN							
$M_{f\,design}$ =	20.5	kNm							
$M_{f\,end}$ =	20.5	kNm							
$M_{f\,wind}$ =	20.2	kNm							
ϕ =	0.9								
F_y =	345	MPa							
Select	W200x31		CSA S16 -09 was followed for design						
b/t =	6.57	≤	9.15	OK	Class 2 or better				
h/w =	29.6	≤	97.7	OK	Class 2 or better				
C_{ro} =	1242.0	kN							
M_{rx} =	104.0	kNm							
kL_x/r_x =	79.0	≤	200	OK					
kL_y/r_y =	109.4	≤	200	OK					
C_{rx} =	708.0	kN							
C_{ry} =	469.1	kN							
C_{ex} =	1264.9	kN					M_u =	102.0	kNm
ω_{1x} =	1.0	uniformly distributed load					M_p =	115.6	kNm
U_{1x} =	1.11						$0.67M_p$ =	77.4	kNm
ω_2 =	1.0	max moment at mid-span					M_r' =	81.7	kNm

	Cross Section Strength Check							
	$\dfrac{C_f}{C_{r0}}$	$+$	$\dfrac{0.85U_{1x}M_f}{M_{rx}}$	$=$	0.29	$\leq$	1	OK
	Overall In-Plane Member Strength Check							
	$\dfrac{C_f}{C_{rx}}$	$+$	$\dfrac{0.85U_{1x}M_f}{M_{rx}}$	$=$	0.36	$\leq$	1	OK
	Lateral Torsional Buckling Stability							
	$\dfrac{C_f}{C_r}$	$+$	$\dfrac{0.85U_{1x}M_f}{M_r'}$	$=$	0.50	$\leq$	1	OK
	Moment Check							
	$\dfrac{M_{fx}}{M_{rx}}$	$=$	0.20	$\leq$	1	OK		

Corner Columns

Load combination:	1.25D + 1.5S + 0.4W						
Column length =	7.0	m			$L_x =$	7000	mm
Column tributary area =	25.00	m^2			$L_y =$	3500	mm
Factored UDL =	4.52	kPa			$C_f =$	112.9	kN
N-S wall wind force =	0.19	kPa			$M_{fx} =$	5.8	kNm
E-W wall wind force =	-0.15	kPa			$M_{fy} =$	4.5	kNm
N-S wall tributary width =	5.00	m			$\phi =$	0.9	
E-W wall tributary width =	5.00	m			$F_y =$	345	MPa
N-S wall corner column UDL =	0.94	kN/m					
E-W wall corner column UDL =	-0.74	kN/m					
Select	W200x31	CSA S16 -09 was followed for design					
b/t =	6.57	$\leq$	9.15	OK	Class 2 or better		
h/w =	29.6	$\leq$	85.9	OK	Class 2 or better		
$L_u =$	1600	mm	Lat-tor buckling				

C_{ro} =	1242.0	kN							
M_{rx} =	104.0	kNm			M_{ry} =	29.1	kNm		
kL_x/r_x =	79.0	≤	200	OK	kL_y/r_y =	109.4	≤	200	OK
C_{rx} =	708.0	kN			λ_y =	1.446			
C_{ex} =	1264.9	kN			C_{ry} =	469.1	kN		
ω_{1x} =	1.0	uniformly distributed load			C_{ey} =	660.7	kN		
U_{1x} =	1.098	≥	1.0	OK	ω_{1y} =	1.0	uniformly distributed load		
ω_2 =	1.0				U_{1y} =	1.206	≥	1.0	OK
M_u =	79.4	kNm			β =	0.85			
M_p =	115.6	kNm							
$0.67M_p$ =	77.4	kNm							
M_r' =	70.9	kNm							

Cross Section Strength Check

$\dfrac{C_f}{C_{r0}}$	+	$\dfrac{0.85U_{1x}M_{fx}}{M_{rx}}$	+	$\dfrac{\beta U_{1y}M_{fy}}{M_{ry}}$	=	0.30	≤	1	OK

Overall In-Plane Member Strength Check

$\dfrac{C_f}{C_r}$	+	$\dfrac{0.85U_{1x}M_{fx}}{M_{rx}}$	+	$\dfrac{\beta U_{1y}M_{fy}}{M_{ry}}$	=	0.42	≤	1	OK

Lateral Torsional Buckling Stability

$\dfrac{C_f}{C_{ry}}$	+	$\dfrac{0.85U_{1x}M_{fx}}{M_r'}$	+	$\dfrac{\beta U_{1y}M_{fy}}{M_{ry}}$	=	0.50	≤	1	OK

Moment Check

$\dfrac{M_{fx}}{M_{rx}}$	+	$\dfrac{M_{fy}}{M_{ry}}$	=	0.24	≤	1.00	OK

Corner Columns										
	Load combination:		1.25D + 0.5S + 1.4W							
	Column length =		7.0	m			$L_x =$	7000	mm	
	Column tributary area =		25.00	m^2			$L_y =$	3500	mm	
	Factored UDL =		2.49	kPa			$C_f =$	62.2	kN	
	N-S wall wind force =		0.66	kPa			$M_{fx} =$	20.2	kNm	
	E-W wall wind force =		-0.52	kPa			$M_{fy} =$	15.8	kNm	
	N-S wall tributary width =		5.0	m			$\phi =$	0.9		
	E-W wall tributary width =		5.0	m			$F_y =$	345	MPa	
	N-S wall corner column UDL =		3.30	kN/m						
	E-W wall corner column UDL =		-2.58	kN/m						
Select	W200x31		CSA S16 -09 was followed for design							
$L_u =$	1600	mm	Lat-tor buckling							
b/t =	6.57	≤	9.15	OK	Class 2 or better					
h/w =	29.6	≤	88.4	OK	Class 2 or better					
$C_{ro} =$	1242.0	kN								
$M_{rx} =$	104.0	kNm				$M_{ry} =$	29.1	kNm		
$kL_x/r_x =$	79.0	≤	200	OK		$kL_y/r_y =$	109.4	≤	200	OK
$C_{rx} =$	708.0	kN				$C_{ry} =$	469.1	kN		
$C_{ex} =$	1264.9	kN				$C_{ey} =$	660.7	kN		
$\omega_{1x} =$	1.0	uniformly distributed load				$\omega_{1y} =$	1.0	uniformly distributed load		
$U_{1x} =$	1.052	≥	1.0	OK		$U_{1y} =$	1.104	≥	1.0	OK
$\omega_2 =$	1.0					$\beta =$	0.85			
$M_u =$	79.4	kNm								
$M_p =$	115.6	kNm								
$0.67M_p =$	77.4	kNm								
$M_r' =$	70.9	kNm								
Cross Section Strength Check										
$\dfrac{C_f}{C_{r0}}$		+	$\dfrac{0.85U_{1x}M_{fx}}{M_{rx}}$		+	$\dfrac{\beta U_{1y}M_{fy}}{M_{ry}}$	=	0.73	≤	1	OK
Overall In-Plane Member Strength Check										
$\dfrac{C_f}{C_r}$		+	$\dfrac{0.85U_{1x}M_{fx}}{M_{rx}}$		+	$\dfrac{\beta U_{1y}M_{fy}}{M_{ry}}$	=	0.76	≤	1	OK

201

Lateral Torsional Buckling Stability

$\dfrac{C_f}{C_{ry}}$	+	$\dfrac{0.85U_{1x}M_{fx}}{M_r'}$	+	$\dfrac{\beta U_{1y}M_{fy}}{M_{ry}}$	=	0.84	≤	1	OK

Moment Check

$\dfrac{M_{fx}}{M_{rx}}$	+	$\dfrac{M_{fy}}{M_{ry}}$	=	0.83	≤	1.00	OK		

Interior Simply Supported Beams

$V_{f, joist}$ =	45.2	kN	Select	W460x60		CSA S16-09 was followed for design			
supported by beam =	4		L_y =	2000	mm				
C_f =	361.3	kN	L_u =	1970	mm	Lat-tor buckling			
Beam length =	7.6	m	b/t =	5.75	≤	9.15	OK	Class 2	
$V_{f, beam}$ =	180.6	kN	h/w =	53.6	≤	91.5	OK	Class 2	
$M_{f, beam}$ =	325.1	kNm	ω_2 =	1.0	max moment at mid-span				
φ =	0.9		M_u =	923.8	kNm				
F_y =	345	MPa	M_p =	441.6	kNm				
			$0.67M_p$ =	295.9	kNm				
			M_r' =	395.9	kNm	OK			
			V_r =	745.9	kN	OK			

Interior Gerber Beams

	Cantilever length =	1.2	m						
	Beam length =	11.2	m						
	Moment arm 1 =	5.0	m						
	Moment arm 2 =	3.0	m						
	Moment arm 3 =	1.0	m						
	Joist reaction center =	90.3	kN	full load everywhere					
	Joist reaction cantilever =	90.3	kN						
	Cantilever reaction =	180.6	kN						
	Column reaction =	451.6	kN						
	V_f =	180.6	kN						
	M_{f+} =	541.9	kNm						
	M_{f-} =	-216.8	kNm						

Joist reaction center =			90.3	kN	full load center, 1/2 LL cantilever and link beam			
Joist reaction cantilever =			49.8	kN				
Cantilever reaction =			99.5	kN				
Column reaction =			370.5	kN				
V_f =			180.6	kN				
M_{f+} =			541.9	kNm				
M_{f-} =			-119.4	kNm				
Joist reaction center =			49.8	kN	1/2 LL center, full load cantilever and link beam			
Joist reaction cantilever =			90.3	kN				
Cantilever reaction =			180.6	kN				
Column reaction =			329.9	kN				
V_f =			99.5	kN				
M_{f+} =			298.5	kNm				
M_{f-} =			-216.8	kNm				
V_f =	180.6	kN						
M_{f+} =	541.9	kNm						
M_{f-} =	-216.8	kNm						
Select	W530x85			ϕ =	0.9		CSA S16 -09 was followed for design	
L_y =	2000	mm		F_y =	345	MPa		
L_u =	2110	mm	No Lat-tor buckling					
b/t =	5.03	≤	9.15	OK	Class 2			
h/w =	48.7	≤	91.5	OK	Class 2			
M_r =	652.1	kNm	OK					
Eave Beams at N-S side								
Load combination: 1.0D + 1.0E + 0.25S								
Axial force from bending of diaphragms								
Total shear force =			565.4	kN				
Building length =			60.0	m				
Building width =			30.0	m				
UDL =			9.4	kN/m				
C_{max} = T_{max} =			141.3	kN				

	Axial force from shear flow							
		$S_nR_y =$	21.7	kN/m				
	Length of Collector =		30	m	Cut-off with $R_dR_o = 2$			
	Axial force $C_{max} = T_{max} =$		651.8	kN	$C_{max} = T_{max} =$	402.8		
		$C_f =$	**402.8**	**kN**				
	Gravity loads =		1.69	kPa	Calculating compressive resistance of top flange			
	Beam tributary width =		1.0	m	I	3631134.4		
	UDL on beam =		1.69	kN/m	R	47.6		
	Beam length =		10	m	kL/R	0		
					$C_r =$	497.0	KN	
		$M_{fx} =$	21.1	kNm	C_r/C_f	1.07	OK	
		$V_f =$	8.4	kN				
Com. force on top flange due to moment			61.4	kN				
		$C_f =$	402.8	kN	$L_y =$	0	mm	
	Total force on top flange		464.3	kNm	$L_x =$	10000	mm	
		$\phi =$	0.9					
		$F_y =$	345	MPa				
		Select	W310x39		CSA S16-09 was followed for design			
		b/t =	8.51	≤	9.15	OK	Class 2 or better	
		h/w =	50.1	≤	76.9	OK	Class 2 or better	
		$T_r = C_{r0} =$	1704.3	kN				
		$M_{rx} =$	189.4	kNm				
		$kL_x/r_x =$	76.3	≤	200	OK		
		$kL_y/r_y =$	0.0	≤	200	OK		
		$C_{rx} =$	906.0	kN		$C_{ry} =$	1533.9	kN
		$C_r =$	906.0	kN				
		$C_{ex} =$	1679.8	kN				
		$\omega_{1x} =$	1.0	uniformly distributed load				
		$U_{1x} =$	1.315					
	Cross Section Strength Check							
	$\dfrac{C_f}{C_{r0}}$	+	$\dfrac{0.85U_{1x}M_f}{M_{rx}}$	=	0.36	≤	1	OK

Overall In-Plane Member Strength Check

$$\frac{C_f}{C_{rx}} + \frac{0.85 U_{1x} M_f}{M_{rx}} = 0.54 \leq 1 \quad \text{OK}$$

Moment Check

$$\frac{M_{fx}}{M_{rx}} = 0.11 \leq 1.00 \quad \text{OK}$$

Tension and Bending

$$\frac{T_f}{T_r} + \frac{M_{fx}}{M_{rx}} = 0.35 \leq 1 \quad \text{OK}$$

Eave Beams at E-W side

Load combination: 1.0D + 1.0E + 0.25S

Axial force from bending of diaphragms

				Probable shear force on diaphragm=	21.7	kN/m
Total shear force =	565.4	kN		Length of Collector =	10	m
Building length =	60.0	m		$C_{max} = T_{max}$ =	217.3	kN
Building width =	30.0	m				
UDL =	18.8	kN/m		Cut-off with $R_d R_o$ = 2		
Axial force $C_{max} = T_{max}$ =	35.3	kN		$C_{max} = T_{max}$ =	268.6	

Gravity loads =	1.69	kPa		
Joist tributary width =	2.0	m		
Joist UDL =	3.37	kN/m		
Joist length =	10.0	m		
Joist reaction =	16.9	kN		
Column reaction =	50.6	kN		
Moment arm 1 =	5.0	m		
Moment arm 2 =	3.0	m		
Moment arm 3 =	1.0	m		
M_{fx}=	101.2	kNm	L_y = 2000	mm
V_f =	33.7	kN	L_x = 10000	mm

Com. force on top flange due to moment		2.52E+02	kN	Calculating compressive resistance of top flange			
	$C_f =$	217.3	kN	I	4833537.3	mm^4	
Total force on top flange =		4.69E+02	kN	R	49.4		
	$\phi =$	0.9		kL/R	40.5		
	$F_y =$	345	MPa	$C_r =$	541.7	KN	
				C_r/C_f	1.15	OK	
	Select	W360x51	CSA S16 -09 was followed for design				
	b/t =	7.37	≤	9.15	OK	Class 2 or better	
	h/w =	46.1	≤	85.5	OK	Class 2 or better	
	$T_r = C_{r0} =$	2225.3	kN				
	$M_{rx} =$	277.6	kNm				
	$kL_x/r_x =$	67.6	≤	200	OK		
	$kL_y/r_y =$	51.5	≤	200	OK		
	$C_{rx} =$	1325.2	kN	$C_{ry} =$	1594.0	kN	
	$C_r =$	1325.2					
	$C_{ex} =$	2783.2	kN				
	$\omega_{1x} =$	1.0	uniformly distributed load				
	$U_{1x} =$	1.085					

Cross Section Strength Check

$$\frac{C_f}{C_{r0}} + \frac{0.85 U_{1x} M_f}{M_{rx}} = 0.43 \leq 1 \quad \text{OK}$$

Overall In-Plane Member Strength Check

$$\frac{C_f}{C_{rx}} + \frac{0.85 U_{1x} M_f}{M_{rx}} = 0.47 \leq 1 \quad \text{OK}$$

Moment Check

$$\frac{M_{fx}}{M_{rx}} = 0.36 \leq 1.00 \quad \text{OK}$$

Tension and Bending

$$\frac{T_f}{T_r} + \frac{M_{fx}}{M_{rx}} = 0.46 \leq 1 \quad \text{OK}$$

Eave Beams at E-W side								
Load combination:	1.25D + 1.5S							
Gravity loads =	4.52	kPa						
Joist tributary width =	2.00	m						
Joist UDL =	9.03	kN/m						
Joist length =	10.00	m						
Joist reaction =	45.16	kN						
Column reaction =	135.47	kN						
Moment arm 1 =	5.00	m						
Moment arm 2 =	3.00	m						
Moment arm 3 =	1.00	m						
M_{fx} =	270.9	kNm						
V_f =	90.3	kN			L_y =	2000	mm	
C_f =	0.0	kN			L_x =	10000	mm	
ϕ =	0.9							
F_y =	345	MPa						
Select	W360x51		CSA S16 -09 was followed for design					
b/t =	7.37	≤	9.15	OK	Class 2 or better			
h/w =	46.1	≤	91.5	OK	Class 2 or better			
$T_r = C_{r0}$ =	2225.3	kN						
M_{rx} =	277.6	kNm						
kL_x/r_x =	67.6	≤	200	OK				
kL_y/r_y =	51.5	≤	200	OK				
C_{rx} =	1325.2	kN		C_{ry} =	1594.0	kN		
C_r =	1325.2							
C_{ex} =	2783.2	kN						
ω_{1x} =	1.0	uniformly distributed load						
U_{1x} =	*1.000*							
Cross Section Strength Check								

$$\frac{C_f}{C_{r0}} + \frac{0.85 U_{1x} M_f}{M_{rx}} = 0.83 \leq 1 \quad \text{OK}$$

Overall In-Plane Member Strength Check

$$\frac{C_f}{C_{rx}} + \frac{0.85U_{1x}M_f}{M_{rx}} = 0.83 \leq 1 \quad \text{OK}$$

Moment Check

$$\frac{M_{fx}}{M_{rx}} = 0.98 \leq 1.00 \quad \text{OK}$$

Tension and Bending

$$\frac{T_f}{T_r} + \frac{M_{fx}}{M_{rx}} = 0.98 \leq 1 \quad \text{OK}$$

Determination of shear strength and shear stiffness of roof diaphragm using SDI method			
Steel			
Steel thickness	tt	0.76	mm
Steel yield strength (for the calculation of Qf of screws according to the SDI method)	Fy	230	MPa
Steel ultimate tensile sterngth (for the calculation of Q_f of welds according to the SDI method)	Fu	310	MPa
Young's modulus	E	203000	MPa
Deck			
Depth of deck	hh	38	mm
Length of web (measured over the inclined distance)	ww	40.16	mm
Pitch (o/c spacing of flutes)	dd	152	mm
Half-length of the lower flange	ee	19.05	mm
Length of the upper flange	ff	88.9	mm
Horizontal projection of the web	gg	12.7	mm
Developed length of steel per flute	ss	207.32	mm
Overall deck width	w_f	914	mm
Overall deck length	LL	10000	mm
Number of intermediate joists	np	4	
Joist spacing (o/c)	Lv	2000	mm
Gross Moment of inertia of the deck	lx	214000	mm^4/m
Connections			
Resistance of the frame connectors	Q_f	6.71	kN
Flexibility of the frame connectors	S_f	0.0413	mm/kN
Resistance of the sidelap connectors	Q_s	3.23	kN
Flexibility of the sidelap connectors	S_s	0.099	mm/kN
Valley spacing (each = 1, alternate = 2, third = 3, fourth = 4) (is every flute connected or not?)	n_pas	2	
$S(x_e/w)$ on the end joists (over w, including the edge connectors)	α_1	1.333	
$S(x_p/w)$ on the intermediate joists (over w, including the edge connectors)	α_2	1.333	
$S(x_e/w)^2$ on the end joists (over w, including the edge connectors)	$\Sigma(x_e/w)^2$	0.556	
$S(x_p/w)^2$ on the intermediate joists (over w, including the edge connectors)	$\Sigma(x_p/w)^2$	0.556	
Number of end connectors (total over width w including those on the edge	n_v	4	
Side-lap spacing		140	mm
Number of frame connectors on the side of the deck (total over length LL excluding those on the joists)	n_e	66	
Number of sidelap connectors (total over length LL excluding those on the joists)	n_s	66	
Resistance			
Corner factor	λ	0.764	
Factor B	B	38.442	
Resistance based on the panel end	Sn	49.65	kN/m
Resistance based on the interior panel	Sn	25.48	kN/m
Resistance based on the corner connection	Sn	19.38	kN/m
Resistance based on the overall shear buckling of the deck (Lower bound 2 span case where coeff = 3.25)	S_{cr}	18.27	kN/m
Nominal shear resistance	**min S$_n$**	**19.4**	kN/m
Flexibility and Rigidity			
Flexibility due to the deformation of a flat steel sheet in shear	Fs	0.0230	mm/kN
Flexibility due to warping of the deck (parameter Dn)	Fn	0.1167	mm/kN
Flexibility due to deformation at the connections (parameter C)	Fslip	0.0143	mm/kN
Flexibilty	**F**	**0.15**	**mm/kN**
Rigidity	**G'**	**6.5**	**kN/mm**

Appendix D:

Detail design of large sized (40m×90m×8m) single-storey steel buildings

Table D1 – Design Summary of Gravity members

Members	Location
	Abbotsford (BC)
Joist top chord section (in.)	⊤ 1 ¾ × 1 ¾ × 5/32
Interior columns	HSS 203 × 203 × 6.4
Exterior columns	W200 × 36
Corner columns	W200 × 36
Gerber cantilever beams	W530 × 85
Gerber link beams	W460 × 60

Table D2 – Design matrix of CBF buildings (System A) (Abbotsford, BC)

Building size	40m×90m×8m	
Diaphragm shear stiffness	SDI G'	70% of SDI G'
Time period limitation	$T_a = 0.4$ s	NL
Design Case	AVL0	AVL2

Table D3 – Seismic properties of CBF buildings (System A) (Abbotsford, BC)

Details	Design case	
	AVL0	**AVL2**
Actual fundamental period with diaphragm flexibility and design period (shown in bracket)		
N-S Direction (s)	0.67 (0.4)	0.75 (0.75)
E-W Direction (s)	0.5 (0.4)	0.55 (0.55)
Actual fundamental period with rigid diaphragm assumption		
N-S Direction (s)	0.41	0.45
E-W Direction (s)	0.41	0.45
Design spectral value S(Ta) (g)	0.77	0.49
Seismic Weight W (kN)	6669	6560
Base shear V[1] (kN)	1317	824
Upper limit on Base Shear[2] (kN)	1129	1110

[1]Corresponds to total base shear, [2]Corresponds to 2/3 S(0.2 s).

Table D4 – Design details of CBF buildings (System A) (Abbotsford, BC)

Details	Design case	
	AVL0	AVL2
Vertical brace (at N-S sides)		
Factored compression force, C_f (kN)	444	368
Brace section (HSS)	$152 \times 152 \times 8.0$	$127 \times 127 \times 9.5$
Factored compression resistance, C_r (kN)	551	390
Probable tension resistance T_u (kN)	1854	1780
Probable compression resistance, C_u (kN)	808	573
Post buckling strength, C'_u (kN)	371	356
Storey shear corresponding to $C_u + T_u$ (kN)	2662	2353
Storey shear corresponding to $C'_u + T_u$ (kN)	2225	2136
Storey shear corresponding to $R_d R_o$=1.3 (kN)	2370	1676
Storey shear corresponding to $R_d R_o$=2.0 (kN)	1540	1089
Column member	W200 × 52	W310 × 39
Beam member	W310 × 52	W310 × 28
Vertical brace (at E-W sides)		
Factored compression force, C_f (kN)	444	368
Brace section	$152 \times 152 \times 8.0$	$127 \times 127 \times 9.5$
Factored compressive resistance, C_r (kN)	551	390
Probable tension resistance, T_u (kN)	1854	1780
Probable compression resistance, C_u (kN)	808	573
Post buckling strength, C'_u (kN)	371	356
Storey shear corresponding to $C_u + T_u$ (kN)	2662	2353
Storey shear corresponding to $C'_u + T_u$ (kN)	2225	2136
Storey shear corresponding to $R_d R_o$=1.3 (kN)	2370	1483
Storey shear corresponding to $R_d R_o$=2.0 (kN)	1540	964
Column member	W250 × 58	W250 × 58
Beam member	W410 × 60	W410 × 60
Perimeter Beams		
N-S sides	W310 × 52	W310 × 39
E-W sides	W310 × 86	W310 × 74
Design of Diaphragm		
Shear force S_f (kN/m)	98.7	75.5
Limiting shear force S_{limit} (kN/m)	38.5	24.1
Factored shear resistance ϕS_n (kN/m)	41.2	25.4
Thickness of deck (mm)	1.52	1.21
Shear stiffness G' (kN/mm)	48.7	35.6
Frame fasteners pattern	36/9	36/7

Table D4 – Design details of CBF buildings (System A) (Abbotsford, BC) Cont..

Details	Design case	
	AVL0	AVL2
Side lap spacing (mm)	100	125
Deflection using SAP models under seismic load at mid span (N-S)		
$\Delta R_d R_o$(mm)†	72.2	84.6
$\Delta_b R_d R_o + \Delta_d$(mm)*	45.4	39.8
Deflection using SAP models under seismic load at mid span (E-W)		
$\Delta R_d R_o$(mm)	47.6	64.7
$\Delta_b R_d R_o + \Delta_d$(mm)	41.5	57.5

* Δ_b - Elastic deformation at brace end, Δ_d - Elastic deformation of diaphragm, † Δ - Total elastic deformation at mid-span

Table D5 – Design matrix of buildings with inelastic diaphragm (System B)

Location	Abbotsford (BC)	
Building size	40m×90m×8m	
Diaphragm shear stiffness	70% of SDI G'	
Time period limitation	T_a=0.4 s	NL
Design Case	BVL0	BVL1

Table D6 – Seismic characteristics of buildings with ductile diaphragm (System B)

Details	Design case	
	BVL0	BVL1
Actual fundamental period with diaphragm flexibility and design period (shown in bracket)		
N-S Direction (s)	0.8 (0.4)	1.34 (1.34)
E-W Direction (s)	0.5 (0.4)	0.68 (0.68)
Actual fundamental period with rigid diaphragm assumption		
N-S Direction (s)	0.34	0.51
E-W Direction (s)	0.34	0.37
Design spectral value S(Ta) (g)	0.77	0.27
Seismic Weight W (kN)	6376	6376
Base shear V[1] (kN)	1289	450
Upper limit on Base Shear[2] (kN)	1105	1105

[1]Corresponds to total base shear, [2]Corresponds to 2/3 S(0.2 s).

Table D7 – Design details of buildings with ductile diaphragm (System B) (Abbotsford, BC)

Details	Design case	
	BVL0	BVL1
Design of Diaphragm		
Shear force S (kN/m)	17.0	8.0
Thickness of deck (mm)	0.76	0.76
Frame fasteners patern	36/7	36/4
Side lap spacing (mm)	100	250
Factored shear resistance ϕS_n (kN/m)	18.0	8.34
SDI Shear stiffness G' (kN/mm)	21.0	6.1
Probable Shear Resistance $R_y S_n$ (kN/m)	33.6	15.6
Vertical brace (at N-S sides)		
Storey Shear corresponding to $R_y S_n$ (kN)	3024	1404
Storey Shear corresponding to $R_d R_o = 2$ (kN)	1473	1028
Beam member	W310 × 60	W310 × 33
Brace section (HSS)	203 × 203 × 8.0	178 × 178 × 8.0
Column member	W310 × 45	W310 × 39
Vertical brace (at E-W sides)		
Storey Shear corresponding to $R_y S_n$ (kN)	1344	624
Storey Shear corresponding to $R_d R_o = 2$ (kN)	1473	515
Beam member	W410 × 85	W310 × 60
Brace section	178 × 178 × 9.5	152 × 152 × 4.8
Column member	W310 × 45	W200 × 31
Perimeter beams		
N-S sides	W310 × 60	W310 × 33
E-W sides	W410 × 85	W310 × 60
Deflection using SAP models under seismic load at mid span (N-S)		
$\Delta R_d R_o$ (mm)†	88.7	146.2
$\Delta_d R_d R_o + \Delta_b$ (mm)*	75.9	130.8
Deflection sign SAP models under seismic load at mid span (E-W)		
$\Delta R_d R_o$ (mm)	58.6	73.8
$\Delta_d R_d R_o + \Delta_b$ (mm)	30.5	47.1

* Δ_b - Elastic deformation at brace end, Δ_d - Elastic deformation of diaphragm, † Δ - Total elastic deformation at mid-span

Table D8 – Design matrix of EBF buildings (System C) (Abbotsford, BC)

Building size	40m×90m×8m	
Diaphragm shear stiffness	70% of SDI G'	
Time period limitation	$T_a = 0.4$ s	NL
Design Case	CVL0	CVL1

Table D9– Seismic properties of EBF buildings (System C) (Abbotsford, BC)

Details	Design case	
	CVL0	CVL1
Actual fundamental period with diaphragm flexibility and design period (shown in bracket)		
N-S Direction (s)	0.91 (0.4)	1.06 (1.06)
E-W Direction (s)	0.66 (0.4)	0.78 (0.78)
Actual fundamental period with rigid diaphragm assumption		
N-S Direction (s)	0.37	0.45
E-W Direction (s)	0.37	0.42
Design spectral value S(Ta) (g)	0.77	0.31
Seismic Weight W (kN)	6376	6376
Base shear V[1] (kN)	818	330
Upper limit on Base Shear[2] (kN)	701	701

[1]Corresponds to total base shear, [2]Corresponds to 2/3 S(0.2 s).

Table D10 – Design details of EBF buildings (System C) (Abbotsford, BC)

Details	Design case CVL0	Design case CVL1
Braced frame (at N-S sides)		
Shear force on link beam V_f (kN)	367	270
Shear resistance of link beam V'_p (kN)	434	328
Probable resistance of link beam $1.3R_yV'_p$ (kN)	630	476
Link beam	W250 × 67	W200 × 31
Length of Link Beam	660	660
Brace section (HSS)	203 × 203 × 13.0	203 × 203 × 9.5
Column member	W310 × 39	W310 × 33
Outer beam member	W250 × 67	W250 × 39
Braced frame (at E-W sides)		
Shear force on link beam V_f (kN)	367	189
Shear resistance of link beam V'_p (kN)	434	328
Probable resistance of link beam $1.3R_yV'_p$ (kN)	630	476
Link beam	W250 × 67	W250 × 39
Length of Link Beam	660	660
Brace section (HSS)	203 × 203 × 13.0	203 × 203 × 9.5
Column member	W310 × 39	W310 × 33
Outer beam member	W250 × 67	W250 × 39
Perimeter Beams		
N-S sides	W310 × 39	W310 × 39
E-W sides	W250 × 67	W360 × 57
Design of Diaphragm		
Shear force S (kN/m)	19.7	11.5
Limiting Shear force S_{limit} (kN/m)	36.8	14.9
Factored shear resistance ϕS_n (kN/m)	20.9	11.57
Thickness of deck (mm)	0.76	0.76
SDI Shear stiffness G' (kN/mm)	21.7	18.1
Frame fasteners patern	36/9	36/7
Side lap spacing (mm)	100	200
Deflection using SAP models under seismic load at mid span (N-S)		
ΔR_dR_o (mm)	99.0	108.0
$\Delta_bR_dR_o + \Delta_d$ (mm)	42.5	54.0
Deflection using SAP models under seismic load at mid span (E-W)		
ΔR_dR_o (mm)	75.6	88.2
$\Delta_bR_dR_o + \Delta_d$ (mm)	62.6	72.7

* Δ_b - Elastic deformation at brace end, Δ_d - Elastic deformation of diaphragm, † Δ - Total elastic deformation at mid-span

Table D11 – Design matrix of CC buildings (System D) (Abbotsford, BC)

Building size	40m×90m×8m	
Diaphragm shear stiffness	SDI G'	70% of SDI G'
Time period limitation	$T_a = 0.4$ s	NL
Design Case	DVL0	DVL2

Table D12 – Seismic properties of buildings with Conventional Construction (System D) (Abbotsford, BC)

Details	Design case	
	DVL0	DVL2
Actual fundamental period with diaphragm flexibility and design period (shown in bracket)		
N-S Direction (s)	0.65 (0.4)	0.72 (0.72)
E-W Direction (s)	0.45 (0.4)	0.48 (0.48)
Actual fundamental period with rigid diaphragm assumption		
N-S Direction (s)	0.35	0.38
E-W Direction (s)	0.35	0.35
Design spectral value S(Ta) (g)	0.77	0.51
Seismic Weight W (kN)	6560	6560
Base shear V[1] (kN)	2590	1717
Upper limit on Base Shear[2] (kN)	2220	2220

[1]Corresponds to total base shear, [2]Corresponds to 2/3 S(0.2 s).

Table D13 – Design details of buildings with Conventional Construction (System D) (Abbotsford, BC)

Details	Design case	
	DVL0	DVL2
Vertical brace (at N-S sides)		
Design force C_f (kN)	863	863
Brace section (HSS)	178 × 178 × 9.5	178 × 178 × 9.5
Brace resistance C_r (kN)	928	928
Column member	W410 × 54	W410 × 54
Beam Member	W310 × 52	W310 × 33
Vertical brace (at E-W sides)		
Design force C_f (kN)	863	670
Brace section	178 × 178 × 9.5	178 × 178 × 8.0
Brace resistance C_r (kN)	928	794
Column member	W410 × 54	W410 × 54
Beam member	W360 × 79	W310 × 79
Perimeter Beams		
N-S sides	W310 × 52	W310 × 33
E-W sides	W360 × 79	W310 × 79
Design of Diaphragm		
Shear force S (kN/m)	33.7	26.1
Factored shear resistance ϕS_n (kN/m)	33.9	29.2
Thickness of deck (mm)	1.21	1.21
Shear stiffness G' (kN/mm)	38.7	38.0
Frame fasteners patern	36/9	36/7
Side lap spacing (mm)	95	95
Deflection using SAP models under seismic load at mid span (N-S)		
$\Delta R_d R_o$(mm)	71.0	65.1
$\Delta_d R_d R_o + \Delta_b$(mm)	60.9	56.0
Deflection using SAP models under seismic load at mid span (E-W)		
$\Delta R_d R_o$(mm)	50.3	55.7
$\Delta_d R_d R_o + \Delta_b$(mm)	31.1	33.1

* Δ_b - Elastic deformation at brace end, Δ_d - Elastic deformation of diaphragm, † Δ - Total elastic deformation at mid-span

Appendix E:

Response of the designed buildings under the simulated design level earthquake signals
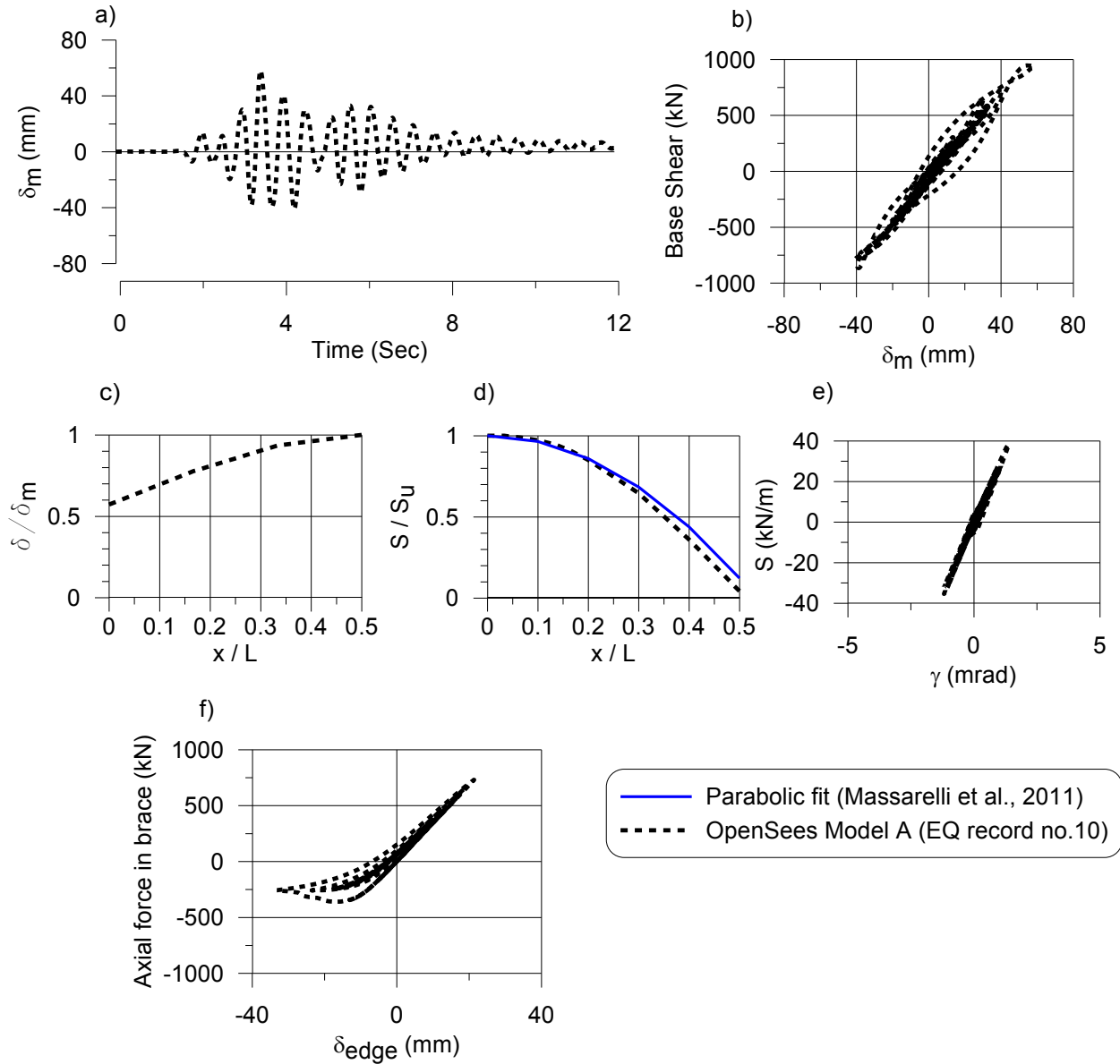
Figure E1 – Building response for AVM0 building (30m×60m×7m) under design level earthquake signal (record no. 10): a) Displacement time history at mid-span; b) base shear vs. mid-span displacement; c) normalized maximum displacement profile along length; d) normalized shear force distribution along length; e) hysteretic response of diaphragm at the building edge and f) hysteretic response of a diagonal brace member.
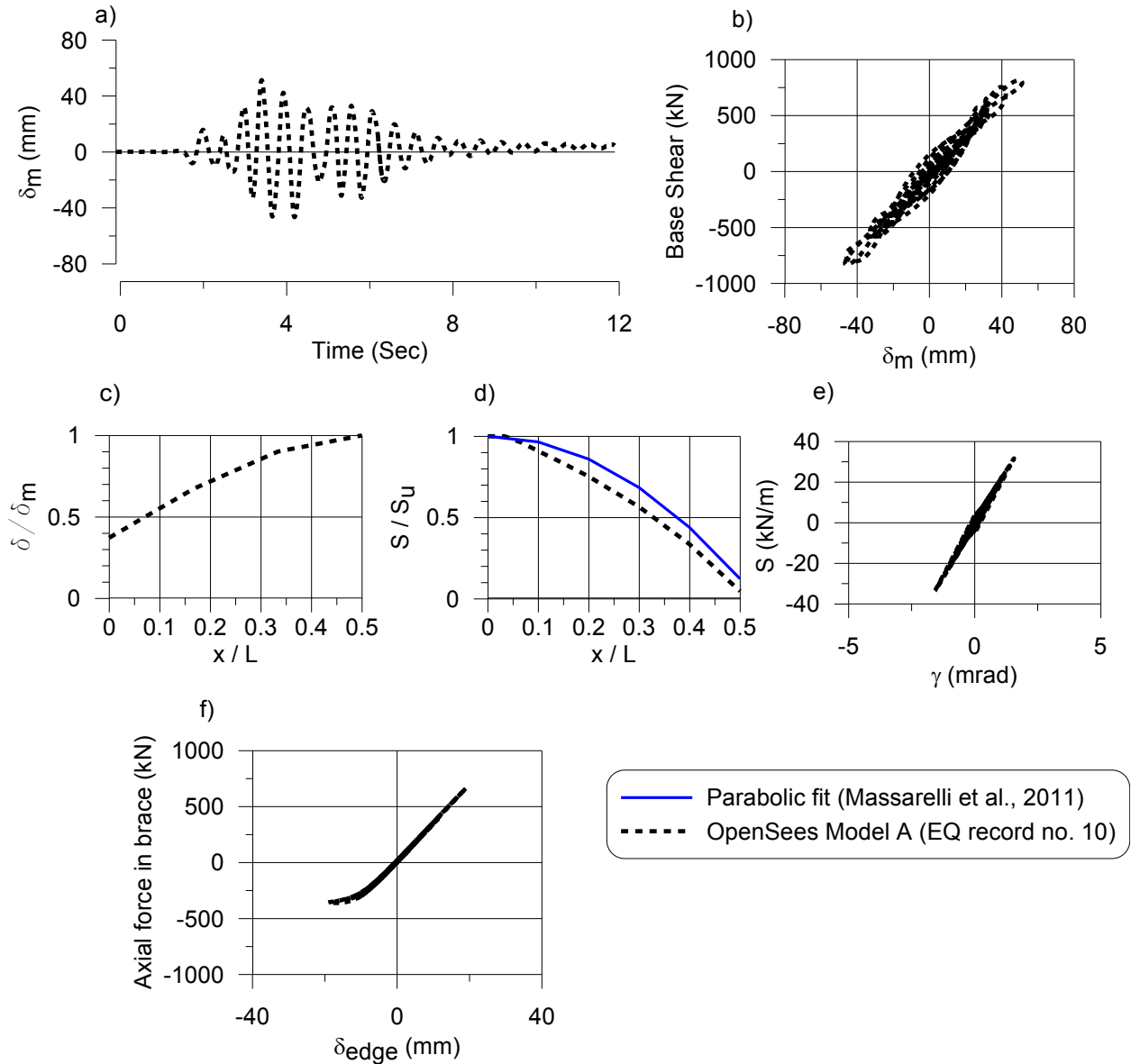
Figure E2 – Building response for AVM1 building (30m×60m×7m) under design level earthquake signal (record no. 10): a) Displacement time history at mid-span; b) base shear vs. mid-span displacement; c) normalized maximum displacement profile along length; d) normalized shear force distribution along length; e) hysteretic response of diaphragm at the building edge and f) hysteretic response of a diagonal brace member.
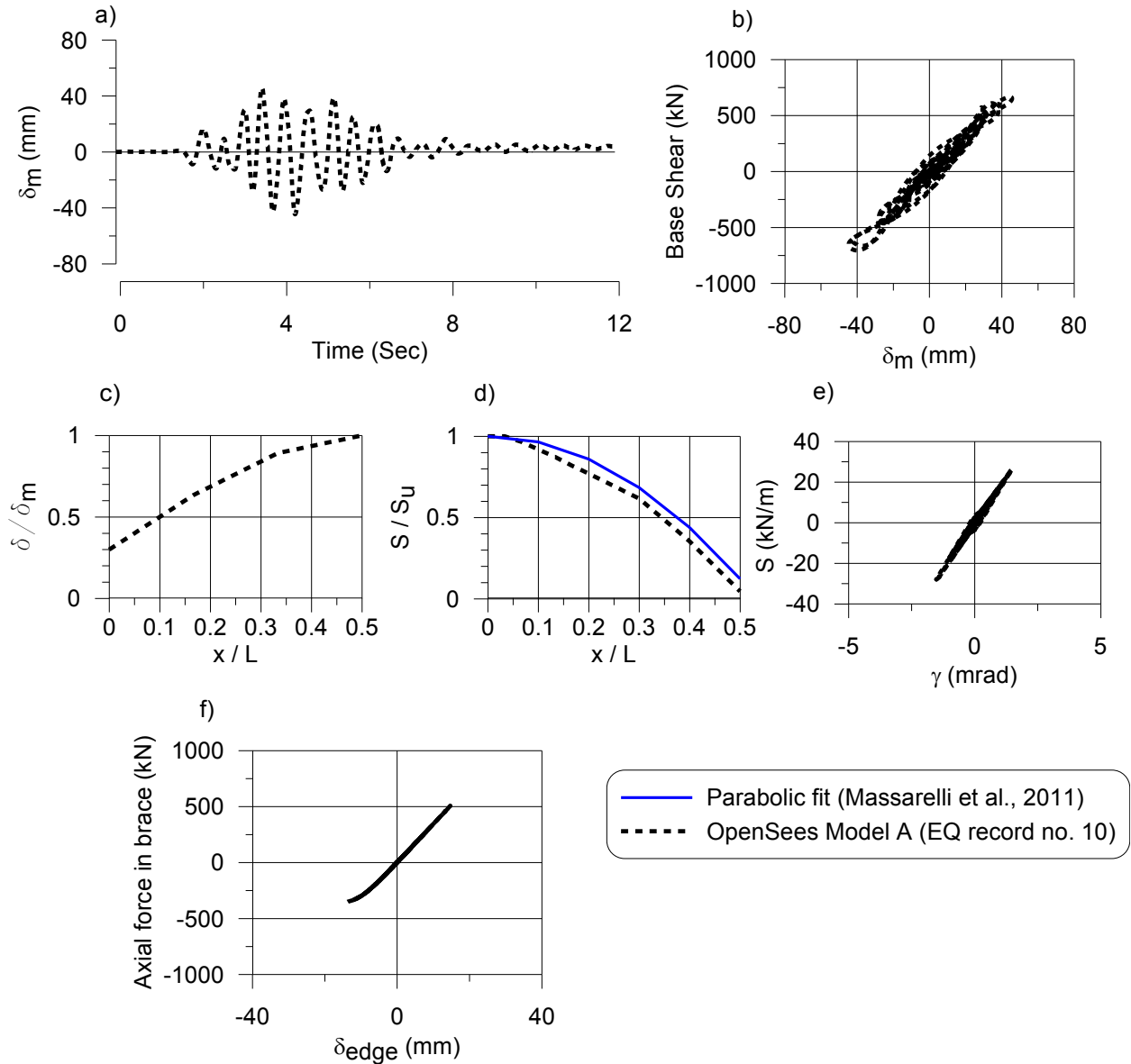
Figure E3 – Building response for AVM2 building (30m×60m×7m) under design level earthquake signal (record no. 10): a) Displacement time history at mid-span; b) base shear vs. mid-span displacement; c) normalized maximum displacement profile along length; d) normalized shear force distribution along length; e) hysteretic response of diaphragm at the building edge and f) hysteretic response of a diagonal brace member.
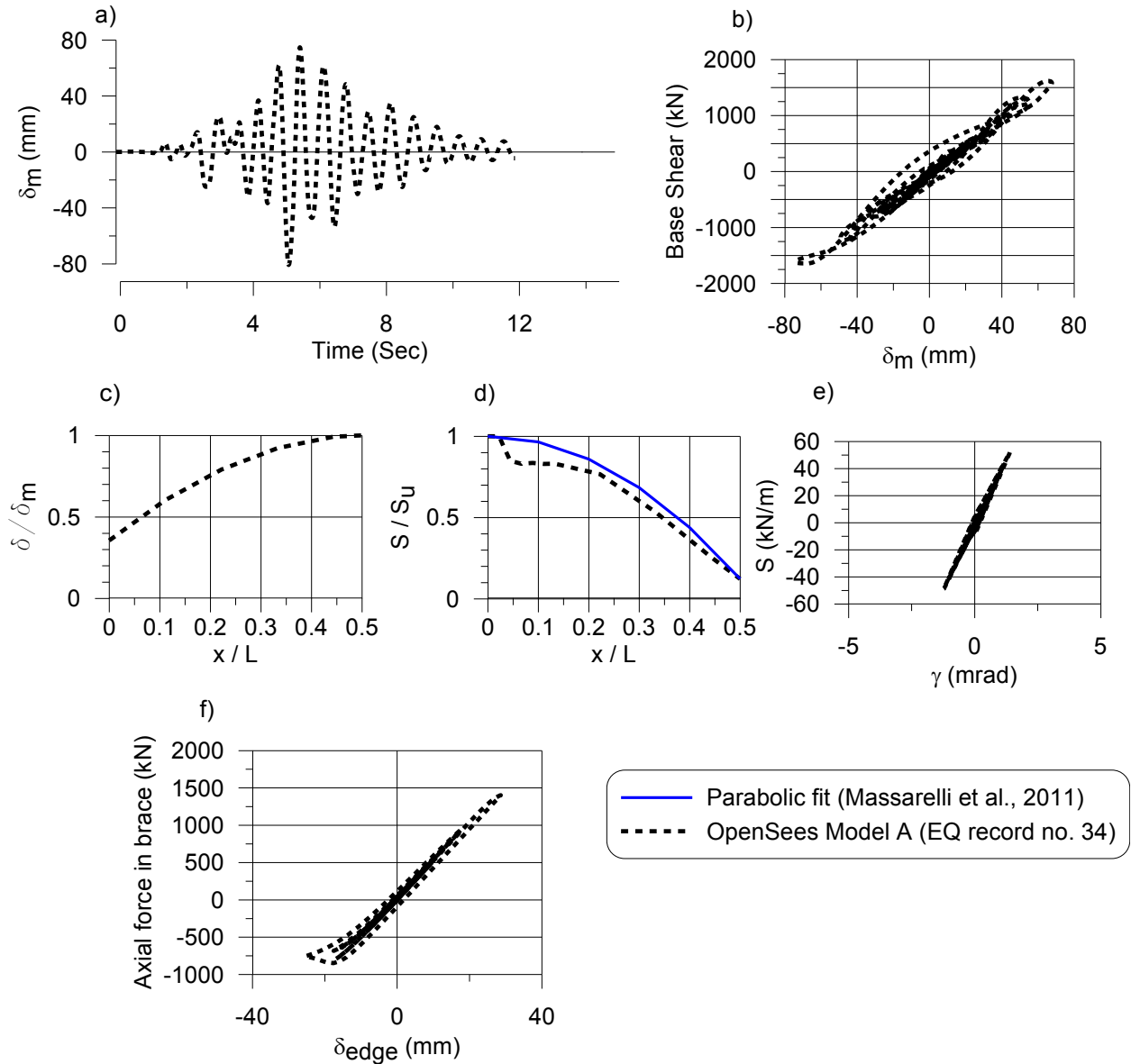
Figure E4 – Building response for AVL0 (40m×90m×8m) building under design level earthquake signal (record no. 34): a) Displacement time history at mid-span; b) base shear vs. mid-span displacement; c) normalized maximum displacement profile along length; d) normalized shear force distribution along length; e) hysteretic response of diaphragm at the building edge and f) hysteretic response of a diagonal brace member.

223
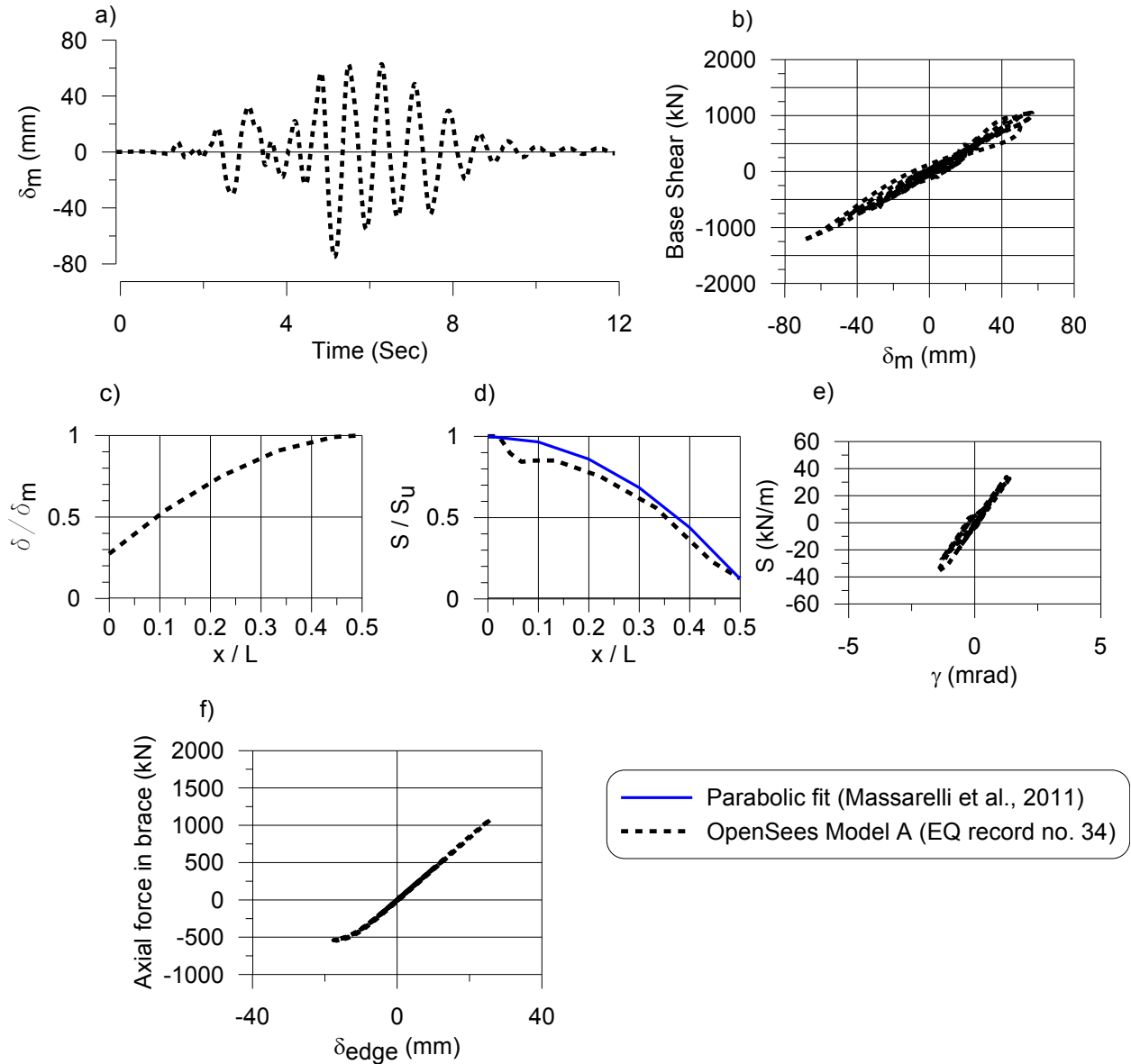
Figure E5 – Building response for AVL2 (40m×90m×8m) building under design level earthquake signal (record no. 34): a) Displacement time history at mid-span; b) base shear vs. mid-span displacement; c) normalized maximum displacement profile along length; d) normalized shear force distribution along length; e) hysteretic response of diaphragm at the building edge and f) hysteretic response of a diagonal brace member.
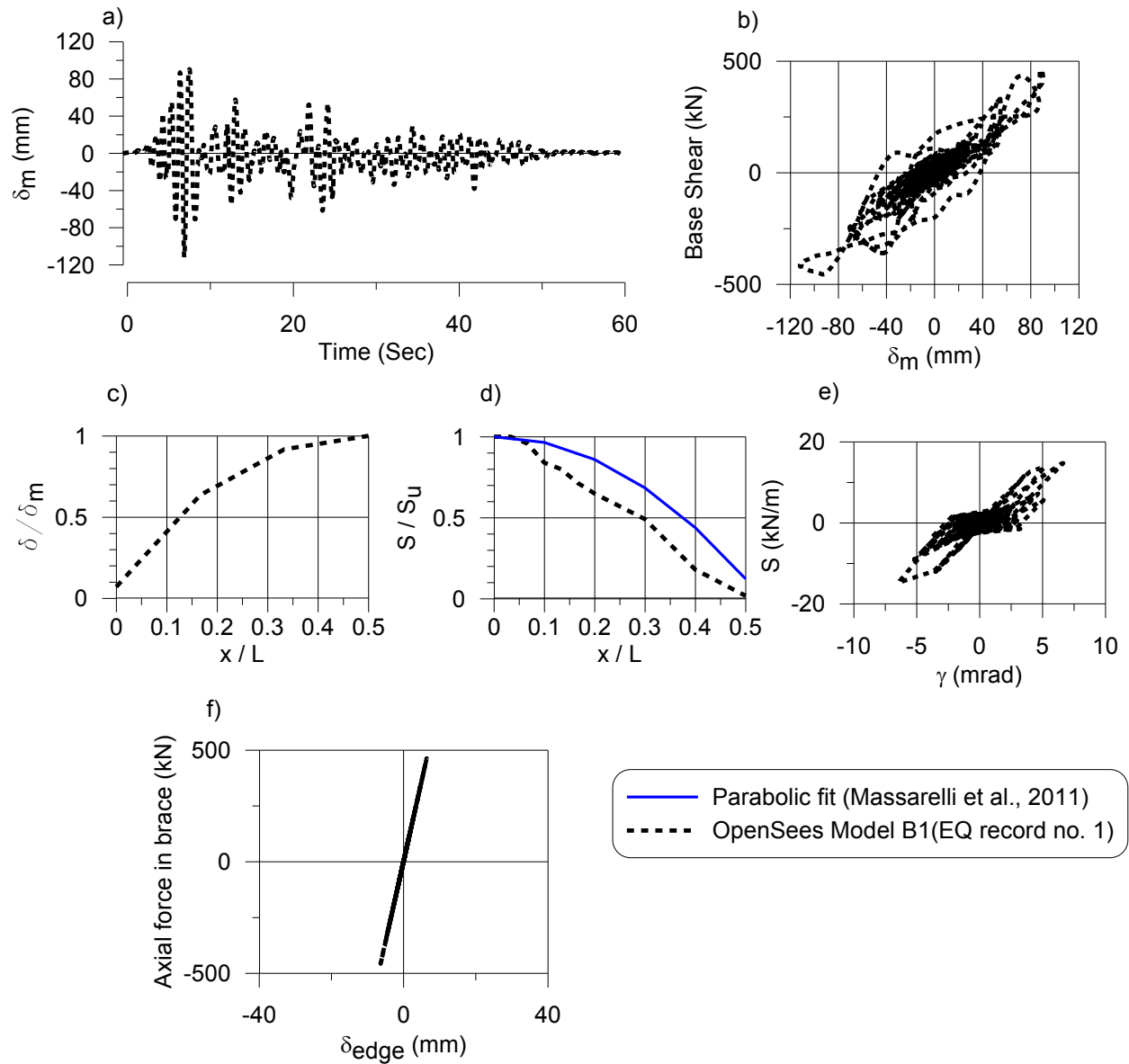
Figure E6 – Building response for Design 2 of BVM0 (30m×60m×7m) building under design level earthquake signal (record no. 1): a) Displacement time history at mid-span; b) base shear vs. mid-span displacement; c) normalized maximum displacement profile along length; d) normalized shear force distribution along length; e) hysteretic response of diaphragm at the building edge.
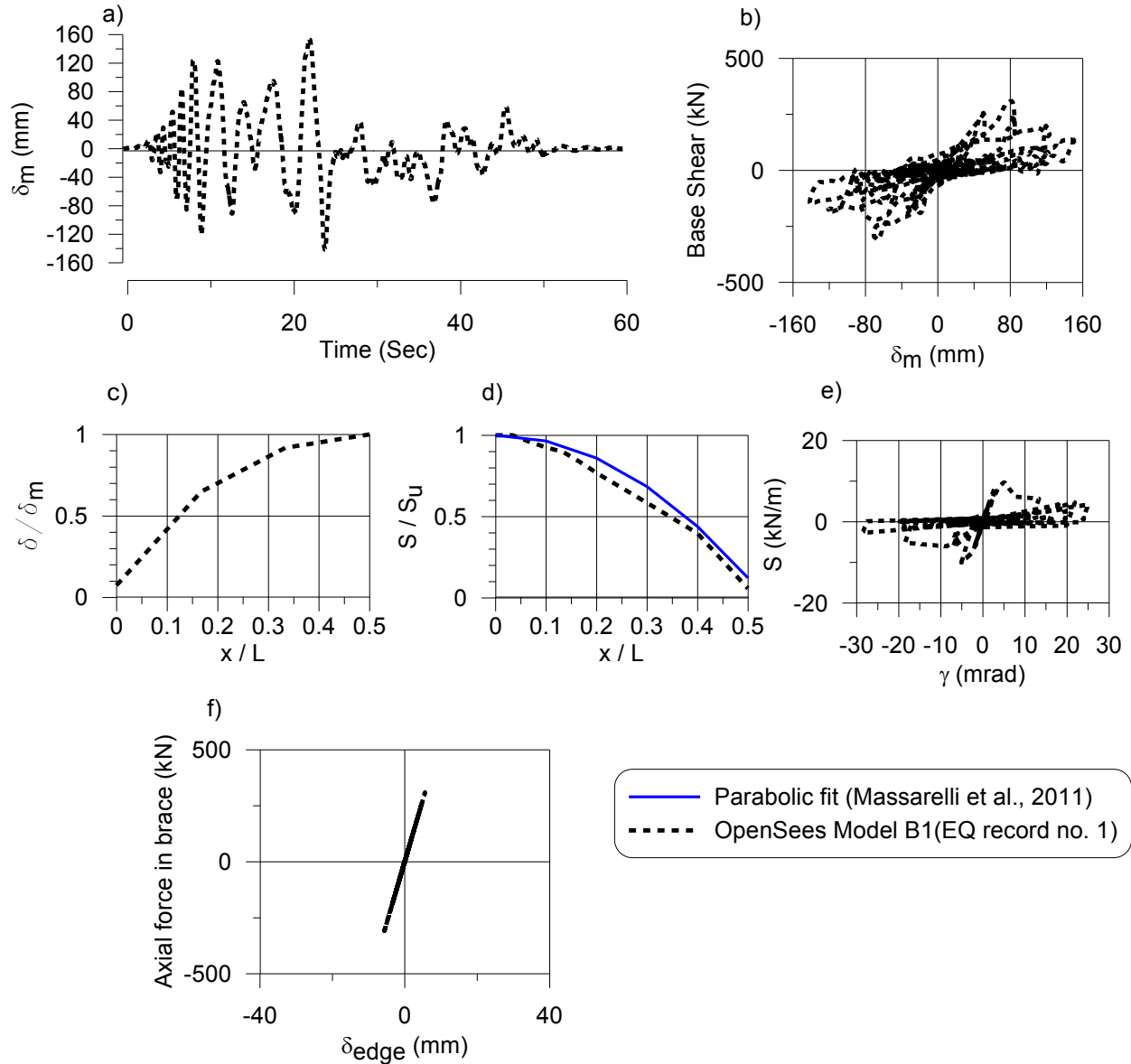
Figure E7 – Building response for Design 2 of BVM1 (30m×60m×7m) building under design level earthquake signal (record no. 1): a) Displacement time history at mid-span; b) base shear vs. mid-span displacement; c) normalized maximum displacement profile along length; d) normalized shear force distribution along length; e) hysteretic response of diaphragm at the building edge.
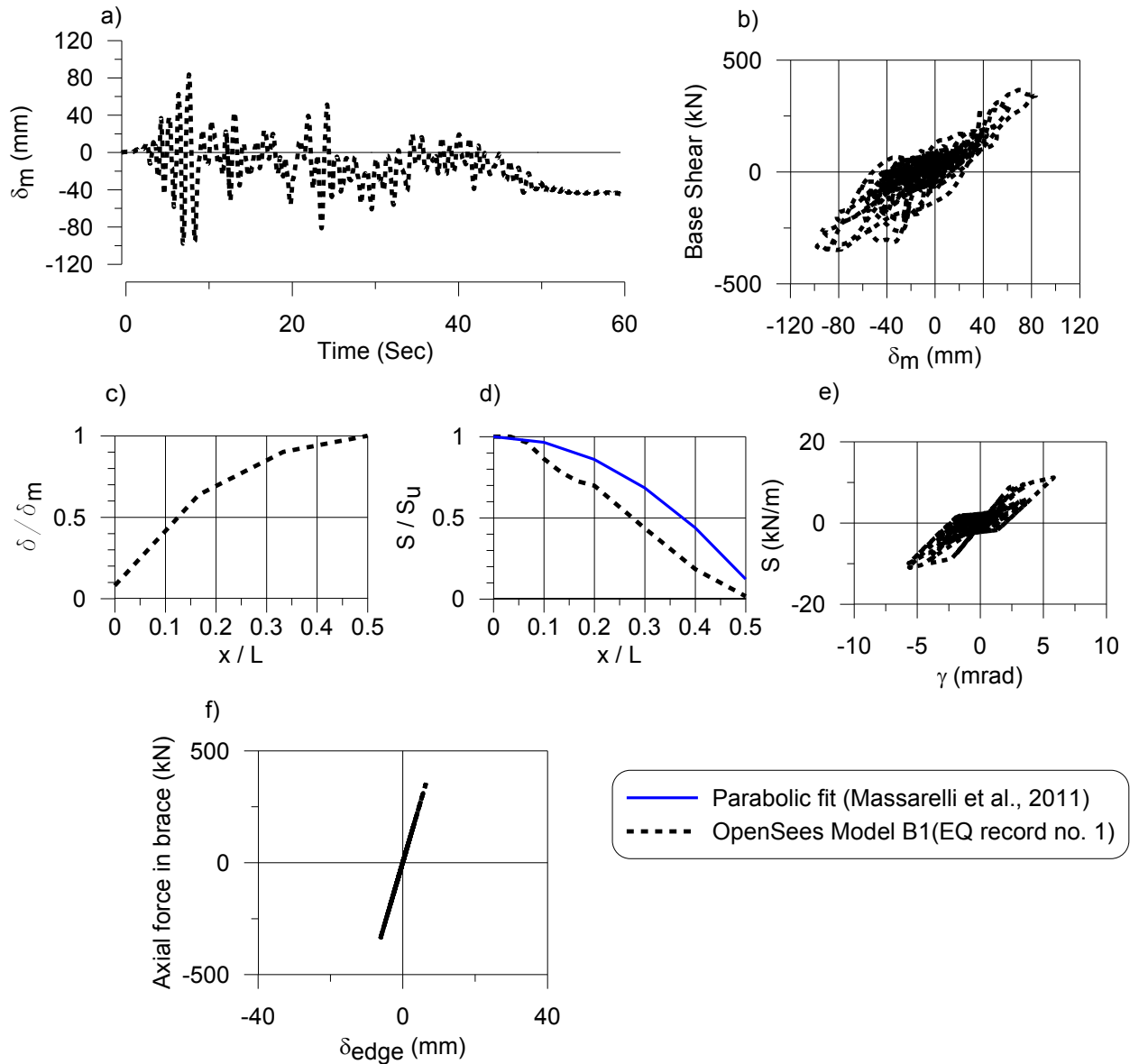
Figure E8 – Building response for Design 1 of BVM1 (30m×60m×7m) building under design level earthquake signal (record no. 1): a) Displacement time history at mid-span; b) base shear vs. mid-span displacement; c) normalized maximum displacement profile along length; d) normalized shear force distribution along length; e) hysteretic response of diaphragm at the building edge.
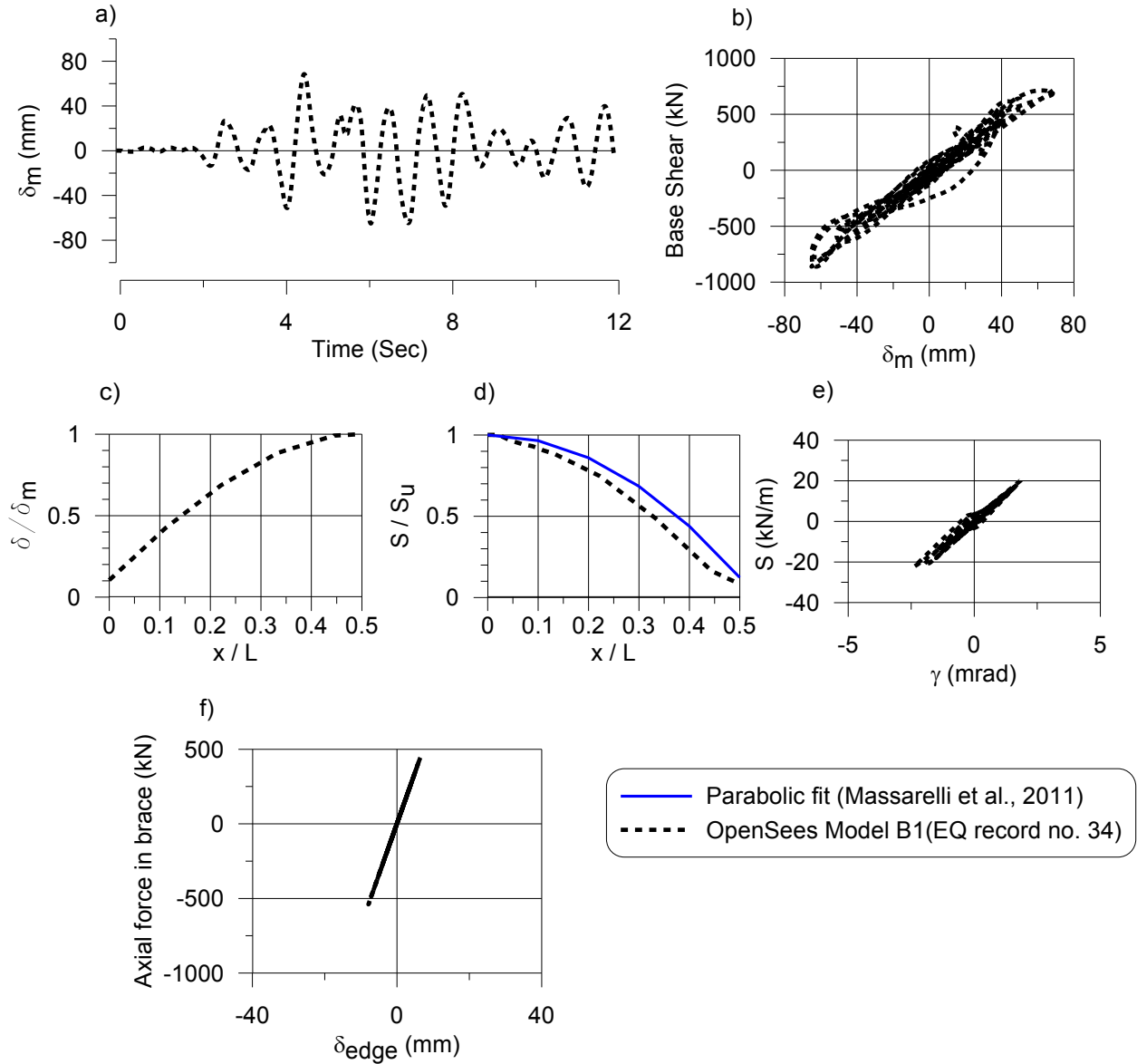
Figure E9 – Building response for BVL0 building (40m×90m×8m) under design level earthquake signal (record no. 34): a) Displacement time history at mid-span; b) base shear vs. mid-span displacement; c) normalized maximum displacement profile along length; d) normalized shear force distribution along length; e) hysteretic response of diaphragm at the building edge; f) response of diagonal brace
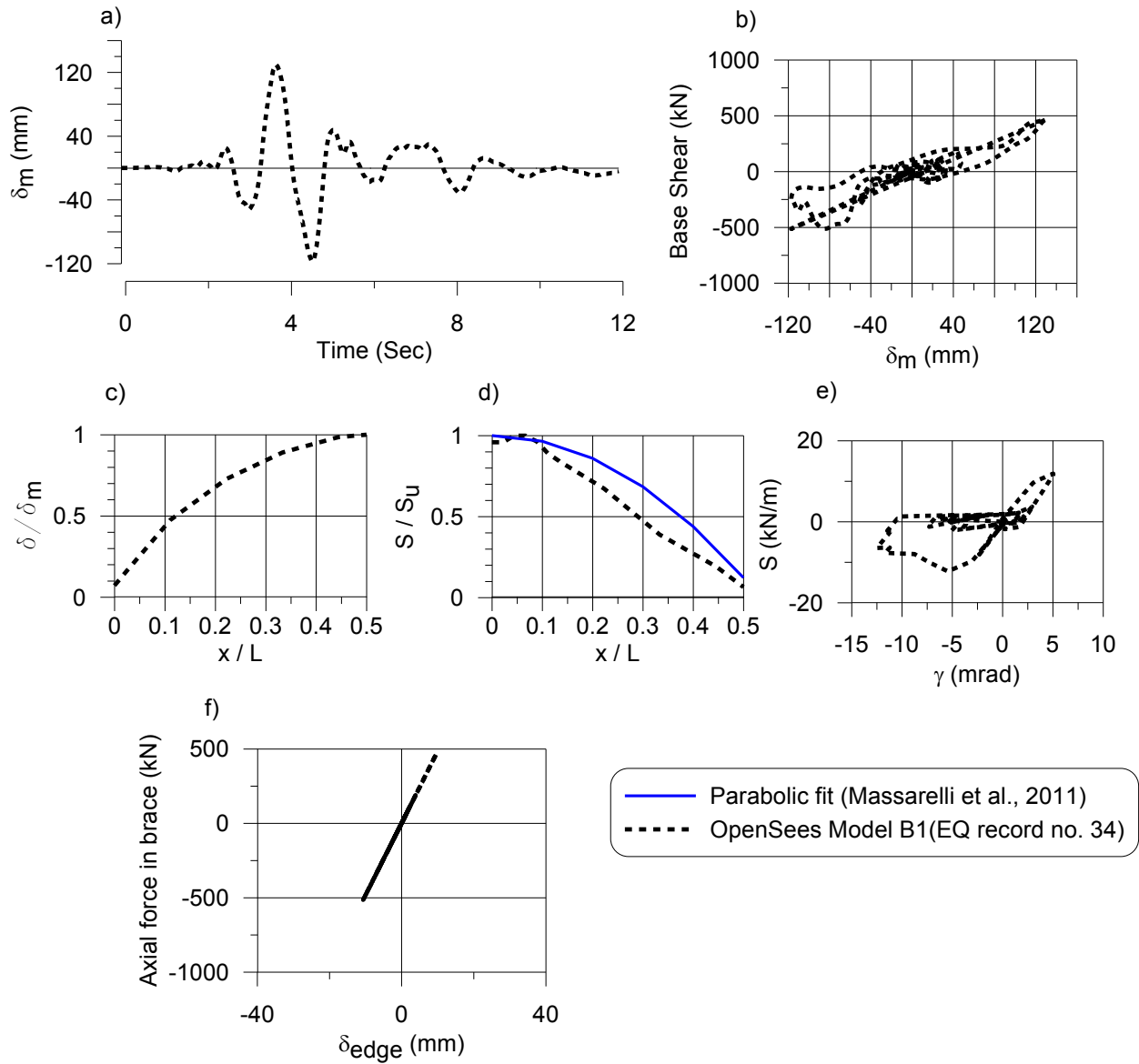
Figure E10 – Building response for BVL1 building (40m×90m×8m) under design level
earthquake signal (record no. 34): a) Displacement time history at mid-span; b) base shear vs.
mid-span displacement; c) normalized maximum displacement profile along length; d)
normalized shear force distribution along length; e) hysteretic response of diaphragm at the
building edge; f) response of diagonal brace
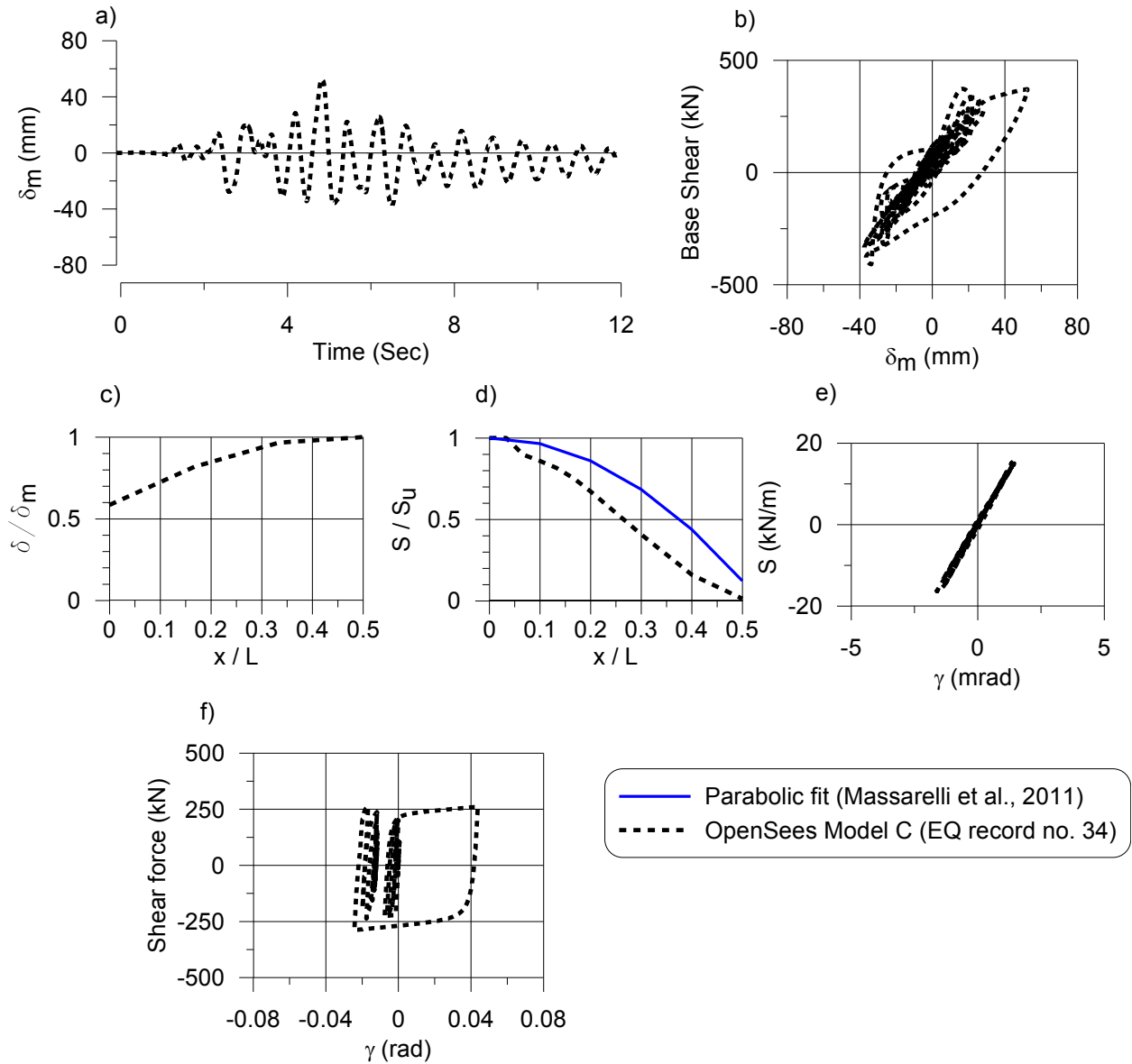
Figure E11 – Building response for CVM0 building (30m×60m×7m) under design level earthquake signal (record no. 34): a) Displacement time history at mid-span; b) base shear vs. mid-span displacement; c) normalized maximum displacement profile along length; d) normalized shear force distribution along length; e) hysteretic response of diaphragm at the building edge and f) hysteretic response of a link beam.
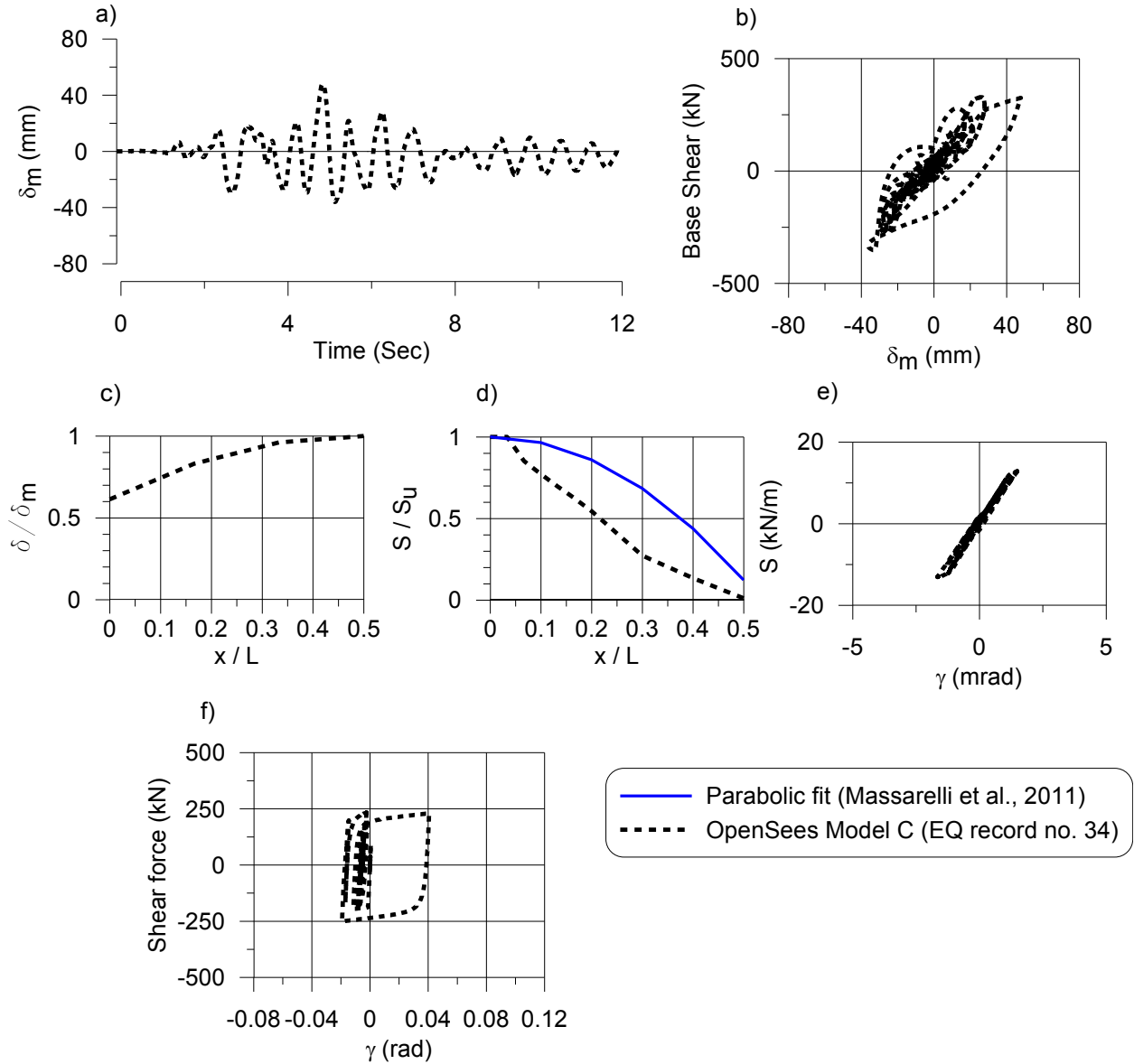
Figure E12 – Building response for CVM1 building (30m×60m×7m) under design level earthquake signal (record no. 34): a) Displacement time history at mid-span; b) base shear vs. mid-span displacement; c) normalized maximum displacement profile along length; d) normalized shear force distribution along length; e) hysteretic response of diaphragm at the building edge and f) hysteretic response of a link beam.
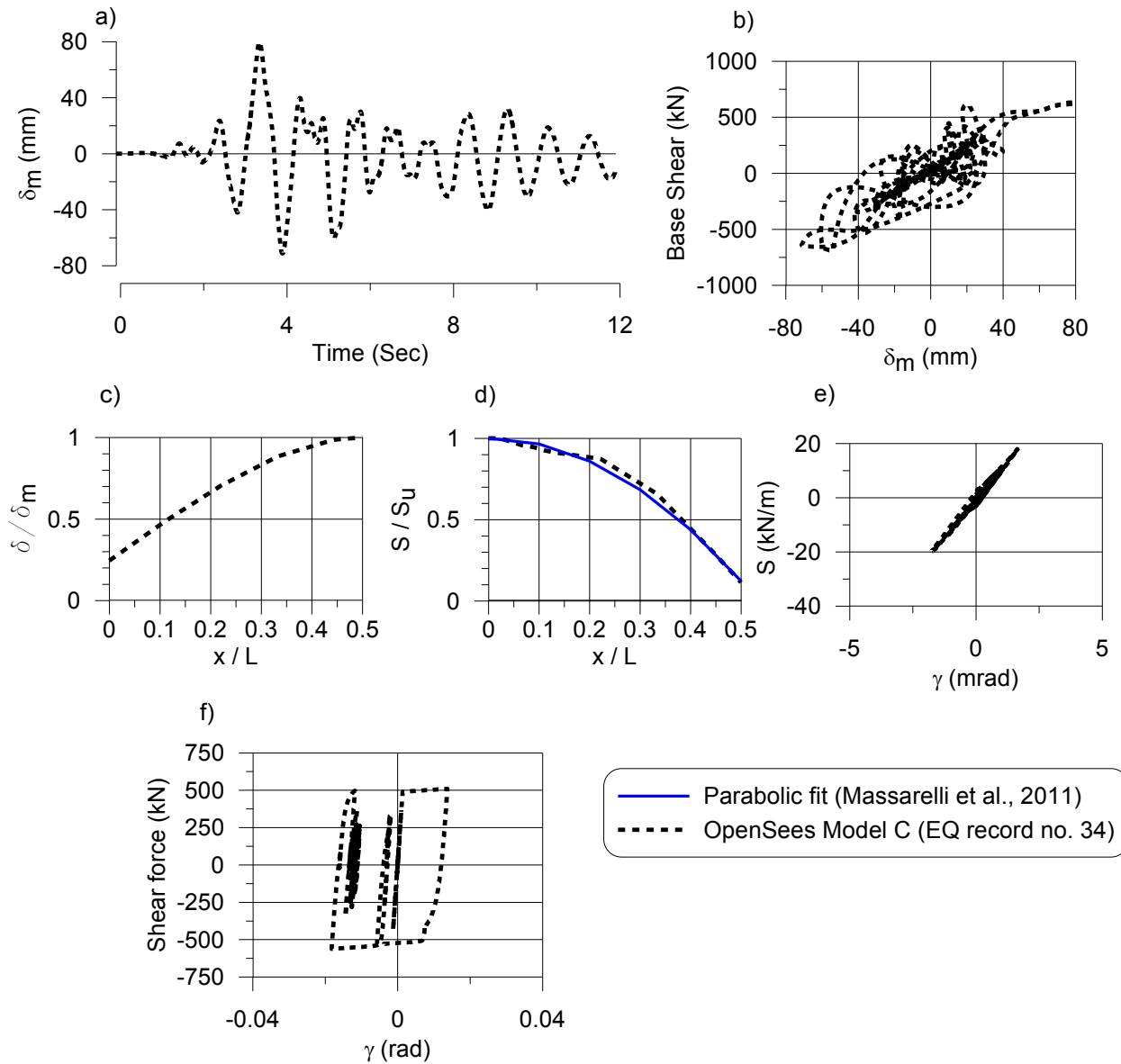
Figure E13 – Building response for CVL0 building (40m×90m×8m) under design level earthquake signal (record no. 34): a) Displacement time history at mid-span; b) base shear vs. mid-span displacement; c) normalized maximum displacement profile along length; d) normalized shear force distribution along length; e) hysteretic response of diaphragm at the building edge and f) hysteretic response of a link beam.
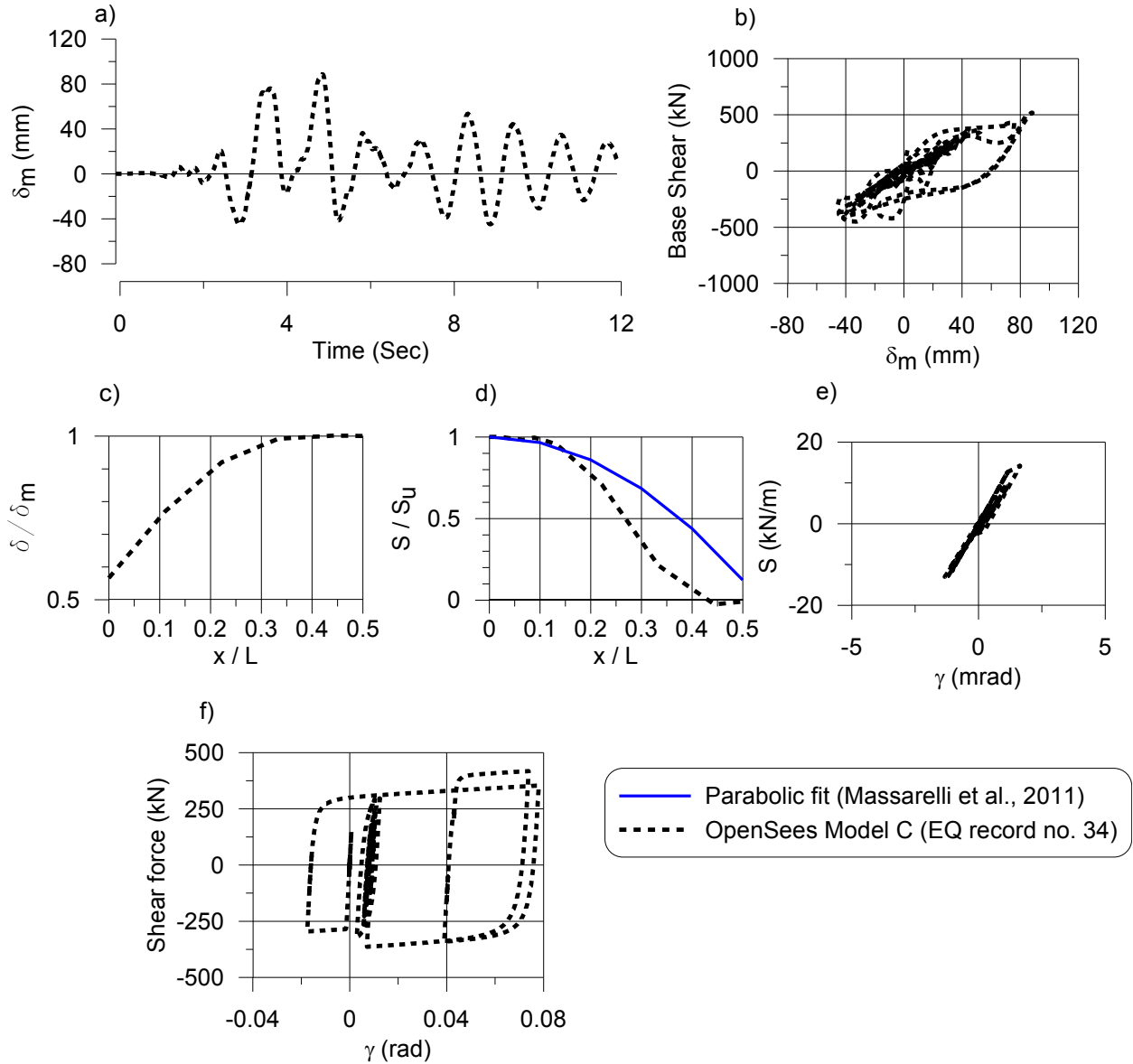
Figure E14 – Building response for CVL1 building (40m×90m×8m) under design level earthquake signal (record no. 34): a) Displacement time history at mid-span; b) base shear vs. mid-span displacement; c) normalized maximum displacement profile along length; d) normalized shear force distribution along length; e) hysteretic response of diaphragm at the building edge and f) hysteretic response of a link beam.
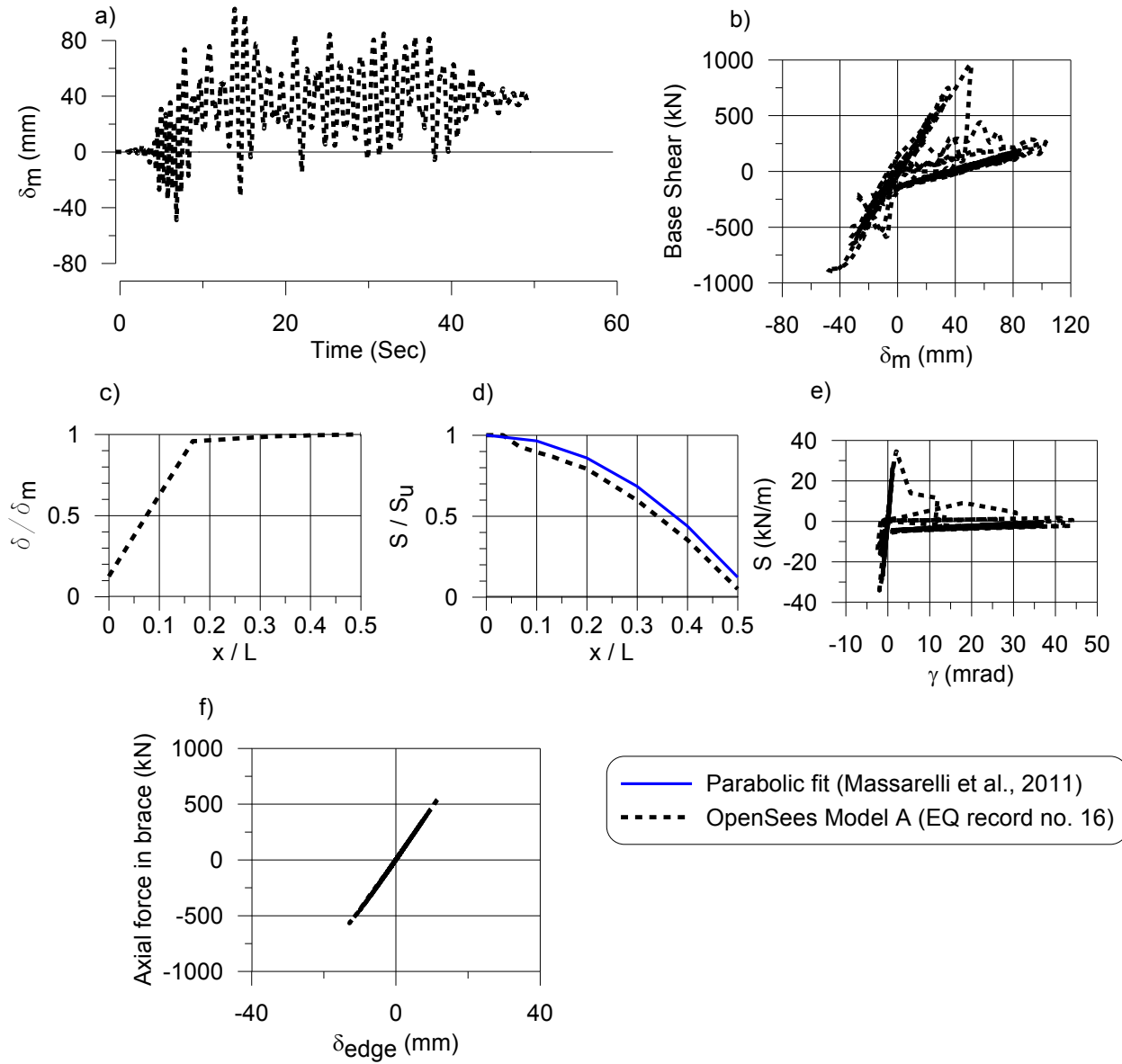
Figure E15 – Building response for DVM0 building (30m×60m×7m) under design level earthquake signal (record no. 16): a) Displacement time history at mid-span; b) base shear vs. mid-span displacement; c) normalized maximum displacement profile along length; d) normalized shear force distribution along length; e) hysteretic response of diaphragm at the building edge and f) response of a diagonal brace member.
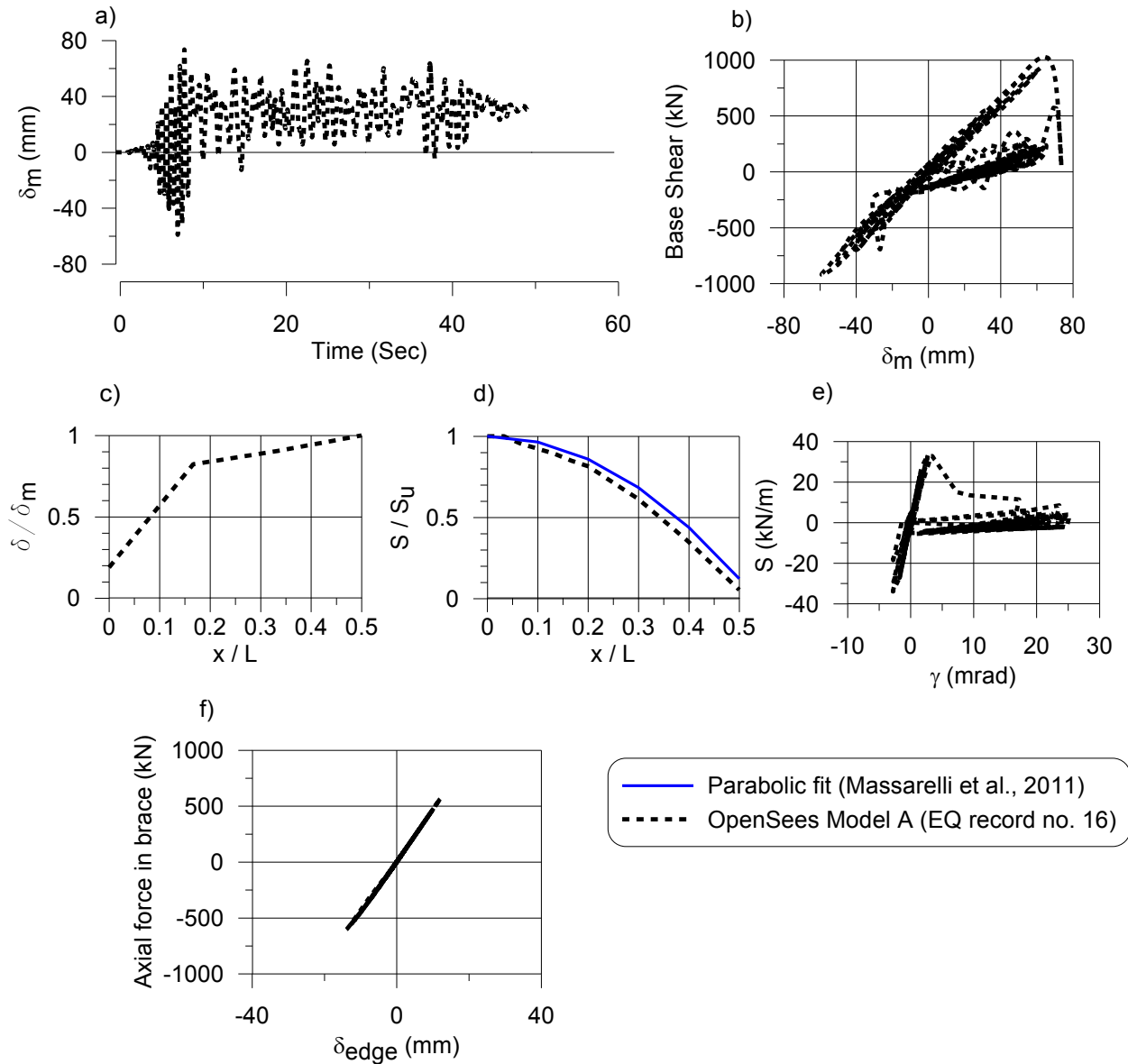
Figure E16 – Building response for DVM1 building (30m×60m×7m) under design level earthquake signal (record no. 16): a) Displacement time history at mid-span; b) base shear vs. mid-span displacement; c) normalized maximum displacement profile along length; d) normalized shear force distribution along length; e) hysteretic response of diaphragm at the building edge and f) response of a diagonal brace member.
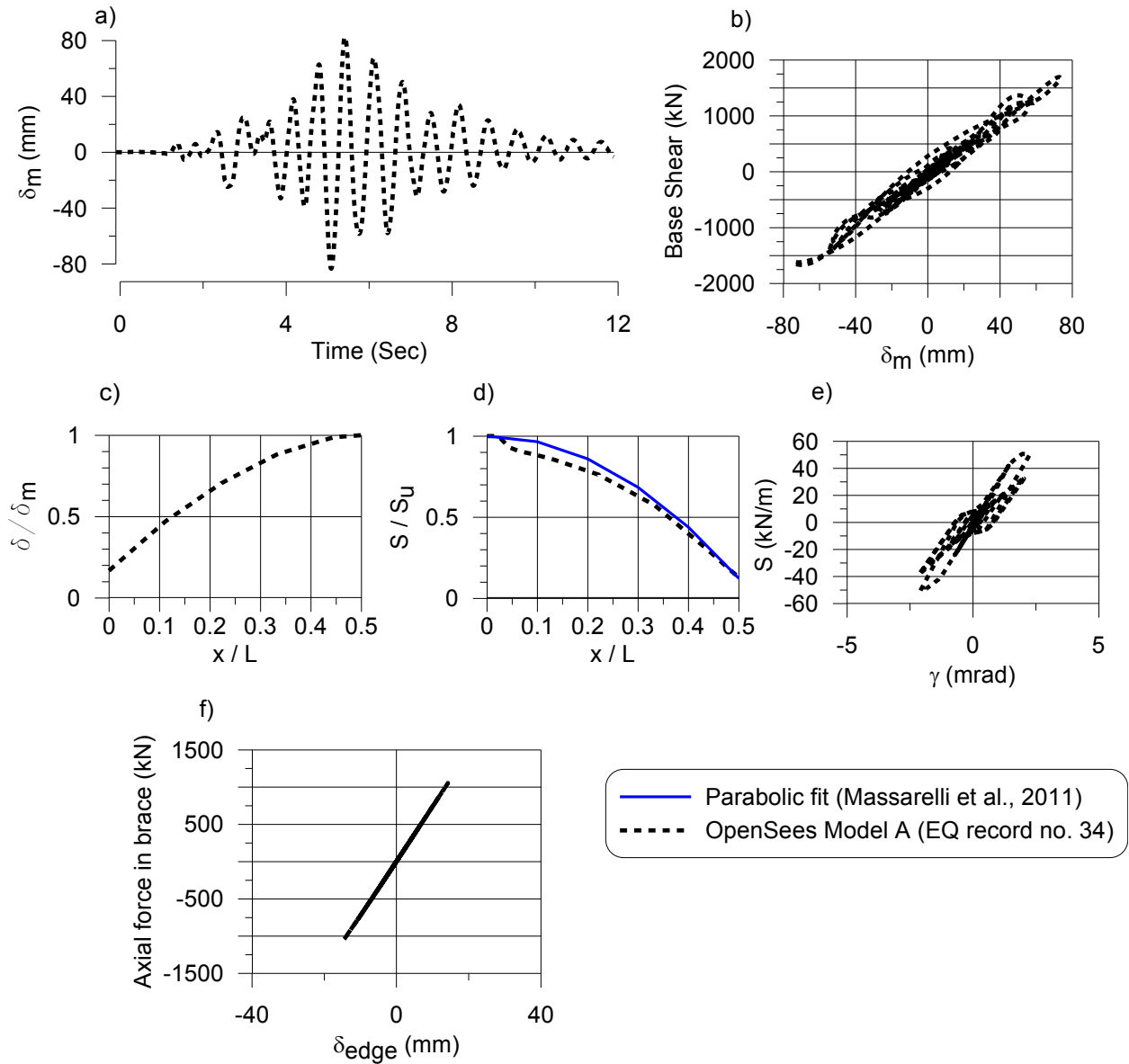
Figure E17 – Building response for DVL0 building (40m×90m×8m) under design level earthquake signal (record no. 34): a) Displacement time history at mid-span; b) base shear vs. mid-span displacement; c) normalized maximum displacement profile along length; d) normalized shear force distribution along length; e) hysteretic response of diaphragm at the building edge and f) response of a diagonal brace member.
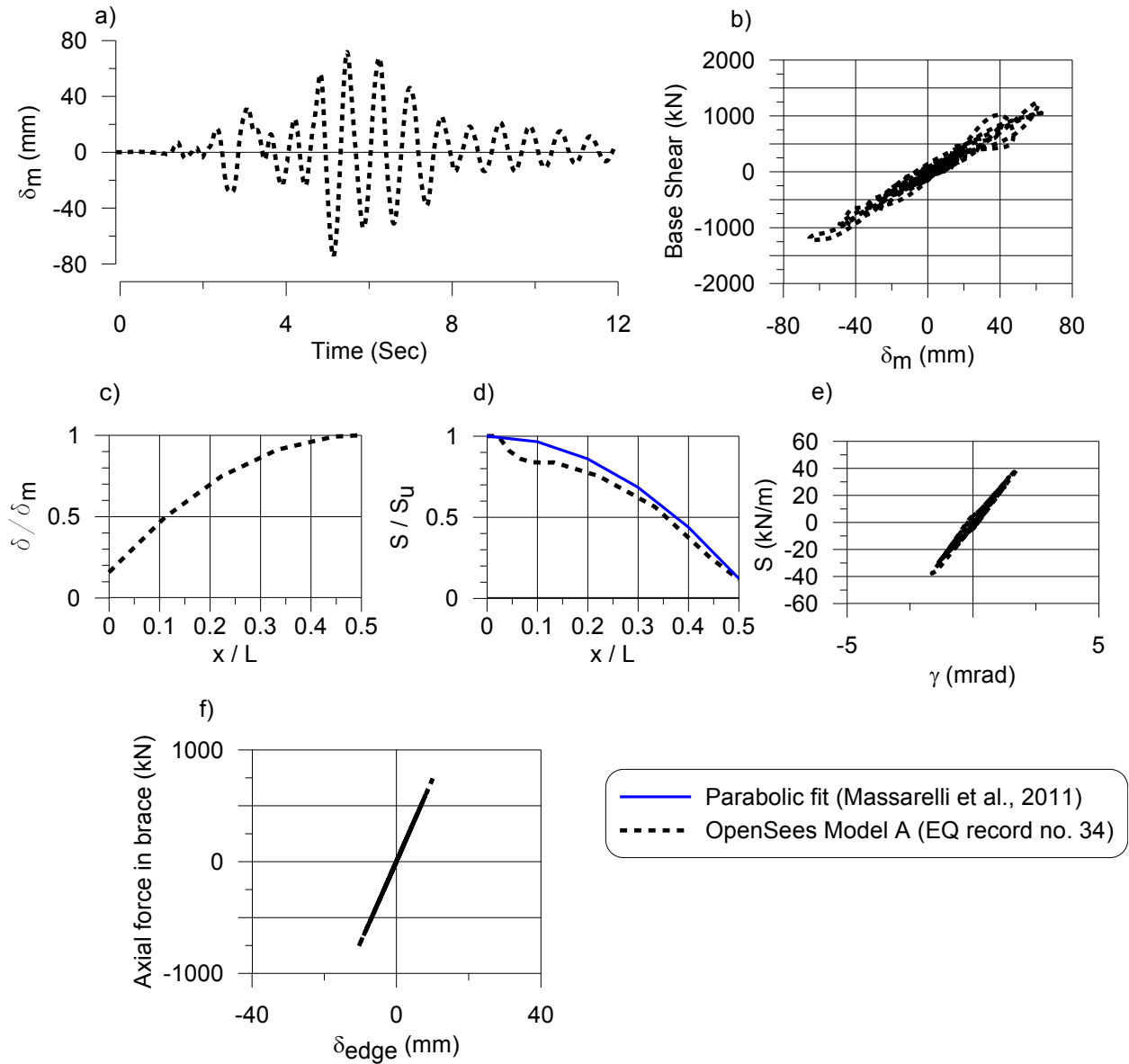
Figure E18 – Building response for DVL2 building (40m×90m×8m) under design level earthquake signal (record no. 34): a) Displacement time history at mid-span; b) base shear vs. mid-span displacement; c) normalized maximum displacement profile along length; d) normalized shear force distribution along length; e) hysteretic response of diaphragm at the building edge and f) response of a diagonal brace member.